Characterisation of cell growth, metabolism and recombinant protein production during transient and steady state conditions for the human cell line AGE1.HN.AAT

Dissertation

zur Erlangung des akademischen Grades

Doktoringenieur
(Dr.-Ing.)

von: Dipl.-Ing.(FH) Alexander Georg Rath

geb. am: 13.09.1978 in Penang, Malaysia

genehmigt durch die Fakultät für Verfahrens- und Systemtechnik der Otto-von-Guericke-Universität Magdeburg

Promotionskommission: Prof. Dr.-Ing. Kai Sundmacher

                            Prof. Dr.-Ing. Udo Reichl

                            Prof. Dr.-Ing. Ralf Pörtner

                            Dr. Volker Sandig

eingereicht am: 19.05.2017

Promotionskolloquium am: 06.12.2017

Meiner Familie

Kurzfassung

In dieser Arbeit erfolgte eine Charakterisierung des Zellwachstums, des Zentralstoffwechsels und der Produktion des rekombinanten Proteins $\alpha 1$-Antitrypsin der humanen Designerzelllinie AGE1.HN.AAT während Batch und kontinuierlichen Kultivierungen. Der Fokus lag dabei vor allem auf der Bestimmung intrazellulärer Metabolite und der maximalen *in vitro* Aktivität von Enzymen der Glykolyse, des Pentose Phosphatweges, des Zitronensäurezyklus und Nukleotide des Energiestoffwechsels. Um diese Ziele zu erreichen, wurden die Schwerpunkte auf folgende Sachverhalte gelegt: zu Beginn der Arbeit erfolgte eine physikalische Charakterisierung der in dieser Arbeit verwendeten Bioreaktoren. Das Ziel dabei war, ein Kriterium zu identifizieren, mit welchem Bioreaktoren mit unterschiedlichen Geometrien verglichen werden konnten. Es erfolgte dann eine Adaptation der Zellen an Adenovirus Expression Medium (AEM) und an glutaminfreies 42-MAX-UB Medium in Schüttelkolben. Anschließend wurde eine neue Methode zur Probennahme und gleichzeitigem Quenchen des Stoffwechsels von Suspensionszellen entwickelt und charakterisiert. In einer Serie von Batchkultivierungen in Bioreaktoren mit unterschiedlichen Arbeitsvolumina, wurden dann das Zellwachstum, die $\alpha 1$-Antitrypsinproduktion und der Stoffwechsel während der charakteristischen Zellwachstumsphasen, welche mit der

Hilfe eines mathematischen Modells bestimmt wurden, untersucht. Im letzten Abschnitt dieser Arbeit erfolgte die Charakterisierung des Zellwachstums, des Stoffwechsels und der α1-Antitrypsinproduktion in kontinuierlichen Kultivierungen mit unterschiedlichen Verdünnungsraten und Substratkonzentration. Basierend auf den Erkenntnissen dieser Arbeit, werden mehrere Ansatzpunkte für die Verbesserung der Kultivierungsbedingungen und des Zentralstoffwechsels in AGE1.HN.AAT Zellen aufgezeigt, mit dem Ziel der Steigerung der Biomasse und der α1-Antitrypsinausbeute. Zudem ergeben sich aus der Bestimmung der Dynamiken der Glykolyse, des Pentose Phosphatweges, des Zitronensäurezyklus und verschiedener Nukleotide des Energiestoffwechsels wertvolle Erkenntnisse, welche zu unserem besseren Verständnis des Zentralstoffwechsels und dessen Regulation in tierischen Produktionszellen beitragen.

Abstract

Main objectives of this thesis were the characterisation of cell growth, the central metabolism and the production of the recombinant protein α1-antitrypsin with the human designer cell line AGE1.HN.AAT during batch and continuous cultivations. Special focus was on the determination of intracellular metabolites and maximum *in vitro* enzyme activities from glycolysis, pentose phosphate pathway, TCA cycle and nucleotides from the energy metabolism. This work comprises (1) the physical characterization of bioreactors with different geometries for the identification of criteria for comparison, (2) the adaptation of the cells to AEM and glutamine-free medium in shaker cultivations, (3) the establishment and characterisation of a novel sampling and quenching method for suspension cells for the determination of intracellular metabolite concentrations, (4) the characterisation of cell growth, the central metabolism and α1-antitrypsin production during distinct growth phases obtained with the help of a mathematical model for batch cultivations in different bioreactors and (5) the characterisation of cell growth, the central metabolism and α1-antitrypsin production for continuous cultivations exploring the effect of the dilution rate and nutrient supply. The obtained results provided several starting points for the improvement of cultivation conditions and the central metabolism with the aim to increase

the overall yield of biomass and α1-antitrypsin. In addition, the results add valuable insights to our understanding of the central metabolism of mammalian cells, in particular of the dynamics of glycolysis, pentose phosphate pathway, TCA-cycle and nucleotides from the energy metabolism.

Acknowledgment

Bei den technischen Assistentinnen Susanne König, Claudia Best, Ilona Behrendt und Felicitas Hasewinkel möchte ich mich ganz herzlich bei der täglichen Unterstützung im Labor bedanken.

Bei den von mir betreuten Bachelor Studenten möchte ich mich für ihre Einsatzbereitschaft und den Fleiß bei der Ausarbeitung ihrer Abschlussarbeiten bedanken und den damit zusammenhängenden Beiträgen zu meiner Promotionsarbeit.

Dem ganzen SysLogics Konsortium danke ich für die hervorragende und erfolgreiche Zusammenarbeit, welche letztendlich in die Veröffentlichung mehrerer Publikationen mündete.

Bei der ProBioGen AG bedanke ich mich für die Überlassung der humanen Designerzellen für meine Forschungsarbeiten sowie beim BMBF für die finanzielle Unterstützung im Rahmen des SysLogics-Projektes.

Allen Doktoranden und Doktorandinnen, welche mich auf meinem Weg begleitet haben, danke ich ganz herzlich für die kurzweiligen und stets interessanten Gespräche, die stetige Unterstützung, den Zuspruch, aber auch für die kritische Auseinandersetzung mit meiner Forschungsarbeit.

Zu guter Letzt gilt der größte Dank meiner Frau Janine und meiner ganzen Familie für ihre Geduld, ihre Unterstützung und stetigen Ermutigungen.

Contents

List of abbreviations and symbols

Abbreviations

1PFK	fructose-1-phosphatekinase
2-KG	2-ketoglutarate
2PG	2-phospho-D-glyceric acid
3PG	3-phosphoglyceric acid
6PFK	fructose-6-phosphatekinase (phosphofructokinase)
6PGDH	6PG dehydrogenase
A1AT	α1-antitrypsin
ACOAL	acetate-CoA ligase
AEC	anion exchanger chromatography
AEM	Adenovirus Expression Medium
ALA	alanine
AlaTA	alanine transaminase
AMM	ammonia
AMPK	AMP-activated protein kinase
ARG	arginine
ASN	asparagine
ASP	aspartate
AspTA	aspartate transaminase
BHK	baby hamster kidney
CHO	chinese hamster ovary
CIS-ACO	cis-aconitate
CIT	citrate
CL	citrate lyase
CQA	critical quality attribute
CS	citrate synthase
CYS	cysteine
DO	dissolved oxygen

EAA	essential amino acid
ECR	energy charge ratio
F1P	fructose 1-phosphate
F6P	fructose 6-phosphate
FBP	fructose 1,6-bisphosphate
FBPA	fructose-bisphosphate aldolase
FPDO	freezing point depression osmometer
FUM	fumarate
FUMase	fumarase
G1P	glucose 1-phosphate
G6P	glucose 6-phosphate
G6PDH	G6P dehydrogenase
GALC	galactose
GAP	glyceraldehyde 3-phosphate
GAPDH	glyceraldehyde 3-phosphate dehydrogenase
GC-MS	gas chromatography-mass spectrometry
GLC	glucose
GLDH	glutamate dehydrogenase
GLN	glutamine
GLNase	glutaminase
GLU	glutamate
GLUT	glucose transporter
GLY	glycine
GS	glutamine synthetase
HE	heat exchanger
HIS	histidine
HK	hexokinase
HPLC	high-performance liquid chromatography
I$_2$	iodine
ICIT	isocitrate
ILE	isoleucine
KI	potassium iodide
LAC	lactate
LC-MS	liquid chromatography-mass spectrometry
LDH	lactate dehydrogenase
LEU	leucine
LIN	liquid nitrogen
LPS	lactate producing state
LYS	lysine
MAL	malate
MDCK	Madin Darby canine kidney
MDH	malate dehydrogenase
ME	malic enzyme
MET	methionine
MFA	metabolic flux analysis
MVDA	multivariate data analysis
NaCl	sodium chloride
NAD-ICDH	NAD$^+$-dependent isocitrate dehydrogenase

NADP-ICDH	NADP$^+$-dependent ICDH
NDP	nucleotide diphosphate
NEAA	non-essential amino acid
NLPS	non-lactate producing state
NMP	nucleotide monophosphate
NMR	nuclear magnetic resonance
NTP	nucleotide triphosphate
OAA	oxaloacetate
OTR	oxygen transfer rate
PBS	phosphate buffered saline
PC	pyruvate carboxylase
PCA	principle component analysis
PCS	process control system
PDH	pyruvate dehydrogenase
PDHK	pyruvate dehydrogenase kinase
PDK4	pyruvate dehydrogenase lipoamide kinase isozyme 4
PEP	phosphoenolpyruvate
PEPCK	PEP carboxykinase
PGAM	2,3-bisphosphoglycerate-dependent phosphoglycerate mutase
PGI	phosphoglucose isomerase
PHE	phenylalanine
PI	propidium iodide
PK	pyruvate kinase
PKM2	pyruvate kinase M2
PLSR	partial least square regression
PPP	pentose phosphate pathway
PRO	proline
PYR	pyruvate
R5P	ribose 5-phosphate
RP-HPLC	reversed phase high-performance liquid chromatography
RSS	residual sum of squares
SD	standard deviation
SER	serine
SOP	standard operating procedure
Na$_2$S$_2$O$_3$	sodium thiosulfate
SUC	succinate
SVM	support vector machines
TA	transaldolase
THR	threonine
TK	transketolase
TPI	triose-phosphate isomerase
TRP	tryptophan
TYR	tyrosine
UDP-GalNAc	uridine diphosphate N-acetyl galactosamine
UDP-GLC	UDP-glucose
UDP-GlcNAc	uridine diphosphate N-acetyl glucosamine
VAL	valine
Vero	African green monkey kidney

Symbols

CD	μm	cell diameter
CV_v	μL/mL	total viable cell volume per volume of media
C_p	mmol/L	produced metabolite concentration
C_s	mmol/L	consumed substrate concentration
d	m	stirrer diameter
D	m	tank diameter
DR	1/h	dilution rate
η	kg/(m s)	dynamic viscosity
F_g	m^3/s	aeration rate
F_i	L/h	feed rate
k_D	1/h	specific cell death rate
$k_{d,gln}$	1/h	spontaneous degradation rate of glutamine
k_{glc}	mmol/L	Monod constant for glucose
k_{gln}	mmol/L	Monod constant for glutamine
$k_L a$	1/h	volume-specific oxygen transfer value
$k_{m,glc}$	mmol/L	saturation constant for glucose
$k_{m,gln}$	mmol/L	saturation constant for glutamine
$k_{m,pyr}$	mmol/L	saturation constant for pyruvate
m_{glc}	μmol/(μL h)	maintenance term for glucose
m_{gln}	μmol/(μL h)	maintenance term for glutamine
m_{pyr}	μmol/(μL h)	maintenance term for pyruvate
$\theta_{0.95}$	s	mixing time at a mixing degree of 95 %
μ	1/h	specific cell growth rate
μ_{max}	1/h	maximum specific cell growth rate
N	rpm	rotational stirrer speed
Ne	-	dimensionless Newton number
N_g	-	dimensionless aeration rate number
P	W	power input
P_0	W	power input of a non-gassed system
P_g	W	power input of a gassed system
q_s	nmol/(μL h)	specific uptake rate for substrates s
q_p	nmol/(μL h)	specific production rate for metabolites p
Q^2	%	predictability of the PCA model
Q_{lac}	mmol/(L h)	volumetric lactate production rate
R^2	%	goodness of fit of the PCA model
Re	-	Reynolds number
ρ	kg/m^3	density
σ	-	unit step function
τ_p	s	response time of the dissolved oxygen probe
τ_t	s	response time of the system regarding oxygen transport
t_m	s	mixing time
$u_{g,0}$	m/s	gas superficial velocity
u_{tip}	m/s	impeller tip speed
v_{max}	mmol/s	maximal enzyme reaction velocity
vvm	1/min	volume gas per volume liquid per minute
wv	L	working volume
X_D	cells/mL	concentration of dead cells

X_T	cells/mL	concentration of total cells
X_V	cells/mL	concentration of viable cells
$Y_{CVv/glc}$	μL/mmol	yield coefficient for produced CV_v per consumed glucose
$Y_{CVv/gln}$	μL/mmol	yield coefficient for produced CV_v per consumed glutamine
$Y_{CVv/pyr}$	μL/mmol	yield coefficient for produced CV_v per consumed pyruvate
$Y_{lac/glc}$	mol/mol	yield coefficient for produced LAC per consumed GLC
$Y_{amm/gln}$	mol/mol	yield coefficient for produced AMM per consumed GLN
$Y_{ala/gln}$	mol/mol	yield coefficient for produced ALA per consumed GLN

Introduction and motivation

When it comes to quality and efficacy of biopharmaceuticals, such as correctly folded and glycosylated recombinant proteins, there exists no alternative to the production of such products with cell-based expression systems. In 2007, with \$97 billion of sales, the biopharmaceuticals sector represented a considerable growing portion of the overall pharmaceutical market. Nowadays, around 60 % of therapeutic proteins on the market are produced in cell-based expression systems [1–5]. Between 2010–2014 the rate of biopharmaceutical approvals in the United States (US) and European Union (EU; Brussels) has remained relatively steady compared with the previous time periods and of the 54 biologics, which were approved in the US and EU, 17 were monoclonal antibodies, 9 were hormones, 8 were blood-related proteins, 6 were enzymes, 4 were vaccines, fusion proteins and granulocyte-colony stimulating factors (G-CSFs; filgrastims), one was interferon and one was a gene therapy-based product [5]. Besides a vast number of different cell lines nowadays available, for more than 25 years DHFR-minus chinese hamster ovary (CHO) cells constitute the major host for the production of recombinant proteins, and many manufacturing processes are still performed in large-scale stirred-tank bioreactors in simple batch and extended batch or fedbatch mode. With improved vectors,

host cell and process engineering, medium development and screening methods, product titers up to 13 g/L are nowadays achievable [1, 6, 7].

Today, chemically defined media exist for the cultivation of mammalian cells, which are usually supplemented with great amounts of glucose and glutamine as these substrates are the main substrates for cell growth of mammalian cells. Studies in the past therefore mainly focused on kinetic and stoichiometric analyses of glucose and glutamine consumption [8–13]. Mammalian cells in culture usually take up these substrates at high rates and secrete lactate and ammonia, which can have cytotoxic effects and thereby can decrease cell viability, growth and productivity [14–16]. Production of biopharmaceuticals with mammalian cell lines is still performed in large-scale stirred-tank bioreactors in mostly batch process mode [17]. The reasons for the broad application of batch cultivations are from a historical point of view the development of processes for the production of vaccines. Back at the 1960s the technology available was suited only for batch applications and the only acceptable cell lines for production were diploid cells, which are limited in their life-span. For the scale-up of these processes, a simple and fast approach was the adoption of stirred tank reactors commonly used for bacterial cultivations. With the development of the recombinant protein technology in the 1970s and 1980s, suspension cells were more and more deployed for the production of biopharmaceuticals and this allows nowadays the application of more advanced cultivation systems such as fedbatch or perfusion systems [18]. Fedbatch as well as perfusion cultivations have shown to successfully prevent accumulation of toxic by-products and cells grown under limiting concentrations of either glucose and/or glutamine shift to a more efficient metabolism with less waste product formation leading to higher cell densities and product yields [19–23]. Others have focused on specific alterations of metabolic pathways, which led to reduced substrate consumption or even enabled the cells to grow in glutamine free medium and thereby reduced formation of lactate and ammonia [24–26]. Besides these approaches, empirical driven studies have also shown that for some cell lines the substitution of glucose or glutamine with alternative substrates can lead to superior growth characteristics with less waste product formation and eventual higher product titers [27–31].

As intracellular metabolite concentrations are more downstream from gene expression to a specific phenotype, the metabolome certainly reflects more closely the physiological activity of a cell, compared to other functional levels such as the

transcriptome or proteome. For example, it has been suggested that when comparing the discriminatory power of metabolic and RNA measurements to distinguish between different potato tuber systems, measuring the intracellular metabolome was superior over expression profiling [32]. While metabolic profiling was done in the past for microorganism, plants and cancer cells [33–35], studies of the dynamics of intracellular metabolites with mammalian cells employed for industrial production processes are greatly lacking [36]. Chrysanthopoulos et al. [37], for example, applied gas chromatography-mass spectrometry (GC-MS) to analyse baby hamster kidney (BHK) cells of different cell ages from perfusion reactors at both laboratory and manufacturing scales. With their approach they could differentiate the cell cultures based on cell age, bioreactor scale and cell source although cell growth, metabolic activity and protein productivity measurements suggested consistency across the employed bioreactors and over the time course of cultivations [37]. In another study, Dietmair et al. [38] analysed CHO cells cultivated in three different media exhibiting different specific growth rates and maximum viable cell concentrations. For the cells with a lower specific growth rate they found mainly nucleotides being lower concentrated and hypothesized that too low CTP concentrations might limit proliferation. To establish, whether a lack of cytosine or cytidine was responsible for the low specific growth rates, they added cytosine and cytidine at the start of a batch culture. But this did not increase growth rates. According to the authors, these result illustrates one of the difficulties associated with the interpretation of metabolomics data, namely the high degree of connectivity of intracellular metabolites [38]. In contrast, for hybridoma cells, intracellular metabolite pools were successfully used for monitoring the physiological state [39]. Therefore, as changing conditions such as the depletion of extracellular substrates might lead to global changes in the metabolome, profiling of intracellular metabolites might add to our understanding of how metabolic networks are regulated and finally linked to cell growth and protein production during manufacturing processes. Moreover, intracellular metabolite profiling might complement other "-omics" as well as metabolic flux studies.

Few is known about the relation of cell growth and productivity to intracellular metabolite dynamics, even though there are in-depth studies on the carbon and energy metabolism of mammalian cells used for the production of biopharmaceuticals [11, 40, 41] and excellent reviews about this topic [42]. Therefore, in this

thesis, intracellular metabolite concentrations and maximum enzyme activities in a novel human designer cell line were determined under different conditions such as transient growth in batch cultivations as well as steady state growth in continuous cultivations. The human parental cell line AGE1.HN and its α1-antitrypsin (A1AT) producing clone AGE1.HN.AAT, both established and designed for the production of recombinant proteins as well as for viruses and viral vectors by the company ProBioGen from Berlin, were used as a model system for these studies. The work described in this thesis was funded by the Federal Ministry of Education and Research (BMBF) and was part of a comprehensive approach to generate experimental datasets of the AGE1.HN and AGE1.HN.AAT cell lines. This was achieved together with seven other research partners [1] and the industrial partner ProBioGen within the Systems Biology of Cell Culture for Biologics (SysLogics) project. During this time, different studies with both cell lines focused on aspects concerning the glycosylation pattern and the *in vitro* anti-inflammatory activity of A1AT [43], the flux distribution within the central cell metabolism [44, 45], effects of varying substrate and waste product concentrations on cell growth and metabolism [46, 47], comparison of cell growth in different cultivation systems [48–50], quantification of the intracellular metabolome, transcriptome and proteome with focus on glycolysis, TCA cycle and oxidative phosphorylation [51], and modelling approaches to describe different growth phases, compare growth and metabolism between both cell lines and calculate the theoretical metabolic burden of A1AT production [50, 52, 53].

Within the scope of this thesis, first working cell banks of the parental and producer cell line and routine cultivations in orbital shaker flasks were established in the Bioprocess Engineering group at the Max Planck Institute in Magdeburg. Then the geometric similarities, power inputs (P), impeller tip speeds (u_{tip}), Reynolds numbers (Re), and mixing times for the bioreactors used were determined (section 4.1.1 on page 57). This served as a basis for comparison of the different bioreactors used within the SysLogics consortium and also for the set-up of proper cultivation conditions for the intended continuous cultivations. In preliminary experiments with shaker flasks and the standard medium (serum-free, chemically defined), basic growth characteristics as well as the dependency of AGE1.HN cells on glutamine

---

[1]Prof. Dr. Noll and Dr. Gösmann (University Bielefeld), Prof. Dr.-Ing. Heinzle (University Saarbrücken), PD Dr.-Ing. Pörtner and Prof. Dr. Zeng (University Hamburg-Harburg), Prof. Dr. Scheper (University Hannover) and Dr. Hauser (Helmholtz Centre for Infection Research in Braunschweig)

supplementation were investigated (section 4.1.2 on page 61). For the quantification of maximum activities of key enzymes and intracellular metabolites from the carbon and nucleotide metabolism two analytical platforms originally developed for the analysis of adherently growing Madin Darby canine kidney (MDCK) cells by Janke [54] and Ritter [55] were adapted for monitoring of cultivations. In contrast to adherently growing cells, the removal of the culture broth upon sampling is crucial for suspension cells. Therefore, a novel sampling and quenching method was established and subsequently characterized (section 4.2 on page 66). This enabled the measurement of intracellular metabolite concentrations and maximum enzyme activities in AGE1.HN.AAT cells growing in batch cultivations at different scales (section 4.3 on page 87). In addition, a series of continuous cultivations under limiting concentrations of glucose (section 4.4 on page 113) was performed to identify strategies for the improvement of cell growth and A1AT yield.

CHAPTER 2

Theoretical background

2.1 The AGE1.HN cell line for production of alpha1-antitrypsin

Since decades, continuous cell lines such as CHO, BHK, hybridoma, MDCK or African green monkey kidney (Vero) cells are used for the production of recombinant proteins, antibodies and vaccines. Their major advantage over primary cell cultures are a prolonged life span due to spontaneous or directed immortalization using different viral oncogenes and their extensive characterisation in various studies concerning cell growth [8, 16, 27, 30, 56–59], productivity [6, 26, 60–67] and metabolism [11, 13, 40, 41, 68–74]. The generation of most cell lines was by chance, driven by their growth characteristics and their applicability for the production of certain biopharmaceuticals. A different approach is the design of cell lines for certain applications by carefully selecting the source of primary cells. This cells are then immortalized and shaped for apoptosis resistance [75] by well known genetic methods such as the integration of genes from adenovirus into the genome of the cells [76, 77]. The human parental cell line AGE1.HN represents such a designed cell line, which was established by the company ProBioGen (ProBioGen

AG, Berlin, Germany) from a tissue sample of a human brain. Main advantage of a continuous cell line of human origin for the production of biopharmaceuticals, is certainly the capability to produce a complex glycosylation pattern close to that of the human body [78]. The AGE1.HN cells express only marker genes characteristic for neuronal cells and lack markers characteristic for glial cells. Immortalization was achieved by insertion of the adenoviral E1 A and B genes of the human adenovirus type 5. The parental cell line was then further modified to express the adenoviral protein 9 (pIX), which is known to be involved in the stabilization of the viral capsid, to act together with the E1 A protein as activator of transcription and to possibly be involved in the control of apoptosis [43, 79]. These modifications are believed to enhance the production of exported proteins, to modulate susceptibility to a variety of viruses and to also have an effect on the metabolism [43]. The parental cell line was then adapted to grow in suspension in a chemically defined medium [44].

The producer cell line AGE1.HN.AAT was established by insertion of the gene for the expression of A1AT, an acute phase glycoprotein required to treat patients having A1AT deficiency. This disease can results in lung emphysema and liver dysfunction [43, 80]. A1AT is mainly produced in the liver by hepatocytes, but also by macrophages, intestinal, and bronchial epithelial cells [80]. The main function of A1AT is to inhibit pancreatic trypsin and many other proteinases including neutrophil elastase, cathepsin G, and proteinase 3 [81]. The human glycoprotein A1AT has a weight of 52 kDa. It consists of a single polypeptide chain with 394 amino acids, and it has about 14 % carbohydrates by weight. Since the 1980s, the augmentation therapy with A1AT has shown to increase lung levels of A1AT in emphysema patients with severe A1AT deficiency. At present, great numbers of patients are treated in Europe as well in the United States of America with A1AT that was purified from human serum. As there is a high risk of infection and the augmentation therapy is expensive and in short of supply, an alternative source of human A1AT is the production of a recombinant protein [43]. The entire development work for the generation of the AGE1.HN cell line was carried out in a dedicated cell culture suite and the complete development history was recorded [44]. The AGE1.HN cell line was adapted to grow in media that are compliant with the stipulations of the guidance on minimizing the risk of transmitting animal spongiform encephalopathy agents via human and veterinary medicinal products

(European Medicines Agency, 2004) [43] and is a proprietary product of the Pro-BioGen AG, covered by the patent application 06807777.5-2406 [44]. The cloning vectors for the immortalization of the parental cell line and the generation of the producer clone are shown in figure 2.1.

Figure 2.1: Cloning vectors for the immortalization of the parental cell line AGE1.HN (a) and for the generation of the A1AT producing clone AGE1.HN.AAT (b).

2.2 Process strategies for mammalian cell cultivations

To avoid the high risk of contaminations, bioreactor cultivations with mammalian cells are typically performed as a batch process. For a batch cultivation, all required substrates are submitted to the bioreactor, followed by the inoculation with cells. The system is then closed and by the end of the process time the product can be harvested (see figure 2.2-a). A batch cultivation is regarded as a closed system. However, this is only true in matters of the liquid phase, as gaseous substrates cannot be provided in a sufficient amount due to their low solubility in water, as well as gases produced during the metabolic processes need to be transported out of the system. In addition, small amounts of acid or base are usually added during the process for the control of the culture pH, and especially for small benchtop biore-

9

actors (working volume (wv) = 0.5–2 L), a significant amount of the liquid phase might be constantly removed due to evaporation, as well as due to daily sampling for different analysis. In contrast to that, an open system such as a continuous cultivation is also open for the liquid phase, which means that during the process time fresh media is added as well as old medium with cells is removed from the system, so that the culture volume remains constant (see figure 2.2-c). In case the dilution rate is controlled, the system is also termed chemostat cultivation. Besides these two process modes, semi-open systems such as fed batch [16, 82, 83], extended batch [1] and semi-continuous [74] processes are under investigation and in case of fed-batch processes are already applied in large scale for the production of recombinant proteins [17]. A fed-batch process is started with a short batch phase followed by a phase, where fresh medium is added, which increases the culture volume, number of viable cells and product titre. Extended batch and semi-continuous processes are harvested at regular intervals, whereby the medium is either replaced at once (extended batch process) or diluted by a continuous feed (semi-continuous process) with fresh medium. Another open system is a perfusion process, where fresh medium is continuously added and old medium removed by retaining cells within the reactor, leading to significantly higher cell numbers and protein titres [84, 85].

Batch and continuous cultivations During a batch cultivation, mammalian cells go through different phases (lag, exponential, stationary and death), which can be typically observed during the process (see figure 2.2-b). Batch cultivations are simple regarding process control and operation, less time consuming and enable a cost-efficient production. However, cells are constantly exposed to a continuously changing environment, which often becomes gradually toxic, due to accumulating waste products [18]. Therefore, datasets obtained from batch cultivations are often difficult to interpret, as the outcome might be the combined result of various different factors. One way to circumvent this problem is to grow the cells in a defined and homogeneous environment, were the physio-chemical conditions can be precisely controlled. This can be achieved by growing cells in a continuous cultivation [86]. Continuous cultivations are usually initiated by a short batch culture, followed by the continuous phase were fresh medium with a limiting concentration of e.g. glucose or glutamine is added to the culture (see figure 2.2-d). Fresh

medium is added during the exponential growth at a suitable rate, whereas the culture broth is removed at the same rate. Growth with a constant rate below the maximum specific cell growth rate (μ_{max}) of the cells proceeds until a steady state is reached, where viable cell numbers and all specific uptake and production rates are constant. Under these conditions different factors such as substrate concentrations, pH value or culture temperature can be varied and the influence on the steady state studied. The most important parameter for a chemostat cultivation is the dilution rate (DR) (see equation 3.26 on page 55). As the total biomass under steady state conditions is constant ($\frac{d[X_T]}{dt} = 0$), it follows that the specific cell growth rate (μ) = DR (only for cell viability = 100 %, refer to section 3.5.4). This means that during steady state, μ can be controlled by adjusting DR, as long as μ is below a critical dilution rate, where cells are washed out of the bioreactor.
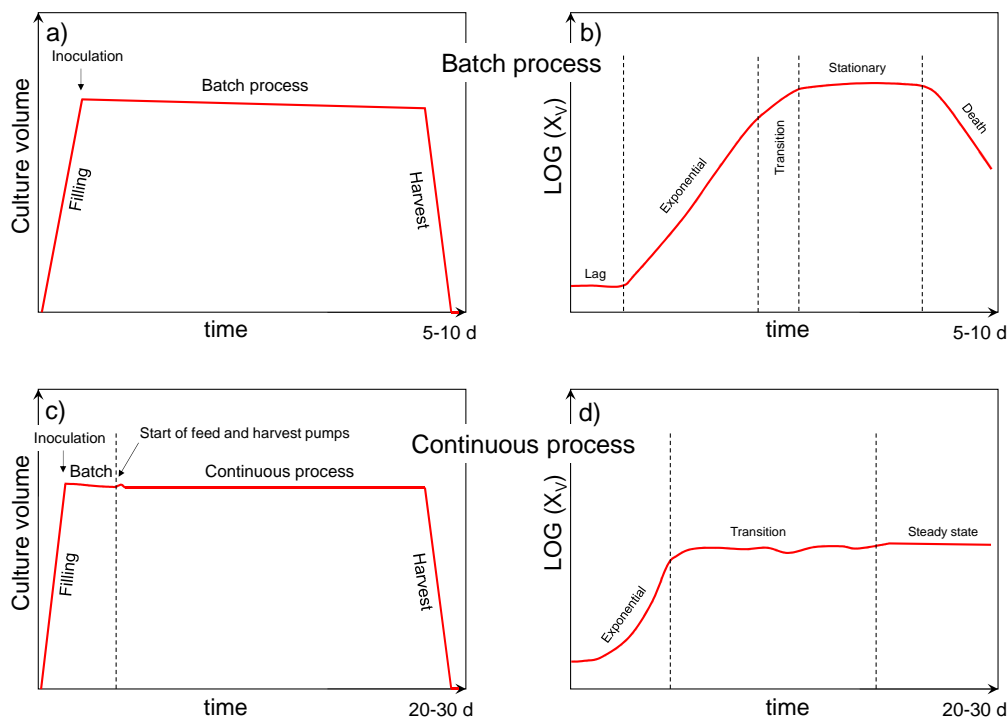
Figure 2.2: Time courses of the culture volume and viable cells of a batch (a, b) and continuous cultivation process (c, d).

The achievable biomass concentration in a continuous cultivation depends only on the yield coefficient for produced biomass per consumed substrate (the limiting

substrate), and the concentration of the limiting substrate in the feed medium. Without a cell retention system it is always lower compared to a batch cultivation. However, a commercial continuous production system might provide a higher operational flexibility, a much smaller facility footprint, higher volumetric productivities, and a consistent product quality [87]. Hence, continuous cultivations for the production of recombinant proteins might be a serious contender for batch production systems. In addition, continuous cultivations are an invaluable tool for cell physiology studies [18], especially when combined with recently emerging omics applications (see section 2.3).

Assumptions for steady state analysis   Crucial for steady state analysis of mammalian cells grown in continuous cultivations, is that characteristic properties regarding growth and metabolism do not change significantly. This means that variations in their concentration are lower than the standard deviation (SD) of the respective analytical method, which might be as high as ± 20 %. In addition, when designing a continuous cultivation the following points should be considered. Firstly, the feed medium added to the bioreactor at a specific point might result in substrate concentration gradients. This might lead to cells being more or less exposed to nutrients, which might influence therefore the uptake of substrates and which add additionally bias when analysing the metabolism, especially on an intracellular level. Secondly, owing to the fact that the cell population consists of cells with different cell sizes, bigger cells might settle faster to the bottom of the bioreactor. Depending on the position of the harvest tube for the removal of culture broth, either smaller cells being selectively removed, in case the harvest is withdrawn from the surface of the cultivation or bigger cells are being removed selectively, when the harvest is withdrawn from the bottom of the bioreactor. Making sure that the mixing time is small enough to circumvent substrate as well as biomass concentration gradients is therefore mandatory for steady state analysis. Constant time profiles after at least three complete volume exchanges are often found in literature as standard value for the achievement of the steady state phase [88–91]. Having a lower specific growth rate compared to other continuous cell lines, it was assumed that the steady state for the experiments with the AGE1.HN cells was achieved after reaching constant time profiles after at least four complete volume exchanges.

2.3 Analytical methods for cell physiology studies

Multi omics approaches More and more data sets are emerging, obtained with recently established omics techniques, such as genomics, proteomics, transcriptomics, metabolomics, fluxomics, and glycomics (figure 2.3). These analytical methods allow the investigation of mammalian cell physiology on a global scale and will aid in developing future engineering strategies to develop high-producer cell lines [92, 93]. In this context, genomics aims at analysing the whole genome sequence and the information contained therein by applying DNA sequencing methods, whereas transcriptomics provides information about both the presence and the relative abundance of mRNA transcripts by applying microarray technologies or by serial analysis of gene expression (SAGE) [94]. On the next level, proteomics aims to identify and quantify the abundance of every single protein that is encoded by the genome. Methods are two-dimensional gel electrophoresis for separation, followed by mass spectrometry for the identification of the separated proteins.
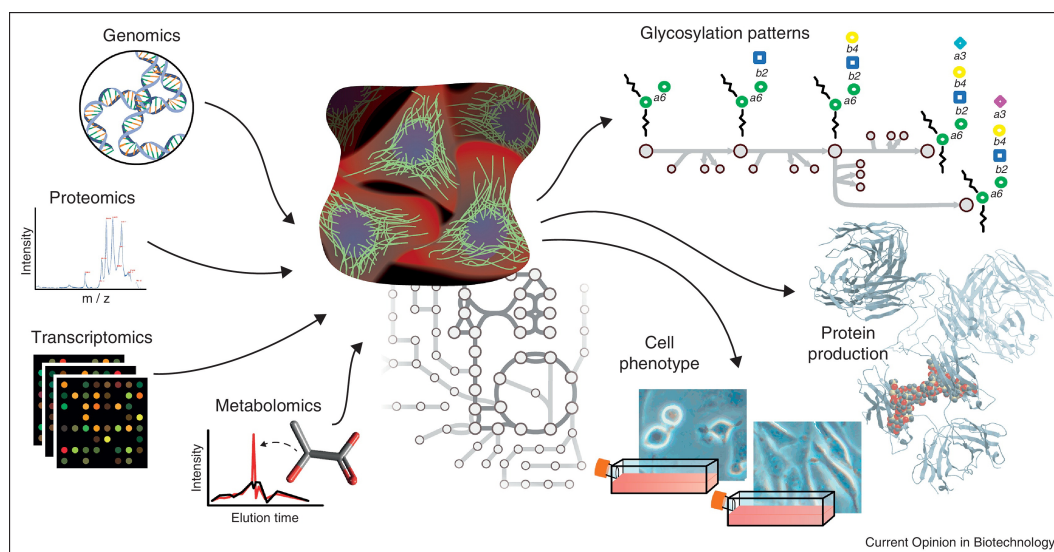
Figure 2.3: Schematic overview of currently available omics methods for the investigation of mammalian cell metabolism and recombinant protein production (Reprinted from Kildegaard et al. [92], with permission from Elsevier).

By applying high-performance liquid chromatography (HPLC) and high-resolution mass spectrometry glycomics seeks to identify the entire complement of carbohydrates and glycans within a cell. Metabolomics aims at the investigation of the

complete set of metabolites (metabolome), which represents the functional end-point of the genome, transcriptome and proteome. Typical methods for analysing the metabolome are HPLC followed by mass spectrometry or nuclear magnetic resonance (NMR) spectroscopy. Besides these methods, more omics techniques are under way such as lipidomics (investigation of the complete inventory of lipids), localizomics (investigation of the subcellular location of proteins), fluxomics (quantification of specific metabolite fluxes) and phenomics (highthroughput determination of cellular fitness in response to genetic / environmental perturbations) [94]. However, the development of these methods is still in its infancy and their applicability has still to be proven.

Targeted analytical methods   In contrast to the above mentioned omics methods, targeted approaches are aiming at the quantification of e.g. proteins or metabolites from specific pathways of interest. In the bioprocess engineering group at the Max-Plank-Institut in Magdeburg, two analytical platforms were recently established aiming at the quantification of maximum activities of key enzymes [54] and intracellular metabolites from the carbon and nucleotide metabolism of adherently growing MDCK cells [55]. For the determination of maximum enzyme activities, Janke [54] adapted 17 different cycling assays used for plant metabolomic studies. Furthermore, the platform was extended to 11 new enzyme assays for biochemical reactions in the central carbon and glutamine metabolism of mammalian cells. In cycling assays, the enzyme activity is measured by quantifying the product formed or substrate consumed per unit time under optimized experimental conditions (e.g. pH, ionic strength) in 96-well microplates [54]. According to Janke [54], the developed enzyme assays allow a sensitive (0.025–0.4 nmol product) and faster determination of enzyme activities compared to most of the existing assays. Further advantages are less laborious preparation steps and the application of highly diluted cell extracts reducing possible interferences from other cellular components. For the determination of maximum enzyme activities in AGE1.HN cells, the assay conditions optimized for MDCK cells were verified and if necessary adapted. For a elaborate description and discussion of the established enzyme assays the reader is referred to Janke [54].

The second analytical platform, established by Ritter [55], is based on a selective extraction method for organic acids, sugar-phosphates and nucleotides from mam-

malian cells. An anion-exchange chromatography method with conductivity, UV and a mass-spectrometry detector, allows the confirmation of metabolite identities according to their mass/charge ratio. After the improvement of the chromatography method, the detection limits were below the micromolar range and the coefficient of correlation was above 0.99 for most analytes [95]. Then two promising extraction methods were further optimized based on experimental design techniques and after combining individual steps of both methods, recoveries close to 100 % for all metabolites could be achieved [96]. As explained in sections 3.4.5 and 4.2, for the determination of intracellular metabolites in AGE1.HN cells, the method of Ritter was slightly adjusted to account for differences in quenching and sampling between adherently growing MDCK cells and AGE1.HN cells growing in suspension.

Challenges when working with suspension cells For the quantification of intracellular metabolites, the applied method should be able to stop the intracellular reactions, i.e. reduce/inactivate enzyme activities sufficiently and fast enough, to stop the turnover of intracellular metabolites. This should be achieved without inducing cell damage or leakage of metabolites from the cell, until the metabolites are being extracted from the cells (figure 2.4). This is usual done by lowering the temperature to or below 0 °C. For bacteria and yeast cells, quenching with -40 °C cold methanol is widely applied, though several authors have shown that leakage of metabolites during quenching with methanol occurs [97, 98]. For adherently growing mammalian cells, such as MDCK cells, quenching can be easily achieved by either adding ice-cold sodium chloride (NaCl) solution, phosphate buffered saline (PBS) or liquid nitrogen to the culture dish after the removal of the culture broth [55, 99, 100]. The fast removal of the culture broth is a crucial point and in case of adherently growing cells, this can be achieved by quickly inverting the culture dish and thereby separating the cells from the liquid phase followed by optional subsequent washing steps. However, for suspension cells the separation is more laborious and time consuming. Dietmair et al. [101], Kronthaler et al. [102], Sellick et al. [103] and Wiendahl et al. [104] proposed centrifugation, whereas Volmer et al. [105] described a filtration approach for separation of cells from the culture broth or quenching solution. For lowering the temperature, quenching in ice-cold NaCl solution is widely deployed [101, 102], whereas Sell-

ick et al. [103] proposed quenching in 60 % methanol supplemented with 0.85 % ammonium bicarbonate (AMBIC) at -40 °C. However, it was shown that quenching with methanol is not suitable for rather sensitive mammalian cells [101, 102, 106]. Therefore, in this thesis, methanol was not considered for quenching. Besides quenching with ice-cold NaCl solution another promising method was proposed by Wiendahl et al. [104]. They used a metallic microstructure heat exchanger which allows cooling of CHO suspension cells from 37 °C to 0 °C in less than one second without any detectable cell damage. However, enzyme activites at 0 °C might still be high enough to alter intracellular metabolite pools during sampling, therefore the established quenching method should be as fast as possible.
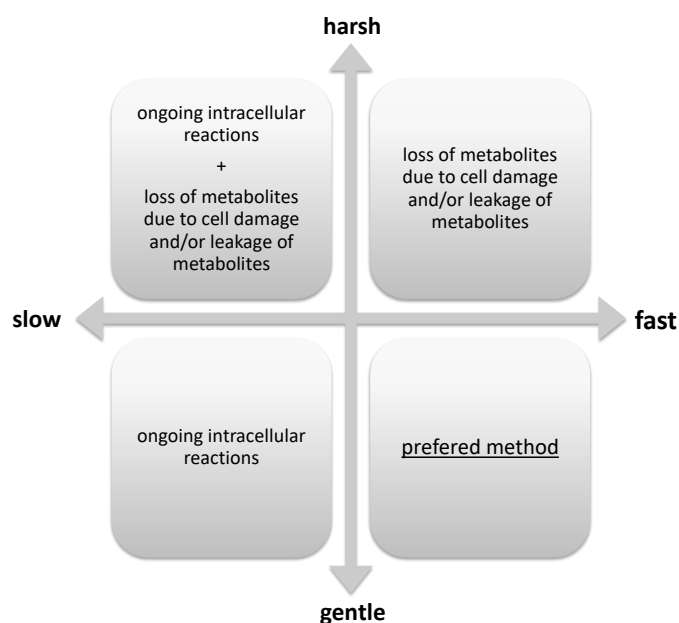
Figure 2.4: Relationship between the required time and quenching conditions, resulting in either not fully stopped intracellular reactions or loss of metabolites.

2.4 Multivariate data analysis

The principle component analysis (PCA) is one of the most deployed multivariate analytical methods [107] and was also used in this thesis for the interpretation of the datasets generated in batch and continuous cultivations. Multivariate ana-

lytical methods or so-called data mining techniques can be categorized in either supervised or unsupervised methods. The goal in supervised methods is to predict the value of an outcome measure (Y variable, e.g. the productivity of a cell) based on a number of input measures (X variables, e.g. intracellular metabolite concentrations), whereas in unsupervised methods the goal is to analyse the underlying patterns or structure among a set of input measures (only X variables) [108]. Examples for supervised methods are discriminant analysis and support vector machines (SVM) for categorical predictions (e.g. sample belongs to group A or to group B), and partial least square regression (PLSR) for quantitative predictions (e.g. level or severity of a disease based on sera samples from patients). Unsupervised methods are for example hierarchical cluster analysis, where the output is a 'tree-like' dendrogram and the PCA. The great advantage of a PCA compared to conventional methods (e.g. univariate analysis) is that underlying structures in the observations (= batch or steady state samples) can be easily visualized and interpreted with regards to the variables (= analysed parameters, e.g. cell numbers, metabolite concentrations etc.). The central idea is the reduction of the dimensionality by identifying underlying variables (= the principle components) in the structure of the data [109]. The starting point for a PCA is a matrix $\underline{X}$ with the samples in rows and the variables (e.g. metabolite concentrations) in columns. In a first step the raw data is centred and often scaled to unit variance. This is done by simply subtracting the mean of each column from each value in the corresponding column. This produces a data set whose mean is zero. Scaling to unit variance is achieved by dividing the SD of each column from each value in the corresponding column. The resulting matrix is then matrix $\widehat{\underline{X}}$. The first principle component (X1) is a linear combination of the variables x_1, x_2, ..., x_i:

$$\underline{X1} = a_{1,1}x_1 + a_{1,2}x_2 + ... + a_{1,i}x_i = \begin{pmatrix} a_{1,1} & a_{1,2} & ... & a_{1,i} \end{pmatrix} \cdot \begin{pmatrix} x_1 \\ x_2 \\ ... \\ x_i \end{pmatrix} \qquad (2.1)$$

or written in matrix form:

$$\underline{X1} = \underline{a_1^T}\ \underline{S} \qquad (2.2)$$

with $\underline{a_1^T}$ the eigenvector of the first principle component, which accounts for the greatest possible variance in the data set and $\underline{S}$, the variables x_1, x_2, ..., x_i written

17

in matrix form. The weights a_{ij} are calculated with the constraint that their sum of squares is 1 [110]:

$$a_{1,1}^2 + a_{1,2}^2 + ... + a_{1i}^2 = 1 \qquad (2.3)$$

Then the second principle component is identified in the same way with the constraint that it is orthogonal to the first principle component. The second principle component accounts for the next highest variance in the dataset. This procedure is repeated until a set of principle components equal to the number of variables has been calculated. The sum of variances of this principle components then equals the sum of the variances of the original data set. The question now is, how can we calculate the eigenvectors of each principle component? If we consider two variables, the wanted eigenvectors of principle component 1 and 2 would point in the direction of maximal variance and would be orthogonal to each other. The solution to this problem is the so called eigenvalue problem. The greatest eigenvalue (δ) and the corresponding eigenvector $\underline{a_1^T}$ for the first principle component is derived from the covariance matrix $\underline{C}$. Assuming two variables x and y the covariance between those variables is calculated with:

$$cov(x,y) = \frac{\sum_{i=1}^{n}(x_i - \bar{x})(y_i - \bar{y})}{(n-1)} \qquad (2.4)$$

The covariance matrix for three variables (x, y and z) would be:

$$\underline{C} = \begin{pmatrix} cov(x,x) & cov(x,y) & cov(x,z) \\ cov(y,x) & cov(y,y) & cov(y,z) \\ cov(z,x) & cov(z,y) & cov(z,z) \end{pmatrix} \qquad (2.5)$$

with the variances for each dimension on the main diagonal. In case of scaled variables (e.g. scaled to unit variance) the correlation matrix instead of the covariance matrix is calculated. Due to cov(x,y) = cov(y,x), the matrix $\underline{C}$ is symmetrical about the main diagonal. The eigenvalue δ of a squared matrix $\underline{A}$ exists if the equation:

$$\underline{A} \cdot \underline{S} = \delta \, \underline{S} \qquad (2.6)$$

has a solution vector $\underline{S} \neq 0$. Such a solution vector is called eigenvector of matrix $\underline{A}$ for eigenvalue δ and is derived from the set of linear equations after conversion of equation 2.6 to:

$$(\underline{A} - \delta \, \underline{E}) \cdot \underline{S} = 0 \qquad (2.7)$$

with matrix $\underline{E}$ the so-called unit matrix. For data sets with more then three variables iterative methods such as the NIPLAS algorithm [111] are implemented within the available software packages for the calculation of the eigenvalues and eigenvectors. All transformations of the original variables results in:

$$\widehat{\underline{X}} = \underline{A}\,\underline{S} \tag{2.8}$$

with the eigenvectors of each principle component in the rows of matrix $\underline{A}$. The eigenvector with the highest eigenvalue being the first principle component followed by the eigenvector with the second highest eigenvalue and so on. Eigenvectors with small eigenvalues are usually ignored at the point at which the following principle components offers only small increase in the overall explained variance. The information explained from this point onwards is mostly pure noise and can therefore be ignored. The mathematical equation for modelling the original set of variables is finally given by:

$$\widehat{\underline{X}} = \underline{A}\,\underline{S} + \underline{R} \tag{2.9}$$

with R being the residual matrix containing the noise (= ignored eigenvectors due two small eigenvalues). In this model, the matrix $\underline{S}$ contains the positions of each observation in the new coordinate system of the principle component, also called scores. The elements of the calculated eigenvectors in matrix $\underline{A}$ are also termed as loadings and are plotted together with the scores for each principle component.

Lets assume a simple example. Imagine three variables (e.g. concentrations of three different metabolites) measured during three experiments (e.g. three batch cultivations):

$$FBP = (100\ 58\ 7), LAC = (100\ 69\ 56), G6P = (55\ 45\ 79)$$

The original data is merged in matrix $\underline{X}$ and results after centering and scaling of the original data to unit variance in:

$$\widehat{\underline{X}} = \begin{pmatrix} 0.97 & 1.11 & -0.27 \\ 0.06 & -0.27 & -0.84 \\ -1.03 & -0.84 & 1.11 \end{pmatrix}$$

then the correlation matrix is calculated:

$$\underline{C} = \begin{pmatrix} 1 & 0.96 & -0.73 \\ 0.96 & 1 & -0.50 \\ -0.73 & -0.50 & 1 \end{pmatrix}$$

from the correlation matrix the eigenvectors and the corresponding eigenvalues are determined:

$$\underline{A} = \begin{pmatrix} -0.63 & -0.58 & 0.51 \\ -0.16 & -0.54 & -0.82 \end{pmatrix}, \underline{\delta} = \begin{pmatrix} 2.47 \\ 0.53 \end{pmatrix}$$

Finally, the coordinates of the original variables in the new coordinate system of the principle components are calculated by multiplying the original data matrix (the mean centred and scaled variables) with the transposed eigenvector matrix $\underline{A}$:

$$\underline{S} = \widehat{\underline{X}} \cdot \underline{A}^T = \begin{pmatrix} 0.97 & 1.11 & -0.27 \\ 0.06 & -0.27 & -0.84 \\ -1.03 & -0.84 & 1.11 \end{pmatrix} \cdot \begin{pmatrix} -0.63 & -0.16 \\ -0.58 & -0.54 \\ 0.51 & -0.82 \end{pmatrix} = \begin{pmatrix} -1.39 & -0.54 \\ -0.3 & 10.83 \\ 1.71 & -0.29 \end{pmatrix}$$

The resulting model is shown in figure 2.5. Last but not least, the goodness of fit is given by the parameter R^2, which is a measure of the explained variance for each principle component. It is calculated from the eigenvalues and the cumulative R^2 for all principle components of the PCA model is a measure of how good the model fits the original data. A high value close to 100 % is desired, however with sufficiently many latent variables, R^2 might not be adequate enough to judge the model quality. For that purpose the prediction error made by the model is estimated (goodness of prediction: Q^2) by cross validation [108]. This is done by keeping a certain part of the data out of the model development, calculate a number of different models from the remaining data set and predict the omitted data with the different models [112]. The predicted values are then finally compared to the original values resulting in a value between 0 and 100 % for Q^2. A model with a high predictive power results in a value close to 100 % and is used together with R^2 to judge the overall performance of the PCA model. In the above invented example, around 82 % of the variance is explained by principle component 1 and 18 % is explained by principle component 2.
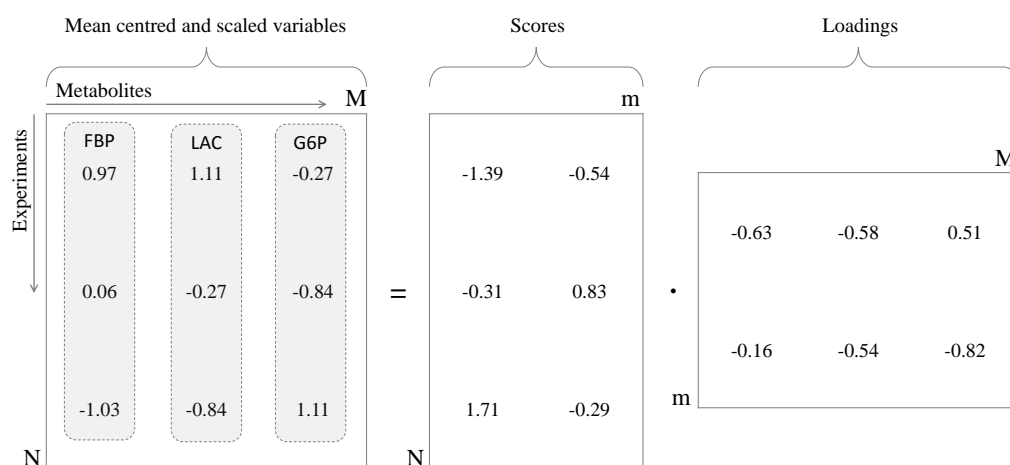
Figure 2.5: Final PCA model for three exemplary variables (metabolite concentrations during three different experiments). For illustration purposes, invented numbers are used to show the relationship between the scores, loadings and the original data (the mean centred and scaled variables).

2.5 Other studies with the AGE1.HN cell lines

To facilitate the classification of the results from this work within the context of the SysLogics project (see chapter 1 for the SysLogics objectives), in the following a summary of the outcomes of the different studies carried out by the other SysLogic partners as well as from other research groups is given.

Metabolic flux analysis in shaker flasks   Niklas et al. [44] studied the central cell metabolism of the parental cell line grown in shaker flasks by applying a dynamic metabolic flux analysis (MFA) approach. This was done by fitting splines to the measured data for biomass and extracellular metabolites. The spline fitted data was then used to calculate specific rates for each metabolite concentration. Intracellular fluxes were subsequently calculated by implementing the data into a metabolic network model. Main result was the finding that a change in metabolism towards a more efficient metabolism was triggered by the depletion of pyruvate, which led to a reduced glucose uptake rate together with the shut down of the lactate production. The authors concluded that the reason for the metabolic inefficiency during the first growth phase might be the low connectivity between

glycolysis and TCA cycle, which resulted in lactate production from intracellulary produced pyruvate due to an overflow of the metabolism. In a follow-up study, the effects of different start concentrations of pyruvate and glutamine on growth and metabolism of the parental cell line in shaker flask cultivations were investigated. In this study also stationary MFA of feeding experiments with the producer clone were performed [46]. It was found that higher pyruvate concentrations (9 mM) led to an inefficient metabolism and lowered cell proliferation. Specifically glucose and pyruvate uptake as well as the production of lactate per cell were increased depending on the pyruvate concentration. Varying the glutamine concentration had only a minor effect on cell growth and metabolism. By reducing the substrate levels during the feeding experiments with the AGE1.HN.AAT cell line it was found that without pyruvate feeding, the cells used the substrates in a higher efficiency leading to higher viable cell densities and A1AT concentration. Moreover, it was concluded that supplementing the media with pyruvate does not increase TCA cycle fluxes, contrary to reports using other mammalian cells [46]. As the metabolic flux distribution around pyruvate and additionally also the compartmentation of the metabolism cannot be determined by stationary or dynamic MFA, ^{13}C tracer experiments and ^{13}C MFA were performed [45]. In this study, it was found that lactate and alanine were produced from the same pyruvate pool and that the consumed alanine was mainly directly metabolized to lactate. It was also found that the activity of the pentose phosphate pathway (PPP) was low (around 2.3 % of the glucose uptake flux), leading to the conclusion that this might be compensated by a high mitochondrial malic enzyme (ME) flux producing NADPH. Moreover, mitochondrial pyruvate transport was almost zero, instead pyruvate carbons were channeled via oxaloacetate into the TCA cycle which was manily fed via 2-ketoglutarate (2-KG) and oxaloacetate (OAA).

Identification of growth phases and glycosylation pattern of A1AT
In addition to the study of Niklas et al. [44], Borchers et al. [52] used a modelling approach to identify different growth phases and the factors influencing cell growth and metabolism during batch cultivations of the parental cell line in shaker flasks and bioreactors. They concluded that the growth in batch culture can be divided into two main growth phases. The initial phase is characterized by exponential growth dynamics. The subsequent phase is characterized by a decrease

in the specific growth rate, which was for the bioreactor cultivation the result of glucose limitation and for the shaker flask cultivations the decreasing pH of the medium [52]. However, Borchers et al. [52] did not include pyruvate in their analysis. Meanwhile, Blanchard et al. [43] showed that the producer cell line is capable of producing a *N*-glycosylation pattern of A1AT, which resembles the one from human plasma A1AT in terms of antennarity and sialylation. But they also found differences, mainly concerning the degree of fucosylation. In addition, in their study, the recombinant A1AT produced was found to be biologically active and to induce anti-inflammatory properties as the commercially available Prolastin®does [43].

Combined metabolome, transcriptome and proteome analysis   In another investigation with the A1AT producer cell line grown in bioreactors, Scholz et al. [51] studied the intracellular metabolome, transcriptome and proteome with focus on glycolysis, TCA cycle and oxidative phosphorylation. The transcriptome data suggested a strong gene expression for enzymes of the central metabolism in the first two days of the cultivation, corresponding with elevated intracellular glucose and pyruvate concentrations. For most genes, the expression decreased over time, whereas the gene for ME showed a high expression throughout the cultivation time. They concluded their study by stating that the expression of the pyruvate dehydrogenase lipoamide kinase isozyme 4 (PDK4) gene in the exponential growth phase possibly inhibited the PDH, leading to a truncated connectivity between glycolysis and TCA cycle [51].

Effect of quercetin and high ammonia concentrations   After quercetin was identified during a screening for a substance, which might be able to increase the metabolic efficiency or to improve A1AT production, Niklas et al. [113] performed stationary MFA of quercetin treated AGE1.HN.AAT cells at different growth phases. They found that quercetin addition to the culture medium resulted in an increase in culture longevity, viable cell density, and final A1AT titer. It was hypothesized that the observed increase in channeling of pyruvate into the mitochondria, led to reduced waste product formation and increased TCA cycle activity. This was probably induced either by inhibitory action of quercetin on specific enzymes, quercetin-induced oxidized state with a reduced NADH/NAD+ ratio, by cytoprotective activity or by any combination of this three events [113]. Next the effect of

different ammonia start concentrations on cell growth, A1AT formation and stationary MFA of the producer cell line grown in shaker flasks was studied by Priesnitz et al. [47]. Main finding was that the amino acid metabolism was significantly changed. Uptake of asparagine (ASN), leucine (LEU), serine (SER), tyrosine (TYR), isoleucine (ILE), phenylalanine (PHE), threonine (THR) and valine (VAL) were reduced, whereas the production of alanine (ALA), proline (PRO) and glycine (GLY) were significantly increased leading to an increased storage of excess nitrogen in extracellular ALA. It was also found that the glutamate dehydrogenase (GLDH) flux was reversed with increasing extracellular ammonia concentration, were free ammonia was taken up. Besides that, the central energy metabolism remained relatively unaffected [47].

Process characterisation of bioreactor and shaker flask cultivations
As the aim of the SysLogics consortium was a combined effort to generate reliable and comparable experimental datasets of both cell lines in four different research laboratories, three studies focused on process standardization and comparability of the results obtained with different laboratory equipment and assay handling [48–50]. Platas Barradas et al. [49] analysed criteria for operation standardization and process transfer for cultivation in five different types of bioreactors and compared the cell growth within varied ranges for power input, mixing time, impeller tip speed, and Reynolds number. Similar specific growth rates could be observed at a mixing time range of 10–12.5 s. Correspondingly, the mixing time was taken as the preferred reference for comparability of laboratory bioreactors with different internal geometry [49]. In addition, specific ranges for the specific power input, impeller tip speed, and the Reynolds number were defined for the cultivation of AGE1.HN cells (see also results and discussion in section 4.1.1). In addition, Schräder et al. [48] and Freund et al. [50] characterised and compared cultivations in different cultivation systems. Main results of these studies were that the exponential growth phase was comparable for shake flasks and bioreactors. However, Freund et al. [50] found significant differences for the parental cell line cultivated in baffled shake flasks and the producer cell line cultivated in non-baffled shake flasks. I.e., the glucose uptake and the lactate production rates were higher in baffled shaker flask and similar to bioreactor cultivations. In their study, no indication

was found that the production of A1AT is a significant burden on cell growth or metabolism.

Metabolite demand for the production of A1AT   In contrast to the aforementioned results showing that the production of A1AT was not a significant burden on cell growth or metabolism, Niklas et al. [53] found in another study that the RNA, lipid and phosphatidylcholine fractions (g/g cell mass) were higher in the producer cell line compared to the parental cell line causing significant metabolic changes in the producer cell line, e.g. increased glycine and glutamate production. In this study, MFA revealed similar energy metabolism in both cell lines, but ALA production was significantly higher in the parental cell line. In addition, the GLC uptake required for glycosylation was lower than 1 % of the overall GLC uptake rate, and is therefore probably not a significant burden for the cell. However, by simulating the theoretical metabolite demand for the production of A1AT, they found that the differences in metabolic profiles between producer and parental cells match the observed increased glycine production and nucleotide demand as well as the increased lipid precursor demand in the producer cell line [53].

Summary   Taken together, providing similar mixing conditions led to comparable results regarding cell growth and metabolism in baffled shake flasks as well as in bioreactors independent of the cell line. However, a slightly increased glycine production and nucleotide and lipid precursor demand in the producer cell line, points towards that the metabolism of the AGE1.HN.AAT cell line might be different compared to the metabolism of the parental cell line AGE1.HN. Moreover, it was also found that the metabolism can be altered or even shifted towards a more efficient metabolism by the depletion of either extracellular pyruvate or glucose, whereas different glutamine concentrations have only a minor effect on cell growth and metabolism. In addition, the activity of the PPP and the connectivity between glycolysis and TCA cycle were found to be low, leading to a phenotype producing lactate in great excess during exponential growth.

CHAPTER 3

Materials and methods

In the following, all materials and methods used for this study are described. A detailed list of all chemicals and the standard operating procedures (SOPs) can be found in the appendix.

3.1 Cell culture and media

3.1.1 Thawing of cells

AGE1.HN and AGE1.HN.AAT cells stored in liquid nitrogen were incubated for 2 min in a water bath pre-warmed to 37 °C. After 2 min, the cryovials were further thawed by retaining them in the hand while gentle reversing the vials. The thawed cell suspension was quickly removed with a 2 mL pipette and transferred to 10 mL 4 °C cold PBS in an 15 mL falcon tube. Then the cells were centrifuged for 5 min at 150 xg (Biofuge primo R, Heraeus, Germany). The supernatant was removed and the cell pellet was resuspended in chemical defined medium (42-MAX-UB, Xell AG, Germany) supplemented with 5 mM glutamine pre-warmed to room temperature to an initial cell density of $1.1 \cdot 10^6$ cells/mL in a 50 mL filtertube (Corning, Amsterdam, Netherlands). The cells were immediately placed in a shaking incubator with an

orbital motion of 50 mm (Multitron 2, Infors GmbH, Germany or Kühner Shaker X, Adolf Kühner AG, Switzerland) set to 37 °C, 5 % CO_2 and 185 rpm.

3.1.2 Routine cultivations and pre-cultures

After thawing, the cells were cultivated either in 10–20 or 50 mL 42-MAX-UB medium supplemented with 5 mM glutamine in 50 mL filtertubes or in 125 mL baffled shaker flasks (Corning, Amsterdam, Netherlands). The medium composition as determined with the stated analytical method is given in table 3.1. The cells were incubated in a shaking incubator at 37 °C, 5 % CO_2 and 185 rpm. To minimize the risk of unwanted effects from genome alterations due to prolonged passaging, only cells with a maximum passage number of 15 (after thawing) were used for the experiments. Cells were directly passaged into new medium every 3 days with an initial cell concentration of $5 \cdot 10^5$ cells/mL for the parental cells and $8 \cdot 10^5$ cells/mL for the producer cells. Pre-cultures for shaker and bioreactor experiments were cultivated either in 50 mL or in 150 mL medium supplemented with 5 mM glutamine in 125 mL and 250 mL baffled shaker flasks respectively. Prior to the inoculation of an experiment, the cells were centrifuged for 7 min at 150 xg and the supernatant discarded. The pellet was then resuspended in fresh medium with different amounts of glucose, galactose and glutamine according to the objective of the experiment. In figure 3.1 the viable cell concentrations together with the viabilities for the AGE1.HN.AAT cell line are shown at time point before passaging. With an average cell concentration of $2.29 \cdot 10^6 \pm 4.93 \cdot 10^5$ cells/mL and an average viability of 88.4 ± 4.5 %, the routine cultivation protocol proved to be robust given the fact that the data shown in figure 3.1 was generated by three different users over two years. In cases were the viable cell concentration dropped below $1.5 \cdot 10^6$ cells/mL, a complete exchange of the media by centrifugation (7 min at 150 xg) was performed to avoid excessive dilution of the new medium with old medium.

Table 3.1: Measured medium composition of the 42-MAX-UB standard medium used for preparation of working cell banks, thawing of cells, routine and pre-cultures.

Substance	Value	Dimension	Analytical method
Pluronic	1.0	g/L	as stated by Xell
NaHCO3	2.1	g/L	as stated by Xell
Osmolality	290.0	mOsm/kg	FPDO[a]
pH value	7.4	-	pH meter
GALC	0.5	g/L	AEC[b]
GLC	5.5	g/L	Bioprofile
AMM	0.3	mM	Bioprofile
LAC	0.0	g/L	Bioprofile
PYR	2.9	mM	AEC
GLU	636.9	µM	AEC
ALA	437.1	µM	AEC
ARG	1588.2	µM	AEC
ASN	920.4	µM	AEC
ASP	2197.9	µM	AEC
CYS	963.1	µM	AEC
GLY	1196.0	µM	AEC
HIS	642.7	µM	AEC
ILE	1744.9	µM	AEC
LEU	1893.2	µM	AEC
LYS	1256.0	µM	AEC
MET	601.3	µM	AEC
PHE	1039.4	µM	AEC
PRO	1040.5	µM	AEC
SER	3027.4	µM	AEC
THR	1502.4	µM	AEC
TRP	383.8	µM	AEC
TYR	1109.7	µM	AEC
VAL	1811.9	µM	AEC

a: freezing point depression osmometer (FPDO); b: anion exchanger chromatography (AEC);

3.1.3 Preparation of working cell banks

For the preparation of working cell banks, the AGE1.HN and the AGE1.HN.AAT cells were harvested during the mid-exponential growth phase from shaker flask cultivations, and centrifuged for 7 min at 150 xg. The supernatant was removed and the cell pellet resuspended in 4 °C cold 42-MAX-UB medium supplemented with 10 % DMSO (v/v) and 5 mM glutamine. The cell concentration was adjusted to $1.1 \cdot 10^7$ cells/vial and 1.5 mL of this suspension was transferred to cryovials placed in an Eppendorf cooler (Eppendorf® IsoTherm Benchtop Cooler, Eppendorf AG,

Germany) pre-chilled to 4 °C. Afterwards the cryovials were immediately trans-
ferred to a freezer set to a -80 °C. After 24 h, the cryovials were placed at -196 °C
in a liquid nitrogen tank until usage of the cells for experiments.
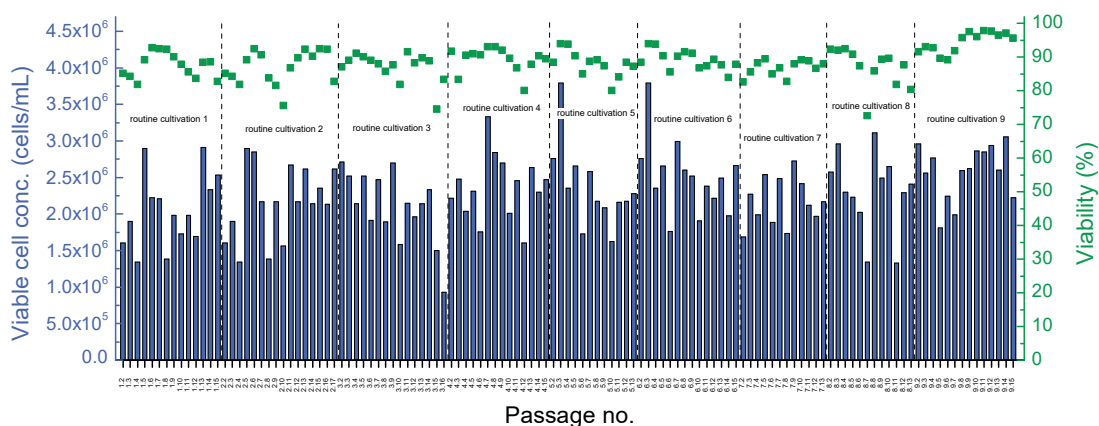
Figure 3.1: Viable cell concentrations (blue bars) and viabilities (green boxes) for pas-
saging of the AGE1.HN.AAT cell line generated by three different users over two years.
Note that the shown passage numbers are representing the given passage within one
routine cultivation run after thawing of the cells (e.g. passage no. 3.8 is the eighth
passage within cultivation run number 3).

3.2 Bioreactors

3.2.1 Physical characterization of the bioreactor systems

To assess criteria for the systematic comparison of bioreactors and for process
transfer within the SysLogics consortium, the geometric similarity, power input (P),
Reynolds number (Re), impeller tip speed (u_{tip}) and mixing time (t_m) were calcu-
lated. For the bioreactors in our laboratory also the volume-specific oxygen trans-
fer value ($k_L a$) was determined. As most cultivations for this work were done with
a DasGip cultivation system (cellferm-pro®, DasGip AG, Germany), DasGip biore-
actors with *wv* of 0.5 and 2.5 L were used for the physical characterization.

3.2.1.1 Geometric similarity

Different dimensionless numbers were determined to assess the geometric simi-
larity, the dimensions of the bioreactor, the type and number of stirrers, and the

presence and number of baffles. Determination of the different bioreactor dimensions was done according to the drawing shown in figure 3.2. A complete overview of all determined geometric dimensions can be found in the appendix A.1.4.
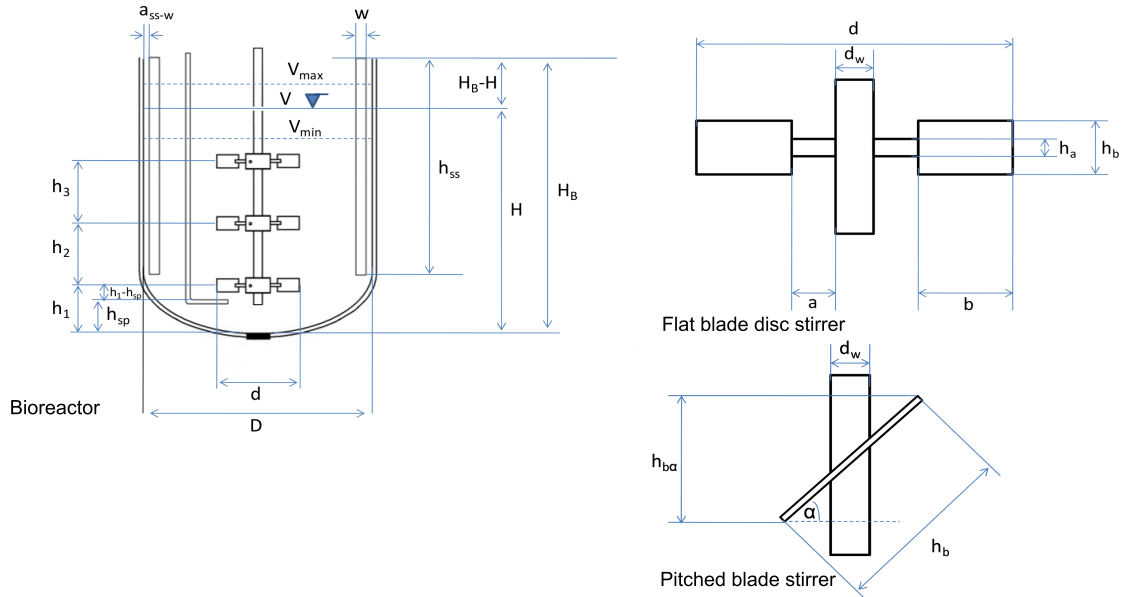
Figure 3.2: Drawing of dimensions with stirrer positions and stirrer types used to asses the geometric similarity and dimensionless numbers of bioreactors.

3.2.1.2 Power input, Reynolds numbers and impeller tip speed

The *P* can be determined by measuring the torque of the agitated system:

$$P = 2 \cdot \pi \cdot n \cdot \left(T_q - T_q, air \right) \tag{3.1}$$

with n: the rotational speed, T_q: torque of the agitated system and $T_{q,air}$: torque measured in air at the respective n. If no torque measurement is available, the power input of a non-gassed system (P_0) can be obtained from correlation formulas. As in an ungassed system the dimensionless Newton number (*Ne*) (or power number):

$$Ne = \frac{P_0}{\rho \cdot n^3 \cdot d^5} \tag{3.2}$$

depends only on *Re*:

$$Re = \frac{\rho \cdot n \cdot d^2}{\eta} \qquad (3.3)$$

with ρ: the density of the fluid, d: the diameter of the stirrer and η: the dynamic viscosity of the fluid, *Ne* can be determined with correlation formulas obtained for different stirrers. For *Re* > 10.000 the flow regime of the system is completely turbulent, and hence *Ne* independent of *Re*. For a known *Ne*, one can then calculate P_0 from equation 3.2. As the power input of a gassed system is reduced compared to a non-gassed system, a second dimensonless number, the dimensionless aeration rate number (N_g) is introduced:

$$N_g = \frac{F_g}{n \cdot d^3} \qquad (3.4)$$

with F_g: the aeration rate. From correlations of P_g/P_0 with N_g for different stirrers, the power input of a gassed system (P_g) can then be obtained. For example, with a value of N_g=2.5 the power input of a gassed system for a system agitated with a pitched blade stirrer is reduced by approximately 50 %. However, with aeration rates between 0.5 - 6.0 sL/h employed in this work, the N_gs were very low and hence the influence of aeration on the power input was neglected. As mentioned above, the determination of the power input requires a torque sensor mounted to the bioreactor. As the 0.5 L DasGip bioreactor was not equipped with such a sensor, the *P*s for the 0.5 L bioreactor (BS0500TPSS) were taken from Platas Barradas et al. [49], whereas for the 2.5L DasGip bioreactors (DR03C), the power input was determined with the inbuilt torque measurement according to equation 3.1. The specific power input per unit liquid volume (P/V) was then used for comparison of the different cultivation systems. The impeller tip speed was calculated according to:

$$u_{tip} = \pi \cdot n \cdot d \qquad (3.5)$$

3.2.1.3 Mixing times

For the determination of the mixing time in the 0.5 L DasGip bioreactor a decolorization method was used. A 1 M I_2/KI (Roth, 7935; Merck, 105043) solution was

titrated against a 1 M sodium thiosulfate ($Na_2S_2O_3$) (Roth, HN25) solution to determine the required volume corresponding to a molar excess of 5 % of $Na_2S_2O_3$ ($\equiv$ mixing degree of 95 %). The bioreactor was filled to the corresponding working volume with a 1 % starch w/v (starch from potatoes, Roth, 9441.1) solution and the I_2/KI solution was added (0.01 % v/v). After a homogeneous blue colour was reached, the stirrer drive was set according to the experiment. Then the titrated volume of $Na_2S_2O_3$ was quickly added from the top of the bioreactor next to the shaft of the stirrer. The iodine (I_2) is decolorized during the reaction with $Na_2S_2O_3$ to colorless iodide: $I_2 + 2Na_2S_2O_3 \rightarrow 2NaI + Na_2S_4O_6$. The decolorization was followed by a digital video camera and the mixing time was determined afterwards by evaluating the recordings on a computer. The mixing time was defined as the time needed for the complete desaturation process. Triplicate determinations were performed for all individual stirrer settings. The mixing time for the 2.5 L DasGip bioreactor (DR03C) was estimated with following equation originally proposed by Van't Riet and Tramper [114] and modified by Bonvillani et al. [115]:

$$t_m = \left[a \cdot \frac{\rho \cdot D^5}{P_g} \cdot \left(\frac{D}{d} \right)^4 \right]^b \tag{3.6}$$

with a=6.08 and b=0.332.

3.2.1.4 Volume-specific oxygen transfer values

To determine the oxygen transfer rate (OTR), the specific contact area (a) between the gas and the liquid phase, the mass transfer coefficient k_L, and the driving force (C_L^* - C_L), with C_L^* = oxygen saturation concentration in the liquid phase and C_L = the present oxygen concentration in the liquid phase has to be determined. The mass transfer coefficient k_L includes only the resistance in the liquid phase as the resistance in the gas phase is usually marginal and thus can be neglected. The transport of oxygen can then be described with following equation:

$$OTR = k_L a \cdot (C_L^* - C_L) \tag{3.7}$$

For the determination of the $k_L a$ for different aeration rates and agitation speeds (at 37 °C) an in-stationary method was used. The reactor was filled either with NaCl solution (8.0 g/L) or with 42-Max-UB medium to the *wv*. Then the oxygen

was removed by adding nitrogen, followed by the start of aeration with air. The oxygen saturation process was followed by a dissolved oxygen (DO) probe. To obtain reliable $k_L a$ values, it is necessary, to take the response time of the dissolved oxygen probe (τ_p) into account. This response can affect the correct determination of the mass transfer coefficient, if the response time of the system regarding oxygen transport (τ_t) (equation 3.8) is of the same order than the response time of the DO probe [116].

$$\tau_t = \frac{1}{k_L a}[s] \tag{3.8}$$

Response lags are mainly caused by the diffusion of oxygen through the membrane of the DO probe and might occur especially for higher $k_L a$ values [117]. If the ratio of τ_t/τ_p is below 1, the response time of the DO probe has to be considered by using a mathematical model. With an assumed τ_p value of 100s for the DO probes used in our lab, the τ_t/τ_p ratio was found to be below 1 only for $k_L a$ values greater then 36 ^{1}/h. Therefore τ_p was neglected and the $k_L a$ value was obtained by a logarithmic transformation of equation 3.7:

$$log(C_L^* - C_L) = k_L a \cdot t \tag{3.9}$$

3.2.2 Batch cultivations

0.5 - 2.5L scale batch cultivations

Bioreactor cultivations with a *wv* of 0.5–2.5 L (42-MAX-UB medium) were carried out either in DasGip bioreactors (0.5 and 2.5 L *wv*) or in a Biostat bioractor (0.8 L *wv*, Biostat® Bplus, Sartorius Stedim Biotech, France and Germany) with control of temperature at 37 °C, DO at 40 % and pH value at 7.15. A piping and instrumentation drawing (P&ID) for the DasGip cultivation system can be found in figure 3.3. For agitation, one 3-blade segment impeller was used for cultivations with a *wv* up to 0.8 L, whereas two 3-blade segment impellers were used for the cultivations with a *wv* of 2.5 L. Stirrer velocity was set to 120–150 rpm. Aeration was accomplished by a continuous gas flow rate of 0.5–6.0 ^{sl}/h via a dip tube. The DO was controlled at 40 % via the oxygen concentrations in the aeration gas controlled by the gas mix unit. Control of the pH was achieved by feeding of Na_2CO_3 and via the CO_2 content in the gas flow stream. The bioreactors were inoculated either with a

concentration of $5 \cdot 10^5$ cells/mL for the parental cells or $8 \cdot 10^5$ cells/mL for the producer cells from exponentially growing precultures in shaker flasks in 42-MAX-UB with a glutamine concentration of 5 mM.
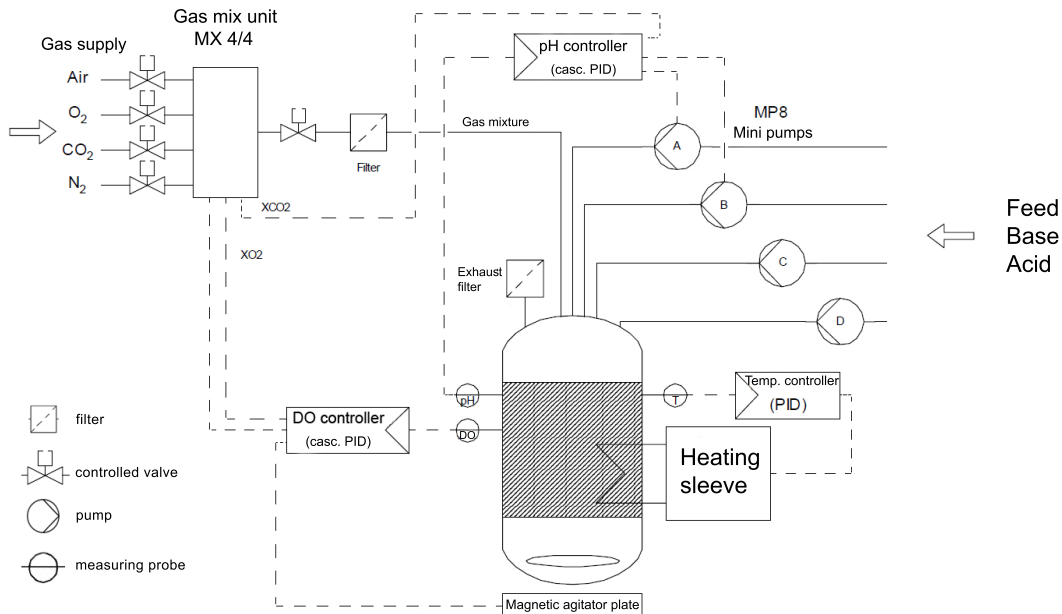
Figure 3.3: Piping, installed controller and gas mix unit of the DasGip cultivation system (P&ID diagram).

20 L scale batch cultivations

20 L bioreactor cultivations were carried out in a Biostat bioreactor (BIOSTAT® C-DCU, Sartorius Stedim S.S. Biotech, France) in the laboratory of a cooperation partner at the University of Bielefeld (Cell culture technology group headed by Prof. Noll). The controller set-points were identical to set-points of the 0.5-2.5 L cultivations. Three rushton impellers (d = 0.092 m) with an initial velocity of 80 rpm and a maximum velocity of 100 rpm were used for agitation. Aeration was accomplished by a continuous airflow of 3 sL/h in the headspace and discontinuous flow of pure oxygen via a ring sparger. The 20 L bioreactors were inoculated with a concentration of $8 \cdot 10^5$ cells/mL from exponentially growing producer cells in 2 L bioreactors (BIOSTAT® Aplus, Sartorius Stedim S.S. Biotech, France).

Figure 3.4: From left to right: Magnetically agitated DasGip bioreactor (BS0500TPSS, *wv* = 0.5 L, cellferm-pro®), DasGip vessel with overhead stirrer (DR03C, *wv* =2.5 L, cellferm-pro®), Biostat Univessel (Bplus, *wv* = 0.8 L, Biostat®) and Biostat stainless steal tank reactor (Cplus, *wv* = 20 L, BIOSTAT®)

3.2.3 Continuous cultivations

For studying the metabolism under steady-state conditions, continuous cultivations were established with the DasGip system using a DasGip bioreactor (BS0500TPSS, *wv* = 0.5 L) with control of temperature at 37 °C, DO at 40 % and pH value at 7.15. For feeding of fresh 42-MAX-UB medium, the in built peristaltic pump of the DasGip system was used after calibration with the corresponding feed tube. The cell suspension was continuously removed from the liquid surface via an external pump with a rate of 2x the DR. The feed rate (F_i) was automatically adjusted during sampling, to avoid oscillation of the dilution rate. Thus, the total sampling volume was determined and entered in the process control system (PCS), where the new feed rate was then calculated and automatically adjusted every 10 seconds based on the reduced *wv* (see script in appendix A.1.6). The feed rate was verified for cultivations A, B, C, D and E after completion of the experiment by recalibration of the pump and comparison of the calibration parameter. As for cultivation E the feed rate was found to be significant differend after the recalibration at the end of the experiment, for the subsequent experiments the dilution rate was verified online. Therfore, the weight of the harvest vessel was continuously determined by a balance connected to the PCS. A second script was implemented for the calculation of the dilution rate based on the delta increase of the harvest weight and the *wv* of the reactor (see appendix A.1.6). The *wv* of the reactor was determined at the

beginning of the experiments by weighing the reactor with all installed probes and pipes after a constant volume was reached. A complete overview of the setup for the continuous cultivations, the installation positions as well as length of the probes and pipes for feeding and aeration are shown in figure 3.5 and in table 3.2. The 42-MAX-UB medium was supplemented with glucose, galactose and glutamine according to the objective of the experiment. For shift experiments, the vessel containing the feed medium was replaced by a new vessel containing the medium with the new concentration of either glucose or glutamine. Old medium remaining in the tubes was removed from the feed hose via a bypass and a sterile filter into a waste bottle. The vessel containing the feed medium was placed in a styrofoam box filled with -20 °C cold thermal packs. The thermal packs were replaced once per day to keep the feed medium at a temperature of 4–8 °C throughout the whole experiment.
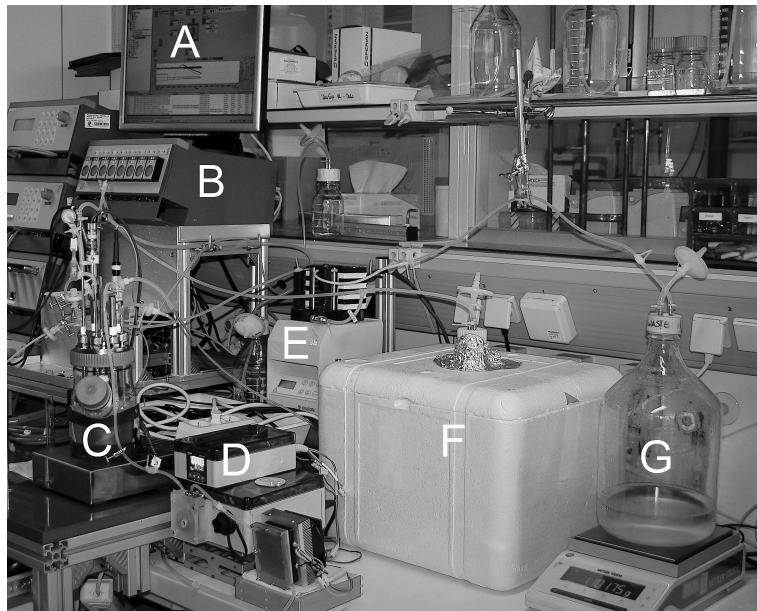
Figure 3.5: The setup for continuous cultivations with the DasGip cultivation system. A: Process control system (cellferm-pro®), B: DasGip pump unit, C: DasGip Bioreactor (BS0500TPSS, *wv* = 0.5 L), D: Sampling system, E: External pump for harvest, F: Feed vessel and G: Harvest vessel.

Table 3.2: Overview of the installation positions and length of the probes and pipes for feeding and aeration used for continuous cultivations (shown is the lid of the reactor from above with the installation length inside the bioreactor measured from the inside of the lid).

#	Description	Installation length (mm)	Inner diameter (mm)
1	Feed	162	2
2	DO probe	130	–
3	Temperatur	163	–
4	Exhaust	–	–
5	pH probe	130	–
6	Aeration	158	2
7	Sampling probe	107	–
8	Harvest	98	2
9	Sampling port	146	2
10	Stirrer	–	–
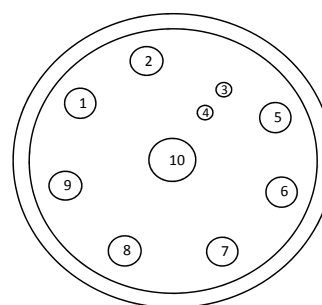
3.3 Sampling and quenching of AGE1.HN cells

In the following, the methods for manually and automated sampling and separation of cells from the culture broth, as well as the quenching procedure and assays used for determination of pH values, cell, extracellular (glucose, lactate, ammonia, pyruvate, galactose and amino acids) and intracellular metabolite concentrations are described.

3.3.1 Sampling for cell, pH and extracellular metabolite measurements

Samples were taken manually through a drain valve and then either the pH value was directly determined with a pH meter (Inolab pH/Cond level 1, WTW, Germany) or the viable and dead cell concentrations were directly measured with an automated cell counter (see section 3.4.1). For the determination of extracellular metabolite concentrations, cells were removed by centrifugation for 1 min at 3500 rpm with a bench-top centrifuge (Multi-spin PCV-3000, Grant Instruments, England).

3.3.2 Experimental set-up for filtration experiments

In the beginning of this work, it was tested whether filtration is suitable for the separation of cells from the culture broth prior to the extraction of intracellular metabolites. Therefore, a Büchner flask with a top-mounted polyoxymethylen open-face filter holder (Open-Face Delrin Filter Holder, 25 mm, Pall Life Sciences) was connected to a water-jet vacuum pump. The internal pressure inside the vacuum flask was measured under the assumption that the internal pressure corresponds to the pressure in the water-jet. A pressure transducer was therefore connected to the outlet of the water-jet vacuum pump (see figure 3.6). For the filtration, a cellulose/nitrate membrane with pore size of 5 μm was used (Cellulose Nitrate Membrane Filters, diameter 25 mm, Whatman®). After adjusting the pressure according to the pressure transducer, the filter membrane was placed on the holder and flushed once with ice-cold 0.9 % NaCl solution. Then, the cell suspension was applied on the filter, followed by a washing step with 1 mL ice-cold 0.9 % NaCl solution. The supernatant was collected and analysed as described under 3.4.2 on page 43.
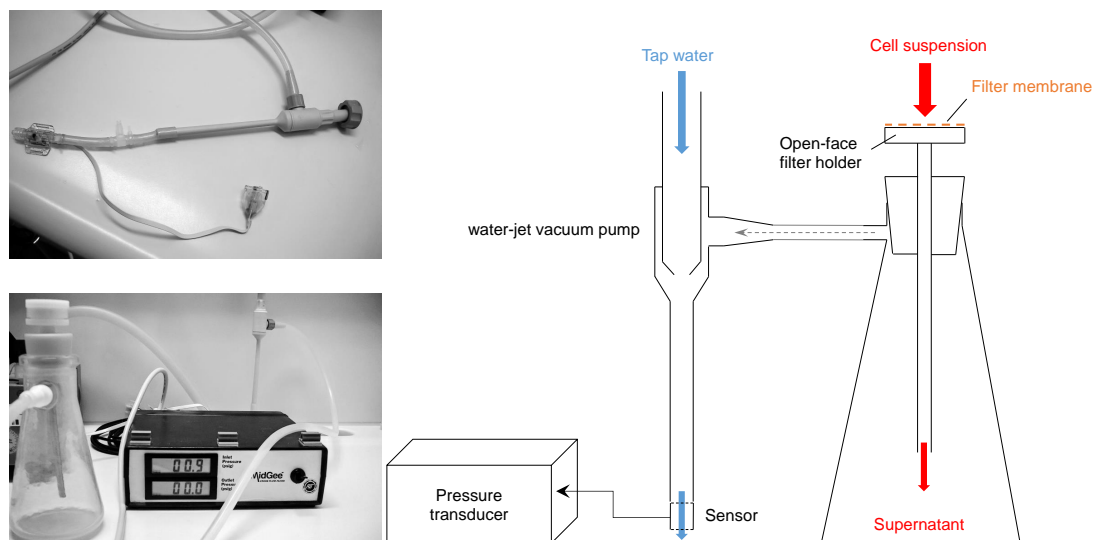
Figure 3.6: Experimental set-up for the filtration of AGE1.HN cells for determination of intracellular metabolites.

3.3.3 Sampling and quenching with a automated sampling system

For sampling of cell suspensions for intracellular measurements, an automated sampling system developed by Dr. Heiner Sann in cooperation with the bioprocess engineering group at the Max Planck Institut in Magdeburg was used. The system consists of a stainless steel probe and a peristaltic pump. The pump can be accessed and programmed by a software installed on a Laptop connected to the pump via a network cable. The system features the possibility to withdraw a predefined sample volume ($\geq$ 0.3 mL) from the bioreactor with a minimal dead volume. When combined with an autosampler, the system also allows automated sampling at predefined times and intervals. As the temperature is a critical issue when taking samples for the determination of intracellular metabolites, a heat-exchanger was coupled to the probe (see figure 3.7 for a schema of the sampling system coupled with a heat exchanger).
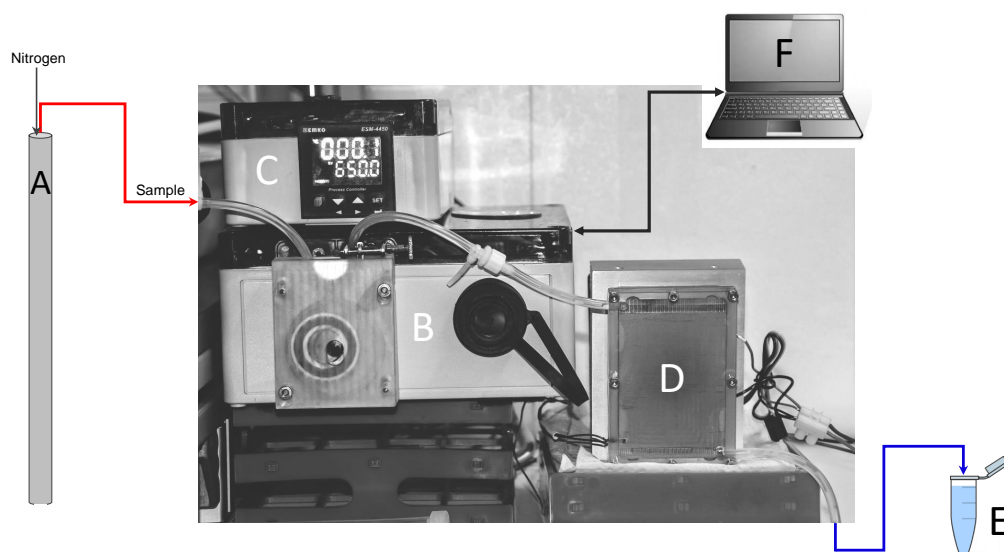
Figure 3.7: Scheme of the sampling system developed by Dr. Heiner Sann coupled with a heat exchanger for fast sampling and cooling of a cell suspension sample during bioreactor cultivations. A: Sampling probe, B: Peristaltic pump, C: Control unit heat exchanger, D: Heat exchanger, E: Reaction tube (on ice), F: Control unit sampling system.

The heat exchanger was designed to cool the cell suspension as fast as possible from the temperature during the experiments (37 °C) to almost zero degree. This was achieved with a peltier element and a stainless steal plate, which directs the

sample stream from the bioreactor through 26 1 mm by 1 mm small channels (see figure A.2). The temperature of the heat exchanger was measured with a PT100 temperature probe and controlled to 0.2 °C by a control unit. With this setting, the whole system allowed samples with a volume of 3 mL to be cooled down from 37 °C to almost zero degree (1.7 ± 0.3 °C) in ≤ 10 s (see figure 4.11). Technical drawings of the heat exchanger can be found in the appendix A.1.7.

3.3.4 Sampling of suspension cells for intracellular measurements

Before start of sampling and sample preparation all solutions used and the sample tubes were cooled to 0 °C. Samples were taken with the sampling system and the heat exchanger directly into tubes placed on ice. Then the cells were centrifuged (35 s at 3000 xg) and washed once with an ice-cold 0.9 % NaCl solution to remove residual amounts of contaminating metabolites and enzymes, or interfering substances such as anions. In parallel, samples were also taken manually through a drain valve and were then either directly centrifuged and washed or rapidly cooled down by placing the sample tube for 5 s into liquid nitrogen followed by centrifugation and washing. After a second centrifugation step, samples for the determination of intracellular metabolite concentrations were further processed as described in section 3.4.5. For determination of maximum enzyme activities, the supernatant was removed and the cell pellet was quickly frozen by immersion of the sample tube in liquid nitrogen. Storage of samples was at -80 °C until measurement. As the sampling system was not available for the 20 L batch cultivations, samples were taken from the bioreactor through a drain valve and then the cell suspension was either rapidly cooled to 0 °C by use of a microstructure heat exchanger [104] or directly centrifuged and then further processed as described under 3.4.5 on page 47.

3.4 Analytics

3.4.1 Viable and dead cell concentrations

3.4.1.1 ViCell cell counter

Determination of viable and dead cell concentrations, and cell diameter was carried out with an automated cell counter (ViCell™ XR, Beckman Coulter, Germany). Detection of dead cells was based on trypan blue exclusion. The total cell number and cell diameters were determined with a camera taking up to 100 stationary pictures of the sample chamber. In the beginning of this work, the detection parameter were adapted to the AGE1.HN cells. As both cell lines have the same morphology, in the ongoing work the same set of parameter was used for the measurement of both cell line. The used detection parameters are given in table 3.3.

Table 3.3: Detection parameter used for the determination of viable and dead cell concentrations, and cell diameter with the ViCell cell counter.

Parameter	Value
Threshold [%]	83
Center threshold [%]	90
Minimum diameter [μm]	9.0
Maximum diameter [μm]	40.0
Minimum center size	10.0
Minimum circularity	0.5
Frames	100
Focus parameter	60
Sample flush cycles	3
Trypan blue mixing cycles	3

3.4.1.2 Validation of the ViCell cell counter procedure

For the validation of the cell counter method, a linear range based on preliminary measurements between $5 \cdot 10^4$ cells/mL and $6 \cdot 10^6$ cells/mL was assumed. To check the homoscedasticity 8 individual stock solutions of AGE1.HN.AAT cells at the lower ($5 \cdot 10^4$ cells/mL) and the upper viable cell concentration ($6 \cdot 10^6$ cells/mL) were produced. From these stock solutions, threefold measurements with the ViCell cell counter were performed and the averages of these measurements were used for the check

of the homoscedasticity. For the validation of the assumed linear range 6 individual stock solutions with viable cells with equidistant distances between $5 \cdot 10^4$ cells/mL and $6 \cdot 10^6$ cells/mL were produced. From this stock solutions, threefold measurements with the ViCell were performed and the averages of this measurements were used for the validation of the linear range. The validation results are summarized in table 3.4. As homoscedasticity could not be shown, a weighted linear regression was applied. The calculation was done with an Microsoft Excel template (temp_vali_AR_v1.8.xls, version 1.8), which calculates automatically the test statistics and compares them to the test criteria. A description of the whole validation process is described by Bock [118]. The equations used for the calculation of the unweighted linear and quadratic and the weighted linear regression were taken from Gottwald [119] and Draper and Smith [120].

Table 3.4: Results of the validation of the ViCell cell counter method.

Parameter	Value
Linearity	yes
Homoscedasticity	no
Weighted residual SD [cells/mL]	4311
Sensitivity	0.93
SD of the method [cells/mL]	$4.7 \cdot 10^3$
Relative SD of the method [%]	6.2
Coefficient of determination	0.996
Limit of detection [cells/mL]	$1.5 \cdot 10^4$
Limit of quantitation [cells/mL]	$4.7 \cdot 10^4$

3.4.2 Quantification of cell damage

For the determination of cell damage induced after different treatments of the cells (e.g. after filtration) the CytoTox 96® Non-Radioactive Cytotoxicity Assay (Promega, G1780) was used. The CytoTox 96® Assay quantifies the enzyme lactate dehydrogenase (LDH), which is released by the cells upon cell lysis. The released LDH is then measured in the supernatant after removal of the cells. In principle, the assay transforms a tetrazolium salt into a red formazan product. The amount of produced colour is then proportional to the number of damaged or lysed cells. The chemical reactions of the assay are as follows:

$$NAD^+ + lactate \xrightarrow{LDH} pyruvate + NADH$$

$$NADH + tetrazolium\ salt \xrightarrow{Diaphorase} NAD^+ + formazan\ (red)$$
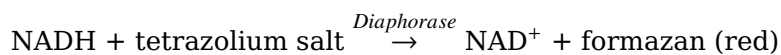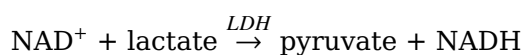
For the determination of the maximum LDH content, 0.5 mL cell suspension was collected in reaction tubes, mixed with 80 µL lysis buffer, and incubated for 45 min on ice. After removal of cell debris by centrifugation at 6000 xg for 3 min (0 °C), the supernatant was stored at -80 °C until measurement. Prior to the measurement the samples were either 1:10 or 1:20 diluted with medium. For the determination of the released LDH after treatment, a sample was taken, and the cells were removed by centrifugation at 3000 xg for 35s (0 °C). The supernatant was collected in a reaction tube and stored at -80 °C until measurement or over night at 4 °C. For the determination of released LDH prior to the treatment of the cells (spontaneous released LDH), a sample was taken before the treatment and the cells were removed by centrifugation at 3000 xg for 35 s. The supernatant was collected in a reaction tube and stored at -80 °C until measurement or over night at 4 °C. Prior to the measurement the samples were thawed at room temperature. Then 50 µL per well were transferred to a 96-microtiter plate with flat bottom. For the measurement of the background the respective medium was used. Then 50 µL of the substrate mix was quickly added, followed by incubation for 30 min at room temperature in the dark. Afterwards 50 µL stop solution (1 M hydrochloric acid) was added and the absorption measured in a microplate reader (Infinite 200, Tecan) at a wavelenght of 490 nm. Threefold determinations were performed for every treatment, followed by threefold measurements on microtiter plates. After correction of the experimental LDH release for spontaneous released LDH and subtraction of the background, cell damage in percent was calculated as follows:

$$Cell\ damage = \frac{Experimental\ LDH\ release}{Maximum\ LDH\ release} \cdot 100\% \tag{3.10}$$

3.4.3 Alpha1-antitrypsin

For the quantification of A1AT in the supernatant of cell culture broth, a sandwich ELISA was established (SOP A/03, see appendix A.1.3). Briefly, 100 µL per well of a diluted rabbit polyclonal antibody solution (anti-human alpha1-antitrypsin, Acris, AP01066PU-N, diluted 1:1000 with coating buffer (1.6 g/L Na_2CO_3, 2.4 g/L

NaHCO$_3$, pH 9.7)) was transferred to a 96 well plate and incubated over night at 4 °C. Then the plate was washed four times with washing buffer (PBS, pH 7.4 + 0.05 % Tween20), followed by blocking of unspecific binding using 300 µL ELISA-Block (hydrolysated gelatin 2.7 g in 100 mL distilled water, Roche, 1112589) per well. After incubation for 1 h at room temperature, the plate was washed again twice with washing buffer, and 200 µL of the sample was applied as well as a commercially available A1AT standard between 5–80 ^{ng}/$_{mL}$ (human alpha1-antitrypsin, Calbiochem, VWR, 178251). Consecutive dilutions of the samples and standard were then performed directly on the plate (1:2 dilutions). After 2 h incubation on a plate shaker at 500 rpm and 20 °C, the plate was washed four times and 100 µL of a second antibody solution (anti-human alpha1-antitrypsin-peroxidase, 1:1000 diluted) was added to each well. After incubation for 1 h (500 rpm, 20 °C), the plate was washed four times and 90 µL substrate solution (SeramunBlau slow, Seramun, S-004-2-TMB) was added to each well. After 5-10 min incubation on a plate shaker (500 rpm, 20 °C), the reaction was stopped using 90 µL stop-solution (0.2 M H$_2$SO$_4$, Merck) per well. Absorption was measured at 450 nm with a reference wave length of 630 nm (Tecan Nano Quant infinite M200, Tecan, Switzerland). Due to the fact that immunoassays have typically a sigmoidal dose response for a wide enough concentration range, the concentration range monitored was between 5 and 80 ^{ng}/$_{mL}$. However, a slightly asymmetrical sigmoidal response was still observable. Therefore, it was decided to use a 5 parameter logistic function to fit the calibration curves for a concentration range between 5–80 ^{ng}/$_{mL}$ using following equation:

$$y = d + \frac{(a-d)}{\left(1 + \left(\frac{x}{c}\right)^b\right)^g} \tag{3.11}$$

with d: the value for the minimum asymptote, b: the Hill slope, c: the concentration at the inflection point, a: the value for the maximum asymptote and g: the asymmetry factor. As some proteins are known to be unstable under typical cultivation conditions, it was verified that this is not the case for A1AT. Therefore, 500 mL supernatant from a cultivation with the AGE1.HN.AAT cell line obtained after removal of the cells by filtration was incubated for 12 days in the DasGip bioreactor at 37 °C and a pH of 7.15 (see figure 3.8). As a result, A1AT was found to be stable over a time period of 12 days.
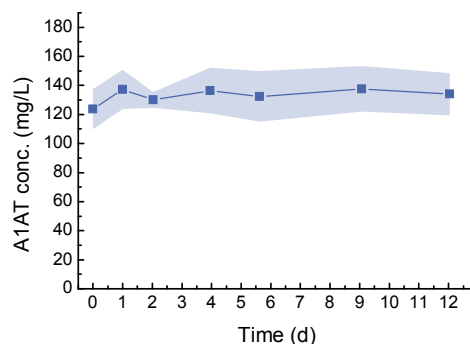
Figure 3.8: Stability of A1AT in the supernatant from a cultivation with the AGE1.HN.AAT cell line during incubation for 12 days in the DasGip bioreactor at 37 °C and pH 7.15.

3.4.4 Extracellular metabolite concentrations

3.4.4.1 Glucose, glutamine, glutamate, lactate, and ammonia

Concentrations of glucose, glutamine, glutamate, lactate, and ammonia in the supernatant of cell culture broth were determined after removal of cells and debris according to a validated method (SOP A/03, see appendix A.1.3) with a Bioprofile 100 Plus (Nova Biomedical, USA). The validation results are summarized in table 3.5. Concentrations of glucose and lactate of 20 L batch cultivations were determined with a YSI 2700S Analyzer (Yellow Springs Instruments, USA). Ammonia concentrations were quantified by mixing ammonia with a derivatization reagent (250 mg ortho-phtalaldehyde, 500 mg thioglycolic acid, 2 mL methanol p.a., 100 mL 0.4M Na-borat buffer, pH 10.4) yielding an isoindole derivate, which was detected with a fluorescence spectrometer (RF-551, Shimadzu, Japan) using an extinction wave length of 415 nm and an emission wave length of 485 nm. The final ammonia concentrations were calculated using a 5.56 mM ammonia standard, which was measured together with the samples.

3.4.4.2 Pyruvate and galactose

Quantification of pyruvate and galactose was done directly after dilution of the samples with water using two anion exchange chromatography systems (BioLC Dx-320 and DX-600, Thermo Scientific, Germany). For separation of pyruvate a IonPac column and for galactose a CarboPac column were used (Dionex IonPac AS11 and

CarboPac PA20, Thermo Scientific, Germany). A detailed description of the method for quantification of pyruvate can be found in Genzel et al. [30]. The validation results of both methods are given in table 3.5.

Table 3.5: Results for the validation of the determination methods of glucose, glutamine, glutamate, lactate, ammonia, pyruvate and galactose.

Parameter	GLC	GLN	GLU	LAC	AMM	PYR	GALC
Linearity	yes	yes	yes	no	yes	yes	yes
Homoscedasticity	no	no	no	yes	no	no	yes
Standard dev. of the method [mM]	0.19	0.04	0.02	0.28	0.02	0.26	0.39
Rel. std. dev. of the method [%]	11.0	4.7	3.4	1.6	2.2	1.0	1.31
Limit of quantitation [mM]	2.00	0.41	0.22	2.78	0.17	2.64	3.91

3.4.4.3 Amino acids

Amino acids were either quantified with a validated method (average relative SD of the method for all detectable amino acids < 5 %) according to Genzel et al. [121] or for the 20 L batch cultivations with a reversed phase high-performance liquid chromatography (RP-HPLC) method. Briefly, for the quantification of amino acids with the RP-HPLC method, proteins were precipitated with 5 % perchloric acid and 0.4 M potassium borate buffer (pH 9.5), followed by derivatization of amino acids with 50 mg ortho-pthalaldehyde, 1 mL methanol, 100 μL 3-mercapto-propionic acid and 9 mL borate buffer (pH 10.4) [122]. Separation was done with a RP18 column (Kromasil C18, 5 μm, 150x4 mm, VDS Optilab Chromatographietechnik GmbH, Germany) on a HPLC system. Isoindole derivates were detected using an extinction wave length of 350 nm and an emission wave length of 450 nm. For quantification, an external standard (L-norvalin) and the integrated peak areas were used.

3.4.5 Intracellular metabolite concentrations

3.4.5.1 Extraction of metabolites from the supernatant

For the determination of intracellular metabolites released to the culture broth or the washing buffer due to cell lysis and/or leakage during sample preparation, 250 µL of the supernatant were mixed with 800 µL MeOH + 0.075 % formic acid for 30s on a vortex mixer followed by incubation for 10 min on ice. Then the sample was

again mixed on a vortex mixer for 30 s, heated at 85 °C for 4 min and centrifuged at 16000 xg for 10 min (0 °C). The supernatant was transferred to a new reaction tube and stored at -80 °C until measurement.

3.4.5.2 Extraction of metabolites from cell pellets

Extraction was performed in triplicates after washing the cells as described in section 3.3.3. The extraction and measurement of intracellular metabolites was based on the work of Ritter et al. [95, 96]. Briefly, 600 µL of a MeOH/CHCl$_3$ solution (2:1) was added to the pellet after the washing solution was discarded. Then 500 µL CHCl$_3$ (100 %) and 900 µL of MeOH/tricine solution (9:10, tricine 3.8 mM) were added, followed by mixing of the reaction tubes on a vortex mixer for 20 s and centrifugation for 5 min at 16000 xg at 0 °C. The water phase was then transferred to a new reaction tube placed in an Eppendorf Cooler at -20 °C and 800 µL of MeOH/tricine solution (9:10, tricine 3.8 mM) were added to the remaining CHCl$_3$ phase to perform a second extraction. Tubes were mixed on a vortex mixer for 20 s, incubated at 0 °C for 5 min, and centrifuged (16000 xg, 5 min, 0 °C). Then, the water phase was transferred to the reaction tube with the water phase from the first extraction. For the inactivation of remaining enzyme activities, the reaction tubes with the pooled water phases were heated at 85 °C for 4 min and then centrifuged again (16000 xg, 10 min, 0 °C). Finally, the liquid phase was evaporated by placing the reaction tubes under a stream of air. All samples were stored afterwards at -80 °C until measurement.

3.4.5.3 Extraction of metabolites directly in culture broth

For the determination of the efficiency of the sampling and quenching procedure for the quantification of intracellular metabolites, a protocol was established for the extraction of metabolites from cells directly in culture broth (in the following referred to as: whole broth extraction) without the time consuming need of removal of the supernatant. 800µL MeOH/tricine solution (110:1, tricine 250 mM) were added to 2 mL reaction tubes placed at -20 °C. 500 µL of a cell suspension was added to the reaction tube, followed by mixing for 30 s on a vortex mixer. Then 700 µL CHCl$_3$ (100 %) was added, followed by 30 s mixing on a vortex mixer and incubation at 0 °C for 5 min. Then the reaction tube was centrifuged for 5 min at

16000 xg at 0 °C. The water phase was transferred to a new reaction tube placed in an Eppendorf Cooler at -20 °C and 800 µL of MeOH/tricine solution (9:10, tricine 3.8 mM) were added to the remaining $CHCl_3$ phase to perform a second extraction. Tubes were mixed on a vortex mixer for 20 s, incubated at 0 °C for 5 min and centrifuged (16000 xg, 5 min, 0 °C). Then the water phase was transferred to the reaction tube with the water phase from the first extraction. For the inactivation of remaining enzyme activities, the reaction tubes with the pooled water phases were heated at 85 °C for 4 min and then centrifuged again (16000 xg, 10 min, 0 °C). Finally, the liquid phase was evaporated by placing the reaction tubes under a stream of air. All samples were stored afterwards at -80 °C until measurement. In addition, the recovery of metabolites from the standard stock solution was determined in water (Milli-Q) and in culture broth (six technical replicates each) by adding 20 µL standard stock solution to 500 µL Milli-Q water or to 500 µL cell suspension from a shaker cultivation.

3.4.5.4 Liquid chromatography-mass spectrometry

For the LC-MS analysis 400–600 µL Milli-Q water according to the expected concentration of intracellular metabolites were added to the reaction tubes, followed by mixing on a vortex mixer for 30 s. Then, chromatographic separation and detection of intracellular metabolites was performed with a anion exchanger chromatography system coupled to a UV, conductivity and mass-spectrometry detector according to [71]. In total, 31 intracellular metabolites were quantified. Based on the measured concentration and the corresponding total cellular volume (determined by simulation, see section 3.5.3) at the respective sample time, intracellular metabolite concentrations were calculated. The volume of a single cell was calculated based on the cell diameter derived from the cell counter under the assumption of a spherical shape. An overview of the used detectors and calibration types for the quantification of intracellular metabolites is given in table 3.6.

Table 3.6: Overview of the detectors used and the calibration types for the quantification of intracellular metabolites.

Metabolite	MS detector	UV detector	Conductivity detector
3PG	Quad[c]	-	-
ADP	-	XLOff[d]	-
AMP	XQOff[e]	XLOff	-
ATP	-	XLOff	-
CDP	Quad	Quad	-
cis-aconitat	Quad	-	-
CIT	XQOff	-	-
CMP	-	XLOff	-
CTP	-	XLOff	XLOff
FBP	XQOff	-	XLOff
F1P	XQOff	-	-
F6P	XQOff	-	-
FUM	Quad	-	-
GDP	-	XLOff	-
G6P	XQOff	-	-
GMP	Quad	XLOff	-
GTP	-	XLOff	-
ICIT	Quad	-	-
2-KG	XQOff	-	-
MAL	Quad	-	-
PEP	Quad	-	-
PYR	Quad	-	XLOff
R5P	Quad	-	-
SUC	XQOff	-	-
UDP	-	XLOff	-
UDP-GalNAc[a]	XQOff	XLOff	-
UDP-GLC	XQOff	-	-
UDP-GlcNAc[b]	XQOff	XLOff	-
UMP	Quad	XLOff	-
UTP	-	XLOff	-

a: uridine diphosphate N-acetyl galactosamine (UDP-GalNAc); b: uridine diphosphate N-acetyl glucosamine (UDP-GlcNAc); c: polynomial 2. order forced through origin (Quad); d: weighted (1/concentration) linear regression (XLOff); e: weighted (1/concentration) polynomial 2. order (XQOff).

3.4.5.5 Verification of the standard stock solution

In the beginning of the work, a new standard stock solution containing all metabolites and substances which are detectable with the liquid chromatography-mass spectrometry (LC-MS) method was established and checked against the existing standard. Based on the established stock solution from Ritter [95], one new metabolite was added (F1P). The composition of the standard stock solution together with

the purchase order numbers of the suppliers can be found in table A.2 in the appendix. The new standard was then verified against the existing standard of Ritter based on measurements of the peak areas of all metabolites and calculation of the recovery of the new standard based on the standard of Ritter. The overall recovery for all metabolites was 96.6 ± 9.7 %, however the recoveries were much smaller for CDP (78.4 %), UDP (66.2 %), ATP (89.9 %), GTP (90.4 %) and UDP-GlcNAc (91.1 %). Therefore, a second stock solution with new weighted amounts of CDP, UDP, ATP, GTP and UDP-GlcNAc was produced and the recoveries were determined. As the exact same concentrations were determined for the second stock solution (overall recovery = 97.5 ± 12.5 %), this stock solution was used for all measurements described in this work. The stock solution was stored in aliquots of 700 μL at -80 °C until measurement.

3.4.6 Intracellular maximum enzyme activities

After washing the cells as described in section 3.3.3, enzymes were extracted from freshly thawed cell pellets according to the work of Janke [54]. The assay conditions were verified and adapted from MDCK cells to the measurement of enzymes extracted from the AGE1.HN cells. For measuring the maximum enzyme activities, pH of the buffers was set to optimal values, while the dilution of the cellular extracts were adjusted to fit the measurement range of the corresponding standard. Briefly, pH values for citrate lyase (CL) and for GLDH were set to 9.0 and 7.5, respectively. Extraction of enzymes was performed in independent duplicates or triplicates followed by quadruplicate measurements on microplates.

3.5 Computations

3.5.1 Pairwise correlation coefficients

The pearson correlation coefficient between two variables x and y was calculated with the following equations:

$$\rho(x, y) = \frac{Cov(x, y)}{\sqrt{Var(x)Var(y)}} \tag{3.12}$$

with the covariance between x and y given by:

$$Cov(x, y) = \frac{\sum_{i=1}^{n}(x_i - \bar{x})(y_i - \bar{y})}{(n - 1)} \tag{3.13}$$

and the variance of x and y:

$$Var(x) = \frac{1}{n - 1} \sum_{i=1}^{n}(x_i - \bar{x})^2 \tag{3.14}$$

$$Var(y) = \frac{1}{n - 1} \sum_{i=1}^{n}(y_i - \bar{y})^2 \tag{3.15}$$

3.5.2 Principle component analysis

Before calculating the principle components, the raw data was pre-processed in Microsoft Excel according to the recommendations published by Steuer et al. [123]. Missing values were replaced by the mean of the remaining steady-state samples, whereas values below the quantification limit were set to zero. Then the data was centred and scaled to unit variance:

$$\widehat{x_i} = \frac{x_i - \bar{x}}{Std(x)} \tag{3.16}$$

with the SD given by:

$$Std(x) = \sqrt{Var(x)} \tag{3.17}$$

The PCA was then performed using the Microsoft Excel add-in Multibase package (Numerical Dynamics, Japan).

3.5.3 Modelling of cell growth and substrate consumption for batch cultivations

The following equations were used to determine yield coefficients for cell growth and specific consumption rates of glucose, glutamine and pyruvate. A Monod kinetic based on the simultaneous limitation of glutamine and glucose was considered for estimation of μ:

$$\mu = \mu_{max} \cdot \frac{[Gln]}{[Gln] + k_{gln}} \cdot \frac{[Glc]}{[Glc] + k_{glc}} \tag{3.18}$$

with μ_{max}, the Monod constant for glutamine (k_{gln}), and the Monod constant for glucose (k_{glc}). For modelling the specific glucose, glutamine and pyruvate uptake rates, the following correlation from Tremblay et al. [124] was used:

$$q_s = \frac{\mu}{Y_s} + m_s \cdot \frac{[S]}{[S] + k_{m,s}}$$
(3.19)

with s: concentrations of glucose, glutamine or pyruvate in the medium, Y_s: the yield coefficient, m_s: the maintenance term and $k_{m,s}$: the saturation constant for the corresponding substrate (s). The following balance equation describes the increase in total cellular volume of viable cells during batch cultivations:

$$\frac{d[CV_V]}{dt} = \mu \cdot CV_V - k_D \cdot CV_V$$
(3.20)

with the total viable cell volume per volume of media (CV_v) and the specific cell death rate (k_D). Uptake of the substrates glucose and pyruvate is described by:

$$\frac{d[Glc]}{dt} = -q_s \cdot CV_v \cdot \sigma$$
(3.21)

$$\frac{d[Pyr]}{dt} = -q_s \cdot CV_v \cdot \sigma$$
(3.22)

with a unit step function (σ), which is 1 for [s]>0 and zero otherwise, to prevent negative substrate concentrations. As glutamine is known to be chemically unstable in cell culture media [125], the spontaneous degradation rate of glutamine ($k_{d,gln}$) was determined in 42-MAX-UB media under controlled conditions of 37 °C and a pH of 7.15 in the 0.5 L DasGip bioreactor. The $k_{d,gln}$ followed a first-order kinetic with $k_{d,gln}$= 0.00150 ± 0.00003 1/h (see figure 3.9). A comparable value ($k_{d,gln}$=0.00159 ± 0.00025 1/h) was found in the supernatant from a cultivation with the AGE1.HN.AAT cell line after removal of the cells by filtration and incubation of the supernatant for 12 days in the DasGip bioreactor at 37 °C and pH 7.15. In both experiments no glutaminase activity could be found, as the glutamate concentrations were stable over the whole incubation times. The $k_{d,gln}$ was considered in the following differential equation for glutamine:

$$\frac{d[Gln]}{dt} = -\left(q_s \cdot CV_v + k_{d,gln} \cdot [Gln]\right) \cdot \sigma$$
(3.23)

All calculations were done with Matlab (Version 7.9.1.671, R2009b, The Math-Works, Inc.). For the estimation of the model parameters the Systems Biology

Toolbox for MATLAB (SBtoolbox2) was used with the global optimization algorithm „fSSmSB" [126].
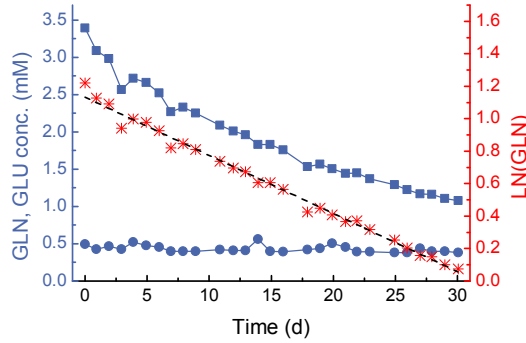
Figure 3.9: Glutamine concentrations (blue squares) and glutamate concentrations (blue circles) in 42-MAX-UB medium during incubation at 37 °C and pH 7.15 in the 0.5 L DasGip bioreactor, together with the logarithmic plot of the glutamine concentrations (red asterisk) and the linear fit (dashed straight line) for the determination of $k_{d,gln}$.

The residual sum of squares (RSS) used for comparing models with different monod kinetics (refer to section 4.3.2) was calculated according to:

$$RSS = \sum_{i=1}^{n}(y_i - f(x_i))^2 \tag{3.24}$$

with y_i the measured value for CV_v, glucose, glutamine or pyruvate and $f(x_i)$ the predicted value for y_i.

3.5.4 Calculation of specific growth, consumption and production rates for continuous cultivations

For the continuous cultivations from material balances in the bioreactor, the specific cell growth rate (μ), the specific uptake rate for substrates s (q_s), and the specific production rate for metabolites p (q_p) during steady-state were determined. The following differential equation describes the increase in total cell number during the continuous cultivations:

$$\frac{d[X_T]}{dt} = \mu \cdot X_V - DR \cdot X_T \tag{3.25}$$

with the concentration of total cells (X_T) and the concentration of viable cells (X_V). The dilution rate (DR) is derived from:

$$DR = \frac{F_i}{wv} \tag{3.26}$$

with the feed rate (F_i) and wv. From equation 3.25, μ was obtained after considering steady-state, $\frac{d[X_T]}{dt} = 0$:

$$\mu = DR \cdot \frac{X_T}{X_V} \tag{3.27}$$

q_s and q_p were calculated from:

$$\frac{d[C_s]}{dt} = DR \cdot (C_s^F - C_s^B) - q_s \cdot CV_v \tag{3.28}$$

$$\frac{d[C_p]}{dt} = DR \cdot (C_p^B - C_p^F) + q_p \cdot CV_v \tag{3.29}$$

with the consumed substrate concentration (C_s) and the produced metabolite concentration (C_p). The superscripts F and B denote the concentration of substrates S or metabolites P in the feed and in the bioreactor. From equations 3.28 and 3.29 q_s and q_p are obtained after considering steady-state ($\frac{d[C_s]}{dt} = 0$ and $\frac{d[C_p]}{dt} = 0$):

$$q_s = \frac{DR}{CV_v} \cdot (C_s^F - C_s^B) \tag{3.30}$$

$$q_p = -\frac{DR}{CV_v} \cdot (C_p^B - C_p^F) \tag{3.31}$$

During the batch (DR=0) and the transient phase, q_s and q_p were calculated with following equations:

$$q_s = \frac{DR \cdot (C_s^F - C_s^B) - \frac{d[C_s]}{dt}}{CV_v} \tag{3.32}$$

$$q_p = -\frac{DR \cdot (C_p^B - C_p^F) - \frac{d[C_p]}{dt}}{CV_v} \tag{3.33}$$

The yield coefficient for produced CV_v per consumed glucose ($Y_{CVv/glc}$), the yield coefficient for produced CV_v per consumed glutamine ($Y_{CVv/gln}$), the yield coefficient for produced LAC per consumed GLC ($Y_{lac/glc}$), and the yield coefficient for produced AMM per consumed GLN ($Y_{amm/gln}$) were calculated as follows:

$$Y_{CVv/glc} = \frac{\mu}{q_{glc}} \tag{3.34}$$

$$Y_{CVv/gln} = \frac{\mu}{q_{gln}} \tag{3.35}$$

$$Y_{lac/glc} = \frac{q_{lac}}{q_{glc}} \tag{3.36}$$

$$Y_{amm/gln} = \frac{q_{amm}}{q_{gln}} \tag{3.37}$$

CHAPTER 4

Results and discussion

4.1 Preliminary studies

4.1.1 Physical characterization of the bioreactor systems

Within the SysLogics consortium different bioreactor systems were deployed for the cultivation of the AGE1.HN and AGE1.HN.AAT cell lines. To assess criteria for bioreactor comparison, we determined in the beginning the geometric similarities, P, u_{tip}, Re and t_m for five different bioreactor systems (figure 4.1), which were used in our laboratory and in the laboratories of two SysLogics cooperation partners[1]. For this comparison, the data of the DasGip bioreactor (BS0500TPSS) with a wv of 0.5 L was used as this reactor scale was for this thesis predominantly employed for batch as well as continuous cultivations. As criterion for the comparison of the different bioreactors a t_m range of 10–12.5 s based on μ as indicator could be successfully identified. The results of this comparison were published in Engineering in Life Sciences by Platas Barradas et al. [49]. In the following, the results of the physical characterization of the DasGip bioreactors with wv of 0.5 and 2.5 L as part

---

[1]Cell culture technology group at the University of Bielefeld and Institute of Bioprocess and Biosystems Engineering at the University of Technology in Hamburg

of my contribution to the publication of Platas Barradas et al. [49] together with determined $k_L a$ values are described and discussed.
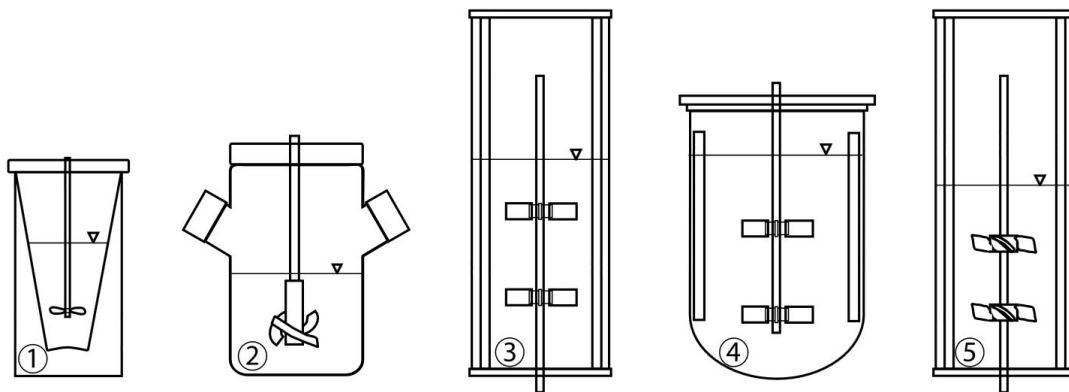
Figure 4.1: Drawing of the different bioreactors used within the SysLogics consortium for the cultivation of the AGE1.HN cell lines. 1: Vario1000 (wv = 0.2 L, Medorex eK, DE), 2: Benchtop bioreactor (wv = 0.5 L, DasGip AG, DE), 3 and 5: VSF2000 (wv = 1.2 L, Bioengineering AG, CH) and 4: Biostat B-DCU (wv = 2 L, Sartorius Stedim Biotech GmbH, DE) (Reprinted from Platas Barradas et al. [49], with permission from Elsevier).

The $k_L a$ values were determined for different aeration rates (F_gs) and rotational stirrer speeds (Ns) in NaCl solution (8.0 g/L) and in 42-MAX-UB medium (all results are summarized in table 4.1). The lowest $k_L a$ of 0.67 1/s was found for 50 rpm and an F_g of 0.5 sL/h in NaCl solution in the 0.5 L bioreactor (BS0500TPSS). As can be seen in table 4.1, N had only a minor effect on the $k_L a$ value within the tested range of 50 to 180 rpm. This might be due to the low power input by the stirrer and the position of the dip tube used for aeration near the vessel wall, circumventing efficient bubble break up by the impeller as the bubbles traversing through the liquid to the surface along the vessel wall. In addition, due to the low power inputs applied for the experiments with the AGE1.HN.AAT cells (and with animal cells in general), cultivations are most likely operated in a transient region between a laminar (Re<100) and a turbulent flow regime (Re>10000, see table 4.1). In contrast to that, an almost 12 fold increase of the $k_L a$ could be determined with increasing aeration rates from 0.5 to 18 sL/h at 125 rpm (table 4.1). This is not surprising as an increase in the number of bubbles with increasing F_g increases the gas-liquid interface a and therefore the product $k_L \cdot a = k_L a$ (assuming independence of bubble sizes from F_g and a constant climb rate of the bubbles). According to Van't Riet [117],

the most important factors which affects the k_La are (besides power consumption and gas superficial velocity) liquid phase properties such as ionic strength, surface tension and viscosity. Compared to the values obtained in NaCl solution, the k_La values were higher in 42-MAX-UB medium (table 4.1) containing Pluronic as surfactant (see table 3.1). Surfactants can affect the k_La in two opposed ways. Firstly, by decreasing the diffusional resistance (k_L) through aqueous pores between the surfactant molecules [127], and secondly by increasing the gas–liquid interface (a) by decreasing bubble sizes [128]. According to Sheppard and Cooper [129], the predominating effect depends on the concentration of the surfactant. An increase in the diffusional resistance, for example, may predominate at low surfactant concentrations. Howeve, at higher concentrations, the effects on the gas–liquid interface may be significant enough to increase the rate of oxygen transfer [129]. Which effect dominates can not be answered without additional experiments. The experimental data suggest a possible positive effect of Pluronic on the k_La through an increased gas-liquid interface. This was also found by Zhang et al. [130] after supplementing various cell culture media with Pluronic. Nevertheless, a positive effect on the k_La might be also due to the composition and the amount of different ions in 42-MAX-UB medium compared to the NaCl solution. The k_La in the 2.5 L bioreactor (DR03C, determined in 42-MAX-UB) was slightly lower compared to the 0.5 L bioreactor (BS0500TPSS). Nevertheless, the k_La values ranging from 1.0–2.7 $^{1}/_{s}$ in 42-MAX-UB are most likely sufficient to meet the oxygen demand of AGE.HN.AAT cells during batch as well as continuous cultivations.

Table 4.1: Determined dimensions and volume-specific oxygen transfer values, mixing times, power input per liquid volume, Reynolds numbers and impeller tip speeds of the 0.5 L and 2.5 L DasGip bioreactor for different aeration rates and rpm values.

Bioreactor media	wv	D	d	N	u_{tip}	F_g	vvm	P/V^a	t_m	k_La	Re^b
	L	m	m	1/min	m/s	sL/h	1/min	W/m^3	s	1/h	-
BS0500TPSS	0.5	0.100	0.054	50	0.14	0.5	0.017	-	39.0	0.67	3390
	0.5	0.100	0.054	74	0.21	0.5	0.017	-	-	0.68	5017
	0.5	0.100	0.054	125	0.35	0.5	0.017	-	10.0	0.77	8474
	0.5	0.100	0.054	180	0.51	0.5	0.017	-	5.3	0.83	12203
	0.5	0.100	0.054	125	0.35	1.5	0.050	-	-	2.14	8473
	0.5	0.100	0.054	125	0.35	3.0	0.100	-	-	3.22	8473
	0.5	0.100	0.054	125	0.35	6.0	0.200	-	-	4.43	8473
	0.5	0.100	0.054	125	0.35	12.0	0.401	-	-	6.31	8473
↑	0.5	0.100	0.054	125	0.35	18.0	0.600	-	-	9.09	8473
NaCl	0.5	0.100	0.054	125	0.35	0.0	0.000	5.9	-	-	8474
42-MAX-UB	0.5	0.100	0.054	125	0.35	0.5	0.017	-	-	0.99	8473
↓	0.5	0.100	0.054	125	0.35	1.0	0.033	-	-	1.96	8473
	0.5	0.100	0.054	125	0.35	1.5	0.050	-	-	2.48	8473
	0.5	0.100	0.054	125	0.35	3.0	0.100	-	-	3.72	8473
DR03C NaCl	2.5	0.128	0.048	100	0.25	0.0	0.000	5.3	9.2	-	5356
NaCl	2.5	0.128	0.048	125	0.31	0.0	0.000	6.7	8.6	-	6696
NaCl	2.5	0.128	0.048	150	0.38	0.0	0.000	8.9	7.8	-	8035
42-MAX-UB	2.5	0.128	0.048	150	0.38	6.0	0.040	-	-	2.71	8035

a: Power input for the DR03C bioreactor was determined at RT without aeration.

b: for the calculation of Re a density of 1012.4 kg/m^3 (500 mM NaCl solution, 37 °C, 1 bar, taken from Potter and Brown [131]) and a dynamic viscosity of 0.000726 kg/(m·s) (500 mmol/kg NaCl solution, 37 °C, 1 bar, taken from Kestin et al. [132]) were used.

For the identification of proper operation ranges for the stirrer to avoid pH or substrate concentration gradients, t_m was experimentally determined for the 0.5 L bioreactor (BS0500TPSS). The t_m is defined as the time required to achieve a certain degree of homogeneity after the addition of a tracer pulse at a single point in the vessel. To ensure comparable results, the addition of sodium thiosulfate ($Na_2S_2O_3$) was from the top of the reactor near the stirrer shaft at the exact same position for all tested conditions. A maximum time of 39 s for decolorization could be determined at 50 rpm (table 4.1). Moreover, at 50 rpm, distinct decolorization regions could be observed near the installed dip tubes and probes, indicating zones of poor macromixing. However, at higher rotational speeds of 125 and 180 rpm (t_m=10 & 5.3 s, table 4.1), the decolorization was uniform and decolorization regions were hardly detectable anymore. According to equation 3.6, the calculated

t_m values for the 2.5 L bioreactor (DR03C) were comparable to the results of the 0.5 L bioreactor (table 4.1). Therefore, rotational speeds of 125–150 rpm seemed to be sufficient to ensure fast and homogeneously mixing of the culture broth, e.g. upon addition of base for pH adjustment, and/or feed media for continuous cultivations.

4.1.2 Shaker cultivations for cell growth studies

In the beginning of this thesis, small scale cultivations in filter-tubes (wv=10 mL) and shaker flasks (wv=50–150 mL) were performed to test firstly if AEM (Gibco-Life Technologies, USA) can be used for the routine cultivations instead of the standard medium 42-MAX-UB, and secondly if AGE1.HN.AAT cells can be adapted to glutamine-free 42-MAX-UB medium. These experiments were motivated by two facts: firstly, the standard medium 42-MAX-UB which was established and provided by cooperation partners for the cultivation of the AGE1.HN cell line was not commercially available from other media manufacturer. Therefore, growth in Adenovirus Expression Medium (AEM) was studied to verify wether this medium can be used as an alternative option. Secondly, it was already shown for different cell lines that the substitution of glutamine with other substrates led to superior growth characteristics with less waste product formation and eventual higher product titers [27–31, 91, 133–135]. For this reason, it was also tried to adapt the AGE1.HN.AAT cell line to glutamine-free 42-MAX-UB medium as well as to 42-MAX-UB medium. For the latter, glutamine was substituted with glutamate, alanine or pyruvate, and with different combinations of them.

4.1.2.1 Cell growth in Adenovirus Expression Medium

AEM was originally developed for suspension culture of PER.C6 cells, a human designer cell line used for the production of recombinant antibodies and proteins as well as adeno- and influenza viruses [136–140]. Therefore, AEM might also be suitable for the growth of the human cell line AGE1.HN. For this study, the parental cell line AGE1.HN grown in 42-MAX-UB medium was directly passaged in 150 mL fresh AEM and in parallel in 150 mL fresh 42-MAX-UB medium in 250 mL baffled shaker flasks. In the first four days, cell growth in AEM was comparable to that in 42-MAX-UB medium. But after 105 h, the cells started to die in AEM, whereas in 42-MAX-UB medium cell growth continued until 131 h (figure 4.2-a). Glutamine

metabolism seemed to be comparable given the fact that the start concentrations in both media where different (figure 4.2-d). Due to the lower glutamine start concentration in AEM, glutamine dropped below 0.5 mM already after 95 h, which might correlate with the earlier decline of cell growth in AEM. In contrast to that, uptake of glucose as well as lactate release seemed to be higher in AEM (figure 4.2-c). Also, the total viable cell volume per volume of media (CV_v) appeared to be slightly higher in AEM (figure 4.2-b) which might explain the higher uptake of glucose as well as (in part) the higher release of lactate. However, the lactate release rate seemed to be higher in AEM, which indicates that the glucose metabolism is different in AEM compared to 42-MAX-UB medium.
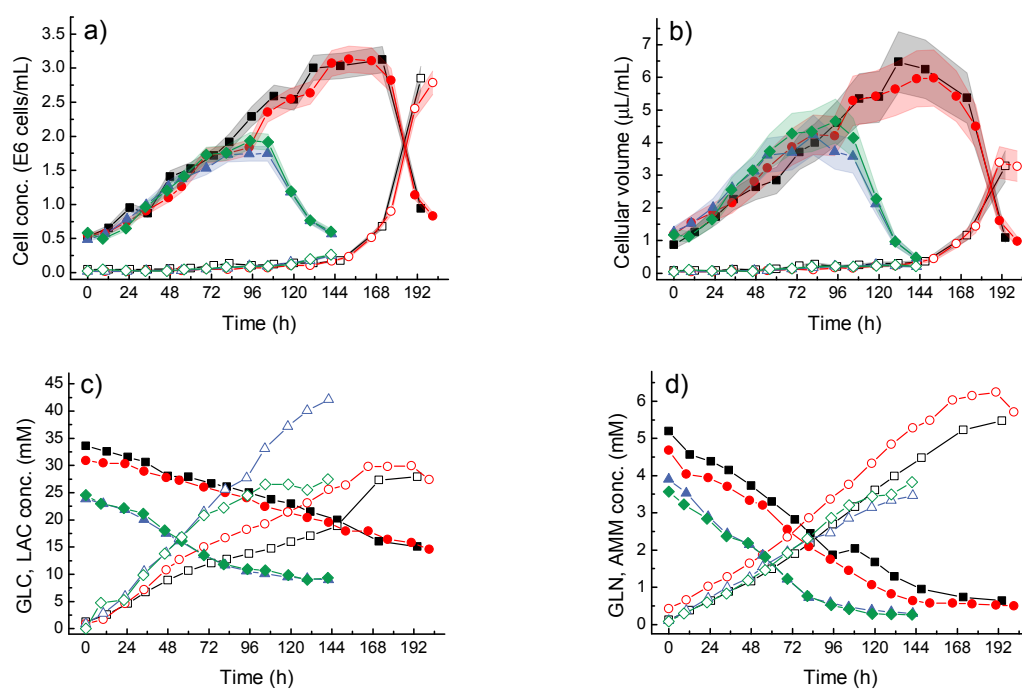
Figure 4.2: a) Concentrations of viable (filled symbols) and dead cells (open symbols) and **b)** cellular volume of viable (filled symbols) and dead cells (open symbols) shown as average of three technical replicates and the SD as shaded background around the symbols and **c)** concentrations of glucose (filled symbols), lactate (open symbols), **d)** glutamine (filled symbols), and ammonia (open symbols) for two replicates of shaker cultivations with AGE1.HN cells in 42-MAX UB medium (■: replicate 1, ●: replicate 2), and for two replicates in AEM (◆: replicate 1, ▲: replicate 2).

Taken together, the performance of 42-MAX-UB medium in terms of the support of viable cell growth as well as the reduced lactate relase in 42-MAX-UB appeared

to be superior over AEM. Therefore, AEM might be used for routine cultivations in case 42-MAX-UB medium is not available. Nonetheless, for the following main experiments, 42-MAX-UB medium was used.

4.1.2.2 Adaptation to glutamine-free medium

For the adaptation of the AGE1.-HN.AAT cell line to glutamine-free 42-MAX-UB medium, the cells were thawed and passaged at least three times in medium with 5 mM glutamine. For the adaptation itself, two different procedures were followed: in a first attempt the glutamine concentration was stepwise reduced from 5 mM to 2 mM to 1 mM and, in a second attempt, the cells were directly passaged from 5 mM containing medium into glutamine-free medium. To ensure that no limitation of glutamine occurs during the first adaptation process, the extracellular concentration along with the concentrations of glucose and glutamate were measured daily (data not shown). The cells were passaged into fresh medium to an initial viable cell concentration of $1.15 \cdot 10^6$ cells/mL, as soon as the extracellular concentration of glutamine dropped below 0.5 mM. After placing the cells in medium with 2 mM glutamine (passage 1), the viable cell concentration decreased from $2.2 \cdot 10^6$ to $1.3 \cdot 10^6$ cells/mL (figure 4.3-a). The viability was more or less stable and decreased after four passages from about 90 % to 85 %. After reducing the glutamine concentration further to 1 mM (passage 5 to 6), the viable cell concentration decreased to $0.8 \cdot 10^6$ cells/mL and the viability decreased to 62 %. After four passages in 2 mM glutamine, a second filter-tube containing glutamine-free 42-MAX-UB medium was inoculated to test if the cells would grow without glutamine. After passaging into the glutamine-free medium, the viability dropped to 6.4 % and no cell growth could be detected (data not shown). The same result was observed during the second adaptation attempt after placing the cells from 5 mM glutamine containing medium directly into glutamine-free medium (figure 4.3-a). No cell growth could be observed and the viability decreased after four passages from 92 % to 45 % and further to 15 % after eight passages. Similar results were also obtained by our cooperation partners, were all adaptation attempts to glutamine-free medium were not successful. In addition, no cell growth was detectable in all media were glutamine was substituted by different concentrations of glutamate, alanine or pyruvate and also with different combinations of them (figure 4.3-b).
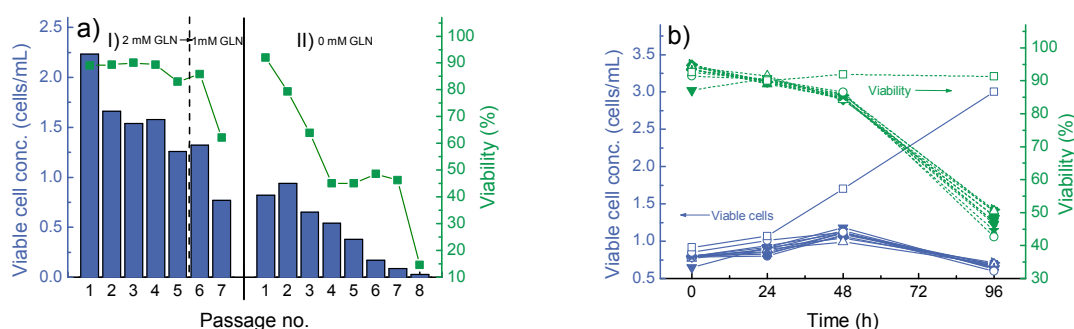
Figure 4.3: a) Concentrations of viable cells (blue bars) and viability (green squares) of AGE1.HN.AAT cells during adaptation to glutamine-free 42-MAX-UB medium in shaker flasks and in filter-tubes and **b)** concentrations of viable cells (blue symbols with straight lines) and viability (green symbols with dashed lines) of AGE1.HN.AAT cells in glutamine-free 42-MAX-UB medium (○) and in glutamine-free 42-MAX-UB medium supplemented with 2 mM (■), 4 mM (●) and 8 mM alanine (▲), 2 mM (▼), 4 mM (◆) and 8 mM glutamate(◄), 5 mM pyruvate + 2 mM alanine (►), 5 mM pyruvate + 2 mM glutamate (△), 2 mM alanine + 2 mM glutamate (★) and 5 mM glutamine (□) in filter-tubes.

In the past, adaptation to glutamine-free medium was also not successful for other cells [133, 141]. For example, Eagle et al. [133] grew mouse fibroblast cells in a glutamine-free medium supplemented with glutamate in a range of 0.1 to 40 mM. All glutamate concentrations failed to substitute for glutamine as the cells did not multiply and after 6d showed degenerative changes. In the study of Capiaumont et al. [141], a hybridoma cell line could not be adapted to a glutamine-free medium. However, in the same study of Eagle et al. [133], Hela cells could be successfully adapted to grow in glutamine-free media supplemented with a high glutamate concentration of 20 mM [133]. Also, Griffiths [134] successfully adapted WI-38 and MRC-5 cells to a glutamine-free medium supplemented with the identical glutamate concentration compared to the glutamine containing medium. Recently, other cell lines were also successfully adapted to grow in glutamine-free medium [27, 30, 91, 135]. Also, in these studies, cell growth depended on the availability of alternative substrates and according to McDermott and Butler [142] and Butler and Christie [27], intracellular glutamate availability might be an important factor governing adaptability of cells to glutamine-free medium. Glutamate can be taken up either directly from the medium or could be derived from degradation of other amino acids (e.g. isoleucine, valine or aspartate). It could be shown, that cells subjected to glutamine-free medium adapt by increasing their glutamate transport

[27, 142]. To ensure an ample supply of glutamine for the synthesis of proteins or nucleic acids, it was also shown that during the adaptation to glutamine-free medium the activity of glutamine synthetase (GS) was induced, enabling the synthesis of glutamine from glutamate [27, 142–145]. With an activity of 279.6–646.1 $^{fmol}/_{(cell\ h)}$ during exponential growth, the activity of GS was found to be high enough to ensure the synthesis of glutamine from glutamate in AGE1.HN.AAT cells (see table 4.2 and section 4.3.3). Therefore, it can be hypothesized that AGE1.HN.AAT cells probably could not be adapted to glutamine-free medium due to an insufficient intracellular amount of available glutamate. This was also found in a study with McCoy cells and MDCK cells. Here, in both cell lines, the activity of GS was increased upon the adaptation to glutamine-free medium. However, only the McCoy cells could grow in glutamine-free medium after doubling of their glutamate uptake rate, whereas the MDCK cells maintained their low glutamate uptake rate during the adaptation [142]. Therefore, not only a sufficient activity of GS is required, but also a sufficient amount of intracellular glutamate. To investigate this further, experiments should focus on how the uptake of glutamate or other amino acids could be increased to raise the intracellular glutamate pool either directly or indirectly (through degradation reactions of other amino acids).

Table 4.2: Comparison of glutamine synthetase activity values in AGE1.HN.AAT cells with values measured in MDCK and McCoy cells after adaptation to glutamine-free medium.

Cell	Reference	GS activity ($^{fmol}/_{(cell\ h)}$)
AGE1.HN.AAT	this study	279.6 - 646.1
MDCK	[145]	390.6
McCoy^a	[142]	202.5

a: for the conversion of the in McDermott and Butler [142] published GS activity from $^{nmol}/_{(mg\text{-}Protein\ min)}$ in $^{fmol}/_{(cell\ h)}$, a cellular protein content of 0.375 $^{ng}/_{cell}$ was assumed.

4.2 Establishment of a sampling and quenching method for suspension cells

As illustrated in section 2.3, for the determination of intracellular metabolite concentrations in mammalian suspension cells to date no standard method is available. Moreover, publications dealing with this topic are sparse and the efficiency of the sampling and quenching methods used in these studies are usually reported only for a few selected metabolites [101–103, 105]. As the investigation of intracellular metabolite concentrations during batch and continuous cultivations was the main focus of this work, a reliable and efficient sampling and quenching procedure was required. This procedure should meet the following requirements:

- a sufficient halt of the cellular metabolism

- a complete separation of intracellular metabolites from substances originating from the supernatant of the cultivation

- a sampling volume between 0.5–2.0 mL to allow for the investigation of small scale cultivations in shaker and benchtop bioreactors

- compatibility with the extraction method established in our group by Ritter et al. [96]

In the following, the results obtained during the establishment of a sampling and quenching procedure for AGE1.HN and AGE1.HN.AAT cells are described and discussed.

4.2.1 Separation of cells from the culture broth

Substances, such as residual amounts of contaminating metabolites and enzymes from lysed cells, might bias the determination intracellular metabolites or, in case of e.g. anions, interfere with the analytical method, leading to biased measurement signals [146]. Therefore, as the first critical point of the sampling procedure, the separation of the culture broth from the cells was examined. Separation can be achieved either by centrifugation or filtration and both methods might provide reproducible results. However, centrifugation takes more time to complete, especially, if additional washing steps are necessary.

4.2.1.1 Separation by filtration

At first it was tested if filtration is suitable for the separation of AGE1.HN cells from the culture broth prior to the extraction of intracellular metabolites. To check, which pore sizes of the filter membrane would give the best results in terms of cell retention and minimum time needed for the filtration procedure, three sizes were tested: 1 µm (Regenerated Cellulose Membrane Filters, Whatman®) and 3 and 5 µm (Cellulose Nitrate Membrane Filters, Whatman®). By applying 2.5–3.0 $\cdot 10^6$ cells per filtration, no cells could be detected in the flow through with all three tested membranes. However, the 1 and 3 µm membranes were clogged immediately leading to substantially longer filtration times compared to the 5 µm membrane. In a next step, it was evaluated, which pressure is gentle enough to separate the cells from the culture broth without damaging the cells and at the same time allowing for a short filtration time. For this test, the 5µm membrane was used with the set-up described under 3.3.2. The lowest applicable pressure was 50 mbar. At this pressure, the whole filtration procedure including the washing step took about 30 s. By increasing the pressure, the filtration time could be reduced down to 10 s. However, already at the lowest pressure of 50 mbar a relative cell damage of 32.6 ± 3.3 % (based on the released LDH) could be detected (see figure 4.4). With increasing applied pressure, the cell damage increased up to 90 %. Moreover, after examining the supernatant of the „flow through" under a microscope, an increasing amount of cell debris with increasing applied pressure was observable.
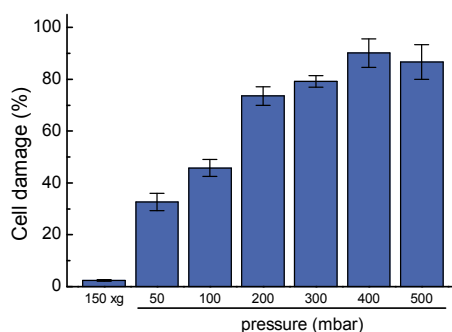
Figure 4.4: Relative cell damage based on the quantification of LDH with the CytoTox assay after filtration of AGE1.HN cells at different applied pre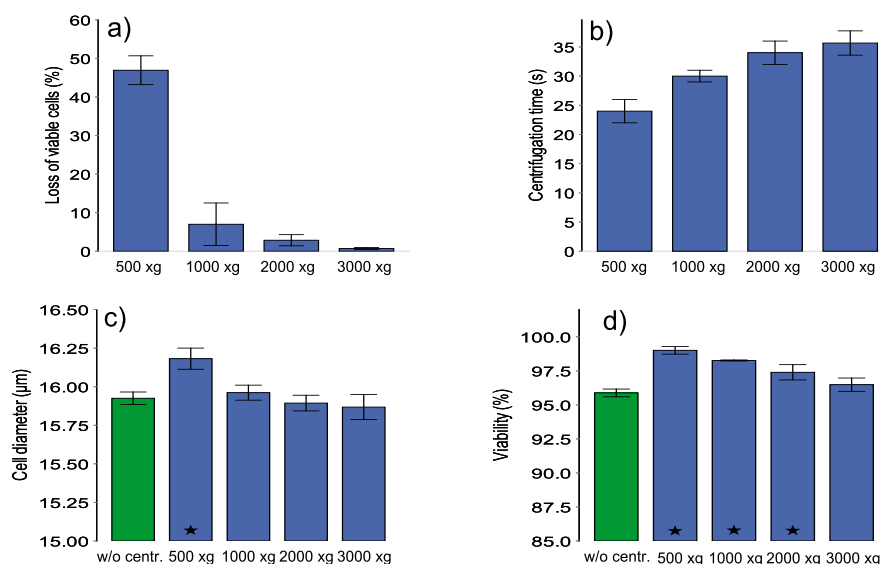ssures compared to centrifugation at 150 xg for 3 min. Shown are the means of three determinations for each setting with the SD as error bar. Exponentially growing cells were taken from routine cultivations in 125 mL shaker flasks (wv=50 mL).

This result is contradictory to the results of Volmer et al. [105]. They established a method for sampling suspended chinese hamster ovary (CHO) cells grown in chemically defined medium based on a fast filtration method. After comparing their method to sampling with a microstructure heat exchanger followed by centrifugation for 1 min or centrifugation without prior quenching, they found that the energy charge ratio (ECR) and the measured intracellular concentrations of glucose, ribose/ribulose 5-phosphate, ADP, ATP, GTP, UDP-glucose (UDP-GLC) were substantially different [105]. Moreover, they determined a relative LDH release of only 4–10 % for applied pressures between 20–80mbar. They used $50 \cdot 10^6$ cells per filtration, which might explain the different result, as the total amount of damaged cells might not be correlated with the total amount of filtered cells. However, applying more cells for filtration would make the investigation of intracellular metabolite concentrations during smaller scale cultivations (wv=0.5–1.0 L) impossible. Moreover, a complete redesign of our extraction method would be necessary, as the original method from Ritter et al. [96] was established for the extraction of 3.0–$6.0 \cdot 10^6$ cells in 2 mL reaction tubes. In addition, Dietmair et al. [101] also found that filtration is not suitable for the separation of CHO cells (grown in serum- and protein-free medium) from the culture broth, as they found only approximately 9 % of the total intracellular metabolite concentration after filtration of the cells.

4.2.1.2 Separation by centrifugation

As filtration seemed not be suitable for this application, centrifugation was chosen as separation method. As can be seen in figure 4.4,. the relative cell damage and the SD for centrifugation at 150 xg was much lower compared to filtration (2.4 ± 0.3 %). However, 3 min for the complete sedimentation of cells is certainly too long. Therefore, it was tested at which centrifugal acceleration and minimum centrifugation time the loss of viable cells is minimal. A volume of 2 mL of exponentially growing AGE1.HN.AAT cells from shaker cultivations were taken and centrifuged in 2.2 mL reaction tubes at different centrifugal acceleration (500, 1000, 2000 and 3000 xg). To assure that the time for centrifugation is as short as possible, the centrifugation was stopped as soon as the pre-set value for the centrifugal acceleration was reached. The supernatant was quickly decanted and the residual supernatant removed by tapping the reaction tube onto a cellulose paper. The cells were

washed with 1 mL 0.9 % NaCl solution and centrifuged again. Then the weight of the reaction tube was determined before and after the NaCl solution was removed and the cells were resuspended in the respective volume of 42-MAX-UB medium followed by the analysis of viable and total cells with the ViCell counter. As can be seen in figure 4.5-a and -b, at 3000 xg the loss of cells was almost zero with an minimum time requirement of 35 s for one centrifugation step. Interestingly, with decreasing centrifugal acceleration the viability increased significantly, which points towards a preferred separation of dead cells (figure 4.5-d). Moreover, also the cell diameter of the sample centrifuged at 500 xg was significantly higher compared to the control sample w/o centrifugation (see figure 4.5-b), probably due to a lower percentage of dead cells with smaller diameters. However, the viability and the cell diameter of cells centrifuged at 3000 xg for 35 s were comparable to the reference (figure 4.5-c and -d). Based on this finding, 3000 xg for 35 s was used as centrifugation setting for the separation of AGE1.HN and AGE1.HN.AAT cells from the supernatant.

Figure 4.5: Evaluation of centrifugation for cell separation. **a)** Loss of viable cells after centrifugation at different centrifugal accelerations, **b)** centrifugation time for one centrifugation step at the respective setting of acceleration, **c)** cell diameter and **d)** viability after centrifugation at different centrifugal accelerations. Exponentially growing AGE1.HN.AAT cells were taken from routine cultivations in 125 mL shaker flasks (wv=50 mL). Shown are the means of three determinations for each setting with the SD as error bar and the significance of difference compared to the sample which was not centrifuged (green bar) based on a one-sided T-Test marked by a star (α=0.05).

4.2.1.3 Evaluation of washing steps

In a next step, it was checked if a washing step is necessary to remove residual amounts of e.g. contaminating extracellular metabolites. A physiological sodium chloride solution (0.9 % NaCl) was used as washing buffer. Overall, $2.5 \cdot 10^6$ AGE1.HN.AAT cells were quenched by transferring the corresponding volume of cell suspension in a reaction tube, followed by 7 s incubation in liquid nitrogen (LIN). Then the cells were centrifuged at 3000 xg for 35 s (0 °C) washed once with 1 mL ice-cold 0.9 % NaCl solution, centrifuged again (3000 xg, 35 s, 0 °C) and extracted. In parallel, a second tube with AGE1.HN.AAT cells was also centrifuged, but without removing the supernatant after the first centrifugation step ($\equiv$ mock washing step). The cell pellet was resuspended in the supernatant, centrifuged again (3000 xg, 35 s, 0 °C) and also extracted. In figure 4.6 and 4.7 the measured metabolite concentrations after the washing step and after the mock

washing step are compared, with significant differences marked by a star. For fructose 6-phosphate (F6P), pyruvate (PYR), succinate (SUC), citrate (CIT) and isocitrate (ICIT) the concentrations in the mock wash samples were higher than in the samples washed with NaCl solution, most likely due to residual concentrations in the supernatant. In contrast to that, higher concentrations were found for fructose 1,6-bisphosphate (FBP), ribose 5-phosphate (R5P), ADP and GDP in the NaCl washed samples, which might be due to ongoing intracellular reactions during sample preparation leading to biased intracellular concentrations. As both time and treatment was the same for the samples with washing step and the samples with a mock washing step, the replacement of the medium by the washing buffer was most likely the cause of this increase in some of the intracellular metabolites after washing with NaCl solution. This increase might indicate a substrate limitation due to the replacement of the medium by the washing buffer, which is further examined and discussed in section 4.2.2.
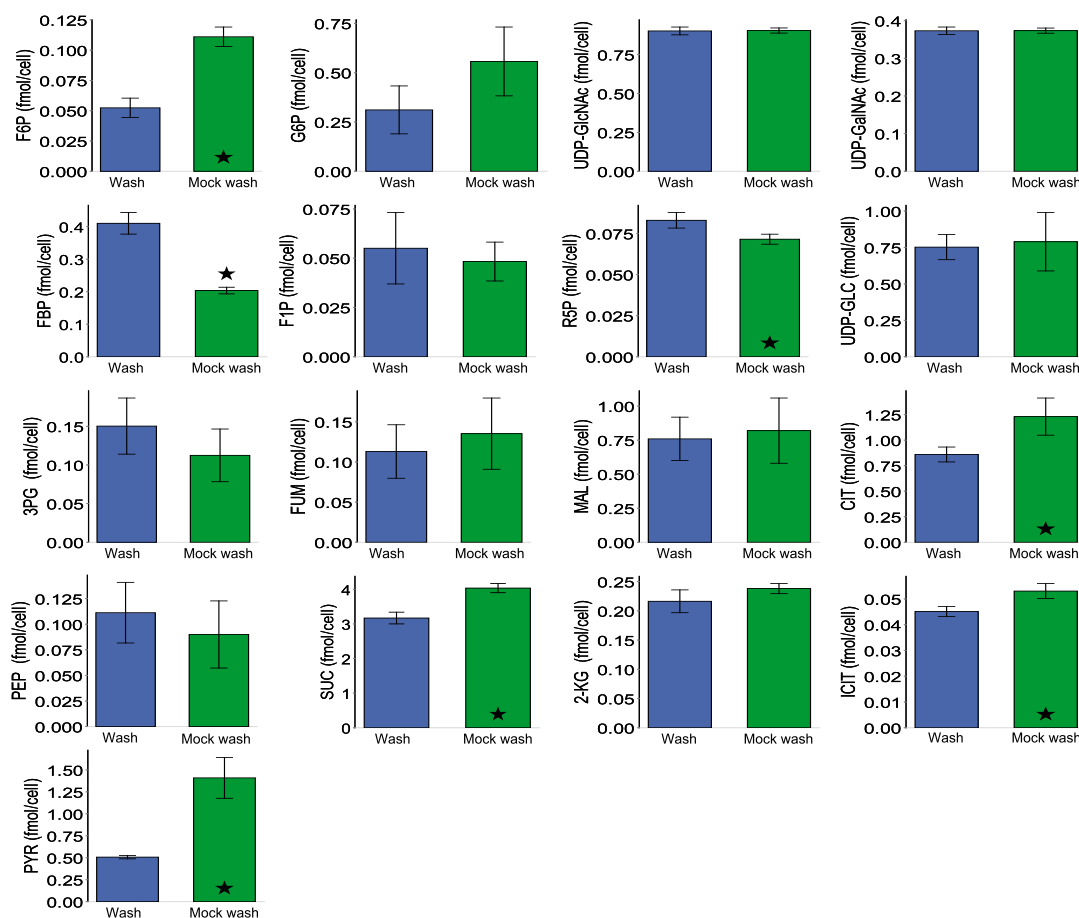
Figure 4.6: Concentrations of intracellular metabolites after a washing step and after a mock washing step in exponentially growing AGE1.HN.AAT cells during a bioreactor cultivation (wv = 2.5 L). The average of three technical replicates and the SD as error bar is shown. Samples with a significant difference based on a one-sided T-Test for equal variance are marked by a star (α=0.05).

For most nucleotides, sugar nucleotides and organic acids, no significant differences were detectable. Though, an increase of intracellular metabolites in the mock wash samples due to metabolites from the supernatant could also be masked by an increase of metabolites in the samples with a washing step due to ongoing intracellular reactions. Therefore, in a second experiment the supernatant of a shaker cultivation with AGE1.HN.AAT cells was measured for intracellular metabolites as described in the materials & methods section (see section 3.4.5.1). Based on the concentration of metabolites in the supernatant, the percentages of metabo-

lites, which would be carried over after extraction of intracellular metabolites with and without a washing step, were calculated for those metabolites, which were found in the supernatant (see figure 4.8-a and -b). For this calculation, a worst case scenario was assumed, with residual amounts of 20µL culture broth or washing buffer after removal of the supernatant and underestimated metabolite concentrations from the supernatant by 70 %. After extraction without a washing step, the intracellular concentrations for cis-aconitate (CIS-ACO), UDP, ICIT, glucose 6-phosphate (G6P), fumarate (FUM), CIT, PYR, AMP, F6P and R5P would be largely build up by metabolites from the supernatant (31.0–94.4 %, see figure 4.8-a). The same metabolites were found to have higher concentrations after a mock washing step (figure 4.6). However, with a washing step the largest contamination was found for PYR with a value of 2.6 % (figure 4.8-b). Based on this risk assessment, one washing step is therefore required and should be sufficient to reduce the percentage of contaminating metabolites from the supernatant.
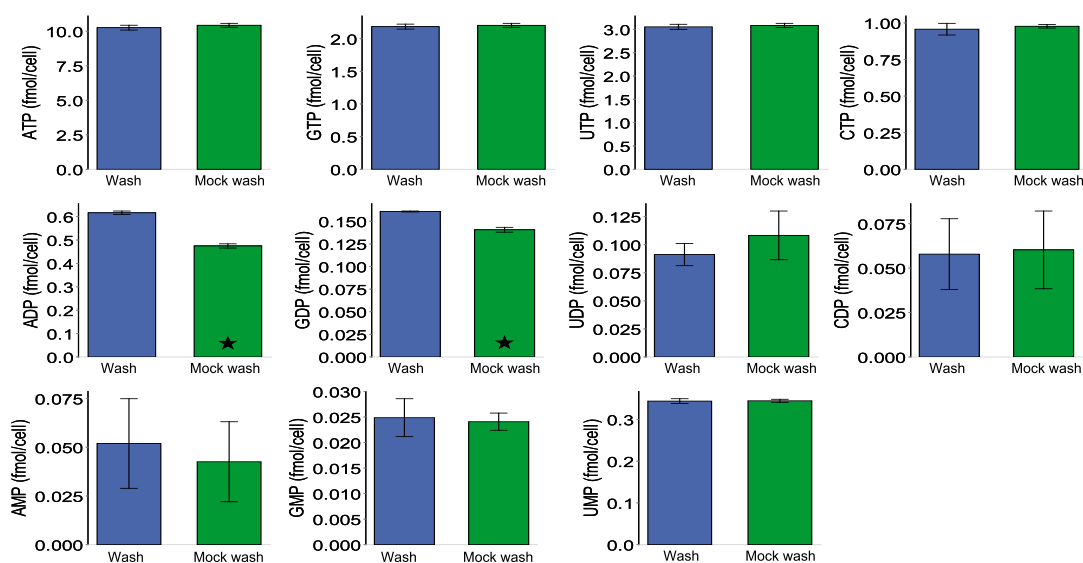
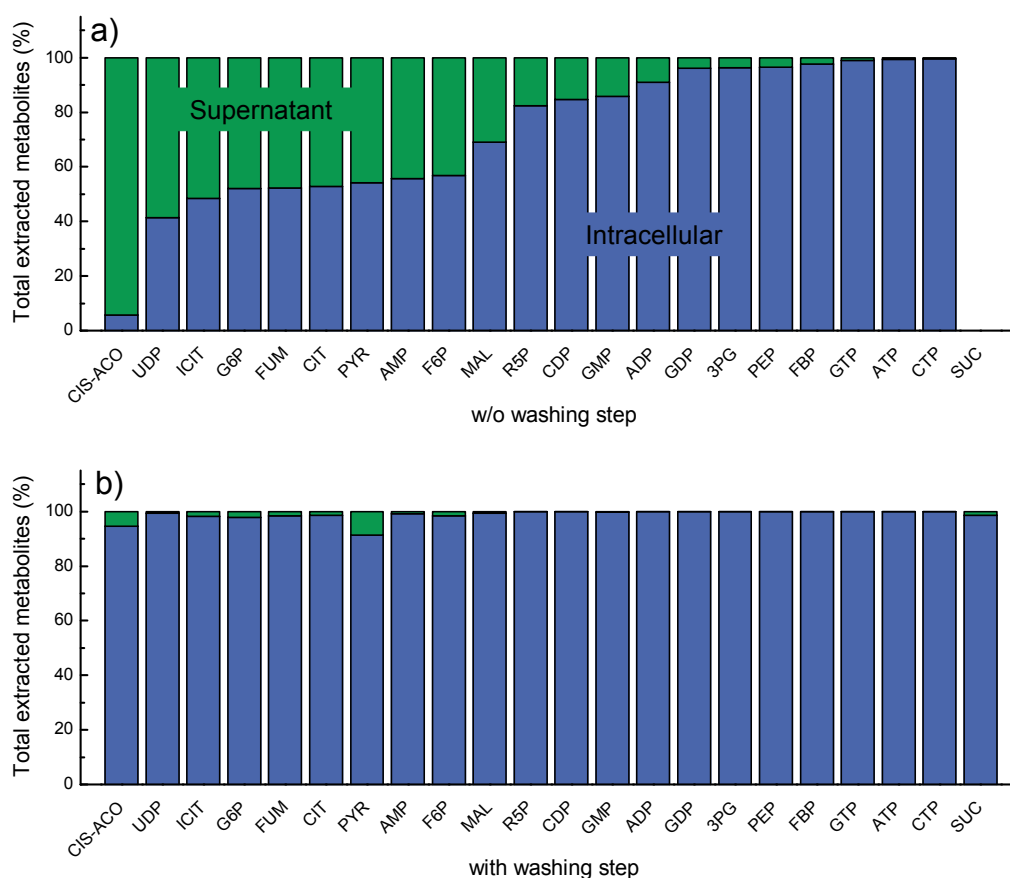**Figure 4.7:** Concentrations of intracellular nucleotides after a washing step and after a mock washing step in exponentially growing AGE1.HN.AAT cells during a bioreactor cultivation (*wv*=2.5 L). The average of three technical replicates and the SD as error bar is shown. Samples with a significant difference based on a one-sided T-Test for equal variance are marked by a star (α=0.05).

Figure 4.8: a) Percentage of intracellular metabolites (blue bars) and metabolites from the supernatant (green bars) after extraction without a washing step and **b)** with a washing step (due to its high concentration in the supernatant, succinate could not be evaluated for the samples without a washing step and is therefore missing in subfigure a)).

Finally, to check if leakage of intracellular metabolites during washing and centrifugation at 3000 xg occurs, AGE1.HN.AAT cells were washed three times with 1 mL ice-cold 0.9 % NaCl solution after sampling from a shaker cultivation without fast cooling prior the first centrifugation step. The respective supernatant after each washing step was then analysed. SUC, CIT, 2-ketoglutarate (2-KG), ATP, malate (MAL), fructose 1-phosphate (F1P), G6P, F6P, UDP-GLC, ICIT and CIS-ACO could be found in the washing buffer after one washing step. However, except for SUC, all concentrations were below the working range of the LC-MS method and therefore possibly near the detection limit (figure 4.9). For most metabolites, leakage is therefore probably not relevant. Even though, this cannot be said for

metabolites, which have low intracellular concentrations (e.g. FUM, CIS-ACO, F1P, F6P and ICIT), therefore leakage might occur to a certain (small) extend for these metabolites.
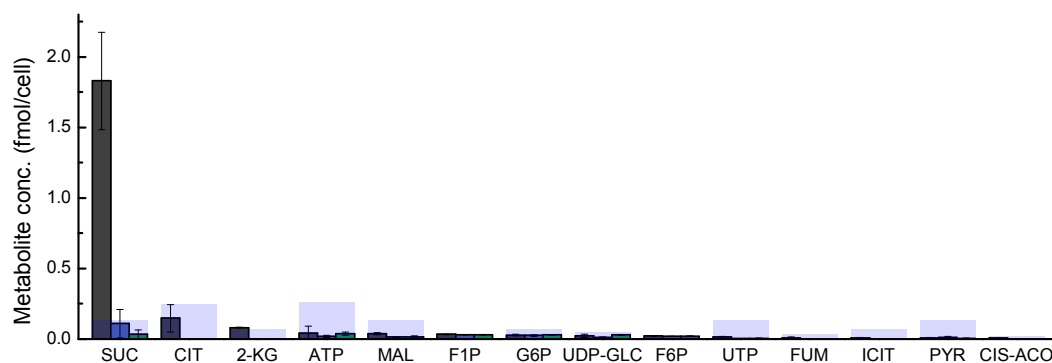
Figure 4.9: Concentrations of intracellular metabolites found in the washing buffer after a single washing step (dark gray bars), after two washing steps (blue bars) and after three washing steps (green bars). Shown are the means of three determinations with the SD as error bar and the lowest standard of the working range as blue background. Exponentially growing AGE1.HN.AAT cells were taken from routine cultivations in 125 mL shaker flasks (*wv*=50 mL).

As found by Kapoore et al. [106], leakage of intracellular metabolites is highly dependent on the cell type and, of course, on the sampling and quenching protocol used. Kronthaler et al. [102], for example, tested different centrifugation settings (1 min @ 1000-2000 xg) as well as additional washing steps with precooled PBS (one, two, and three times) for a CHO cell line grown in a chemically defined medium and found that none of the tested settings led to a significant change of viability as measured by trypan blue staining with a ViCell counter. This is in contrast to the results with the AGE1.HN.AAT cell line (see figure 4.5), but could be explained by the longer centrifugation times of 1 min in the study of Kronthaler et al. [102], allowing the complete sedimentation of dead cells at centrifugation settings < 3000 xg. By applying propidium iodide (PI) staining, Dietmair et al. [101] tested, if quenching and washing of CHO cells (Super-CHO, C2.8 SPF) with ice-cold NaCl solution, could induce leakage due to disruption of the cell membrane. They argued that in case PI is able to enter the cells, it is reasonable to expect that smaller intracellular metabolites might be able to leak from the cells. Neither the high centrifugation speed (1 min @ 1000 xg) did damage the cells, nor did washing and quenching with ice-cold NaCl solution damage the cells to a significant amount.

Then, they verified the extent of leakage based on the quantification of ATP, ADP, AMP, serine and NAD in the supernatant and in the cell extract after quenching and washing with ice-cold NaCl solution. For these metabolites, in agreement with the result obtained here for the AGE1.HN.AAT cell line, they could not find that leakage occurs to a significant amount [101]. In contrast to that, Volmer et al. [105] found that in their study with a different CHO cell line (CHO DP12, ATCC, CRL-12445), using physiological NaCl solution for washing, about 50 % of the total PYR bled from the cells. They argued that the efflux of PYR was caused by concentration driven transport, rather than by diffusion across the membrane and concluded that the higher release of PYR from the cells compared to lactate dehydrogenase (LDH) release during sampling was caused by transporters rather than cell disruption [105]. However, for the AGE1.HN.AAT cell line, significant concentrations of PYR could not be found in the supernatant after washing with ice-cold NaCl solution and centrifugation at 3000 xg (see figure 4.9).

4.2.2 Quenching of cell metabolism

As illustrated in section 2.3, the applied method for the quantification of intracellular metabolites should be able to stop the metabolism sufficiently enough to stabilize the intracellular metabolite profiles without inducing cell damage or leakage of metabolites from the cell. To check whether maximum enzyme activities could be sufficiently reduced at 0 °C, the activities of hexokinase (HK), G6P dehydrogenase (G6PDH), phosphoglucose isomerase (PGI), fructose-6-phosphatekinase (phosphofructokinase) (6PFK) and fructose-bisphosphate aldolase (FBPA) were determined after quenching of AGE1.HN cells from 37 °C to 0 °C with liquid nitrogen (LIN) (cells were taken from shaker flask cultivations). As can be seen in figure 4.10, the residual maximum activities of all five enzymes of the upper part of the glycolylsis could be reduced to values below 10 % compared to their activities at 37 °C. However, the total enzyme activity, especially of PGI, was still high at 0 °C (1502 fmol/(cell h)) compared to a specific glucose uptake rate during the exponential growth phase in bioreactors of 130 fmol/(cell h). PGI is a dimeric enzyme that catalyses the reversible isomerization of G6P to F6P. During batch cultivations (see section 4.3.4.1) the trajectories of G6P and F6P were highly correlated (R>0.99) indicating that the reactions catalyzed by PGI are near-equilibrium and the glycolytic

flux is probably controlled at other points then the PGI reaction. However, this results underpins the need for a reliable and fast sampling procedure, as also other enzymes (possibly catalysing non-equilibrium reactions) are still active enough at 0 °C to alter the intracellular metabolite pools during sampling. Therefore, to reduce the overall sampling time, the centrifugation steps were optimized to a minimum as described before. In a next step, two different quenching methods were compared: first, quenching with a heat exchanger coupled to a sampling system (see section 3.3.3 for the set-up) and second, quenching with liquid nitrogen (LIN). For adherent cells, quenching with LIN was already reported in literature [100]. However, for suspension cell lines no data on quenching with LIN was available so far.
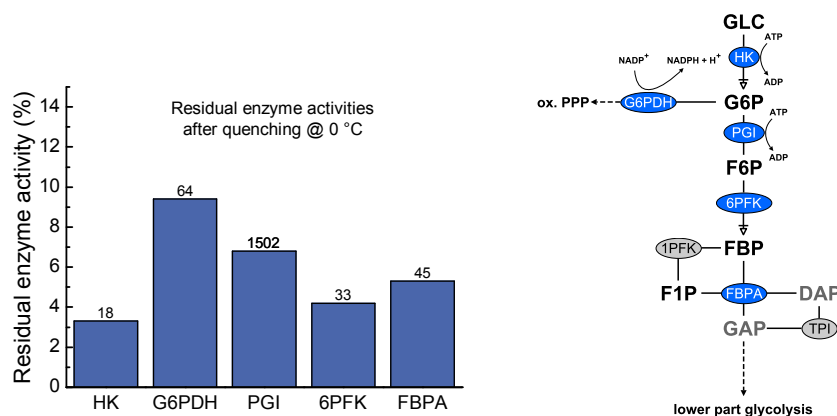
Figure 4.10: Residual enzyme activities at 0 °C of enzymes of the upper part of glycolysis (see illustration on the right side of the diagramm) after quenching at 37 °C. The bars represents the residual activity in percent and the numbers above the bars the absolute activities in fmol/(cell h) at 0 °C.

For the characterization of both quenching methods, the temperature of the cell suspension directly after quenching and the energy charge ratio (ECR) were determined during two bioreactor cultivations (*wv* = 2.5 L) with AGE1.HN.AAT cells in 42-MAX-UB. According to Vuckovic [147], the ECR can be used to evaluate the metabolism quenching potential of different sample preparation methods. ATP, ADP and AMP have fast turnover rates with half lives less than 0.1 s, which makes the calculated ratio ([ATP]+0.5[ADP])/([ATP]+ [ADP]+[AMP]) ideal for evaluating the efficiency of the quenching method [147]. In figure 4.11-a the ECR after quenching with a heat exchanger coupled to a sampling system and after quenching with LIN are shown, together with unquenched control samples (manually taken through a

drain valve). All three conditions show the same increasing trend during the exponential growth phase starting at 0.94 and reaching almost 0.97. However, the ECR after quenching with the heat exchanger was clearly below the ECR of the unquenched samples. In between are the samples, which were quenched with LIN. Typically, a ratio of 0.80–0.95 can be expected for growing mammalian cells [147], but also for yeast, plant and *E. coli* cells similar ratios are reported in literature [148]. As can be seen in figure 4.11-a, after the exponential growth phase, the ECR decreased for the samples quenched with the heat exchanger below 0.93. For the unquenched sample, as well as for the samples quenched with LIN, only a slight decrease of the ECR was observable. As the decrease of the ECR in the heat exchanger samples was perfectly correlated with the onset of the transition from exponential to stationary growth (which will be illustrated and discussed later on in section 4.3) and therefore also with changes in other metabolites (e.g. from glycolysis), it seems that the heat exchanger allowed a more efficient quenching of the cell metabolism as with LIN. The reason for this might be due to the fact that with the LIN quenching method it is not possible to achieve as reproducible end-temperatures of the cell suspension as with the heat exchanger. In figure 4.11-b it can be seen that the overall range as well as the interquartile range was much higher for the samples quenched with LIN compared to the heat exchanger samples. Moreover, the cell suspension quenched with LIN showed a large temperature gradient, with temperatures around 10 °C at the surface and temperature of almost zero degree at the bottom of the reaction tube (compare overall range for LIN in figure 4.11-b). In contrast to that, the cell suspension quenched with the heat exchanger had a homogeneous temperature profile from the surface to the bottom of the reaction tube with a mean of 1.67 °C and a median of 1.55 °C. Therefore, LIN seems not adequate for quenching of the cell metabolism of AGE1.HN.AAT cells. In contrast to that, the sampling system coupled with a heat exchanger provided reproducible quenching results in terms of reached end-temperature of the cell suspension. Moreover, the obtained ECR profile could be linked to different growth phases, which were determined based on specific uptake rates obtained with a simple cell growth model (see section 4.3.2).
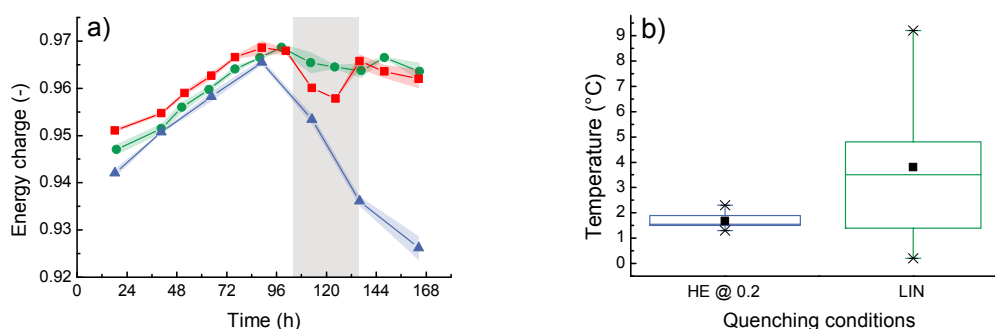
Figure 4.11: a) ECR during two bioreactor cultivations with AGE1.HN.AAT cells. Shown are averages of three technical replicates and the SD as shaded background (■: samples w/o quenching, ▲: samples quenched with heat exchanger (cultivation 1) and ●: samples quenched in LIN (cultivation 2)) and **b)** box plot of temperatures after quenching with heat exchanger (blue) and LIN (green). The transition from the exponential to the stationary phase is indicated by a light grey background (a) and the highest and lowest measured temperatures (b) are indicates by asterisks (HE = heat exchanger).

Finally, the proposed sampling procedure is shown in figure 4.12. In the next two sections, this sampling and quenching procedure is characterized in terms of cell damage and overall efficiency.
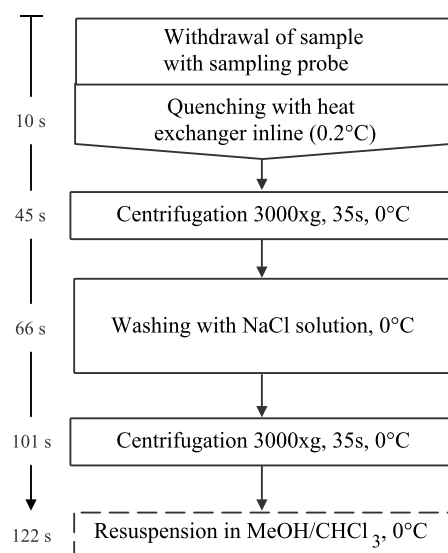
Figure 4.12: Flow chart for sampling and quenching of AGE1.HN and AGE1.HN.AAT cells for the determination of intracellular metabolites. The required time for each step is given in seconds on the left side.

4.2.3 Cell damage during automated sampling and quenching

Cell damage due to automated sampling and quenching with the heat exchanger was investigated for a bioreactor cultivation (wv = 2.5 L) with AGE1.HN.AAT cells. As control, samples were taken manually followed by the determination of viable cell concentrations, viabilities and cell diameters with the ViCell counter. As can be seen in figure 4.13, the concentrations of viable cells and the viability seemed to be slightly lower after quenching with the heat exchanger compared to the control samples, whereas the cell diameter seemed to be clearly increased after sampling and quenching with the heat exchanger.
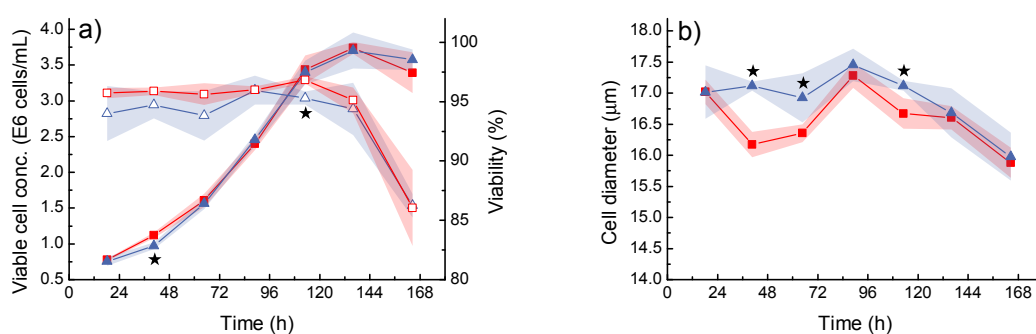
Figure 4.13: a) Viable cell concentrations (filled symbols) and viability (open symbols) and **b)** cell diameters during bioreactor cultivations (wv = 2.5 L) with AGE1.HN.AAT cells. Shown are averages of four technical replicates and the SD as shaded background. (■: samples w/o quenching and ▲: samples quenched with heat exchanger). Samples with a significant difference are marked by a star (α=0.05, one-sided T-Test for equal variance).

To clarify, if the decrease in viable cell concentrations and increase in cell diameters were induced by the sudden temperature drop or the sampling system (including the heat exchanger), exponentially growing cells from a second bioreactor cultivation were sampled either with the sampling system and the heat exchanger set to 0.2 °C or with the uncooled heat exchanger at room temperature. As can be seen in figure 4.14, the decrease of the viable cell concentration and the viability was independent of the heat exchanger temperature. Also, the increase in cell diameter and the increased release of LDH to the supernatant were not induced by the sudden temperature drop. Accordingly, the observed cell damage was most likely induced by shear stress within the tubes and/or channels of the sampling system and the heat exchanger. As the with the ViCell counter determined circularity of the cells also decreased, the observed increase in cell diameter was probably an

artefact of the ViCell counter, as the software tends to overestimate the diameter of cells, which are not perfectly round (not shown). However, taken together, the observed cell damage induced by the sampling system and the heat exchanger was tolerable given the advantages of a reproducible and fast temperature drop of a cell suspension sample for the determination of intracellular metabolites. However, to obtain reliable values for the cell volume during experiments, cell diameters should be determined from manually taken samples to avoid overestimation of the cell volume.
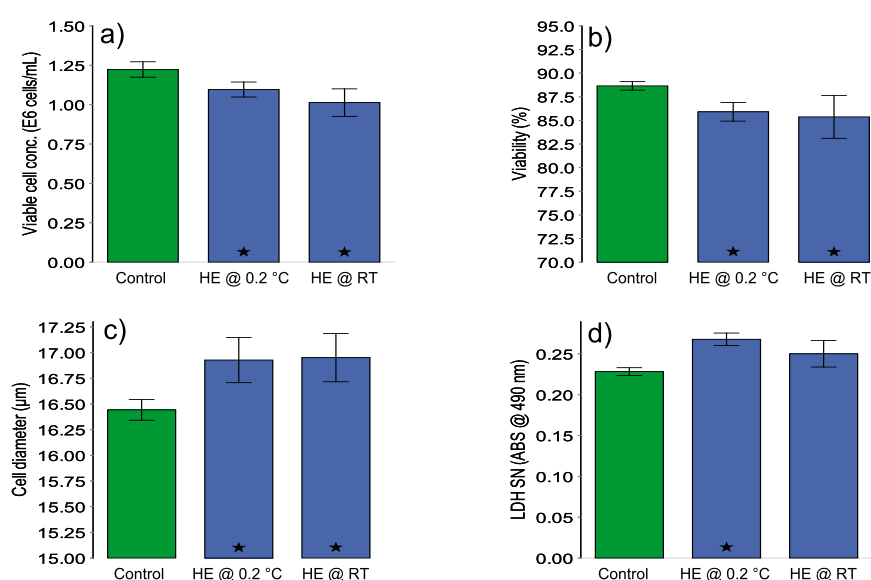
Figure 4.14: a) Concentrations of viable cells, **b)** viabilities, **c)** cell diameters and **d)** LDH in the supernatant from exponentially growing AGE1.HN.AAT cells in 42-MAX-UB during a bioreactor cultivation (*wv* = 0.5 L) after sampling with a sampling system coupled to a heat exchanger set to 0.2 °C and at room temperature compared to samples, which were taken manually through a drain valve without quenching (control). Shown are the averages of four technical replicates and the SD as error bars, with the significance of difference compared to the control samples based on a one-sided T-Test marked by a star (α=0.05).

4.2.4 Efficiency of the sampling and quenching procedure

As it was hypothesized earlier in section 4.2.1, a substrate limitation caused by the sample preparation procedure might have led to biased intracellular metabolite concentrations during the mock-wash experiment. To clarify to which extend

and at which point during the sampling and quenching procedure the intracellular metabolite concentrations are being adulterated, a full mass balance for metabolites in different sample fractions from AGE1.HN.AAT cells grown in a bioreactor and a shaker flask was determined. For this, a protocol was established for the extraction of metabolites from cells directly in culture broth (see section 3.4.5.3). The recovery of metabolites from the standard stock solution was determined in water and in culture broth by adding 20 µL standard stock solution to 500µL Milli-Q water or to 500 µL cell suspension from a shaker cultivation. The recovery in water was very high with an average of 96.9 ± 4.2 %. Except for 3PG (129.2 ± 33.5 %) and R5P (47.9 ±18.7 %) the recoveries in culture broth were between 80.1 and 106 % with an average recovery of 92.9 ± 6.0 % (table 4.3). The mass balances were then calculated according to the scheme shown in figure 4.15. Briefly, after sampling with the sampling system and quenching with the heat exchanger, intracellular metabolite concentrations were determined after removal of the culture broth with and without washing step and in the supernatant after the first and the second centrifugation step. The mass balances calculated by adding up all sample fractions, were then compared to the whole broth extraction.
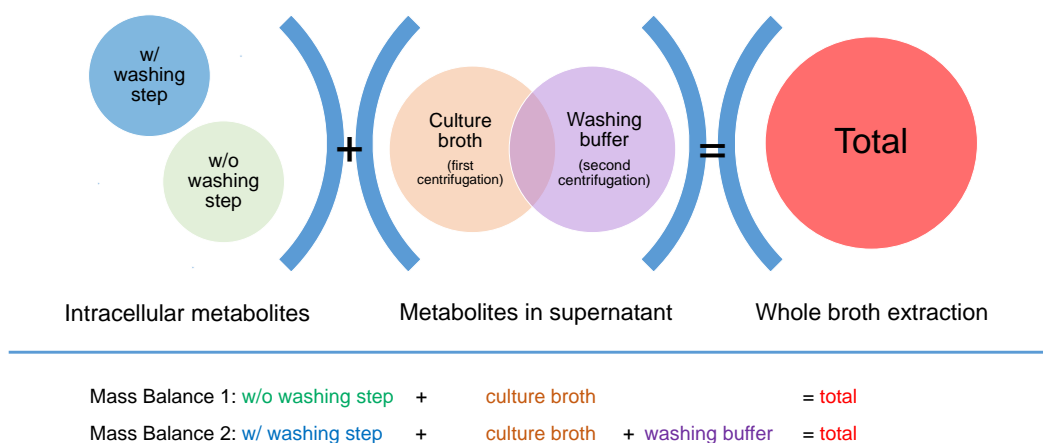
Figure 4.15: Scheme for the determination of metabolites in different sample fractions and the calculation of mass balances for the estimation of the efficiency of the whole sampling and quenching procedure. w/ = with; w/o = without.

Table 4.3: Recoveries of standard metabolites in water and culture broth (spiked with 20 µL standard mix) after whole broth extraction with the established extraction method. Shown are the averages of six technical replicates and the SDs.

Metabolite	Recoveries of standard in	
	Water %	Culture broth %
3PG	90.8 ± 31.7	129.2 ± 33.5
ADP	95.2 ± 6.1	87.9 ± 4.2
AMP	95.2 ± 5.6	86.3 ± 13.7
ATP	95.5 ± 5.6	94.8 ± 5.7
CDP	100.6 ± 31.9	96.2 ± 10.6
CIT	91.7 ± 15.4	87.0 ± 19.6
CTP	95.0 ± 5.9	93.3 ± 15.1
FBP	93.6 ± 5.8	91.8 ± 9.4
F1P	103.2 ± 27.6	104.4 ± 21.0
F6P	102.0 ± 27.9	99.3 ± 24.8
FUM	105.7 ± 41.9	84.9 ± 19.3
GDP	96.9 ± 5.3	92.7 ± 4.8
G6P	100.1 ± 28.5	103.0 ± 21.7
GMP	98.2 ± 8.0	96.5 ± 10.4
GTP	94.9 ± 6.5	101.7 ± 5.7
ICIT	97.9 ± 13.9	91.9 ± 9.2
2-KG	96.9 ± 23.8	92.1 ± 20.2
MAL	104.9 ± 16.4	90.3 ± 20.3
PEP	96.0 ± 26.4	93.5 ± 16.3
PYR	88.6 ± 6.4	91.5 ± 5.3
R5P	97.9 ± 25.8	47.9 ± 18.7
SUC	89.8 ± 16.6	80.1 ± 10.4
UDP	98.9 ± 7.9	106.0 ± 31.2
UDP-GalNAc	95.4 ± 5.5	91.2 ± 4.6
UDP-GLC	97.4 ± 22.6	90.7 ± 35.0
UDP-GlcNAc	94.8 ± 5.9	88.3 ± 6.5
UMP	101.8 ± 33.0	91.5 ± 15.8
UTP	95.1 ± 5.7	89.3 ± 2.8

As can be seen in table 4.4 mass balance closure could not be achieved for all metabolites, which indicates the turnover of metabolites due to not fully stopped enzymatic reactions. For the samples from the bioreactor cultivations, significant higher concentrations were found for 3PG (+32 %), FBP (+40) and PEP (+30 %), whereas significant lower concentrations were found for G6P (-26 %), 2-KG (-23 %), GDP (-24 %) and UDP (-27 %). In addition, for the samples from the shaker flask cultivation, significant lower concentrations were also found for ADP (-28 %) and F6P (-32 %). For all other metabolites only slight differences were found after performing the full mass balance compared to the whole culture broth extraction. Moreover, the differences were larger for mass balance 2 and hence after the washing step. Same metabolites were found having significant higher or lower concentrations during the mock-wash experiment and accordingly confirms the aforementioned hypothesis that biased concentrations for some metabolites after the whole sample and quenching procedure are induced by substrate limitation. However,

differences between mass balance 1 and the whole broth extraction could also be observed for some metabolites (e.g. for FBP). An explanation for this might be a limitation of the cells already induced by the first centrifugation step as cells near the bottom of the reaction tube are sooner isolated from the culture broth as cells on top of the pellet.

Table 4.4: Concentrations of metabolites after extraction of the whole culture broth (total) and calculated mass balances MB1 and MB2 according to the scheme shown in figure 4.15.

Metabolite[a]	Bioreactor cultivation			Shaker cultivation		
	Total fmol/cell	MB1 fmol/cell	MB2 fmol/cell	Total fmol/cell	MB1 fmol/cell	MB2 fmol/cell
3PG ↑ (+32 %)	0.12 ± 0.00	0.12 ± 0.02	0.15 ± 0.01 *	1.24 ± 0.42	1.30 ± 0.33	1.22 ± 0.54
ADP ↓ (-28 %)	0.87 ± 0.04	0.75 ± 0.02 *	0.73 ± 0.03 *	0.88 ± 0.07	0.49 ± 0.00 *	0.63 ± 0.16
AMP	0.11 ± 0.00	0.13 ± 0.04	0.12 ± 0.04	0.17 ± 0.05	0.17 ± 0.04	0.18 ± 0.06
ATP	10.09 ± 0.25	10.02 ± 0.11	9.96 ± 0.21	6.93 ± 0.29	7.41 ± 0.11 *	7.64 ± 0.11 *
CDP	0.21 ± 0.02	0.19 ± 0.07	0.19 ± 0.07	0.14 ± 0.01	0.12 ± 0.03	0.14 ± 0.02
CIT	21.80 ± 1.15	18.84 ± 0.50 *	18.61 ± 0.78 *	12.48 ± 0.77	13.88 ± 1.00	13.49 ± 0.86
CTP	1.18 ± 0.02	1.03 ± 0.03 *	1.00 ± 0.03 *	0.77 ± 0.06	0.78 ± 0.03	0.81 ± 0.03
FBP ↑ (+40 %)	1.09 ± 0.02	1.18 ± 0.05 *	1.52 ± 0.12 *	0.56 ± 0.12	0.93 ± 0.07 *	1.14 ± 0.12 *
F1P	0.53 ± 0.03	0.50 ± 0.03	0.50 ± 0.04	0.41 ± 0.10	0.40 ± 0.09	0.37 ± 0.09
F6P ↓ (-32 %)	0.38 ± 0.02	0.41 ± 0.07	0.33 ± 0.06	0.58 ± 0.10	0.43 ± 0.07	0.40 ± 0.07 *
FUM	0.74 ± 0.05	0.67 ± 0.05	0.66 ± 0.05	1.03 ± 0.08	0.96 ± 0.13	1.05 ± 0.33
GDP ↓ (-24 %)	0.16 ± 0.01	0.13 ± 0.01 *	0.12 ± 0.01 *	0.60 ± 0.09	0.52 ± 0.01	0.55 ± 0.02
G6P ↓ (-29 %)	1.17 ± 0.05	1.25 ± 0.18	0.83 ± 0.09 *	1.87 ± 0.30	1.53 ± 0.27	1.44 ± 0.29
GMP	0.03 ± 0.00	0.04 ± 0.00 *	0.03 ± 0.00	0.04 ± 0.00	0.05 ± 0.00	0.05 ± 0.01
GTP	2.10 ± 0.05	2.06 ± 0.02	2.07 ± 0.05	1.63 ± 0.02	1.75 ± 0.03 *	1.82 ± 0.02 *
ICIT	1.18 ± 0.09	1.02 ± 0.03 *	1.01 ± 0.05 *	1.22 ± 0.13	1.15 ± 0.10	1.24 ± 0.12
2-KG ↓ (-23 %)	1.08 ± 0.03	0.93 ± 0.07 *	0.83 ± 0.11 *	0.21 ± 0.06	0.21 ± 0.11	0.19 ± 0.11
MAL	3.77 ± 0.09	3.75 ± 0.40	3.67 ± 0.46	4.74 ± 0.94	4.14 ± 0.55	4.30 ± 0.98
PEP ↑ (+30 %)	0.11 ± 0.01	0.10 ± 0.01	0.14 ± 0.00 *	0.08 ± 0.02	0.08 ± 0.01	0.08 ± 0.02
PYR	70.64 ± 16.01	51.94 ± 8.73	50.82 ± 9.04	5.51 ± 1.41	5.83 ± 1.13	6.42 ± 0.12
R5P	0.06 ± 0.01	0.06 ± 0.01	0.08 ± 0.01	0.12 ± 0.06	0.14 ± 0.03	0.15 ± 0.06
SUC	51.22 ± 1.91	44.91 ± 2.09 *	43.94 ± 4.29	116.21 ± 14.63	97.01 ± 3.15	108.76 ± 2.66
UDP ↓ (-27 %)	0.16 ± 0.02	0.12 ± 0.01	0.11 ± 0.01 *	0.37 ± 0.23	0.32 ± 0.03	0.36 ± 0.02
UDP-GalNAc	0.42 ± 0.01	0.45 ± 0.03	0.44 ± 0.02	0.29 ± 0.01	0.32 ± 0.01 *	0.33 ± 0.01 *
UDP-GLC	0.59 ± 0.06	0.69 ± 0.09	0.62 ± 0.14	0.20 ± 0.04	0.23 ± 0.06	0.21 ± 0.06
UDP-GlcNAc	0.96 ± 0.04	1.00 ± 0.03	0.98 ± 0.03	0.91 ± 0.06	0.79 ± 0.02 *	0.84 ± 0.03
UMP	0.38 ± 0.03	0.40 ± 0.11	0.35 ± 0.11	0.62 ± 0.08	0.62 ± 0.13	0.53 ± 0.11
UTP	2.64 ± 0.07	2.81 ± 0.03 *	2.80 ± 0.07 *	0.84 ± 0.03	1.00 ± 0.01 *	1.00 ± 0.02 *

Samples were taken during a bioreactor cultivation (*wv*=0.5 L) and a shaker cultivation (*wv*=0.02 L) with AGE1.HN.AAT cells. Shown are averages of three technical replicates and the SDs. Significant different concentrations based on a one-sided T-Test (α=0.05) of mass balance 1 and 2 compared to the total measurement are marked with an asterisk.

a: Downward pointing arrows indicates significant lower, whereas upward pointing arrows indicates significant higher concentrations after the whole sample preparation procedure (MB2) for those metabolites with a magnitude of difference > 20 % compared to the whole broth extraction of samples from the bioreactor cultivation.

So far, most authors evaluated their sampling and quenching method on the basis of ATP, AMP and ADP concentrations only [101–103, 105]. For example, Dietmair et al. [101] showed that the concentration of intracellular ATP in cell extracts from NaCl quenched cultures was significantly higher than in an unquenched control sample.

Furthermore, they could demonstrate that after incubating cells in ice-cold NaCl for 10, 5, or 0 min, the intracellular ATP concentrations of NaCl quenched cells was not significantly different from the ATP concentrations of directly extracted cultures, but was significantly higher than in unquenched control samples [101]. In contrast to that, Volmer et al. [105] found higher ATP concentrations in filtered cells compared to cells quenched with a heat exchanger followed by centrifugation. However, the evaluation of a sampling and quenching method for mammalian suspension cells based on the quantification of a large range of metabolites from glycolylsis, TCA-cycle and nucleotide metabolism has not been carried out so far. In both mass balance experiments performed here, the intracellular concentration of ATP after quenching with the heat exchanger were the same or slightly higher compared to the ATP concentrations obtained after the whole broth extraction (see table 4.4). However, comparing also other metabolites, larger differences were found (e.g. for FBP), demonstrating that the sampling preparation method has an impact on the intracellular metabolite concentrations. By taking only a few „representative" metabolites for the evaluation of sampling and quenching methods into account, over- and underestimated concentrations of other metabolites remain certainly undetected. For example in the study of Dietmair et al. [101], the time were the cells were most likely subject to a substrate limitation after quenching in NaCl solution was much longer then in this work.

For yeast cells, Canelas et al. [149] carried out a full mass balance, to determine the extent of leakage during a study of different quenching conditions. However, for the AGE1.HN.AAT cells, leakage could not be determined in this work as the metabolite concentrations found in the washing buffer were for most metabolites negligible. In the study of Canelas et al. [149], the „true" intracellular metabolite concentrations were determined by the so called „differential method", by subtracting the supernatant from the culture broth from the whole broth extraction. According to Canelas et al. [149], a major disadvantage of this method is the error propagation associated with the subtraction, because metabolite concentrations in the supernatant of the culture broth might be very dilute and difficult to assay reliably. Moreover, the error is further amplified if the extracellular concentration is large compared to the intracellular concentration (two large numbers being subtracted to obtain a small number). This was also observed in this work, especially for all metabolites, which can be found in large quantities in the culture

broth, e.g. PYR, FUM, SUC, MAL, CIT, ICIT, G6P, F6P, AMP and UDP. A routine application of the differential method is therefore at least for the investigation of AGE1.HN.AAT cells not advisable. Moreover, as the amount of extracted metabolites is restricted due to the presence of the culture broth, the differential method would only be applicable for experiments with cell concentrations greater than $2 \cdot 10^6$ cells/mL. Therefore, the method of choice would still be a procedure allowing immediate and full quenching of the metabolism, together with the complete separation of cells from the culture broth.

4.2.5 Summary

Taken all results together, after fast sampling with a probe and simultaneously quenching with a heat exchanger, intracellular concentration of metabolites from nucleotide metabolism were significantly different compared to unquenched cells. Following fast separation without loss of cells through centrifugation at 3000 xg for 35 s and an inevitable washing step, intracellular concentrations of most metabolites remained unchanged according to the mass balance, with the exception of 3PG, FBP, PEP, F6P, G6P, 2-KG, ADP, GDP and UDP. Therefore, as for the investigation of AGE1.HN.AAT cells during batch and continuous cultivations the sampling and quenching procedure was the same (if not stated otherwise), the impact of not fully stopped enzymatic reactions during sampling was assumed to be constant and for most metabolites only a small error.

4.3 Batch cultivations

To study the response of intermediates of the central metabolism, of nucleotides, and of maximum enzyme activities to changing culture conditions that are typically observed during batch cultivations, two biological replicates with AGE1.HN.AAT cells were performed for batch cultivations with 20 L, 2.5 L and 0.5 L *wv*, respectively. To obtain comparable results, setup and equipment were the same for all replicate cultivations. The setup was kept simple and as close as possible to a typical industrial recombinant protein production process with mammalian cells. The following results and the discussion about the metabolism of AGE1.HN.AAT cells during this batch cultivations were published in the Journal of Biotechnology [150].

4.3.1 Cell growth, metabolism and A1AT production

Batch cultivations with the AGE1.HN.AAT cell line in three different scales were performed with control of the temperature at 37 °C, dissolved oxygen (DO) at 40 % and pH value at 7.15 as described in section 3.2.2. Each cultivation for the respective scale was performed twice, yielding in total six independent batch cultivations. As can be seen in figure 4.16-a, cell growth was similar for all six cultivations with maximum viable cell concentrations between $3.7 - 4.9 \cdot 10^6$ cells/mL reached after about 131–140 h. Also, the time courses of the cell diameters were comparable, with values between 15.6–16.6 μm (0–72 h) and after about 120 h steadily decreasing to values of 13.8–16.3 μm (figure 4.16-b). However, the cell diameters at 0 h were quite different, with the highest diameters of 16.5–16.6 μm for the first replications of the 20 L and the 2.5 L cultivations and the lowest diameter of 15.6 μm for replication 2 of the 20 L cultivations. The product A1AT showed a similar trend to the time profiles of the viable cell concentrations and reached the highest concentration after about 140 h (figure 4.16-c). However, the end concentrations of A1AT in the 20 L were noticeably lower, yielding only low cell-specific A1AT productivities of 5.09 and 6.95 pg/cell day, whereas the productivities in the other four cultivations were much higher (8.37–14.03 pg/cell day). Additionally, the lactate concentrations at the end of both 20 L cultivations were also noticeably lower compared to the other four cultivations (see figure 4.16-d), with comparatively low yields of lactate from glucose of 1.24–1.34 mol/mol. For the smaller scale cultivations the lactate yield

from glucose was higher, with values between 1.50–1.74 mol/mol, which were also reported for other mammalian cells grown in batch mode [8, 9].
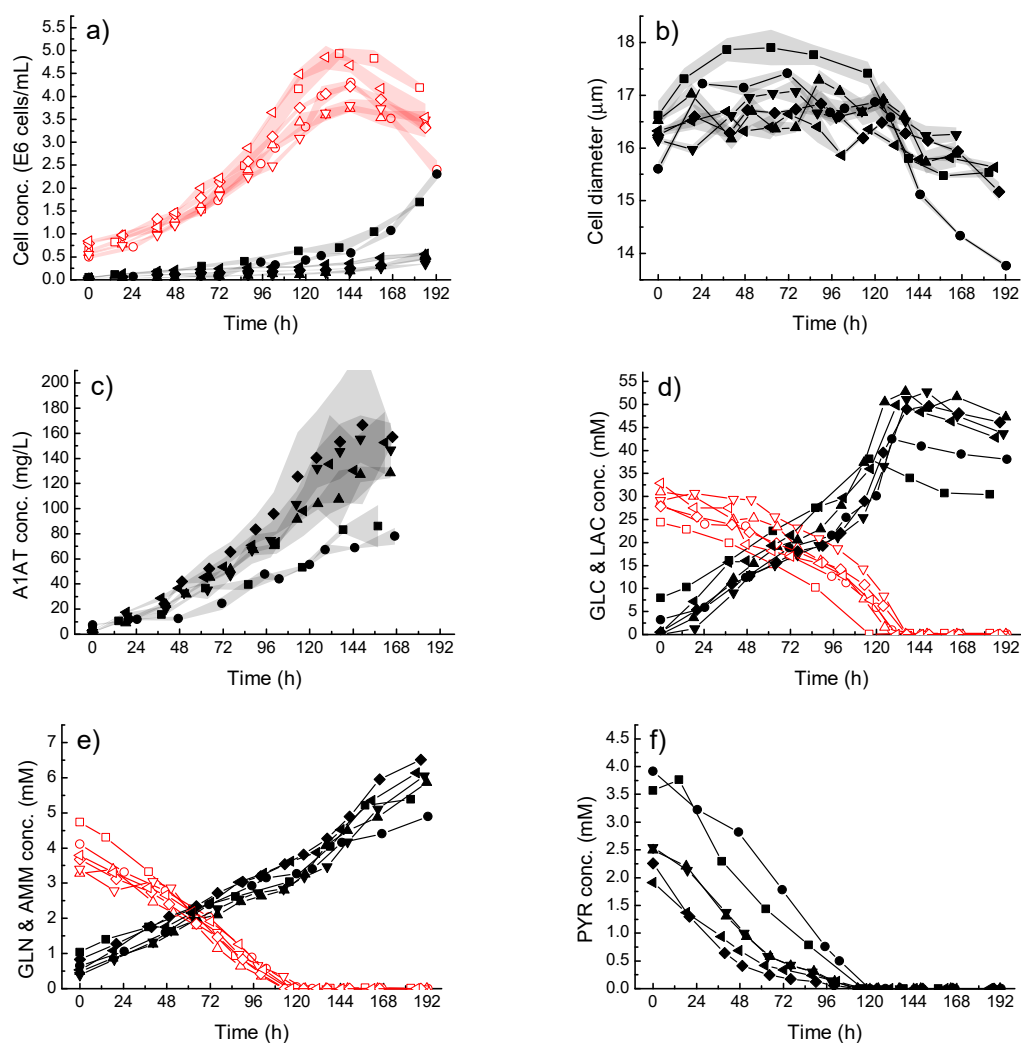
Figure 4.16: Cell, product and metabolite concentrations and cell diameter for six batch cultivations with AGE1.HN.AAT cells (■,●: 20 L *wv*; ▲,▼: 2.5 L *wv*; ◆,◄: 0.5 L *wv*). **a)** Viable (open symbols) and dead cell concentrations (full symbols), **b)** cell diameters **c)** A1AT concentrations, **d)** glucose (open symbols) and lactate concentrations (full symbols), **e)** glutamine (open symbols) and ammonia concentrations (full symbols) and **f)** pyruvate concentrations. In diagrams a) and c) the average of three technical replicates and the SD as shaded background around the symbols is shown.

As can be seen in figures 4.16-d, -e and -f, higher start concentrations of lactate, pyruvate and glutamine and lower start concentrations for glucose in the 20 L cul-

tivations compared to the smaller scale cultivations could be detected. This might be explained by the difference in the inoculation procedure. For the 0.5 and 2.5 L cultivations, the old medium from the precultures was completely removed via centrifugation, whereas for the 20 L cultivations a complete removal of the old medium was not possible and spent medium was therefore partly carried over during inoculation. Probably this, together with the higher biomass, was the reason for the faster consumption of glucose during the first replication of the 20 L cultivations (figure 4.16-d), whereas pyruvate was significantly later depleted during both 20 L cultivations compared to the smaller scale cultivations (figure 4.16-f). However, the time profiles for glutamine and ammonia were quite comparable, with only minor differences between the various scales. Comparable yields of ammonia from glutamine between 0.64–0.82 $^{mol}/_{mol}$, indicated similar behaviour of glutamine metabolism (figure 4.16-e).

In contrast to the low lactate concentrations in the 20 L cultivations, the concentrations of dead cells were much higher, especially at the end of both 20 L cultivations (figure 4.16-a). It is well known that cell death in agitated and aerated stirred bioreactors is triggered by physical damage of the cell membrane leading to necrosis and lysis and/or through an active mechanism called apoptosis [151, 152]. During the 20 L cultivation, the agitation was stepwise increased after 92h from 80rpm to a maximum velocity of 100 rpm, yielding in a u_{tip} of 0.48 $^m/_s$ compared to a maximum value of 0.38 $^m/_s$ for the smaller scale cultivations. Chisti [152] reported a damaging threshold value for u_{tip} of 0.5 $^m/_s$ for hybridoma cells cultivated in a stirred tank reactor in serum-supplemented medium (7.5 %, surface aerated). Without the protective effect of serum, not present in chemically defined media such as 42-MAX-UB, the u_{tip} damaging threshold might be even lower than reported in literature [152–154]. In addition, with a *Re* value of 19678 at 100 rpm, during the 20 L cultivations the cells were exposed to a turbulent flow regime, as opposed to the 0.5 and 2.5L cultivations (compare chapter 4.1.1). As was shown for another hybridoma cell line cultivated in both laminar and turbulent flow regimes, turbulent shear caused a higher degree of cell damage than laminar shear [155]. In addition to the physical damage due to harsh cultivation conditions, it was as also shown by Al-Rubeai et al. [151] that by increasing the power input through increasing the agitation rate, not only necrosis was a significant mechanism of cell death, but there was also evidence of apoptosis. But, as was stated by Oh et al.

[156], it is also necessary to distinguish between the effects of agitation alone and those arising from sparging or the entrainment of bubbles. As the 20 L cultivations were additionally supplied with oxygen via a ring sparger after 96 h onwards (see Materials & Methods section 3.2.2), this might have been also a reason for the increase in dead cells during the 20 L cultivations. Moreover, together with a higher number of damaged cells, the stability of the extracellular protein A1AT might have been severely compromised through the action of a higher amount of released proteases from the damaged cells, yielding lower product titres during the 20 L cultivations [152]. In addition, Keane et al. [157] could show for adherently growing CHO cells that the cell-specific glucose uptake rate increased and the cell-specific recombinant protein and the lactate productivity decreased as the shear stress was increased during a series of shear stress experiments [157].

Taken together, the main differences between the 20 L and the smaller scale cultivations are most likely due to the flow regime and the aeration. This resulted in a higher shear stress and in significant lower A1AT productivities and lactate concentrations. In contrast, the A1AT productivities in the smaller scales were comparable to values obtained for other batch cultivations with mammalian cells reported in literature. For example, Tissot et al. [158] calculated for a CHO-IgG cell line producing a monoclonal antibody a specific productivity of around 10 $^{pg}/_{cell\ day}$ and for another CHO cell line expressing a Fc fusionprotein (tumor necrosis factor receptor) a specific productivity of around 20 $^{pg}/_{cell\ day}$. In addition, even higher productivities up to 50–60 $^{pg}/_{cell\ day}$ can nowadays be achieved for mammalian cells cultivated in fedbatch mode. This shows the potential of further media and feed development as well as bioprocess modifications, which are together resulting in more and healthier cells over a longer cultivation period [17].

In a next step, a mathematical model was developed to correlate the response of intracellular metabolite concentrations and maximum enzyme activities to cell-specific rates at distinct growth phases during this six batch cultivations.

4.3.2 Identification of specific rates in distinct growth phases

To determine cell-specific rates and to identify distinct growth phases, a simple unstructured model was applied in a next step. The model considers the total cellular volume and the concentration profiles of glucose, glutamine and pyruvate.

The total cellular volume was used instead of cell numbers, simply because it is evident that the increase in cell numbers lag behind the increase in cell volume as long as osmolarity effects can be excluded [159]. Therefore, metabolic rates based on cell volume are more likely to reflect changes in growth and biomass dynamics. From preliminary investigations performed in shaker cultivations, it was found that cell growth stops immediately after glutamine depletion (see also section 4.1.2). However, also glucose is certainly limiting cell growth, therefore a Monod kinetic taking into account the simultaneous limitation of glucose and glutamine was applied (model 2, see figure 4.17 for the model fit). This model was then compared to a model including only glutamine as limiting substrate (model 1, fit not shown) and a model including only glucose as limiting substrate (model 3, fit not shown). To determine which model describes the time profiles of CV_v, glucose, glutamine and pyruvate best, the residual sum of squares (RSS) were calculated and compared for all three models. The RSS and the estimated model parameters can be found in tables 4.5 and 4.6. The matlab-scipts used for simulating all six batch cultivations with model two are given in appendix A.1.5. Based on the overall RSS, the fit with model 3 was worse than with model 1 and model 2. The differences between model 1 and 2 were only minor, therefore it was decided to use a Monod kinetic taking into account the simultaneous limitation of glutamine and glucose as this would allow a more generalized application of the model.

Table 4.5: Residual sum of squares (RSS) for three different models obtained after fitting to 6 batch cultivations with the AGE1.HN.AAT cell line.

	Model		Residual sum of squares						
			20 L cultivation		2.5 L cultivation		0.5 L cultivation		
	Name	Kinetic	Repl. 1	Repl. 2	Repl. 1	Repl. 2	Repl. 1	Repl. 2	**SUM(RSS)**
1	**Gln-Limitation:**	$\mu = \mu_{max} \cdot \frac{[Gln]}{[Gln]+k_{gln}}$	2.94	13.17	17.87	33.91	26.97	63.61	**158.47**
2	**Gln & Glc-Limitation:**	$\mu = \mu_{max} \cdot \frac{[Gln]}{[Gln]+k_{gln}} \cdot \frac{[Glc]}{[Glc]+k_{glc}}$	2.77	14.32	17.54	35.37	29.28	64.75	**164.03**
3	**Glc-Limitation:**	$\mu = \mu_{max} \cdot \frac{[Glc]}{[Glc]+k_{glc}}$	33.64	14.11	38.45	58.14	27.61	64.88	**236.84**

Based on the specific growth rate from the model, the time durations for the exponential, transition and stationary growth phases were then calculated. Therefore a value of 95 % of the determined μ_{max} was set as start of the transition phase, which continued until a value of 5 % of μ_{max} was reached. After the transition phase the stationary phase follows, which lasted until the end of the cultivations. Exponential growth of all 6 cultivations started without significant delay at 0 h and lasted

according to the model until 104–113 h with a μ_{max} of 0.024h^{-1}. As the directly calculated values for μ_{max} with values between 0.014–0.018 $^1/$h are not incorporating cell death, the obtained model value was therefore higher to compensate for the estimated specific cell death rate (k_D) of 0.0086 $^1/$h, necessary to fit the decreasing CV_v after the exponential growth phase. After subtracting k_D from μ_{max} a similar value for μ_{max} of 0.0154 $^1/$h compared to the directly calculated values could be obtained. However, as the determination of the dead cell concentrations was based on the trypan-blue exclusion technique, lysed cells were not detected, which means that the true μ_{max} is probably even higher. Compared to values for other mammalian cells grown in batch cultivation mode, the μ_{max} for the AGE1.HN.AAT cell line seems to be at the lower end of the range reported in literature (see table 4.7). However, as mentioned above, as the true μ_{max} depends on the true number of dead cells, differences in culture conditions (e.g. different levels of shear stress due to agitation and aearation) can result in varying values for the apparent μ_{max}. The transition to the stationary/death phase was calculated to last until 128–141 h (indicated by a light blue background in the following figures). In all experiments, the highest viable cell concentrations of 3.7–4.9 $\cdot 10^6$ cells/mL were reached after about 131–140 h (see figure 4.16-a), whereas the increase of the cellular volume ceased already between 118–130 h (see figures 4.17-a, 4.18-a and 4.19-a).

Table 4.6: Estimated parameters for three different models to fit simultaneously the total cellular volume and the concentration profiles of GLC, GLN and PYR of AGE1.HN.AAT cells during six batch cultivations.

| | **Value** | | | |
Parameter	Model 1	Model 2	Model 3	Unit
μ_{max}	0.0237	0.0243	0.0238	$^1/$h
k_{gln}	0.0047	0.0101	-	mmol/L
k_{glc}	-	0.0003	1.5994	mmol/L
$Y_{CVv/glc}$	9.00 $\cdot 10^3$	7.91 $\cdot 10^4$	4.67 $\cdot 10^5$	μL/μmol
$Y_{CVv/gln}$	1.23 $\cdot 10^4$	3.83 $\cdot 10^7$	3.76 $\cdot 10^8$	μL/μmol
$Y_{CVv/pyr}$	6.77 $\cdot 10^5$	2.39 $\cdot 10^7$	5.95 $\cdot 10^7$	μL/μmol
m_{glc}	0.043	0.0465	0.0432	μmol/(μL h)
m_{gln}	0.0092	0.0098	0.0097	μmol/(μL h)
m_{pyr}	0.0196	0.0213	0.0191	μmol/(μL h)
$k_{m,glc}$	0.0002	0.8883	0.0003	mmol/L
$k_{m,gln}$	0.3212	0.3934	0.3974	mmol/L
$k_{m,pyr}$	1.3332	1.4759	1.2864	mmol/L
k_D	0.0089	0.0086	0.0075	$^1/$h
$k_{d,gln}$	0.0015	0.0015	0.0015	$^1/$h

To better describe the biological situation, were the uptake of a substrate also depends on its extracellular concentration and the affinity of the corresponding transporter, a declining maintenance term according to Tremblay et al. [124] was included in the model (see materials and methods section 3.5.3). This was motivated by two facts: first of all, in a situation where cells have to adapt to new environmental conditions (e.g. after the inoculation into fresh medium), the fraction of substrates used for maintenance might be higher in the beginning of the cultivation. Secondly, with a declining maintenance term an abrupt and unrealistic change in the uptake rates towards zero (due to the unit step function used to avoid negative metabolite concentrations) should be avoided. However, due to the large values of the estimated $Y_{CVv/glc}$, $Y_{CVv/gln}$ and $Y_{CVv/pyr}$ (see table 4.6), the first term of equation 3.19 is shifted towards zero ($\frac{\mu}{Y_s} \approx 0$). To distinguish the substrate uptake for cell growth from the substrate uptake for cell maintenance in AGE1.HN.AAT cells, the correlation from Tremblay et al. [124] is therefore not suitable and to model both correctly, the equation for q_s might be revised in a follow-up work. Nonetheless, as the model fit of the glucose, glutamine and pyruvate time profiles of all six cultivations was excellent, the overall specific uptake rates calculated with the model can still be compared to literature values. Reported literature values of q_{GLC} and q_{GLN} for hybridoma, BHK and CHO cells were higher compared to the values obtained with the AGE1.HN.AAT cell line (see table 4.7). As the yield of viable cells in these studies was much lower, it seems that the human cell line AGE1.HN.AAT was using glucose more efficiently. Furthermore, for another human cell line (PER.C6), the specific glucose and glutamine uptake rates were in the same range as those found for the AGE1.HN.AAT cell line (table 4.7).

As can be seen in figures 4.17-a, -b, 4.18-a, -b and 4.19-a, -b, for all six cultivations, the specific cell growth rates (based on the increase of the total cellular volume) and the specific uptake rates for glucose and glutamine remained constant during the exponential phase and showed a strong decrease during the transition phase. Similar trends of the specific growth rate and the specific glucose and glutamine uptake rates throughout batch cultivations with other mammalian cells were also reported in literature [9, 160–162]. When taking the cellular volume into account rather then the delayed increase of the viable cell number, in the first replications in the experiments with a *wv* of 20 L and 2.5 L, the main substrates were consumed slightly faster in these cultivations (see figures 4.17 and 4.18). Therefore,

93

modelling the increase of the total cellular volume, allows the consideration of the determined growth phases as well as uptake rates of glucose, glutamine and pyruvate correctly. Recently, similar results for an adherent growing MDCK cell line were found by Rehberg et al. [163]. In their study, a segregated model linking cell numbers with mean cell diameters was successfully applied to describe the delay between cell number and cell volume increase. The authors argued that differences between pre-cultures were most likely to cause variations in the observed mean cell diameter. This could have been also the case for the batch cultivations in this thesis. In addition, the already in the preceding section discussed differences in the inoculum procedure might have additionally led to differences in the mean cell diameters of the respective cultivations (see section 4.3.1).

Table 4.7: Comparison of cell-specific growth and substrate uptake rates from the mid exponential growth phase of AGE1.HN.AAT cells during batch cultivations to values from literature.

Cell	Scale (L)	μ_{max} (1/h)	q_{GLC} (fmol/cell h)[a]	q_{GLN} (fmol/cell h)[a]	Reference
AGE1.HN.AAT	20	0.024	133 / 118	26 / 22	This study
AGE1.HN.AAT	2.5	0.024	102 / 121	19 / 21	This study
AGE1.HN.AAT	0.5	0.024	103 / 111	20 / 21	This study
BHK-21	0.3	-	720	198	[40]
CHO	15	0.015	50	25	[162]
CHO	0.3	-	468	270	[40]
Hybridoma	1.5	0.035	680	250	[57]
Hybridoma	0.8	0.038	600	130	[10]
Hybridoma	0.5	0.040	500	-	[164]
Hybridoma	2.4	0.058	200	120	[160]
Hybridoma	1.5	0.042	216	46	[9]
PER.C6	2.0	-	110	30	[137]

a: cell volume-specific glucose and glutamine uptake rates were converted to cell-specific rates by taking the corresponding cell volume at the respective time points into account.

As a result of modelling the increase of the total cellular volume together with the consumption of glucose, glutamine and pyruvate, it was found that by applying a Monod kinetic with glucose and glutamine as simultaneous limiting substrates, the trajectories of CV_v, glucose, glutamine and pyruvate could be adequately described (see figures 4.17-b, -c, 4.18-b, -c and 4.19-b, -c). Other authors have also included the growth inhibitory effect of lactate and/or ammonia [8, 165, 166]. Regarding the

inhibitory effect of ammonia, Priesnitz et al. [47] could show for the AGE1.HN.AAT cell line cultivated in shaker flasks, that the cells are capable of adapting to ammonia concentrations usually present during typical batch cultivations, by changing their metabolism with only slightly reduced cell growth and A1AT production. They found that ammonia concentrations below 5 mM did not reduce the specific growth rate. As for the batch cultivations in this thesis, the ammonia concentrations during the transition phase were below 5 mM, ammonia could be probably ruled out as reason for the observed decrease in μ. As for ammonia, lactate could also inhibit cell growth, but according to Cruz et al. [16] a 10-fold higher concentration would be needed to achieve the same growth inhibition as with ammonia for a BHK cell line. In their study, at lactate concentrations higher than 40 mM, the specific growth rate was clearly reduced. Also Glacken et al. [167] found for hybridoma cells that lactate levels as high as 40 mM did not significantly affect the growth rate. For another hybridoma cell line, Ozturk et al. [15] reported even higher tolerable lactate concentrations, after correcting the results for osmolarity effects. With lactate concentrations of about 40 mM during the transition phase, lactate most likely had only a minor inhibitory effect on the growth of the AGE1.HN.AAT cells. But not only lactate and ammonia could have an effect on cell growth, also pyruvate could influence cell growth and metabolism of AGE1.HN.AAT cells. For example, Niklas et al. [44] found for shaker flask cultivations with the parental cell line AGE1.HN three distinct growth phases with two of them correlating with the depletion of pyruvate and glutamine. The authors argued that the depletion of pyruvate triggered a shift towards a more efficient metabolism, whereas upon the depletion of glutamine the cells stopped growing immediately. However, in the cultivations considered for this thesis both pyruvate und glutamine were depleted at about the same time (see figures 4.17-c, -d, 4.18-c, -d and 4.19-c, -d), thus a clear discrimination of the influence of both substrates on cell growth and/or metabolism was not possible. Nevertheless, in accordance with the results of Niklas et al. [44], the results for this thesis confirm the importance of glutamine for growth of the producer cell line AGE1.HN.AAT.
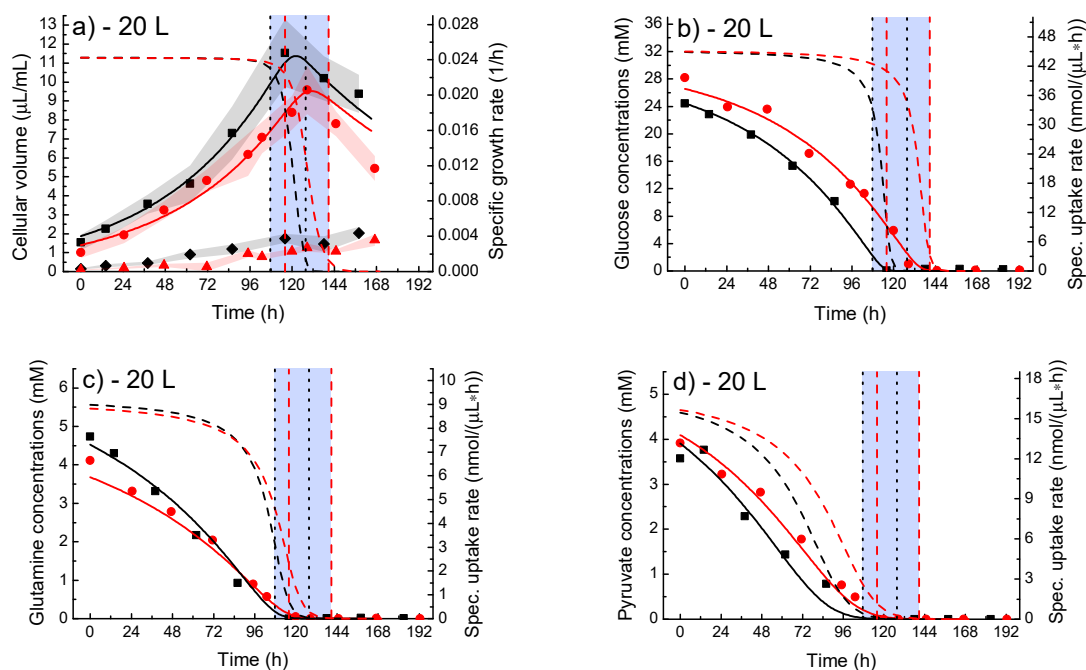
Figure 4.17: a) Cellular volume of viable (■,●) and dead cells (◆,▲), **b)** GLC concentrations, **c)** GLN concentrations and **d)** PYR concentrations for two 20 L batch cultivations with AGE1.HN.AAT cells (■,◆: first replicate; ●,▲: second replicate). Solid lines: model fit, dashed lines: specific growth (a) or specific uptake rates (b, c, d). The transition phase is indicated by a light blue background with the individual transition times indicated by two black dotted vertical lines (first replicate) and two red dashed vertical lines (second replicate). In diagram a), the average of three technical replicates and the SD as shaded background around the symbols are shown.
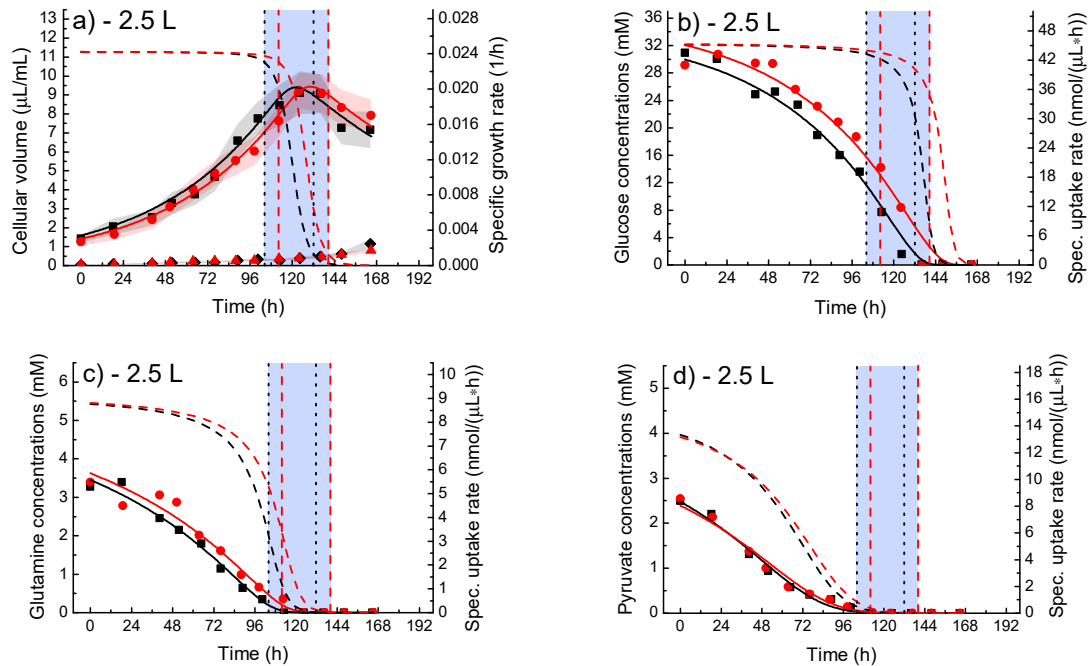
Figure 4.18: a) Cellular volume of viable (■,●) and dead cells (◆,▲), **b)** GLC concentrations, **c)** GLN concentrations and **d)** PYR concentrations for two 2.5 L batch cultivations with AGE1.HN.AAT cells (■,◆: first replicate; ●,▲: second replicate). Solid lines: model fit, dashed lines: specific growth (a) or specific uptake rates (b, c, d). The transition phase is indicated by a light blue background with the individual transition times indicated by two black dotted vertical lines (first replicate) and two red dashed vertical lines (second replicate). In diagram a), the average of three technical replicates and the SD as shaded background around the symbols are shown.
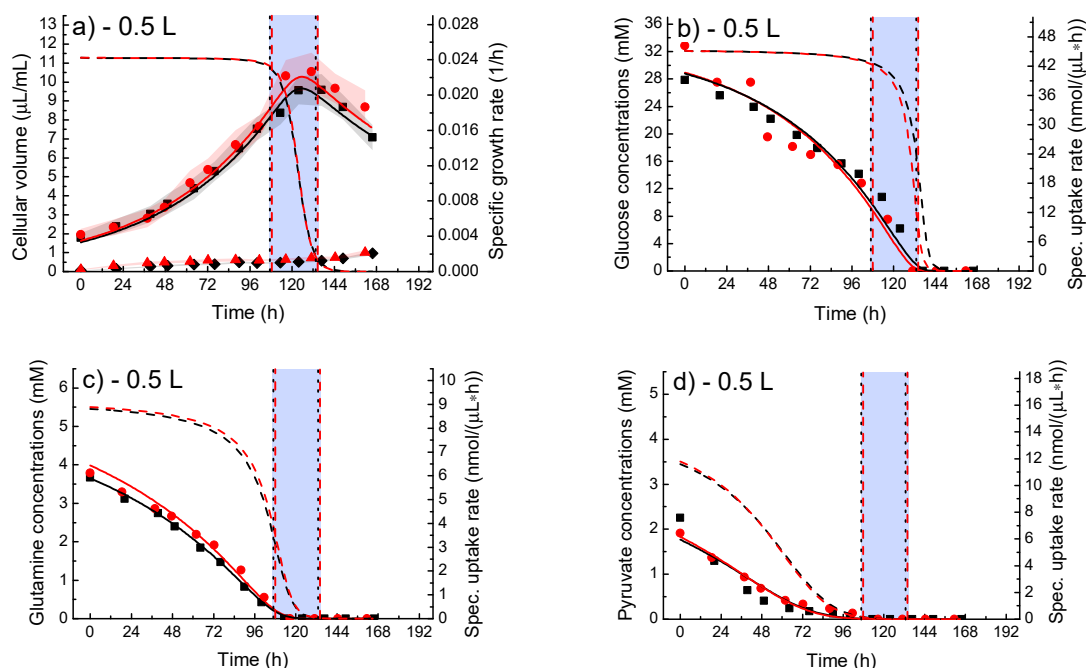
Figure 4.19: a) Cellular volume of viable (■,●) and dead cells (◆,▲), **b)** GLC concentrations, **c)** GLN concentrations and **d)** PYR concentrations for two 0.5 L batch cultivations with AGE1.HN.AAT cells (■,◆: first replicate; ●,▲: second replicate). Solid lines: model fit, dashed lines: specific growth (a) or specific uptake rates (b, c, d). The transition phase is indicated by a light blue background with the individual transition times indicated by two black dotted vertical lines (first replicate) and two red dashed vertical lines (second replicate). In diagram a), the average of three technical replicates and the SD as shaded background around the symbols are shown.

4.3.3 Maximum enzyme activities during 20 L batch cultivations

Although *in vitro* studies on enzyme reactions are not fully representative for biochemical reactions occurring *in vivo*, they still might give valuable information on metabolic fluxes [54]. One crucial point is the optimization of the assay conditions, in a way that they mimic as closely as possible the *in vivo* conditions (pH, ionic strength etc.). As the enzyme assay platform was developed for MDCK cells, the assay conditions were verified and adapted for the measurement of enzymes extracted from the AGE1.HN cells (see also section 3.4.6). As can be seen in tables 4.8 and 4.9, even if the number of sampling points is rather low for the corresponding growth phases, there is a clear tendency that maximum enzyme activities increased from the exponential to the stationary growth phase. Time points for the

determination of maximum enzyme activities during the 20 L cultivations were 62 h and 71.5 h during the exponential growth phase and 138 h and 145 h during the stationary growth phase. Except for GLDH, LDH, malate dehydrogenase (MDH), glutaminase (GLNase), glutamine synthetase (GS), hexokinase (HK), fructose-6-phosphatekinase (phosphofructokinase) (6PFK) and PEP carboxykinase (PEPCK) the total enzyme activities per cell remained more or less constant (see figure 4.20 and tables 4.8 and 4.9). Therefore, this increase over time was most likely caused by the decrease in the average cellular volume during the stationary growth phase. During the exponential growth phase very high activities (>1000 $^{nmol}/_{\mu L\ h}$) were found for phosphoglucose isomerase (PGI), triose-phosphate isomerase (TPI), glyceraldehyde 3-phosphate dehydrogenase (GAPDH), pyruvate kinase (PK), LDH, fumarase (FUMase), MDH and aspartate transaminase (AspTA). In contrast, enzyme activities were low (<10 $^{nmol}/_{\mu L\ h}$) for GLNase, pyruvate dehydrogenase (PDH) and pyruvate carboxylase (PC) (figure 4.20). The latter was also found in other transformed cell lines as well as in cancer cells, where only low or even no activity of PDH and PC was reported [40, 168], which clearly represents the characteristics of the Warburg effect. All other enzyme activities were in a range of 10–1000 $^{nmol}/_{\mu L\ h}$ (figure 4.20 and table 4.8). Comparable results of maximum *in vitro* enzyme activities were also found for adherently growing MDCK cells cultivated in glutamine-containing medium during the exponential growth phase [145].
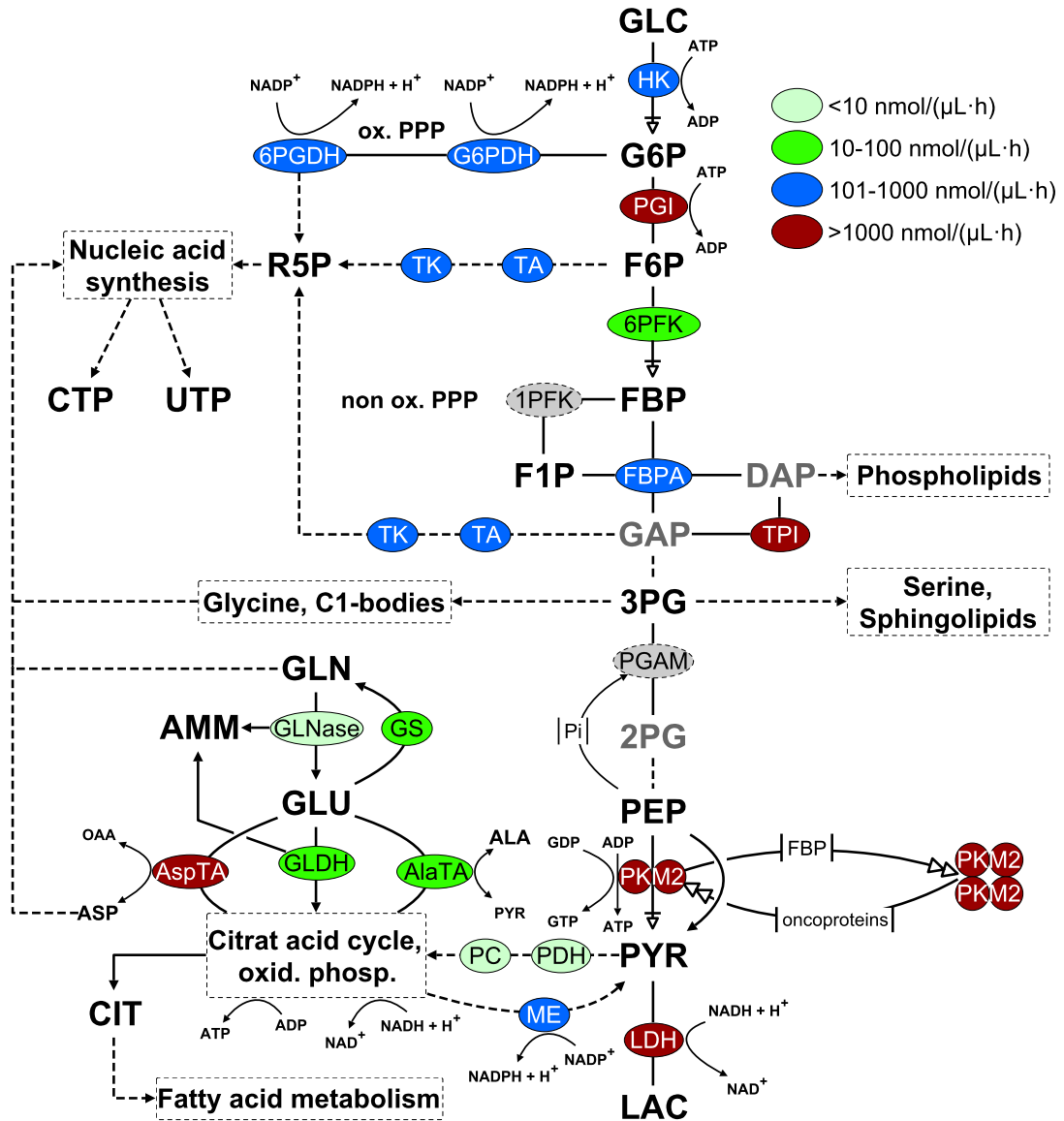
Figure 4.20: Average maximum *in vitro* activities of enzymes from glycolysis, PPP and glutaminolysis in AGE1.HN.AAT cells for two replicates of a 20 L batch cultivation. Enzymes with a dashed border as well as metabolites printed in grey letters were not measured. Lumped reactions are represented with dashed lines. The regulation scheme of PKM2 is adapted from [169, 170]. Shown is the average from samples of the exponential phase of both replicate cultivations.

Table 4.8: Maximum *in vitro* activities of enzymes from glycolysis, PPP, TCA cycle and glutaminolysis in AGE1.HN.AAT cells during exponential growth of two replicates of a 20 L batch cultivation.

Enzyme (EC)	Maximum *in vitro* activities during exponential growth phase			
	Cult. 1[a] nmol/µL h	Cult. 2[a] nmol/µL h	Mean[b] nmol/µL h	Rel.SD[c] %
HK (2.7.1.1)	202.52	195.78	199.15 ± 4.77	2.40
PGI (5.3.1.9)	3455.47	4598.22	4026.84 ± 808.04	20.07
PFK (2.7.1.11)	75.79	74.69	75.24 ± 0.78	1.03
FBPA (4.1.2.13)	443.20	421.68	432.44 ± 15.22	3.52
TPI (5.3.1.1)	1586.07	2332.42	1959.25 ± 527.75	26.94
GAPDH (1.2.1.12)	1235.43	920.75	1078.09 ± 222.51	20.64
PK (2.7.1.40)	5595.92	6831.73	6213.82 ± 873.85	14.06
LDH (1.1.1.27)	6454.51	6127.90	6291.21 ± 230.95	3.67
G6PDH (1.1.1.49)	210.50	243.71	227.10 ± 23.48	10.34
6PGDH (1.1.1.44)	647.24	547.09	597.17 ± 70.82	11.86
TA (2.2.1.2)	444.63	356.66	400.64 ± 62.20	15.53
TK (2.2.1.1)	252.34	217.75	235.04 ± 24.46	10.41
PDH (1.2.4.1)	0.89	2.70	1.79 ± 1.28	71.29
PC (6.4.1.1)	6.54	4.73	5.63 ± 1.28	22.78
CS (2.3.3.1)	120.62	220.34	170.48 ± 70.51	41.36
CL (2.3.3.8)	60.43	40.93	50.68 ± 13.79	27.21
NAD-ICDH (1.1.1.41)	21.33	14.52	17.92 ± 4.81	26.84
NADP-ICDH (1.1.1.42)	84.51	102.30	93.40 ± 12.58	13.47
FUM (4.2.1.2)	1928.18	2657.78	2292.98 ± 515.90	22.50
MDH (1.1.1.37)	15066.32	15214.84	15140.58 ± 105.02	0.69
GLNase (3.5.1.2)	5.38	1.92	3.65 ± 2.45	67.04
GS (6.3.1.2)	94.15	240.61	167.38 ± 103.56	61.87
GLDH (1.4.1.2)	56.75	69.15	62.95 ± 8.77	13.93
AlaTA (2.6.1.2)	29.19	18.85	24.02 ± 7.31	30.43
AspTA (2.6.1.1)	1919.07	1179.26	1549.16 ± 523.13	33.77
PEPCK (4.1.1.32)	726.58	614.05	670.31 ± 79.57	11.87
ME (1.1.1.40)	103.65	109.39	106.52 ± 4.06	3.81

a: Average of four technical replicates.

b: Average and SD of two biological replicates.

c: Relative SD of two biological replicates.

Table 4.9: Maximum *in vitro* activities of enzymes from glycolysis, PPP, TCA cycle and glutaminolysis in AGE1.HN.AAT cells during stationary growth of two replicates of a 20 L batch cultivation.

Enzyme (EC)	Maximum *in vitro* activities during stationary growth phase			
	Cult. 1[a] nmol/µL h	Cult. 2[a] nmol/µL h	Mean[b] nmol/µL h	Rel. SD[c] %
HK (2.7.1.1)	192.09	205.44	198.77 ± 9.44	4.75
PGI (5.3.1.9)	4349.60	5064.19	4706.89 ± 505.29	10.74
PFK (2.7.1.11)	48.99	61.34	55.17 ± 8.73	15.83
FBPA (4.1.2.13)	519.28	550.94	535.11 ± 22.39	4.18
TPI (5.3.1.1)	1833.30	6430.09	4131.69 ± 3250.42	78.67
GAPDH (1.2.1.12)	1004.32	1283.01	1143.66 ± 197.06	17.23
PK (2.7.1.40)	7736.66	8649.77	8193.21 ± 645.67	7.88
LDH (1.1.1.27)	6337.41	7607.62	6972.52 ± 898.17	12.88
G6PDH (1.1.1.49)	306.25	337.13	321.69 ± 21.84	6.79
6PGDH (1.1.1.44)	679.38	842.26	760.82 ± 115.17	15.14
TA (2.2.1.2)	453.49	568.38	510.94 ± 81.24	15.90
TK (2.2.1.1)	324.62	331.93	328.27 ± 5.17	1.57
PDH (1.2.4.1)	3.91	1.24	2.57 ± 1.89	73.49
PC (6.4.1.1)	6.12	6.20	6.16 ± 0.06	0.94
CS (2.3.3.1)	223.59	152.76	188.18 ± 50.09	26.62
CL (2.3.3.8)	69.38	59.73	64.56 ± 6.82	10.57
NAD-ICDH (1.1.1.41)	19.22	13.49	16.36 ± 4.05	24.77
NADP-ICDH (1.1.1.42)	124.25	125.82	125.03 ± 1.11	0.89
FUM (4.2.1.2)	2827.78	3146.15	2986.96 ± 225.13	7.54
MDH (1.1.1.37)	17017.71	18112.06	17564.89 ± 773.83	4.41
GLNase (3.5.1.2)	2.09	0.45	1.27 ± 1.16	91.41
GS (6.3.1.2)	380.82	490.72	435.77 ± 77.71	17.83
GLDH (1.4.1.2)	56.89	65.42	61.15 ± 6.03	9.86
AlaTA (2.6.1.2)	49.03	45.61	47.32 ± 2.42	5.10
AspTA (2.6.1.1)	2339.24	1734.97	2037.11 ± 427.29	20.98
PEPCK (4.1.1.32)	622.45	813.74	718.09 ± 135.26	18.84
ME (1.1.1.40)	125.72	139.45	132.58 ± 9.71	7.32

a: Average of four technical replicates.

b: Average and SD of two biological replicates.

c: Relative SD of two biological replicates.

4.3.4 Intracellular metabolite dynamics in 20, 2.5 and 0.5 L batch cultivations

In general, according to the SDs in figure 4.21, 4.22 and 4.23, the level of confidence regarding the observable differences in intracellular metabolite concentrations seems to be high for most metabolites. Nonetheless, the plotted SD is merely

a measure for the variance of the technical replicates. As the metabolism of suspension cells cannot be completely quenched directly after sampling due to the need to remove the supernatant from the cells, the time needed for this step is critical (refer to the section 4.2.4). As the activity of some enzymes is very high at 37 °C (see table 4.8), there is still a chance for a certain activity at 0 °C (refer also to section 2.3), which might had an influence on the total amount of quantified metabolites as soon as the supernatant is replaced by the washing buffer. This might be especially the case for 3PG, FBP, PEP, F6P, G6P, 2-KG, GDP and UDP, as these metabolites were found to have significant higher or lower concentrations after sampling and quenching with a heat exchanger and performing a washing step with NaCl solution (see section 4.2.4). However, as the sampling and quenching procedure during the experiments was the same for all samples, the impact of not fully stopped enzymatic reactions can be assumed as a constant and for most metabolites small error.

Starting at the upper part of the glycolysis, during the exponential growth phase of both 20 L batch cultivations F6P and G6P showed a slight increase, whereas the concentration of FBP remained unchanged (see figure 4.21). Also the concentrations of F1P, R5P, UDP-GlcNAc, UDP-GalNAc and UDP-GLC, together with 3PG and PEP from the lower part of the glycolysis remained more or less unchanged during the exponential growth phase. Moreover, also intermediates from the TCA-cycle (FUM, MAL, CIT, ICIT, 2-KG and SUC) and also most nucleotides were constant during the exponential phase (see figures 4.21 and 4.22). With the onset of the transition phase, together with the decrease of the specific glutamine and glucose uptake rates (see figure 4.17) almost all measured intracellular metabolite concentrations dropped near or below the quantification limit. In contrast to that, the concentrations of nucleoside monophosphates increased in both cultivations, whereas only for replicate 2 the concentrations of FBP, F1P and R5P together with the extracellular lactate concentration sharply increased during the transition phase (figure 4.21). To study this in detail, during the batch cultivations in 2.5 L and 0.5 L *wv*s, special emphasize was therefore on the quantification of FBP, F1P, R5P, ATP, GTP, UTP and CTP. The increase of the total cellular volume, the model fit and the specific growth rates as well as the resulting transition times for these cultivations can be found in figures 4.17 and 4.18. As can be seen in figure 4.23, for all four cultivations, the same peak-like accumulation of FBP, F1P and R5P during

the transition from exponential to stationary growth as in the second 20 L cultivation were found. Also, the volumetric lactate production rates increased during the transition from exponential to stationary growth.
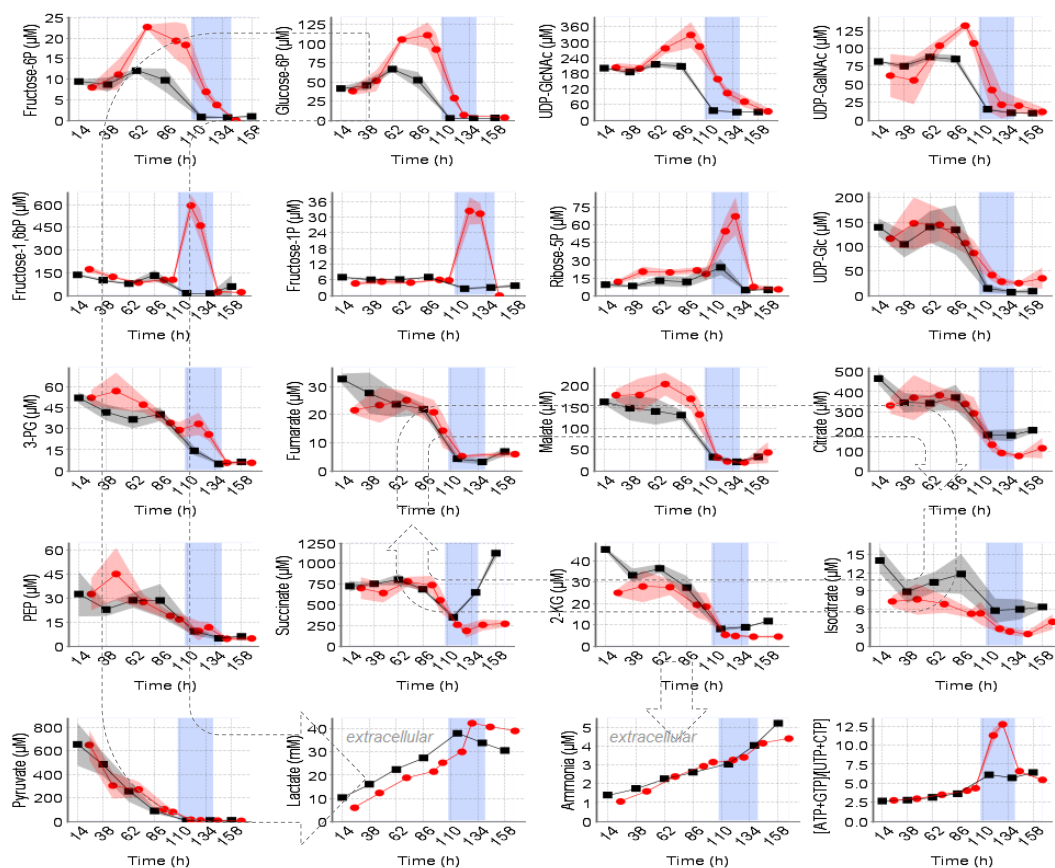
Figure 4.21: Intracellular metabolite concentrations, ratio of (ATP+GTP)/(UTP+CTP), and extracellular LAC and AMM concentrations for two replicates of a 20L batch cultivation with AGE1.HN.AAT cells (■: first cultivation; ●: second cultivation). Transition from the exponential to the stationary phase is for both cultivations indicated by a light blue background. For intracellular metabolites, the average of three technical replicates and the SD as shaded background around the symbols is shown. Indicated by arrows are the flux directions of glycolysis and TCA cycle.
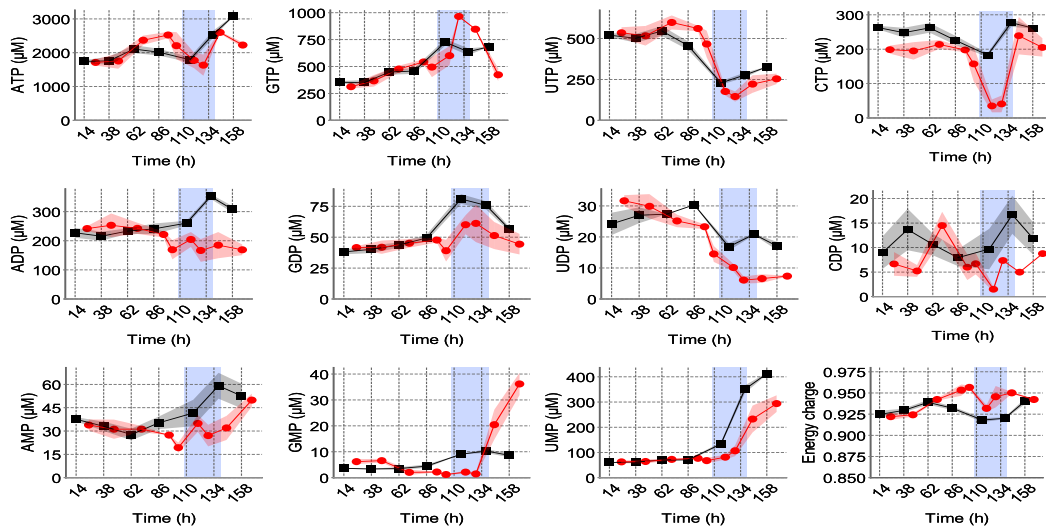
Figure 4.22: Intracellular nucleotide concentrations and the ECR in AGE1.HN.AAT cells for two replicates of a 20 L batch cultivation (■: first cultivation; ●: second cultivation). The transition phase is for both cultivations indicated by a light blue background. The average of three technical replicate extractions and the SD as shaded background around the symbols is shown.
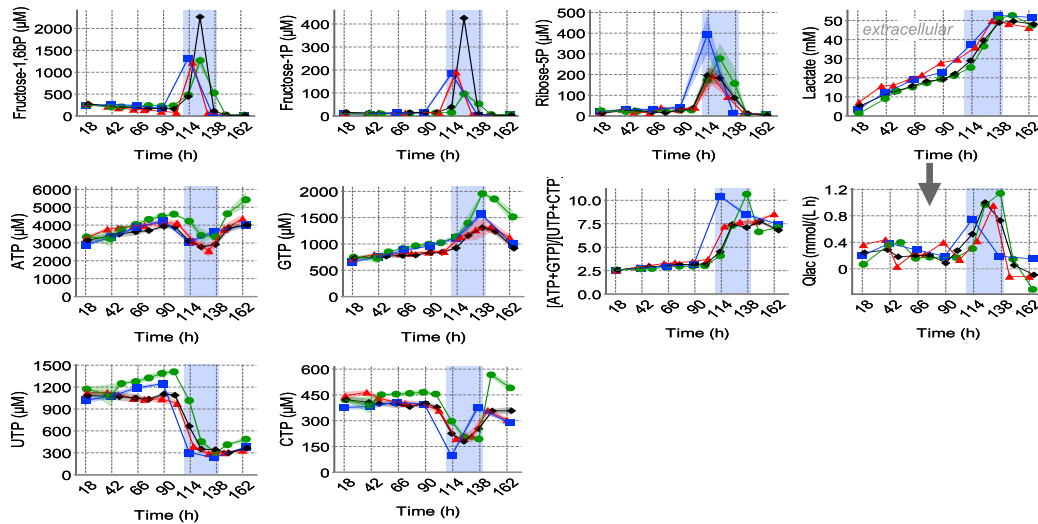
Figure 4.23: Intracellular metabolite concentrations, ratio of (ATP+GTP)/(UTP+CTP), extracellular LAC concentrations and Q_{lac} for four cultivations with AGE1.HN.AAT cells (■,●: 2.5 L *wv*; ▲,◆: 0.5 L *wv*). The transition phase is indicated by a light blue background. For intracellular metabolites, the average of three technical replicates and the SD as shaded background around the symbols is shown.

4.3.4.1 Dynamics of glycolysis, PPP and amino hexoses

Besides the active uptake of glucose from the lumen of the small intestine and prox-imal tubule of the kidney, the transport of glucose across cell membranes occurs by facilitated diffusion via transporters of the glucose transporter (GLUT) family [171]. However, as early as 1976 it was reported that glucose uptake is increased by facilitated diffusion and active uptake in transformed cell lines [172, 173]. The increased uptake is due to an increase in the number of glucose transporter pro-teins in the cell membrane, which is reflected in an unchanged Monod saturation constant for glucose ($k_{m,glc}$) and increased maximal enzyme reaction velocity (v_{max}) [173]. In case of the facilitated uptake via GLUT, the driving force for the glucose uptake is the concentration gradient over the cell membrane. After entry into the cell, glucose is converted almost immediately to G6P by HK to prevent efflux from the cell. It is then metabolized by glycolysis and PPP. In non-immortalized cells, glucose derived pyruvate is fed into the TCA cycle, where it is completely oxidized in favor of ATP generation. In continuous cell lines, however, most of the glucose is used for the generation of two molecules of lactate, which is referred to as aerobic glycolysis or more commonly termed as the Warburg effect [174]. Even though this might be regarded as a waste of energy, some authors are convinced that the up-regulation of glycolysis is sufficient to produce enough energy to meet the de-mand of rapidly proliferating cells [175]. As can be seen in figure 4.22, ATP with an intracellular concentration between 2-3 mM was the most abundant intracellular metabolite measured. In addition to that, the ECR was on a high level above 0.92, irrespective of the different growth phases (figure 4.22). A high glycolytic flux might be required to supply the cell with precursors for synthetic pathways, but decreases the NAD$^+$/NADH ratio. This in turn forces the cell to regenerate NAD$^+$ to ensure a proper NAD$^+$/NADH ratio, allowing the cell to maintain a high oxidative capacity needed to keep glycolysis running. Among the glycolytic enzymes, LDH together with PK showed the highest maximum enzyme activities (see figure 4.20). Therefore, the AGE1.HN.AAT cells had a large capacity for pyruvate conversion and regeneration of NAD$^+$ via a highly active LDH, which is the reason for the build up of high lactate concentrations during the batch cultivations. However, apart from the glycolytic conversion of G6P to pyruvate, G6P can also enter the oxidative PPP via G6PDH and 6PGDH or can be converted to UDP-GLC or by an isomerization

reaction catalyzed by PGI to F6P. F6P can then be further directed to pyruvate or via the reaction of TK into the non-oxidative PPP or serve as a precursor for the formation of UDP-GlcNAc and UDP-GalNAc.

Compared to the specific glucose uptake rate of 45.0 $^{nmol}\!/_{\mu L\ h}$ during the exponential growth phase, the maximum activities of the first enzymes of the upper part of glycolysis together with the activity of G6PDH were much higher than the glucose uptake rate (see figures 4.17-b and 4.20 and table 4.8). During the exponential growth phase most intermediates of glycolysis and PPP remained rather constant, whereas during the transition from the exponential to the stationary phase almost all intermediates of the glycolysis and PPP dropped below or near the quantification limit (figure 4.21), which clearly coincided with the drop of the glucose uptake rate (figure 4.17-b). Therefore, it can be assumed that glucose uptake via GLUT and conversion of glucose by HK is a rate limiting step for the upper part of the glycolysis in AGE1.HN.AAT cells. In fact, this was also found for human breast cancer cells [176], rat hepatocarcinoma cells [177], mouse mammary tumor cells [178], and was also proposed for adherent MDCK cells cultivated in T-flasks [179]. Moreover, intracellular glucose concentrations were always below the detection limit, which was also the case in other studies with mammalian cells [179, 180]. Therefore, it is suggested that GLUT rather than HK mediated flux control on the upper part of glycolysis in AGE1.HN.AAT cells. In addition, the profile of FBP showed a peak-like accumulation during the transition from the exponential to the stationary growth phase, which was accompanied with a peak-like accumulation of F1P and R5P. Interestingly, this transient accumulation was only found during the second 20 L cultivation. A simple explanation for this might be the lack of sampling points during the short transition time for the first cultivation. Indeed, during the replicate cultivations in the 2.5 L and 0.5 L *wv*s, the same peak like accumulation for these intracellular metabolites was found, which will be discussed in the following section.

4.3.4.2 Regulation of pyruvate kinase adjusts metabolite dynamics

Besides the contribution of GLUT and HK on the glycolytic flux pattern, 6PFK is a well-known regulatory site for various fast proliferating cells as well as different cancer cell types [181]. However, due to the increase of glycolytic intermediates

in enzymatic reactions preceding PK during the transition from exponential to stationary growth of the second 20L and the four 2.5 and 0.5L cultivations, i.e. of FBP, F1P and R5P another, maybe PK-mediated, regulatory influence seemed to be present (compare figures 4.21 and 4.23). Among the four known isoenzymes of PK, the type M2 (PKM2) is described to be expressed in several fast proliferating cells and tumor cells (see Mazurek [169] for an overview of PK and its different isoenzymes). A distinctive feature of PKM2 is that it might occur in a highly active tetrameric or in a nearly inactive dimeric form with a low affinity for PEP [182]. Additionally, the tetrameric form may be associated with other glycolytic enzymes leading to a highly effective conversion of glucose to lactate in the cytosol [183]. This dimeric to tetrameric interconversion was shown to be induced by an increasing concentration of FBP and is believed to be a major *in vivo* cellular regulatory mechanism [184]. As a consequence, accumulation of all glycolytic intermediates above PKM2 occurs for the dimeric form and coincides with lower ATP and GTP concentrations (products of the PK reaction) and higher CTP and UTP concentrations resulting from an enhanced nucleic acid synthesis (see figure 4.20 for schematic representation). Accordingly, the ratio of (ATP+GTP)/(UTP+CTP) was found to be low in proliferating mouse embryonic fibroblast cells having a large amount of the dimeric form of PKM2 [183]. Ryll and Wagner [39] also correlated the (ATP+GTP)/(UTP+CTP) ratio to different physiological states of a BHK and a hybridoma cell line showing that the cease of cell growth could be detected 24h earlier than by classical microscopic techniques. This correlates well with the findings in this thesis, as during the transition from the exponential to the stationary growth phase of the second 20 L and the four 2.5 L and 0.5 L cultivations the (ATP+GTP)/(UTP+CTP) ratio increased sharply together with FBP, F1P and R5P concentrations (see figures 4.21 and 4.23). This may result from a drop of the nucleic acid synthesis, which typically precedes the cease of cell growth, and in turn led to the interconversion of PKM2 from the dimeric to the tetrameric form by FBP. The lactate production was also increased as expected from a high activity of a tetrameric PK during the transition from exponential to stationary growth, which is supported by the increased volumetric lactate production rate in figure 4.23. According to Vander Heiden and coworkers, the transfer of the phosphate group of PEP to the PGAM instead to ADP or GDP in PKM2-expressing cells (see scheme in figure 4.20) might pose an alternative flux in the direction of lactate via pyruvate.

They argued that the decreased PK activity allows phosphorylation of PGAM via PEP, which provides a bypass of the PK-mediated reaction. As a consequence, this would decouple the production of ATP from PK-mediated phosphotransfer, which in turn allows for a sustained glycolytic flux under a reduced activity of a dimeric PK to support the anabolic metabolism observed in proliferating cells [170]. Taken together, this would explain the reduced lactate production during the exponential growth phase, as well as the sharp increase in lactate production together with the transient accumulation of FBP, F1P and R5P during the transition from exponential to stationary growth and accounts for the fact that fast proliferating cells must not only provide enough precursors for biomass production, but also have to avoid ATP production in excess to circumvent allosteric inhibition of rate limiting glycolytic enzymes [170].

4.3.4.3 Dynamics of the TCA cycle and glutaminolysis

In primary cells, the conversion of pyruvate to CIT is the starting point for a complete oxidation of glucose-derived pyruvate via the reaction catalyzed by PDH and CS. Besides that, the TCA can also be supplied via various anaplerotic reactions. For example, pyruvate can be fed into the TCA via PC, or glutamate derived from glutamine via GLDH and/or aminotransferases. Production of NADH, FADH2 and GTP in the TCA enables the conversion of ADP to ATP via oxidative phosphorylation. For most continuous cell lines as well as for different cancer cells, glutamine is known to be the major substrate for the TCA [185–189]. As the activity of the PDH and PC was low during exponential as well as stationary growth phase in AGE1.HN.AAT cells, glutamine may compensate the cellular demand of TCA intermediates. This is supported by a specific uptake rate of glutamine between 8.4–9.0 $^{nmol}/_{(\mu L\ h)}$ in both cultivations, and a highly active AspTA (1549.2 $^{nmol}/_{(\mu L\ h)}$) during the exponential growth phase. As mentioned earlier with a value of 3.65 ± 2.45 $^{nmol}/_{(\mu L\ h)}$ during the exponential growth phase, the GLNase activity was rather low and even decreased further to 1.27 ± 1.16 $^{nmol}/_{(\mu L\ h)}$ in the stationary growth phase. This might indicate that GLNase was close to saturation and, hence, might pose another bottleneck in TCA cycle of AGE1.HN.AAT cells. Interestingly, the latter is different from what was reported for other fast proliferating cells. For example, Janke et al. reported for MDCK cells a 40 times higher GLNase activity [145]. It

was also reported by other authors that a prerequisite for the glutaminolysis pathway is an overexpression of GLNase, an inactivation of GS and an overexpression of ME [190, 191]. In the experiments of this thesis, not only a low GLNase activity, but also a moderate maximum GS activity of 160.35 nmol/(µL h) in the exponential growth phase was found. Maximum GS activity even further increased during the stationary growth phase to 455.95 nmol/(µL h). This might lead to the dissipation of ATP due to futile cycling as in the human body GLNase and GS are usually not expressed together [192, 193].

However, it was also found that the glutamine uptake rate was strongly correlated with all TCA intermediates (figures 4.17-c, 4.18-g and -k, and 4.21). Interestingly, also the time course of most extracellular amino acid concentrations was correlated with TCA intermediates (figure 4.24). During the exponential growth phase, the concentrations of 2-KG, SUC, FUM, MAL, CIT, and ICIT were more or less constant, whereas during the transient transition from exponential to stationary growth all intermediates dropped near or below the quantification limit. Highest concentrations were found for CIT and SUC (500–750 µM), whereas ICIT was hardly detectable with concentrations of 5–15 µM, which is not surprising due to its role as intermediate of aconitase-mediated reactions. Low concentrations of ICIT were also reported for other cell lines, e.g. MDCK [179]. Also, Reitzer described for HeLa cells low intracellular concentrations of ICIT, and the role of CIT in the regeneration of acetyl-CoA for fatty acid synthesis with CIT leaving the TCA cycle [186]. Lu and coworkers likewise observed in CHO cell cultivations high concentrations for CIT and no detectable concentrations of ICIT during experiments with different starting concentrations of glucose. In general, intracellular concentrations of TCA intermediates remained unchanged upon variation of the initial glucose concentrations [194]. Sharfstein et al. found for a hybridoma cell line that 37.5 % of CIT was used for the synthesis of fat and only 5.8 % was channeled to 2-KG [195]. Besides, Niklas et al. calculated for the AGE1.HN cell line that the flux from CIT to 2-KG was low compared to the flux through CS and the flux from 2-KG to OAA. This was due to the CL-catalyzed production of cytosolic OAA and acetyl-CoA from CIT for fatty acid synthesis. Moreover, in the experiments of this thesis the low activity of the NAD-ICDH (17.92 ± 4.81 nmol/(µL h)) catalyzing the reaction from ICIT to 2-KG supports the idea of a low flux through this branch of the TCA [45]. Taken together, these findings suggest a TCA more or less decoupled from

glycolysis, which is mostly fed by glutamine via the possible rate limiting step of the GLNase reaction. In addition, TCA-derived CIT seems to be exported into the cytosol in favor of acetyl-CoA production.
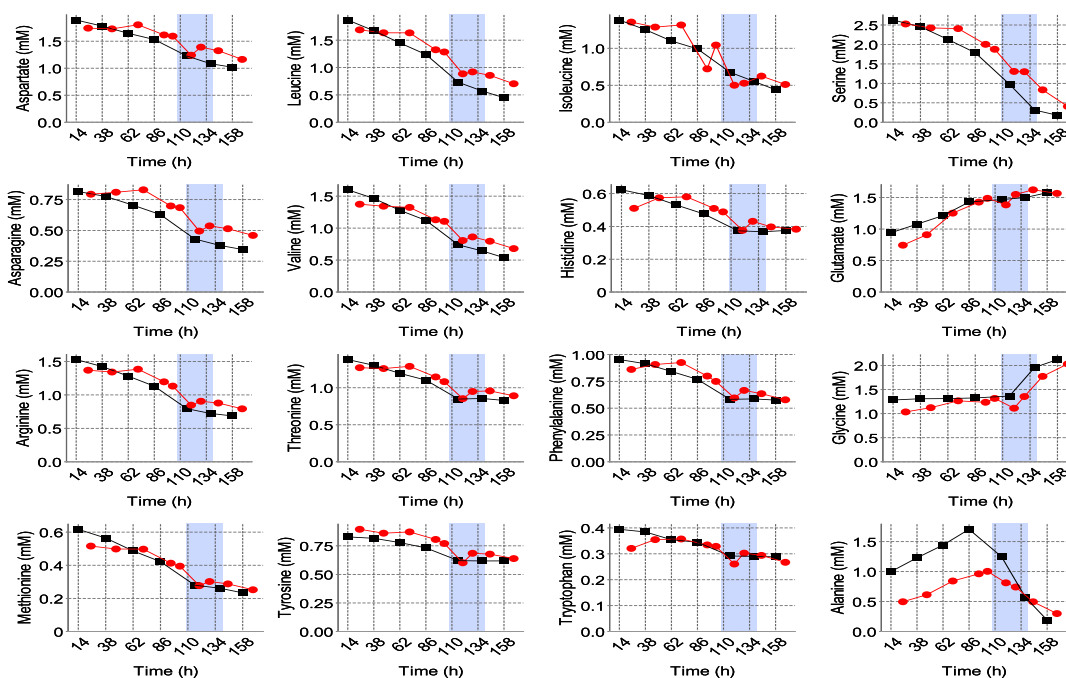
Figure 4.24: Extracellular amino acid concentrations for two replicates of a 20 L batch cultivation with AGE1.HN.AAT cells (■: first cultivation; ●: second cultivation). The transition from exponential to stationary growth is indicated by a light blue background.

4.3.5 Summary

Taken together, the results indicate that during batch cultivations of AGE1.HN.AAT cells the dynamics of intracellular metabolite pools is closely linked to cell growth and to the dynamics of the uptake rates of glucose and glutamine, indicating that the glucose uptake and probably also the conversion by HK are rate limiting steps for the upper part of the glycolysis. In addition, PK seems to exert an important regulatory point as witnessed by the increase of lactate production together with the transient accumulation of FBP, F1P and R5P during the switch from exponential to stationary growth. Moreover, due to its low activity, GLNase might pose a rate limiting step for glutamine metabolism. In addition, the link between glycolysis

and TCA cycle seemed to be weak due to the low maximum *in vitro* enzyme activities of PDH and PC, which might be further decreased during exponential growth through inhibition by PDK4 [51]. Due to the only minor changes in maximum enzyme activities from the exponential to the stationary growth phase, it could also be concluded that the activities of key enzymes, besides their regulation by products and substrates, were most likely modulated by allosteric regulators rather than by changes in gene expression levels. This assumption might by supported by the outcome of a large scale gene expression profiling study of a hybridoma cell line grown in continuous cultivation [196]. Here, a 3–5 fold reduction of glycolytic fluxes was found upon a metabolic shift to a more glucose efficient metabolism. The author stated that the large change in the cellular metabolism was accompanied by only a moderate change in gene expression in terms of the number of genes and the extent of their differential expression. Their results therefore indicated that the observed metabolic shift is a relatively small perturbation on the global scale of the mammalian physiology and the metabolic shift evolves from the modulation of reaction rates through nutrient and metabolic intermediate concentrations together with (small) changes at enzyme levels [196].

In the following sections, the results of a series of continuous cultivations with the AGE1.HN.AAT cells grown under steady-state conditions exploring the influence of the dilution rate and different glucose, galactose and glutamine feed concentrations on the metabolism and production of A1AT are shown and discussed.

4.4 Glucose-limited continuous cultivations

In the previous section it was shown that AGE1.HN.AAT cells take up glucose and glutamine at high rates and produce lactate and ammonia during batch cultivations, which could have negative effects on cell viability, growth and productivity. This was also demonstrated for other mammalian cell lines [14–16, 58]. It is also established that when growing cells in fedbatch, perfusion or continuous mode under limiting concentrations of either glucose and/or glutamine, the cells might shift to a more efficient metabolism with reduced formation of lactate and/or ammonia leading to higher cell concentrations and product yield [16, 19–21, 23, 197]. Despite these and other results from different studies with mammalian cells growing under substrate limitation in continuous cultivation mode [8, 12, 56, 57], our knowledge of how exactly intracellular metabolites are linked to glucose and glutamine metabolism and eventually to product yield is still very limited. In the previous section (section 4.3) it was shown, how intracellular metabolites are correlated to the transient conditions during different batch cultivations, i.e. that the dynamics of intracellular metabolites is strongly connected to cell growth. To decouple the cellular response from transient growth conditions, AGE1.HN.AAT cells were therefore grown in continuous cultivation mode. To study the response of cell growth, metabolism and A1AT production during steady-state, different feed concentrations of glucose and glutamine were then applied.

In total, six continuous cultivations were performed (experiments A–F), with cultivation times between 20–32 d (see table 4.10), resulting in six steady-states (A–F01). In addition, in cultivation F after five days of steady-state growth the concentration of the glutamine feed was also shifted down (5→2 mM, F02), whereas after additional five days the concentration of the glucose feed was shifted up (10→20 mM, F03). In addition, as galactose might have an influence on the glucose metabolism and therefore on the lactate production, the batch medium as well as the feed medium for cultivation F were prepared without galactose. For all six continuous cultivations the dilution rate ranged between 0.0100 and 0.0150 $^1\!/\mathrm{h}$, which is clearly below μ_{max} for this cell line (0.0243 $^1\!/\mathrm{h}$, refer to table 4.6). However, only for cultivations A, B and C different settings of the dilution rate (DR) were intended. For cultivations D, E and F the set point for the DR was 0.0150 $^1\!/\mathrm{h}$. But, during this work it was found that the feed rate was easily affected by different factors, with

113

bubbles within the feed tube leading to wrong estimates of the pumped volume and the total calibration time being probably the two main factors who had the greatest impact on the actual feed rate during cultivation E. For that reason, for the following experiment (cultivation F) the *DR* was monitored online by weighing of the harvest vessel throughout the whole experiment as explained in the material and methods section 3.2.3. However, as can be seen in table 4.10, the *DR* was lower after removing and reconnecting the feed tube after the medium exchange during cultivation F, although the feed tube was the same as used for the pump calibration.

Table 4.10: Overview of the dilution rates, preculture ages and feed compositions of the continuous cultivations with the AGE1.HN.AAT cell line and the lowest and highest relative SDs for each steady-state.

Exp. ID	*DR*	Preculture	GLC	GLN	GALC	GLC/GLN[a]	Rel. SD[b]
	(^{1}/h)	(passage no.)	(mM)	(mM)	(mM)	(^{mol}/$_{mol}$)	(%)
A	0.0140	7	10	5	3	2	1.5–15.2
B	0.0120	7	10	5	3	2	0.5–13.8
C	0.0100	5	10	5	3	2	0.9–14.2
D	0.0150	8	10	2	3	5	1.5–12.9
E	0.0133	4	8	2	3	4	1.1–18.5
F01	0.0150	10	10	5	0	2	1.3–10.8
F02	0.0150	10	10	2	0	5	0.3–52.6
F03	0.0144	10	20	2	0	10	2.3–42.6

a: Ratio of glucose to glutamine in the feed medium.
b: The lowest and highest relative SD of X_V, X_D, CD, LAC, GLN, GLU, AMM, GALC, PYR, ALA, ASP and A1AT during steady-state. Note that the relative SDs for glucose (all 8 experiments) and lactate (only exp. A, B and C) during steady-state were not taken into account, as the measured values were close to zero and therefore outside of the validated range of the analytical method.

Steady-state was assumed to be reached when viable and dead cell concentrations and extracellular metabolite concentrations were approximatively stationary corresponding to at least four complete volume exchanges, except for cultivation A which had to be stopped already after 4.3 volume exchanges due to a leaking feed tube. As the relative SDs of the viable and dead cell concentrations, the cell diameter (*CD*), and the residual metabolite concentrations (LAC, GLN, GLU, AMM, GALC, PYR, ALA, ASP and A1AT) during steady-state were comparable to the other cultivations (B–F01), it was assumed that the steady-state was already reached after about 3.3 volume exchanges (see table 4.10). Also for the other steady-states (cul-

tivations B, C, D, E and F01), the relative SDs were for almost all parameters below 18 %. In contrast to that, the relative SDs for the glutamine (F02) and glucose (F03) shifts were clearly higher (up to 52.6 %), presumably indicating that steady-state conditions during experiments F02 and F03 were not completely reached.

4.4.1 Principal component analysis of steady-state samples

As brief overview on the obtained steady-state results, a PCA with all steady-state samples (A, B, C, D, E and F01) was calculated. The variables used for the PCA are shown in table 4.11 and in table 4.12. The PCA was applied firstly to check if any outliers were detectable and secondly to extract the main differences between the obtained steady-states. After the fourth principle component the increase in the goodness of fit of the PCA model (R^2) was negligible, therefore only the first four principle components with an overall R^2 of 93 % and a predictability of the PCA model (Q^2) of 75 % were further examined. As can be seen in figure 4.25-b and -d the individual samples from steady-states A, B, C, D, E and F01 are close together indicating that each sample is a good representation of the obtained steady-state with no detectable outliers.

The main difference explained by the PCA can be found along principle component one (x-axis, 55.6 % of data variation explained), which is the emerging of two metabolic states. During the steady-states located on the right hand-side (D, E, and F01) the cells produced lactate, whereas during the steady-states located on the upper left hand-side (A, B and C) the cells produced no lactate at all (see figure 4.25-b). Positive correlated with the non-lactate producing state (NLPS) are the concentration of viable cells (X_V), the concentration of dead cells (X_D), the CV_v, the A1AT concentrations, the $Y_{CVv/glc}$ and the extracellular concentrations of ammonia (figure 4.25-a and -c). In contrast to that, positive correlated with the lactate producing state (LPS) are the yield coefficient for produced LAC per consumed GLC ($Y_{lac/glc}$), the specific rates of lactate, A1AT, pyruvate and glucose, the extracellular concentrations of lactate and the mean cell diameters (figure 4.25-a and -c).
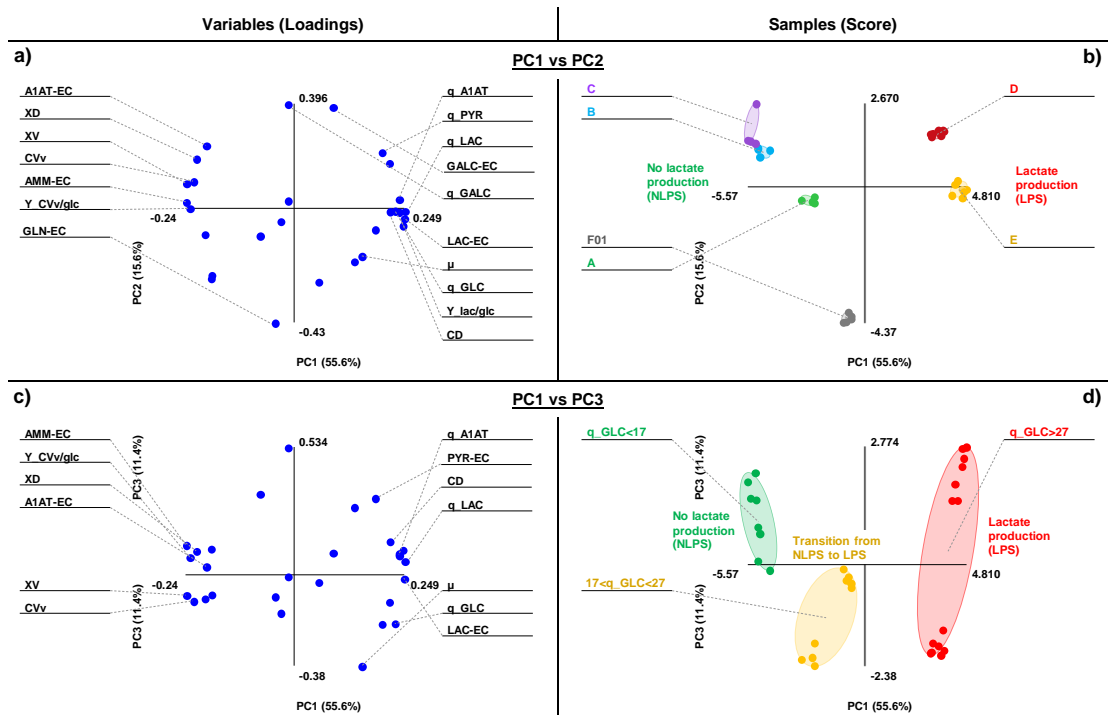
Figure 4.25: Loadings (left diagrams) and scores (right diagrams) of the first three principle components calculated from steady-state samples of continuous cultivations with different glucose and glutamine feed concentrations (experiments A, B, C, D, E and F01, see table 4.10).

By grouping the steady-state samples according to the specific glucose uptake rate (figure 4.25-d), it can be seen that the shift from LPS to NLPS along principle component one occurs most likely for a specific glucose uptake rate of 17–27 $^{nmol}/_{\mu L\ h}$. Below this range no lactate production occurred (left hand side of figures 4.25-a–d), whereas above this range lactate was produced (right hand side of figures 4.25-a–d). These results strongly suggests that the specific glucose uptake rate is linked to two metabolic states and that the cells might be shifted from one state into the other by manipulating the glucose uptake rate. In addition, in figure 4.25-a and -b it can be seen that the extracellular concentrations of galactose and the specific rate of galactose uptake are negatively correlated along principle component two (y-axis) with steady-state F01. As cultivation F was carried out without galactose in the batch as well as in the feed medium, this result is not surprising. However, as these two variables are orthogonal to the emerging of the LPS and the NLPS, the galactose concentrations by itself had most likely an indirect influence on the

shift from one state to the other state. This will be discussed in more detail in the following sections, with special emphasis on specific uptake rates and intracellular metabolite concentrations during this two different metabolic states.

4.4.2 Cell growth, metabolism and A1AT production

All six continuous cultivations with the AGE1.HN.AAT cell line were performed with control of the temperature at 37 °C, DO at 40 % and pH value at 7.15 as described in section 3.2.3. Exponentially growing cells not older than passage 15, were used for inoculation of the bioreactor (see table 4.10). The 42-MAX-UB medium used for the initial batch phase of cultivations A–E was supplemented with 20 mM glucose, 5 mM glutamine and 2.8 mM galactose, whereas the medium for cultivation F was prepared without galactose. After a short batch phase of 2.5–3.0 d the continuous operation mode was started with different feed concentrations of glutamine and glucose according to table 4.10.

4.4.2.1 Cell growth and A1AT production

As can be seen in figures 4.26-a and 4.27-a, cell growth during the exponential phase was comparable between cultivations A, B, C, D and F. However, in cultivation E, the formation of biomass was higher not only during the exponential, but also during the transition phase before a steady-state was reached, which can be seen in the increase in viable cell concentrations and cellular volumes. Also the concentrations of A1AT were higher at the beginning of cultivation E (see figure 4.26-d). In addition, also in cultivation C, the viable cell concentrations were significantly higher during the transition phase compared to cultivations A, B, D and F. This faster increase in biomass was probably due to higher start concentrations (t = 0 h) of glucose in cultivation C (27 mM instead of 20 mM) and glutamine in cultivation E (8 mM instead of 5 mM) compared to the other cultivations. This was not intended, however having similar feed compositions, during the following continuous phase cultivation E reached a steady-state comparable to steady-states D and F01 with a viable cell concentration of $1.0 \cdot 10^6$ cells/mL and a CV_v of 3.40 μL/mL (compare figures 4.26 and 4.27 and tables 4.11 and 4.12).
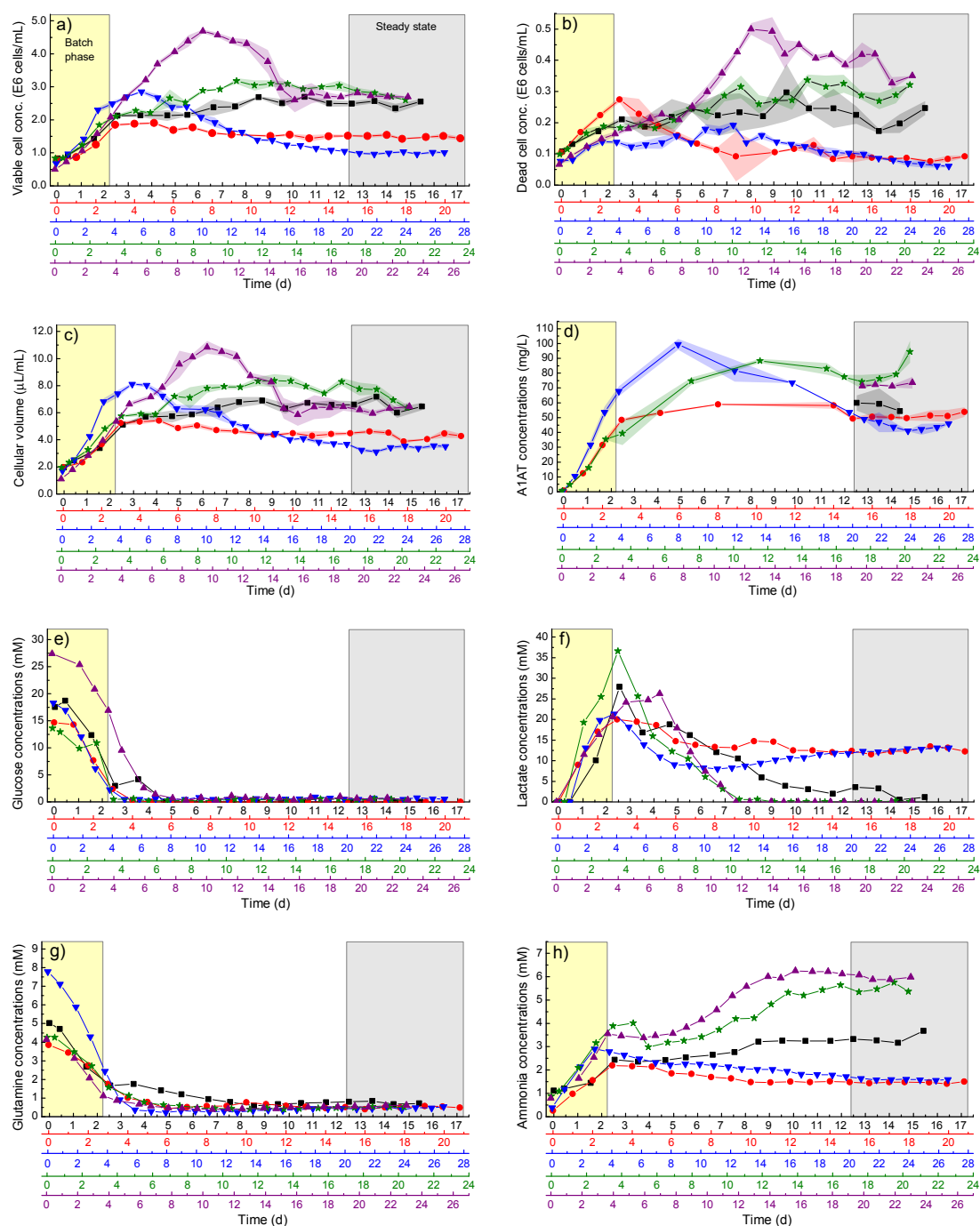
Figure 4.26: Results of continuous cultivations A (■), B (★), C (▲), D (●) and E (▼). **a)** Viable and **b)** dead cell concentrations, **c)** cellular volume, **d)** A1AT, **e)** GLC, **f)** LAC, **g)** GLN and **h)** AMM concentrations. In diagrams a)–d) the averages of three replicate measurements with the SD as shaded background around the symbols are shown. Further analysed steady-state samples are marked by a grey background, whereas the batch phase is marked by a yellow background.

Furthermore, cultivation C reached a similar steady-state as cultivations A and B with a viable cell concentration of 2.7 $\cdot 10^6$ cells/mL and a CV_v of 6.23 μL/mL. As can be seen in figures 4.26 and 4.27, the steady-states reached in cultivation A, B and C were clearly different to the steady-states D, E and F01. In cultivation A, B and C the viable and dead cell concentrations and the total cellular volumes were clearly higher by having smaller cell diameters and thus lower specific cell volumes at the same time (see figures 4.27-b, 4.28-a and tables 4.11 and 4.12). As was already mentioned above, for continuous cultivations A, B and C the dilution rate and hence the specific cell growth rate (μ) was stepwise decreased. As can be seen in figure 4.26-b and in table 4.11, during cultivation A, B and C with a value of -0.81, the increase of the dead cell concentrations was strongly correlated with the decrease of μ (see figure 4.29). A higher amount of dead cells was also found by others, after decreasing the dilution rate stepwise to lower values during continuous cultivations with hybridoma and CHO cells [56, 90, 198]. However, due to a high positive correlation coefficient of 0.90 for the extracellular ammonia concentration with the X_D, the increase in X_D for cultivations A, B and C might be a consequence of an increasing ammonia induced toxification of the cells (see figure 4.29). Again, this is in agreement with the earlier mentioned results from Priesnitz et al. [47], who showed that for ammonia concentrations above 5 mM cell growth of AGE1.HN.AAT cells was negatively affected. In contrast to that, Lee et al. [90] found that the increase in the specific death rate of a hybridoma cell line cultivated in continuous mode, was not due to increased ammonia concentrations, but rather due to an unknown low-molecular-weight component [90]. Therefore, to clarify whether the increase of X_D of the AGE1.HN.AAT cell line during cultivations A, B and C was a function of the specific cell growth rate alone or due to an ammonia induced toxification, additional experiments would be needed.
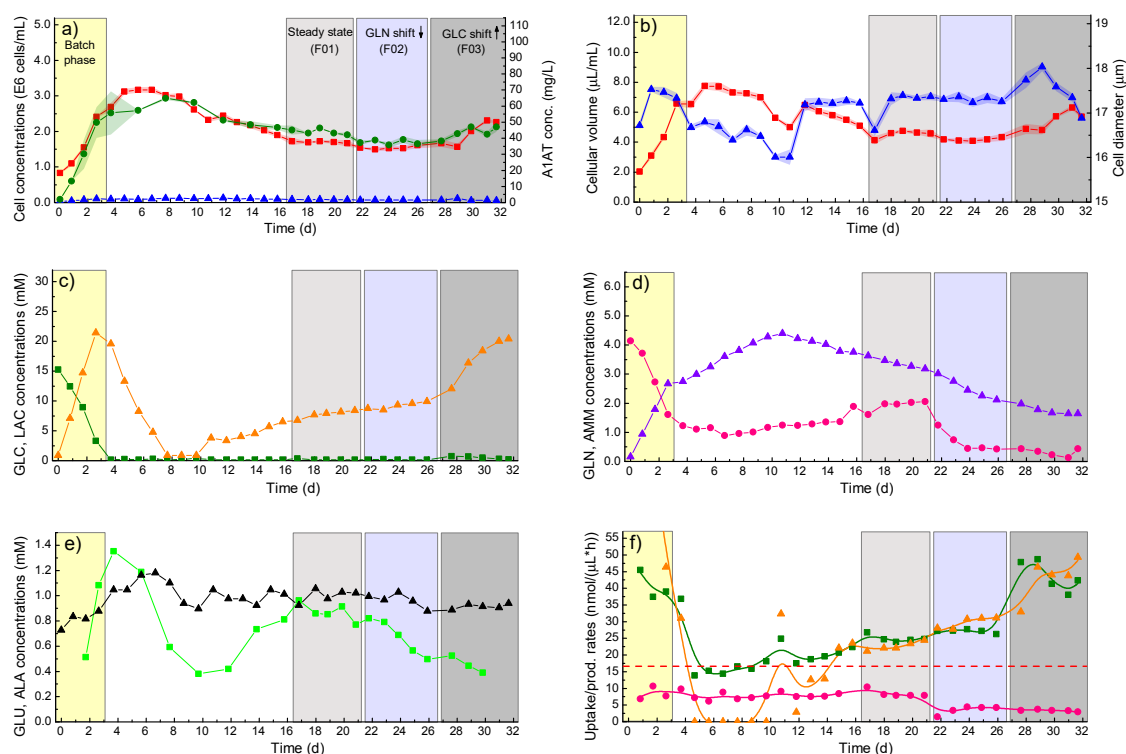
Figure 4.27: Results of continuous cultivation F. **a)** Viable cells (■), dead cells (▲) and A1AT conc.(●), **b)** cellular volume (■) and cell diameters (▲) , **c)** GLC (■) and LAC conc. (▲), **d)** GLN (●) and AMM conc. (▲), **e)** GLU (▲) and ALA conc. (■) and **f)** specific GLC uptake (■), GLN uptake (●), LAC production rates (▲) and threshold for lactate production of the specific glucose uptake rate (red dashed line) (symbols = calculated values, lines = spline interpolated values according to [199]). In diagrams a) and b) the averages of three replicate measurements with the SD as shaded background around the symbols are shown. The batch phase and steady-state F01 are marked by a yellow and a grey background. Experiments F02 and F03 are marked with a blue and a dark grey background.

Along with the biomass, also the A1AT concentrations during steady-states A, B and C were higher compared to steady-states D, E and F01. However, the specific A1AT production rate was clearly higher in cultivation D and E and comparable to the productivities during the batch cultivations with 2.5 L and 0.5 L working volumes (see table 4.11 and section 4.3.1) and therefore positive correlated with the LPS. In addition, a moderate positive correlation of μ with the specific A1AT production rate could be found (see figure 4.29). In contrast to that, the specific A1AT production rate was strongly positive correlated with the specific lactate pro-

duction rate (0.94). Highest t-PA productivities were also found during continuous cultivations with a CHO cell line for the highest glucose feed concentration and the highest specific lactate production rate [91]. For a CHO cell line, Hayter et al. [56] found an increasing specific rate of interferon-γ production with increasing specific growth rate during glucose-limited chemostat cultures. In contrast to that, for different hybridoma cell lines grown in continuous cultivations, a inverse relationship between the specific antibody production rate and μ was found [8, 200]. However, even though A1AT production during batch and continuous cultivations was most likely growth dependent, the overall yield of produced A1AT during the continuous cultivations depended on the overall yield of biomass, which was highest during the NLPS.
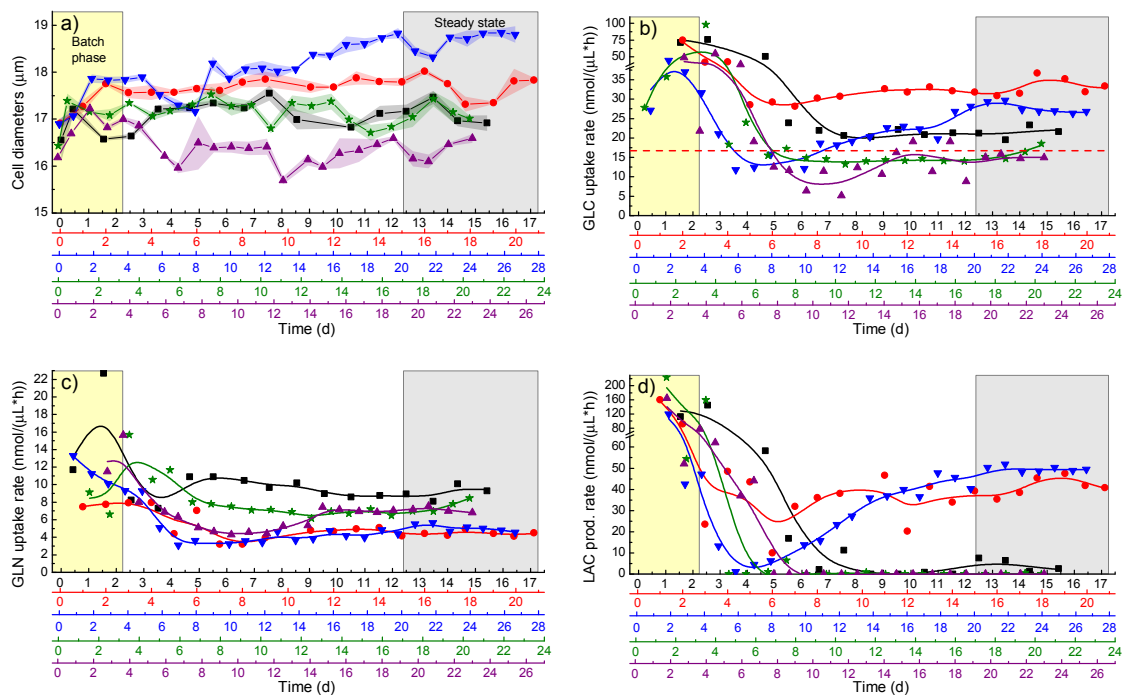
Figure 4.28: Cell diameter and specific rates of continuous cultivations A (■), B (★), C (▲), D (●) and E (▼). **a)** Cell diameters and **b)** specific GLC, **c)** GLN and **d)** LAC production rates (symbols = calculated values, lines = spline interpolated values according to [199]). In diagram a) the averages of three replicate measurements with the SD as shaded background around the symbols is shown. Further analysed steady-state samples are marked by a grey background, whereas the batch phase is marked by a yellow background. In diagramm b), the threshold for lactate production of the specific glucose uptake rate is indicated by a red dashed line.

121

4.4.2.2 Glucose metabolism

Glucose was almost instantly taken up by the cells and residual concentrations of glucose were close to the detection limit by the time the steady-states were reached (see figure 4.26-e and 4.27-c). In cultivations A, B and C lactate was almost not detectable any more after reaching steady-state leading to a $Y_{lac/glc}$ close to zero in contrast to values of 1.2, 1.8 and 0.9 $^{mol}\!/_{mol}$ for steady-states D, E and F01 (see tables 4.11 and 4.12). In addition, having a smaller specific cell volume the glucose uptake rates were also significantly lower during steady-state of cultivations A, B and C compared to steady-states D, E and F01 (see figures 4.27-f and 4.28-b). In contrast to that, the lower glutamine feed concentration of 2 mM in cultivation D and E was accompanied by a lower glutamine uptake rate by a factor of 1.7 and a slightly increased glucose uptake rate (see figure 4.28-b and -c). Moreover, it can be seen, when comparing the time courses of the specific glucose and lactate rates, that the switch from the LPS to a metabolic state without lactate production was strongly coupled to the specific glucose uptake rate. Despite producing lactate during steady-state, the lactate production rate in cultivation E was almost zero two days after switching from batch to continuous mode (see figure 4.28-d). Shortly after, the glutamine uptake rate reached its lowest value followed by an increase in the glucose uptake rate (see figures 4.28-b and -c). At the same time the cells started immediately producing lactate. Also, when comparing cultivation A to cultivations B and C, it can be seen that having a higher glucose uptake rate at the beginning of the continuous mode, the decrease of the specific lactate production rate in cultivation A was clearly later (figure 4.28). In addition, in cultivation A a complete NLPS was not reached as can be seen in the average lactate concentration of 2.1 mM during steady-state (see table 4.11).

As was also observed for cultivation E, the lactate concentrations in cultivation F immediately started to decrease approaching zero after seven days (see figure 4.27-c). However, after day nine the cells surprisingly started to release lactate and reached after five complete volume exchanges a steady-state, which was marked by a $Y_{lac/glc}$ value of 0.9 $^{mol}\!/_{mol}$. Again, in agreement with cultivations A, B, C, D and E, a strong correlation of the glucose uptake rate with the onset of lactate production could be found in cultivation F. Being initially high, after switching from batch to continuous mode the specific glucose uptake rate dropped to a value of

13.9 $^{nmol}/_{\mu L\,h}$ at day four and then steadily increased until reaching a value of 18.1 $^{nmol}/_{\mu L\,h}$ at day nine. This was followed immediately by a sharp increase in the lactate production rate. As can be seen in figure 4.27-b together with the sharp increase in the lactate production rate (figure 4.27-f), the mean cell diameter also increased after day ten from 16.0 µm to its initial value from the batch phase of 17.2 µm. This increase after day ten was preceded by a gradual decrease of the mean cell diameters (figure 4.27-b). As was found by various studies, in case the intracellular osmolarity exceeds the extracellular osmolarity, water flows into the cell following its osmotic gradient and the cell swells. In contrast, if extracellular osmolarity exceeds the intracellular osmolarity water exits, leading to cell shrinkage [201]. After switching from batch to continuous mode, a gradual removal of osmotic active compounds (e.g. lactate) from the culture medium might have led to a decrease in the extracellular osmolarity. As this would induce cell swelling, the cells counteract by volume regulatory mechanisms decreasing the intracellular osmolarity, leading to a regulatory cell volume decrease [201]. After day ten the cells switched from a more efficient glucose metabolism to a highly glycolytic state with high lactate production. As pointed out by Lang et al. [202], an activation of glycolysis might foster cell swelling by the intracellular accumulation of lactate and H^+ and subsequent activation of the Na^+/H^+ exchanger. This would explain the sharp increase of the mean cell diameter during cultivation F with the onset of lactate production after day ten. Interestingly, even though cultivations A, B, C and F were performed with the same glucose and glutamine feed concentrations, the specific glucose uptake rate was higher during steady-state F01. According to the manufacturer of the 42-MAX-UB medium (Xell AG, Germany), galactose was added to the formulation to reduce the production of lactate. This was also found by Altamirano et al. [31] showing that cell growth was improved with a combination of 5 mM glucose and 20 mM galactose compared to growth on 20 mM glucose without galactose. Accordingly, the higher specific glucose uptake rate during cultivation F was presumably the result of the galactose-free medium used for this experiment. However, due to a rather strong positive correlation of μ with the specific glucose uptake rate (0.79), a certain contributing effect of μ on the emerging of the above discussed differences between steady-states A, B, C and D, E and F01 can not be completely excluded.

The observed decrease of $Y_{lac/glc}$ in cultivations A, B and C together with the increase in the $Y_{CVv/glc}$ clearly indicates a metabolic shift towards a more efficient glucose metabolism with a higher biomass yield, which seemed to be accompanied by a decrease in the specific glucose uptake rate below a certain threshold. Also Le et al. [197] found for CHO cells grown in batch and fedbatch cultivations that the specific glucose consumption rates significantly differed between high-titer and low-titer runs. In high-titer runs, the cells consumed glucose at reduced rates and produced less lactate or even consumed lactate compared to those with low titer and high lactate production rates. Therefore, they speculated that a key factor of low lactate production probably appears to be a low specific glucose consumption rate [197]. Comparable results were also found by others [56, 91, 197, 198, 203]. However, not only the specific glucose uptake rate could probably raise the intracellular metabolite concentrations to a level at which a shift in the central metabolism is triggered, as also the specific pyruvate uptake rates differed clearly between the steady-states of cultivation A, B, C, and F01 compared to D and E (see tables 4.11 and 4.12). Therefore, in section 4.4.3 the origin of the metabolic shift will be further discussed considering the levels of intracellular metabolite pools during steady-state, as well as during the shift experiment.

4.4.2.3 Glutamine metabolism

Besides the clear differences in extracellular ammonia concentrations, the $Y_{amm/gln}$ was comparable with values betwwen 0.8–1.3 $^{mol}\!/_{mol}$ for all six steady-states. However, having the same glutamine feed concentration as cultivations A, B and C, the extracellular ammonia concentration during steady-state F01 was clearly lower compared to steady-states B and C, and comparable to steady-state A. In addition, alanine was produced during steady-states A, E und F01, whereas aspartate was produced during steady-states D and E (see tables 4.11 and 4.12). In contrast to that, alanine and aspartate were consumed in steady-states B and C. According to Häggström [42], values for $Y_{amm/gln}$ approaching or exceeding one is a strong indication that the GLDH pathway is used for catabolism of glutamine (see also figure 4.20), whereas a net production of alanine and/or aspartate might indicate that glutamine is converted via transaminase reactions. This was also observed for other cell lines, where the GLDH pathway was up-regulated at glucose limitation,

while the pathways through AspTA and alanine transaminase (AlaTA) dominated during growth conditions with excess substrates [42]. For the AGE1.HN.AAT cells, this might indicate that during cultivations B and C the glutamine metabolism was shifted to a more energy efficient use of glutamine as the complete catabolism of glutamine through the GLDH pathway generates more energy than the incomplete oxidation via AlaTA or AspTA [42]. Upregulation of the GLDH was also found for baculovirus infected insect cells, were the up-regulation of the GLDH during infection might have contributed to maintain the post-infection energetic status of the cells [204]. In addition, the alanine uptake during steady-states B and C might have additionally contributed to the higher extracellular ammonia concentrations compared to steady-states A, D, E and F01 (see table 4.11) and might explain the lower ammonia concentration during steady-state F01 even though the same glutamine feed concentration of 5 mM was provided (see tables 4.11 and 4.12). This is in contrast to the 13C tracer experiments performed by Niklas et al. [45] with the parental AGE1.HN cell line. In their study, it was found that the consumed alanine was mainly directly metabolized to lactate during batch cultivations in shaker flasks. However, this merely underlines how AGE1.HN cells can easily adapt to different cultivation conditions by modifications of the central cell metabolism.

4.4.2.4 Glutamine and glucose shifts during steady-state

As the lower glutamine feed concentration in cultivations D and E probably resulted in a metabolic state with high lactate production, the effect of shifting the glutamine concentrations during steady-state was also examined in addition to the experiments with different feed concentrations of glucose and glutamine. Therefore, in cultivation F initiated with identical glucose and glutamine feed concentrations as experiments A, B and C, the glutamine concentration in the feed medium was shifted from 5 to 2 mM after reaching a steady-state. After two more complete volume exchanges, the glucose concentration was then shifted from 10 to 20 mM to test whether the dynamic of intracellular metabolite concentrations are correlated with the specific glucose uptake rate. However, as during cultivation F the cells already shifted from a NLPS to a LPS before the steady-state was reached (after day nine), the intended effect of the glutamine shift during the steady-state was only minor. As can be seen in figure 4.27-c and -d, shifting the glutamine feed

125

concentration from 5 to 2 mM decreased the extracellular ammonia concentration from 3.4 to 2.5 mM and increased the extracellular lactate concentration from 7.8 to 9.2 mM (see table 4.12). In addition, the X_V together with the CV_v decreased, leading to a reduction of about 9 % in the $Y_{CVv/glc}$ (see table 4.12). As can be seen, the decrease of the CV_v after the glutamine shift was correlated with the increase in the specific glucose uptake rate from 24.9 to 27.1 nmol/μL h. Also, the specific lactate production rate slightly increased, whereas the specific A1AT production rate remained more or less constant with a value between 8.7–9.2 pg/cell d.

In contrast to the moderate effect of the glutamine shift on cell growth and metabolism, the shift of the glucose feed concentration from 10 mM to 20 mM had a much more pronounced effect, especially on cell growth. As can be seen in figure 4.27-a and- b, the mean cell diameter instantly increased, whereas the viable cell concentrations lagged behind and increased only after two days from 1.54 to 1.96 $\cdot 10^6$ cells/mL which corresponds to about 27 % (see table 4.12). Also, the CV_v increased by a value of about 31 %. The extracellular lactate concentrations increased as well, however the $Y_{lac/glc}$ remained constant, indicating a comparable metabolic state as before the shift. This shows, at least for the investigated glucose/glutamine ratio, that the yield of biomass during continuous cultivations was strongly limited by the glucose availability. Similar results were also found by Cruz et al. [205] for BHK cells grown in continuous mode with different glucose and glutamine feed concentrations. Shifting the glutamine concentration from 4 to 2.5 mM had only a minor effect on cell growth, whereas upon shifting the glucose concentration from 16.7 to 5.6 mM, led to a decrease of around 28 % of the total cell concentration [205].

	A1AT-EC	XD	q_ASP	XV	CVv	AMM-EC	Y_CVv/glc	q_AMM	GLU-EC	q_GLN	Y_ala/gln	CD	PYR-EC	μ	Y_CVv/gln	q_PYR	q_GLC	ASP-EC	q_A1AT	Y_lac/glc	LAC-EC	q_LAC	GALC-EC	q_GALC	GLC-EC	Y_amm/gln	q_ALA	GLN-EC	ALA-EC	q_GLU
A1AT-EC	1.00	0.89	0.84	0.84	0.81	0.81	0.75	0.36	0.57	0.33	-0.61	-0.61	-0.61	-0.67	-0.50	-0.40	-0.73	-0.74	-0.59	-0.81	-0.81	-0.77	0.15	0.41	0.12	0.21	0.18	-0.34	-0.51	0.08
XD	0.89	1.00	0.95	0.89	0.80	0.90	0.80	0.48	0.58	0.44	-0.51	-0.75	-0.57	-0.81	-0.66	-0.55	-0.84	-0.82	-0.76	-0.87	-0.90	-0.85	0.06	0.40	0.25	0.27	0.10	-0.25	-0.39	0.04
q_ASP	0.84	0.95	1.00	0.92	0.88	0.86	0.84	0.43	0.70	0.56	-0.43	-0.71	-0.57	-0.71	-0.72	-0.56	-0.86	-0.83	-0.80	-0.90	-0.94	-0.90	0.10	0.41	0.15	0.05	-0.17	-0.24	-0.17	0.20
XV	0.84	0.89	0.92	1.00	0.97	0.90	0.90	0.55	0.77	0.63	-0.64	-0.84	-0.80	-0.55	-0.71	-0.62	-0.83	-0.94	-0.91	-0.99	-0.96	-0.97	-0.17	0.21	-0.07	0.12	-0.12	0.00	-0.28	0.15
CVv	0.81	0.80	0.88	0.97	1.00	0.82	0.92	0.43	0.81	0.56	-0.59	-0.69	-0.74	-0.46	-0.64	-0.59	-0.81	-0.87	-0.85	-0.93	-0.91	-0.93	-0.08	0.20	-0.12	0.00	-0.20	-0.05	-0.21	0.24
AMM-EC	0.81	0.90	0.86	0.90	0.82	1.00	0.91	0.77	0.69	0.63	-0.48	-0.79	-0.60	-0.75	-0.82	-0.80	-0.93	-0.88	-0.86	-0.89	-0.94	-0.92	-0.29	0.08	0.27	0.50	0.19	0.11	-0.34	-0.01
Y_CVv/glc	0.75	0.80	0.84	0.90	0.92	0.91	1.00	0.64	0.83	0.64	-0.36	-0.62	-0.54	-0.62	-0.80	-0.83	-0.95	-0.84	-0.84	-0.87	-0.93	-0.92	-0.22	0.01	0.18	0.27	-0.04	0.10	-0.13	0.19
q_AMM	0.36	0.48	0.43	0.55	0.43	0.77	0.64	1.00	0.58	0.81	-0.17	-0.67	-0.40	-0.37	-0.86	-0.85	-0.66	-0.65	-0.67	-0.61	-0.67	-0.68	-0.76	-0.42	0.19	0.61	0.15	0.63	-0.01	-0.03
GLU-EC	0.57	0.58	0.70	0.77	0.81	0.69	0.83	0.58	1.00	0.79	-0.23	-0.53	-0.48	-0.25	-0.79	-0.69	-0.73	-0.73	-0.72	-0.77	-0.81	-0.82	-0.27	-0.10	-0.10	-0.06	-0.37	0.21	0.19	0.64
q_GLN	0.33	0.44	0.56	0.63	0.56	0.63	0.64	0.81	0.79	1.00	-0.10	-0.65	-0.44	-0.14	-0.90	-0.72	-0.60	-0.67	-0.71	-0.69	-0.74	-0.76	-0.58	-0.28	-0.10	0.05	-0.42	0.51	0.37	0.33
Y_ala/gln	-0.61	-0.51	-0.43	-0.64	-0.59	-0.48	-0.36	-0.17	-0.23	-0.10	1.00	0.72	0.92	0.13	0.06	0.02	0.21	0.64	0.56	0.65	0.46	0.54	0.15	-0.23	0.45	-0.11	-0.20	0.06	0.74	0.17
CD	-0.61	-0.75	-0.71	-0.84	-0.69	-0.79	-0.62	-0.67	-0.53	-0.65	0.72	1.00	0.86	0.39	0.65	0.49	0.57	0.87	0.87	0.88	0.79	0.83	0.45	-0.09	0.18	-0.26	0.01	-0.24	0.35	0.07
PYR-EC	-0.61	-0.57	-0.57	-0.80	-0.74	-0.60	-0.54	-0.40	-0.48	-0.44	0.92	0.86	1.00	0.11	0.35	0.25	0.38	0.81	0.76	0.82	0.65	0.74	0.36	-0.10	0.51	-0.05	0.06	-0.17	0.47	0.03
μ	-0.67	-0.81	-0.71	-0.55	-0.46	-0.75	-0.62	-0.37	-0.25	-0.14	0.13	0.39	0.11	1.00	0.52	0.55	0.79	0.49	0.47	0.50	0.63	0.52	-0.19	-0.38	-0.70	-0.52	-0.41	0.32	0.38	0.17
Y_CVv/gln	-0.50	-0.66	-0.72	-0.71	-0.64	-0.82	-0.80	-0.86	-0.79	-0.90	0.06	0.65	0.35	0.52	1.00	0.87	0.83	0.75	0.76	0.75	0.85	0.82	0.46	0.14	-0.24	-0.29	0.18	-0.36	-0.21	-0.23
q_PYR	-0.40	-0.55	-0.56	-0.62	-0.59	-0.80	-0.83	-0.85	-0.69	-0.72	0.02	0.49	0.25	0.55	0.87	1.00	0.88	0.65	0.73	0.62	0.74	0.74	0.55	0.33	-0.34	-0.52	-0.05	-0.49	-0.10	-0.07
q_GLC	-0.73	-0.84	-0.86	-0.83	-0.81	-0.93	-0.95	-0.66	-0.73	-0.60	0.21	0.57	0.38	0.79	0.83	0.88	1.00	0.78	0.79	0.80	0.87	0.87	0.16	-0.07	-0.39	-0.38	-0.05	-0.05	0.11	-0.12
ASP-EC	-0.74	-0.82	-0.83	-0.94	-0.87	-0.88	-0.84	-0.65	-0.73	-0.67	0.64	0.87	0.81	0.49	0.75	0.65	0.78	1.00	0.91	0.95	0.92	0.94	0.36	-0.10	0.09	-0.23	0.06	-0.19	0.28	-0.11
q_A1AT	-0.59	-0.76	-0.80	-0.91	-0.85	-0.86	-0.84	-0.67	-0.72	-0.71	0.56	0.87	0.76	0.47	0.76	0.73	0.79	0.91	1.00	0.92	0.89	0.94	0.43	0.00	0.10	-0.22	0.14	-0.29	0.16	-0.08
Y_lac/glc	-0.81	-0.87	-0.90	-0.99	-0.93	-0.89	-0.87	-0.61	-0.77	-0.69	0.65	0.88	0.82	0.50	0.75	0.62	0.80	0.95	0.92	1.00	0.97	0.98	0.24	-0.17	0.11	-0.13	0.14	-0.06	0.26	-0.14
LAC-EC	-0.81	-0.90	-0.94	-0.96	-0.91	-0.94	-0.93	-0.67	-0.81	-0.74	0.46	0.79	0.65	0.63	0.85	0.74	0.91	0.92	0.89	0.97	1.00	0.98	0.20	-0.16	-0.09	-0.19	0.13	-0.04	0.15	-0.18
q_LAC	-0.77	-0.85	-0.90	-0.97	-0.93	-0.92	-0.92	-0.68	-0.82	-0.76	0.54	0.83	0.74	0.52	0.82	0.74	0.87	0.94	0.94	0.98	0.98	1.00	0.30	-0.08	0.05	-0.16	0.16	-0.14	0.15	-0.17
GALC-EC	0.15	0.06	0.10	-0.17	-0.08	-0.29	-0.22	-0.76	-0.27	-0.58	0.15	0.45	0.36	-0.19	0.46	0.55	0.16	0.36	0.43	0.24	0.20	0.30	1.00	0.68	0.23	-0.46	-0.07	-0.96	-0.09	0.13
q_GALC	0.41	0.40	0.41	0.21	0.20	0.08	0.01	-0.42	-0.10	-0.28	-0.23	-0.09	-0.10	-0.38	0.14	0.33	-0.07	-0.10	0.00	-0.17	-0.16	-0.08	0.68	1.00	0.01	-0.29	-0.07	-0.75	-0.27	0.04
GLC-EC	0.12	0.25	0.15	-0.07	-0.12	0.27	0.18	0.19	-0.10	-0.10	0.45	0.18	0.51	-0.70	-0.24	-0.34	-0.39	0.09	0.10	0.11	-0.09	0.05	0.23	0.01	1.00	0.52	0.48	-0.24	-0.06	-0.19
Y_amm/gln	0.21	0.27	0.05	0.12	0.00	0.50	0.27	0.61	-0.06	0.05	-0.11	-0.26	-0.05	-0.52	-0.29	-0.52	-0.38	-0.23	-0.22	-0.13	-0.19	-0.16	-0.46	-0.29	0.52	1.00	0.81	0.36	-0.50	-0.50
q_ALA	0.18	0.10	-0.17	-0.12	-0.20	0.19	-0.04	0.15	-0.37	-0.42	-0.20	0.01	0.06	-0.41	0.18	-0.05	-0.05	0.06	0.14	0.14	0.13	0.16	-0.07	-0.07	0.48	0.81	1.00	-0.06	-0.76	-0.53
GLN-EC	-0.34	-0.25	-0.24	0.00	-0.05	0.11	0.10	0.63	0.21	0.51	0.06	-0.24	-0.17	0.32	-0.36	-0.49	-0.05	-0.19	-0.29	-0.06	-0.04	-0.14	-0.96	-0.75	-0.24	0.36	-0.06	1.00	0.29	-0.08
ALA-EC	-0.51	-0.39	-0.17	-0.28	-0.21	-0.34	-0.13	-0.01	0.19	0.37	0.74	0.35	0.47	0.38	-0.21	-0.10	0.11	0.28	0.16	0.26	0.15	0.15	-0.09	-0.27	-0.06	-0.50	-0.76	0.29	1.00	0.45
q_GLU	0.08	0.04	0.20	0.15	0.24	-0.01	0.19	-0.03	0.64	0.33	0.17	0.07	0.03	0.17	-0.23	-0.07	-0.12	-0.11	-0.08	-0.14	-0.18	-0.17	0.13	0.04	-0.19	-0.50	-0.53	-0.08	0.45	1.00

Figure 4.29: Pearson correlation coefficients of different parameters from steady-states A, B, C, D, E, and F01 (see table 4.10). Positive and negative correlations are highlighted in red and blue, respectively, whereas the strength of the individual correlation pair is depicted by the colour saturation (EC = extracellular concentration).

Table 4.11: Steady-state values of different parameters from continuous cultivations with varying GLC and GLN feed concentrations and with 3 mM galactose. Shown are the averages and the absolute and relative SDs of 4–7 steady-states values.

	Exp. A		Exp. B		Exp. C		Exp. D		Exp. E	
Variable	Average ± SD	Rel. SD (%)	Average ± SD	Rel. SD (%)	Average ± SD	Rel. SD (%)	Average ± SD	Rel. SD (%)	Average ± SD	Rel. SD (%)
Setpoints:										
DR (1/h)	0.0140	-	0.0120	-	0.0100	-	0.0150	-	0.0133	-
GLC feed conc. (mM)	10.0	-	10.0	-	10.0	-	10.0	-	8.0	-
GLN feed conc. (mM)	5.0	-	5.0	-	5.0	-	2.0	-	2.0	-
GALC feed conc. (mM)	3.0	-	3.0	-	3.0	-	3.0	-	3.0	-
GLC/GLN ratio (mol/mol)	2	-	2	-	2	-	5	-	4	-
X_V (E6 cells/mL)	2.490 ± 0.100	4.0	2.745 ± 0.118	4.3	2.735 ± 0.056	2.0	1.489 ± 0.043	2.9	0.998 ± 0.025	2.5
X_D (E6 cells/mL)	0.210 ± 0.032	15.2	0.291 ± 0.021	7.4	0.378 ± 0.047	12.5	0.086 ± 0.006	6.5	0.075 ± 0.014	18.5
CV_v (μL/mL)	6.56 ± 0.48	7.4	7.19 ± 0.67	9.4	6.23 ± 0.21	3.4	4.33 ± 0.27	6.3	3.40 ± 0.17	4.9
μ (1/h)	0.0152 ± 0.0002	1.2	0.0133 ± 0.0001	1.1	0.0114 ± 0.0002	1.4	0.0159 ± 0.0001	0.6	0.0143 ± 0.0002	1.4
CD (μm)	17.1 ± 0.25	1.5	17.2 ± 0.19	1.1	16.3 ± 0.24	1.5	17.7 ± 0.30	1.5	18.7 ± 0.20	1.1
GLC (mM)	0.0 ± 0.00	-	0.0 ± 0.00	-	0.0 ± 0.00	-	0.0 ± 0.00	-	0.0 ± 0.00	-
LAC (mM)	2.1 ± 1.52	-	0.0 ± 0.00	-	0.0 ± 0.00	-	12.5 ± 0.60	5.0	12.7 ± 0.40	3.0
GLN (mM)	0.8 ± 0.08	10.0	0.5 ± 0.02	3.5	0.6 ± 0.04	7.3	0.5 ± 0.10	11.1	0.5 ± 0.10	13.7
AMM (mM)	3.4 ± 0.22	6.7	5.5 ± 0.19	3.5	5.9 ± 0.09	1.5	1.5 ± 0.03	2.1	1.6 ± 0.02	1.6
GALC (mM)	1.9 ± 0.08	4.5	1.9 ± 0.06	2.9	1.7 ± 0.02	0.9	2.1 ± 0.10	2.5	2.4 ± 0.10	3.2
PYR (mM)	0.2 ± 0.00	1.8	0.1 ± 0.00	3.2	0.1 ± 0.00	3.2	0.3 ± 0.04	12.6	1.1 ± 0.10	5.3
GLU (mM)	1.2 ± 0.08	6.2	1.3 ± 0.01	0.5	1.0 ± 0.05	5.0	0.7 ± 0.10	12.9	0.8 ± 0.10	12.8
ALA (mM)	1.4 ± 0.09	6.4	0.2 ± 0.03	13.8	0.1 ± 0.01	14.2	0.3 ± 0.02	8.9	1.0 ± 0.05	5.2
ASP (mM)	1.6 ± 0.06	3.9	1.5 ± 0.05	3.2	1.3 ± 0.02	1.2	2.4 ± 0.17	7.1	2.8 ± 0.30	10.8
A1AT (mg/L)	57.9 ± 3.03	5.2	81.0 ± 9.21	11.4	72.1 ± 1.09	1.5	50.9 ± 1.50	2.9	44.6 ± 2.80	6.2
$Y_{CVv/glc}$ (μL/mmol)	711 ± 47	6.6	827 ± 77	9.4	753 ± 17	2.3	482 ± 30	6.3	518 ± 18	3.5
$Y_{CVv/gln}$ (μL/mmol)	1679 ± 140	8.3	1770 ± 145	8.2	1601 ± 52	3.3	3617 ± 215	6.0	2837 ± 201	7.1
$Y_{lac/glc}$ (mol/mol)	0.2 ± 0.15	-	0.0 ± 0.01	-	0.0 ± 0.00	-	1.2 ± 0.10	5.3	1.8 ± 0.10	3.2
$Y_{amm/gln}$ (mol/mol)	0.8 ± 0.05	6.6	1.2 ± 0.04	3.6	1.3 ± 0.03	1.9	1.0 ± 0.05	4.9	1.1 ± 0.10	4.8
$Y_{ala/gln}$ (mol/mol)	0.2 ± 0.02	9.5	0.0 ± 0.00	-	0.0 ± 0.00	-	0.0 ± 0.00	-	0.6 ± 0.04	7.9
q_{GLC} (nmol/μL h)[a]	21.43 ± 1.56	7.3	16.17 ± 1.76	10.9	15.13 ± 0.51	3.4	33.05 ± 2.17	6.6	27.64 ± 1.33	4.8
q_{LAC} (nmol/μL h)[a]	-4.43 ± 3.05	-	0.00 ± 0.00	-	0.00 ± 0.00	-	-41.23 ± 4.13	10.0	-49.68 ± 1.30	2.6
q_{GLN} (nmol/μL h)[a]	9.10 ± 0.82	9.0	7.55 ± 0.72	9.5	7.12 ± 0.31	4.3	4.40 ± 0.28	6.4	5.07 ± 0.41	8.1
q_{AMM} (nmol/μL h)[a]	-7.19 ± 0.67	9.3	-9.21 ± 0.97	10.5	-9.55 ± 0.30	3.2	-4.48 ± 0.35	7.8	-5.66 ± 0.33	5.9
q_{GALAC} (nmol/μL h)[a]	1.94 ± 0.21	10.8	1.55 ± 0.22	14.3	2.46 ± 1.26	51.1	1.92 ± 0.24	12.3	1.61 ± 0.37	23.3
q_{PYR} (nmol/μL h)[a]	5.82 ± 0.52	8.9	4.70 ± 0.57	12.1	4.48 ± 0.11	2.4	9.10 ± 0.64	7.1	7.04 ± 0.55	7.8
q_{GLU} (nmol/μL h)[a]	-1.31 ± 0.18	14.0	-1.05 ± 0.10	9.4	-0.52 ± 0.09	17.9	-0.71 ± 0.31	43.5	-0.88 ± 0.38	43.8
q_{ALA} (nmol/μL h)[a]	-2.14 ± 0.27	12.8	0.39 ± 0.03	6.7	0.54 ± 0.03	5.9	0.10 ± 0.12	127.8	-2.81 ± 0.26	9.4
q_{ASP} (nmol/μL h)[a]	1.19 ± 0.19	15.9	1.20 ± 0.10	8.1	1.49 ± 0.05	3.5	-0.41 ± 0.62	150.7	-2.16 ± 1.15	53.1
q_{A1AT} (pg/cell d)[a]	-7.87 ± 0.19	2.4	-8.54 ± 1.34	15.7	-6.33 ± 0.19	3.0	-12.31 ± 0.60	4.9	-14.29 ± 1.08	7.5

a: Substrate uptake is indicated by a positive rate, whereas a negative value indicates a production rate.

Table 4.12: Steady-state values of different parameters from continuous cultivations with varying GLC and GLN feed concentrations and without galactose. Shown are the averages and the absolute and relative SDs of 5 steady-states values.

	Exp. F01		Exp. F02		Exp. F03	
Variable	Average ± SD	Rel. SD (%)	Average ± SD	Rel. SD (%)	Average ± SD	Rel. SD (%)
Setpoints:						
DR (1/h)	0.0150	-	0.0150	-	0.0144	-
GLC feed conc. (mM)	10	-	10	-	20	-
GLN feed conc. (mM)	5	-	2	-	2	-
GALC feed conc. (mM)	0	-	0	-	0	-
GLC/GLN ratio (mol/mol)	2	-	5	-	10	-
X_V (E6 cells/mL)	1.701 ± 0.023	1.3	1.540 ± 0.042	2.7	1.963 ± 0.335	17.1
X_D (E6 cells/mL)	0.081 ± 0.004	5.1	0.070 ± 0.001	1.5	0.074 ± 0.023	31.7
CV_v (μL/mL)	4.54 ± 0.24	5.2	4.17 ± 0.09	2.3	5.48 ± 0.63	11.5
μ (1/h)	0.0156 ± 0.0000	0.2	0.0155 ± 0.0000	0.1	0.0150 ± 0.0003	1.9
CD (μm)	17.2 ± 0.33	1.9	17.3 ± 0.06	0.3	17.5 ± 0.43	2.5
GLC (mM)	0.0 ± 0.00	-	0.0 ± 0.05	-	0.0 ± 0.00	-
LAC (mM)	7.8 ± 0.64	8.2	9.2 ± 0.58	6.3	17.4 ± 3.41	19.6
GLN (mM)	1.9 ± 0.18	9.3	0.7 ± 0.35	52.6	0.3 ± 0.13	42.6
AMM (mM)	3.4 ± 0.17	5.1	2.5 ± 0.37	14.6	1.7 ± 0.14	8.2
PYR (mM)	0.4 ± 0.02	6.6	0.4 ± 0.04	9.8	0.4 ± 0.11	28.2
GLU (mM)	1.0 ± 0.05	5.2	1.0 ± 0.06	5.8	0.9 ± 0.02	2.3
ALA (mM)	0.9 ± 0.07	8.2	0.7 ± 0.14	20.8	0.5 ± 0.07	14.8
ASP (mM)	1.9 ± 0.21	10.8	1.9 ± 0.15	7.8	1.8 ± 0.13	7.3
A1AT (mg/L)	44.0 ± 1.71	3.9	37.5 ± 1.41	3.8	43.5 ± 3.68	8.5
$Y_{CV_v/glc}$ (μL/mmol)	626 ± 25	4.0	573 ± 11	2.0	355 ± 35	10.0
$Y_{CV_v/gln}$ (μL/mmol)	1865 ± 201	10.8	3856 ± 520	13.5	4605 ± 369	8.0
$Y_{lac/glc}$ (mol/mol)	0.9 ± 0.07	8.2	1.1 ± 0.07	6.6	1.0 ± 0.20	19.5
$Y_{amm/gln}$ (mol/mol)	1.3 ± 0.04	3.1	1.8 ± 0.15	8.4	1.3 ± 0.22	16.5
$Y_{ala/gln}$ (mol/mol)	0.2 ± 0.02	8.5	0.3 ± 0.17	49.5	0.2 ± 0.07	44.1
q_{GLC} (nmol/μL h)[a]	24.9 ± 1.08	4.3	27.1 ± 0.55	2.0	43.6 ± 4.53	10.4
q_{LAC} (nmol/μL h)[a]	-22.6 ± 1.27	5.6	-29.7 ± 1.70	5.7	-43.3 ± 6.22	14.4
q_{GLN} (nmol/μL h)[a]	8.4 ± 1.07	12.7	4.1 ± 0.48	11.9	3.4 ± 0.29	8.7
q_{AMM} (nmol/μL h)[a]	-10.9 ± 1.13	10.3	-8.8 ± 1.41	15.9	-4.5 ± 0.87	19.2
q_{PYR} (nmol/μL h)[a]	4.5 ± 0.31	6.9	4.8 ± 0.13	2.8	3.4 ± 0.22	6.4
q_{GLU} (nmol/μL h)[a]	-0.7 ± 0.15	20.4	-0.7 ± 0.21	30.3	-0.3 ± 0.07	20.1
q_{ALA} (nmol/μL h)[a]	-1.99 ± 0.33	16.3	-1.45 ± 0.52	35.6	-0.53 ± 0.22	42.1
q_{ASP} (nmol/μL h)[a]	1.65 ± 0.64	39.0	0.81 ± 0.52	63.9	1.34 ± 0.42	31.2
q_{A1AT} (pg/cell d)[a]	-9.2 ± 0.25	2.7	-8.7 ± 0.48	5.5	-7.8 ± 1.15	14.8

a: Substrate uptake is indicated by a positive rate, whereas a negative value indicates a production rate.

4.4.3 Intracellular metabolite concentrations

To this point, it was established in this thesis that during batch cultivations, the dynamics of intracellular metabolites, especially in the glycolytic pathway, were strongly connected to the specific glucose uptake rate. It was also shown that the switch from the NLPS to the LPS during the continuous cultivations was coupled to a range of 17–27 nmol/μL h of the specific glucose uptake rate. As these two observed metabolic states were quite different regarding the concentration of extracellular metabolites, a higher glycolytic flux towards lactate during the LPS might be also reflected in the concentrations of intracellular metabolites when compared to the NLPS. Therefore, intracellular metabolite concentrations were measured during all six steady-states and further analysed with a PCA. In addition, intracellular

metabolite concentrations were measured over the whole cultivation time of cultivation F, resulting in 28 trajectories of intracellular metabolites from glycolysis, PPP, TCA-cycle and nucleotide metabolism.

4.4.3.1 Intracellular metabolite concentrations during steady-state

Again, to obtain an overview of the steady-state results and to check for outliers, a PCA was calculated for cultivations A, B, C, D, E and F01. Therefore, intracellular metabolite concentrations during steady-state, the ECR and the ratios of $^{ATP}/_{ADP}$ and $^{ATP}/_{AMP}$ were applied (see tables 4.13 and 4.14). For steady-state samples B, C, D, E and F01 averages of three technical samples per sampling point and for steady-state A, single determinations per sampling point were used. Four principle components were calculated with an overall R^2 of 94 % and a Q^2 of 75 %.

As can be seen in figure 4.30-b and -d the two metabolic states are clearly separated along principle component 1, which explains 51.7 % of the data variation. In addition, no outliers were detected. The main differences in intracellular metabolite levels between the NLPS and the LPS can be seen in figure 4.30-a and -c. The LPS (steady-states D, E and F01) is correlated with high concentrations of metabolites mainly from glycolysis (G6P, F6P, FBP, 3PG and PEP), but also from the TCA-cycle (CIT, ICIT and MAL). Also the ECR and the ratios of $^{ATP}/_{ADP}$ and $^{ATP}/_{AMP}$ were higher, when the cells produced lactate. In addition, during steady-states A, D, E and F01 the intracellular pyruvate pool was significantly higher (10–44 fold increased) compared to steady-states B and C (see tables 4.13 and 4.14). In contrast to that, after switching to a more efficient glucose metabolism without lactate production, the concentrations of almost all nucleotides (ATP, ADP, AMP, UTP, UDP, GTP, GDP, GMP, CTP and CDP) together with R5P were higher, whereas concentrations of the glycolytic metabolites were much lower concentrated. However, nucleotide triphosphates (NTPs) were only during steady-state of cultivation A clearly increased. During steady-state of cultivations B and C ATP, GTP, UTP and CTP were only slightly increased (see figure 4.30-a and table 4.13). In contrast, the concentrations of nucleotide diphosphates (NDPs) and nucleotide monophosphates (NMPs) were significantly increased during steady-state of cultivations A, B and C compared to cultivations D, E and F01. In addition, also the ratios of $^{ATP}/_{ADP}$ and $^{ATP}/_{AMP}$ were higher during the LPS. The reason for the increase of NDPs and NMPs might be

the higher biomass and A1AT formation, which probably led to an increased demand of NTPs together with an increased formation of NDPs and NMPs. Moreover, the increased concentrations of R5P, CTP and UTP during the NLPS might indicate an increased flux through the oxidative and/or non oxidative branches of the PPP to meet the increased demand of nucleotides for the increased proliferation rate [206–208]. Therefore, the proliferative capacity of AGE1.HN cells might be also limited by the abundance of its nucleotide pool, which is also discussed for other cell lines [207].
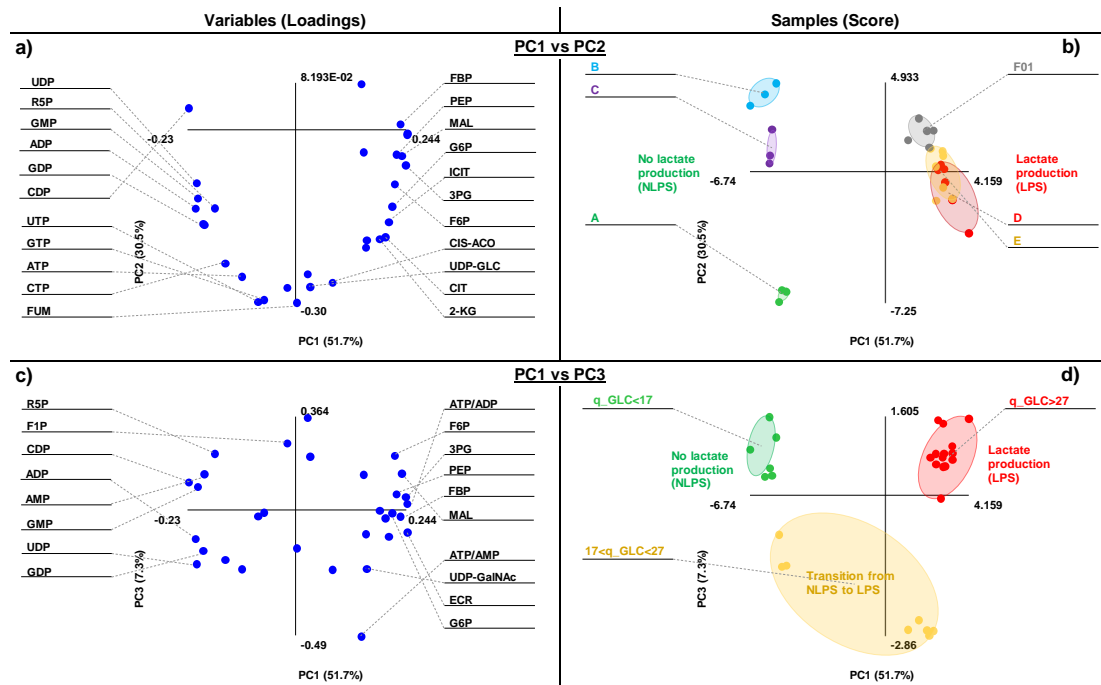
Figure 4.30: Loadings and scores of steady-state samples during continuous cultivations with different GLC and GLN feed concentrations (experiments A, B, C, D, E and F01, see table 4.10). Shown are the first three principle components with the concentrations of intracellular metabolites from glycolysis, TCA-cycle, PPP and nucleotide metabolism and the ECR and the ratio $^{ATP+GTP}/_{UTP+CTP}$ as variables.

The discriminatory power of multivariate data analysis was also used to differentiate between high- and low-producer clones in a study of Chong et al. [209] with different CHO cell lines producing monoclonal antibodies. In their study, different intracellular metabolites linked to the generation of energy, the regulation of cellular redox potential and precursors for protein glycosylation (e.g. nucleotide-

activated sugar precursors such as GDP-fucose and uridine diphosphate N-acetyl glucosamine (UDP-GlcNAc) were positive correlated with the high producer cell lines. The authors concluded their study, by suggesting that high producers had elevated levels of these metabolites to better regulate their redox status and to facilitate the generation of energy and activated sugar precursors to better meet the demands for production of glycosylated recombinant monoclonal antibodies [209]. Also, in AGE1.HN.AAT cells during the LPS, the specific A1AT production rate was higher, together with increased intracellular concentrations of UDP-GlcNAc and UDP-GalNAc (see tables 4.13 and 4.14). In another study, using multivariate data analysis, a range of intracellular metabolites correlating with different μ could be identified for CHO cells grown in different media [38]. The set of identified metabolites consisted mainly of NTPs (dCTP, CTP, GTP, ATP, and NAD) which were higher concentrated in cells growing with a higher μ. This again is in agreement with the findings in this thesis, as especially NTPs were higher concentrated during steady-state A, which had the highest μ among the non lactate producing cultivations (A, B and C). Therefore, as already mentioned above, the *DR* and hence μ had probably in addition to the different feed concentrations, a distinct effect on the emergence of the two different metabolic states.

4.4.3.2 Dynamics of intracellular metabolites during shift experiment

As can be seen in figure 4.31, almost all metabolites from glycolysis, PPP and TCA cycle increased during the batch phase to their highest concentrations. Also, the ECR increased during the batch phase (see figure 4.32). After starting the feed with 10 mM glucose and 5 mM glutamine, together with the specific glucose uptake rate almost all intracellular metabolites and the extracellular lactate concentration decreased rapidly to their lowest concentrations. As can be seen in figure 4.32, together with the decrease of the mean cell diameter directly after the batch phase (compare figure 4.27), the intracellular concentrations of ATP, but also GTP and UTP decreased. Lang et al. [202] mentioned that the maintenance of a constant cell volume by the cell requires the expenditure of energy to fuel the Na$^+$-K$^+$-ATPase, which is required to establish the ionic gradients across the cell membrane. This might explain the decrease of ATP along with the decrease of the mean cell diam-

eter as the cell is forced to counteract the aforementioned hypothesized change
in extracellular osmolarity (refer to section 4.4.2). The increase in biomass forma-
tion during the NLPS probably consumed more energy, which could have also led
additionally to a decrease in the concentrations of NTPs. In contrast to that, the
intracellular concentration of CDP increased up to day ten and then gradually de-
creased after the onset of lactate production. This might indicate that during the
NLPS the formation of CDP was increased due to the formation of phosphatidyl-
choline via the CDP-choline pathway to meet the increased demand for the build
up of cellular membranes [210]. After day nine, together with the aforementioned
increase in the mean cell diameter and the onset of lactate production, the con-
centrations of intracellular metabolites from glycolysis (G6P, F6P, 3PG, PEP, PYR)
increased clearly, even though being diluted by the increase of the specific cell vol-
ume (figure 4.31). Also the intracellular concentrations of FUM, MAL, 2-KG and
CIT, UDP-GlcNAc and UDP-GalNAc increased after the onset of lactate production.
Shifting the glutamine feed concentration from 5 to 2 mM had only a minor effect
on most of the intracellular metabolite concentrations (see green symbols in figure
4.31 and 4.32). Only for the concentrations of 3PG and PEP a slight increase could
be observed, together with a slight increase in the specific glucose uptake rate and
the $Y_{lac/glc}$. This might indicate that the glycolytic flux was slightly adjusted to com-
pensate for the lower glutamine availability. In addition, at the end of steady-state
F02, the concentrations of ATP, GTP and UTP dropped about 15 %. Nonetheless,
the overall effect of the glutamine shift on the intracellular metabolites was only
small. In contrast to that, after the glucose shift from 10 to 20 mM, all metabo-
lites from glycolysis as well as some organic acids increased immediately together
with the specific glucose uptake rate, followed by a decrease after five days (see
red symbols in figures 4.31 and 4.32). This indicates again, in agreement with the
results of the batch cultivations, that the glucose uptake via GLUT had a distinct
impact on the dynamic of the glycolysis in AGE1.HN.AAT cells, which seemed to be
especially pronounced in the dynamics of G6P, F6P, FBP, 3PG and PEP. However,
also intermediates from the TCA-cycle (fumarate (FUM) and MAL) were increased
upon the increase in the specific glucose uptake rate.
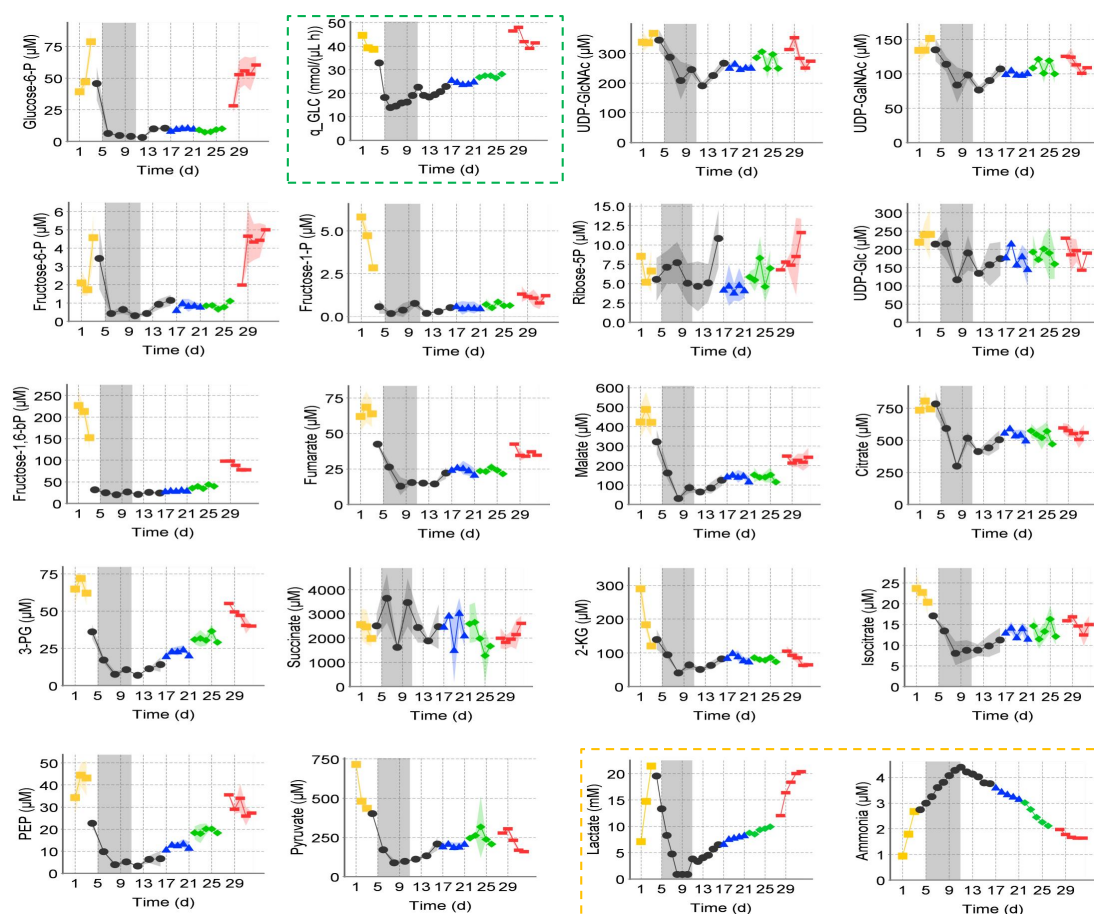
Figure 4.31: Intracellular metabolite concentrations, the specific glucose uptake rate (green frame) and extracellular lactate and ammonia concentrations (orange frame) during the shift experiment (cultivation F). Shown are samples from the batch phase (■), the transition from batch to steady-state with GLC and GLN feed concentrations of 10 and 5 mM (●), steady-state F01(▲), GLN shift from 5 to 2 mM (◆) and GLC shift from 10 to 20 mM (■). The NLPS is marked by a light-grey background. The average of three technical replicates and the SD as shaded background around the symbols is shown.
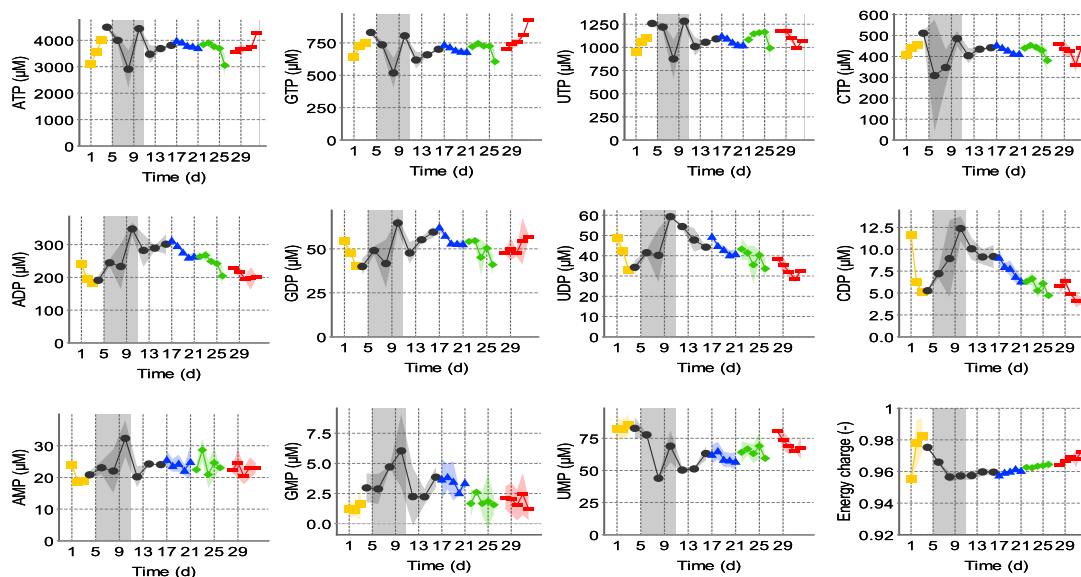
Figure 4.32: Intracellular nucleotide concentrations and the ECR during the shift experiment (cultivation F). Shown are samples from the batch phase (■), the transition from batch to steady-state with GLC and GLN feed concentrations of 10 and 5 mM (●), steady-state F01(▲), GLN shift from 5 to 2 mM (◆) and GLC shift from 10 to 20 mM (■). The NLPS is marked by a light-grey background. The average of three technical replicates and the SD as shaded background around the symbols is shown.

4.4.3.3 The origin of the observed metabolic shifts

As explained in section 4.3.4.1, compared to the continuous cultivations, the glucose uptake rate was much higher during the exponential growth phase of the batch cultivations. This was probably due to a higher concentration gradient over the cell membrane and the fact that the cells were growing with their maximum growth rate during the exponential phase of the batch cultivations. The higher glycolytic flux then left the cell no other choice as to regenerate NAD^+ via a highly active LDH to maintain a high oxidative capacity. In contrast to that, during the continuous cultivations, glucose was taken up with residual extracellular concentrations close to zero, indicating that the transport of glucose through the cell membrane was probably achieved via an active transport by sodium-dependent glucose transporters, as a facilitated transport would be solely driven by the concentration gradient [171]. Lowering the glucose uptake rate and therefore the glycolytic flux as indicated by the lower concentrated intracellular glycolytic metabolites might

therefore have led to a flux regime were the cells were not forced to regenerate NAD^+ via LDH. For a hybridoma cell line, Ljunggren and Häggström [20] found that for glucose and glutamine limited fed batch cultures, the overflow metabolism to lactate, alanine, and some other amino acids was reduced. They speculated that the main reasons for these changes were the decreased uptake rates of glucose and glutamine, which in turn led to a reduction of the pyruvate pool and a restriction of the flux through GLNase and LDH. A shift in the central metabolism during batch cultivations of the parental AGE1.HN cell line cultivated in 42-MAX-UB supplemented with 5 mM glutamine was also found by Niklas et al. [44]. The cells were grown for almost ten days in shaker flasks showing at least three distinct growth phases. The main event triggering the shift from the first phase to the second phase (90–160 h) was according to Niklas et al. [44] the depletion of pyruvate, leading to a reduced glucose uptake rate of 13.4 $^{nmol}/_{\mu L\, h}$ together with an immediate stop of the lactate production. During the first growth phase (0–90 h) the lactate production as well as the glucose uptake rate (> 30 $^{nmol}/_{\mu L\, h}$) were high. The flux calculation revealed that the highest flux through the glycolytic pathway was during the first growth phase. In the second growth phase, the glycolytic activity was significantly lower and remained nearly constant, whereas the TCA cycle activity was higher compared to the first phase. They concluded their study by stating that in AGE1.HN, the available intracellular pyruvate is probably triggering the conversion of pyruvate to lactate. High uptake rates of glucose and pyruvate, as observed in the first growth phase, might therefore have led to an increase of the intracellular pyruvate pool, which triggered the overflow metabolism into lactate/alanine and eventually resulted in an increased secretion of these waste metabolites [44]. Clearly higher specific pyruvate uptake rates were also found during the lactate producing steady-states of continuous cultivations D and E compared to A, B and C. However, clearly increased intracellular pyruvate pools were found for steady-states A, D, E and F01, all four cultivations where lactate was produced during steady-state. Nonetheless, if the increased intracellular pyruvate pools during steady-states D, E and F01 were the reason or the consequence of the observed metabolic shift towards an inefficient overflow metabolism, with increased secretion of lactate, alanine and aspartate cannot be said without further experiments.

Table 4.13: Steady-state values of intracellular metabolites for continuous cultivations with different GLC and GLN feed concentrations and with 3 mM galactose.

	Exp. A		Exp. B		Exp. C		Exp. D		Exp. E	
Variable	Avg ± SD (µM)	Rel.S.D (%)	Avg ± SD (µM)	Rel.S.D (%)	Avg ± SD (µM)	Rel.S.D (%)	Avg ± SD (µM)	Rel.S.D (%)	Avg ± SD (µM)	Rel.S.D (%)
3PG	10.7 ± 2.28	21.3	3.7 ± 2.77	74.2	4.5 ± 0.52	11.5	28.8 ± 7.38	25.6	25.8 ± 4.20	16.3
F1P	6.1 ± 0.30	5.0	2.3 ± 0.97	42.2	3.7 ± 1.30	35.6	3.8 ± 0.87	23.1	4.4 ± 0.68	15.4
F6P	1.3 ± 0.54	42.7	0.0 ± 0.00	-	0.0 ± 0.00	-	4.2 ± 1.15	27.0	4.4 ± 0.73	16.8
FBP	15.6 ± 1.24	7.9	14.8 ± 1.67	11.2	18.3 ± 1.53	8.4	45.6 ± 8.21	18.0	34.5 ± 2.84	8.2
G6P	9.4 ± 2.18	23.3	0.0 ± 0.00	-	0.0 ± 0.00	-	16.6 ± 5.91	35.7	13.3 ± 2.73	20.4
PEP	6.6 ± 1.34	20.3	4.4 ± 3.22	72.8	3.6 ± 0.75	20.6	17.3 ± 3.70	21.4	12.7 ± 4.15	32.7
PYR	182.8 ± 121.52	66.5	19.1 ± 4.57	24.0	9.8 ± 1.93	19.7	235.1 ± 71.60	30.5	835.2 ± 203.54	24.4
R5P	32.2 ± 7.44	23.1	18.1 ± 2.89	16.0	36.0 ± 8.19	22.8	15.1 ± 4.57	30.3	11.7 ± 3.54	30.2
UDP-GalNAc	117.0 ± 4.39	3.8	58.6 ± 8.97	15.3	71.6 ± 2.45	3.4	100.4 ± 11.67	11.6	115.7 ± 13.68	11.8
UDP-GlcNAc	310.6 ± 58.95	19.0	136.0 ± 41.94	30.8	153.7 ± 7.16	4.7	271.6 ± 21.41	7.9	308.3 ± 49.09	15.9
UDP-GLC	314.6 ± 24.69	7.8	160.7 ± 24.73	15.4	245.7 ± 51.41	20.9	278.3 ± 58.08	20.9	238.6 ± 45.17	18.9
2-KG	75.2 ± 6.98	9.3	32.2 ± 1.77	5.5	51.7 ± 19.05	36.8	100.2 ± 20.52	20.5	93.7 ± 14.72	15.7
CIS-ACO	6.7 ± 0.48	7.1	2.9 ± 0.50	17.1	4.2 ± 0.04	0.9	5.3 ± 1.61	30.2	4.9 ± 1.03	21.0
CIT	542.3 ± 36.64	6.8	242.5 ± 10.06	4.1	303.9 ± 39.29	12.9	589.5 ± 140.86	23.9	583.0 ± 89.10	15.3
FUM	33.5 ± 6.12	18.2	9.70 ± 0.95	9.7	15.6 ± 2.89	18.5	29.9 ± 9.38	31.3	26.2 ± 4.33	16.5
ICIT	11.2 ± 0.46	4.1	3.9 ± 0.85	22.0	5.9 ± 1.97	33.5	13.7 ± 3.52	25.6	11.8 ± 2.04	17.2
MAL	241.9 ± 48.43	20.0	66.6 ± 1.40	2.1	105.1 ± 19.94	19.0	227.1 ± 57.40	25.3	194.9 ± 22.89	11.7
SUC	1920.3 ± 254.53	13.3	982.9 ± 182.09	18.5	2303.8 ± 121.26	5.3	1917.2 ± 541.02	28.2	OCR	-
ADP	620.0 ± 10.19	1.6	426.4 ± 37.94	8.9	462.0 ± 11.31	2.4	247.2 ± 31.62	12.8	243.1 ± 22.40	9.2
AMP	59.3 ± 6.22	10.5	42.4 ± 0.09	0.2	41.5 ± 4.96	12.0	26.3 ± 2.70	10.3	25.8 ± 1.98	7.7
ATP	5678.7 ± 205.80	3.6	3449.8 ± 85.87	2.5	4121.0 ± 185.85	4.5	3746.1 ± 434.78	11.6	3419.3 ± 218.04	6.4
CDP	28.6 ± 6.18	21.6	46.3 ± 1.98	4.3	37.1 ± 3.48	9.4	7.4 ± 2.47	33.4	7.3 ± 1.88	25.8
CTP	723.7 ± 15.06	2.1	444.5 ± 27.56	6.2	494.4 ± 18.93	3.8	413.9 ± 39.18	9.5	401.5 ± 25.72	6.4
GDP	108.4 ± 0.85	0.8	70.3 ± 8.57	12.2	78.9 ± 2.97	3.8	49.0 ± 7.61	15.5	46.0 ± 4.73	10.3
GMP	14.5 ± 2.58	17.8	10.5 ± 2.28	21.7	13.9 ± 0.37	2.7	6.7 ± 1.17	17.6	5.6 ± 0.67	12.0
GTP	1097.1 ± 44.80	4.1	671.6 ± 30.08	4.5	808.2 ± 34.76	4.3	839.8 ± 98.53	11.7	717.4 ± 52.34	7.3
UDP	89.5 ± 11.67	13.0	65.9 ± 5.80	8.8	58.8 ± 1.55	2.6	24.7 ± 3.84	15.5	27.3 ± 4.24	15.5
UMP	125.0 ± 4.04	3.2	79.6 ± 3.30	4.2	91.0 ± 3.26	3.6	118.2 ± 23.90	20.2	99.6 ± 17.23	17.3
UTP	1789.9 ± 44.66	2.5	1070.1 ± 111.72	10.4	1246.5 ± 59.89	4.8	1201.5 ± 144.86	12.1	1235.7 ± 75.88	6.1
ECR (-)	0.94 ± 0.001	0.1	0.93 ± 0.01	1.2	0.94 ± 0.00	0.0	0.96 ± 0.001	0.1	0.96 ± 0.001	0.1
ATP/ADP (-)	9.16 ± 0.20	2.2	8.12 ± 0.50	6.2	8.92 ± 0.19	2.1	15.19 ± 0.61	4.0	14.09 ± 0.58	4.1
ATP/AMP (-)	96.23 ± 7.14	7.4	80.17 ± 0.94	1.2	99.99 ± 8.15	8.2	142.68 ± 11.23	7.9	132.49 ± 4.08	3.1

OCR: out of calibrated range; Avg: averages of 3–7 samples from steady-state with 3 technical replicates per sample (except for cultivation A: single determination per sample)

Table 4.14: Steady-state values of intracellular metabolites for continuous cultivations with different GLC and GLN feed concentrations and without GALC.

Metabolite	Exp. F01		Exp. F02		Exp. F03	
	Avg ± SD (µM)	Rel.S.D (%)	Avg ± SD (µM)	Rel.S.D (%)	Avg ± SD (µM)	Rel.S.D (%)
3PG	21.7 ± 2.61	12.0	30.8 ± 4.12	13.4	45.1 ± 5.71	12.6
F1P	1.8 ± 0.22	12.3	2.0 ± 0.29	14.7	2.2 ± 0.31	14.1
F6P	1.8 ± 0.24	13.4	1.8 ± 0.21	11.6	4.7 ± 1.19	25.5
FBP	38.1 ± 2.65	6.9	48.1 ± 5.08	10.6	95.5 ± 9.91	10.4
G6P	10.8 ± 1.92	17.8	10.0 ± 1.34	13.4	52.8 ± 12.70	24.1
PEP	12.4 ± 1.62	13.1	18.8 ± 3.18	16.9	30.2 ± 4.91	16.3
PYR	225.5 ± 44.03	19.5	255.0 ± 42.94	16.8	231.7 ± 79.17	34.2
R5P	3.5 ± 1.26	36.0	4.7 ± 1.61	34.3	6.0 ± 1.75	29.0
UDP-GalNAc	109.1 ± 10.08	9.2	118.3 ± 11.89	10.0	123.7 ± 14.46	11.7
UDP-GlcNAc	256.5 ± 10.53	4.1	278.6 ± 30.77	11.0	294.1 ± 40.62	13.8
UDP-GLC	185.5 ± 34.85	18.8	197.0 ± 44.58	22.6	207.0 ± 37.25	18.0
2-KG	81.8 ± 11.43	14.0	78.6 ± 9.63	12.2	78.5 ± 18.87	24.0
CIS-ACO	5.1 ± 0.63	12.4	5.2 ± 0.88	17.0	5.6 ± 0.64	11.5
CIT	520.0 ± 42.84	8.2	516.4 ± 62.20	12.0	536.7 ± 50.10	9.3
FUM	23.1 ± 3.26	14.1	23.6 ± 3.73	15.8	35.4 ± 6.33	17.9
ICIT	12.5 ± 1.43	11.5	13.0 ± 2.11	16.3	14.7 ± 1.80	12.2
MAL	165.9 ± 20.05	12.1	168.9 ± 24.88	14.7	242.9 ± 31.63	13.0
SUC	2178.6 ± 248.72	11.4	2175.7 ± 453.74	20.9	2200.8 ± 562.74	25.6
ADP	285.2 ± 20.90	7.3	240.8 ± 33.33	13.8	210.3 ± 25.80	12.3
AMP	15.4 ± 1.47	9.5	14.9 ± 2.46	16.5	14.4 ± 1.49	10.3
ATP	3822.6 ± 129.91	3.4	3550.5 ± 469.98	13.2	3722.5 ± 314.61	8.5
CDP	7.3 ± 1.19	16.2	5.6 ± 0.78	13.9	4.8 ± 1.03	21.4
CTP	432.8 ± 18.79	4.3	423.8 ± 47.53	11.2	432.7 ± 31.83	7.4
GDP	56.2 ± 4.23	7.5	48.9 ± 7.20	14.7	51.0 ± 6.91	13.6
GMP	4.4 ± 1.80	41.1	3.9 ± 1.11	28.3	1.8 ± 0.86	46.7
GTP	687.9 ± 25.47	3.7	670.9 ± 83.09	12.4	763.8 ± 84.80	11.1
UDP	42.2 ± 3.60	8.5	37.3 ± 6.41	17.2	31.8 ± 4.72	14.8
UMP	61.8 ± 6.46	10.5	66.0 ± 7.12	10.8	70.8 ± 8.68	12.3
UTP	1070.5 ± 42.01	3.9	1082.0 ± 127.02	11.7	1103.6 ± 96.31	8.7
ECR (-)	0.96 ± 0.001	0.1	0.96 ± 0.001	0.1	0.97 ± 0.003	0.3
ATP/ADP (-)	13.43 ± 0.51	3.8	14.76 ± 0.31	2.1	17.80 ± 2.21	12.4
ATP/AMP (-)	248.80 ± 8.89	3.6	239.03 ± 18.11	7.6	258.13 ± 18.68	7.2

Avg: Averages of 5 samples from steady-state with 3 technical replicates per sample.

4.4.4 Summary

Cultivations A, B and C displayed a more efficient glucose metabolism with no/lower lactate production together with a more energy efficient usage of glutamine via GLDH in cultivations B and C, leading to a phenotype producing more biomass as well as A1AT. In contrast to that, the cells produced lactate during steady-states D, E and F01 comparable to batch cultivations and yielded less biomass and A1AT. In addition, it was found that the intracellular concentrations of UDP-GlcNAc and UDP-GalNAc were positive correlated with the specific A1AT production rate,

highlighting the increased demand for producing more glycosylated A1AT per cell during the LPS of cultivations D, E and F01. Moreover, complete glutamine usage during steady-states A, D, E and F01 was probably via transamination reactions through AlaTA and/or AspTA. In addition, it was shown that the specific cell volume increased significantly with the onset of lactate production. Moreover, the shift from the LPS to the NLPS was strongly coupled to the specific glucose uptake rate. Exceeding a range of about 17-27 $^{nmol}/_{\mu L\ h}$, the cells produced lactate, whereas below 17 $^{nmol}/_{\mu L\ h}$ the cells produced no lactate at all. What exactly triggered the shift from LPS to NLPS cannot be said without additional experiments. At least, clearly decreased intracellular pyruvate pools are indicative for the observed metabolic shift. The reduced intracellular pyruvate pools are likely to be the consequence of the reduced glucose and pyruvate uptake, resulting in a higher NAD^+/NADH ratio and therefore a higher oxidative capacity. Therefore, fluxes might be redirected towards a more energy efficient usage of glucose, e.g. precursors derived from G6P might be channelled into other pathways for the generation of nucleotides and fatty acids. However, also a contributing effect of μ cannot be completely excluded, as with the increase in μ also the specific uptake rates of glucose, glutamine and pyruvate increased. In addition, μ was also found to be negative correlated with the increase in the steady-state concentrations of ammonia, probably confirming the ammonia sensitivity of AGE1.HN.AAT cells above 5 mM as shown by Priesnitz et al. [47]. Intracellular metabolite measurements during steady-state as well as during the whole cultivation of experiment F showed that, in agreement with the results from the batch cultivations, the dynamics of glycolysis is strongly coupled to the specific glucose uptake rate and the shift to a metabolic state with no lactate production can be triggered by the decrease of the specific glucose uptake rate below a certain threshold. Moreover, upon the shift to the NLPS, a change in energy metabolism was clearly indicated by increased concentrations of nucleotides (NDPs and NMPs) and R5P.

CHAPTER 5

Summary and Outlook

Optimization of mammalian based bioprocesses aims at cell lines with high biomass yield and high cell-specific productivity with robust growth properties. This is achieved by selection of high-producer cells through cell screenings, cell engineering approaches, and scale-up studies. For media improvement and cell line engineering, in depths understanding of how the metabolism is regulated and connected with product formation is therefore needed. In this thesis, the extracellular and intracellular dynamics of metabolites from glycolysis, PPP, TCA cycle and nucleotides from energy metabolism together with maximum enzyme activities were determined during batch and continuous cultivations with the new human cell line AGE1.HN.AAT producing A1AT. In the following, the main results are summarized and several possible strategies to improve the culture performance with the AGE1.HN.AAT cell line are given, followed by recommendations for possible follow-up experiments.

5.1 Main results from batch and continuous cultivations

By comparing specific rates obtained from a simple unstructured cell growth model with the dynamics of intracellular metabolite concentrations during batch cultiva-

tions, it was found that the dynamics of intracellular metabolite pools was closely linked to cell growth and to the dynamics of the uptake rates of glucose and glutamine. In particular, the glucose uptake had a distinct impact on the dynamics of the upper part of glycolysis. This assumption was also supported by the results of the glucose shift experiment during continuous cultivation F, were all metabolites from glycolysis as well as some organic acids were positive correlated with the increase of the specific glucose uptake rate after a shift of the glucose feed concentration from 10 to 20 mM. In addition, based on the dynamics of FBP, F1P and R5P as well as the increased lactate production during the transition from exponential to stationary growth, it was concluded that the PK might exert an important control point for the glycolysis. Furthermore, after determination of maximum *in vitro* enzyme activities, it was found that the link between glycolysis and TCA cycle seemed to be weak due to the low maximum *in vitro* enzyme activities of PDH and PC. Due to the low activity of GLNase, glutamate formation might pose a rate limiting step for glutamine metabolism. In addition, it was found for the adaptation experiments in shaker flasks that AGE1.HN.AAT cells stopped immediately with proliferation when the extracellular glutamine concentration dropped to zero.

In contrast to the strong lactate producing metabolic state during all batch cultivations, the AGE1.HN.AAT cells could be shifted during continuous cultivations from a phenotype with lactate production to a phenotype with no lactate production. Comparison of specific uptake and production rates indicated that this metabolic shift was most likely triggered by the specific glucose uptake rate below a certain threshold. In addition, intracellular measurements revealed decreased intracellular pyruvate pools for all continuous cultivations with no lactate production. This might indicate a correlation of the intracellular pyruvate concentration with the metabolic shift. However, if the decreased pyruvate pool is the reason or the consequence of the observed metabolic shift still needs to be verified, as the reduced nutrient uptake might have also resulted in a higher $NAD^+/NADH$ ratio and therefore in a higher oxidative capacity, enabling the cells to redirect fluxes towards a more energy efficient usage of glucose. In addition, an influence of μ on the NLPS was observed, and therefore it cannot be completely excluded that the metabolic shift to the NLPS was also supported by a lower μ. Moreover, upon the shift to the NLPS, a change in energy metabolism was observed with increased concentrations of nucleotides (NDPs and NMPs) and R5P. Finally, there was a positive correlation

of μ with the specific A1AT production rate. However, even though A1AT production during batch and continuous cultivations was most likely growth dependent, the volumetric yield of A1AT during the continuous cultivations depended on the overall yield of biomass, which was highest for the NLPS.

5.2 Strategies to improve A1AT production

Based on the above mentioned results, strategies to increase the A1AT production should focus on the increase of the volumetric yield of biomass. This might be achieved by focusing on the increase of the availability of building blocks for biomass synthesis by increasing the glucose as well as glutamine fluxes during batch cultivations. Such an increase of intracellular building blocks for biomass synthesis might be achieved, for example, by over-expression of GLUT, provided that the oxidative capacity is not limiting the glycolytic flux. As was also suggested by Niklas et al. [45], increasing the connectivity of glycolysis with the TCA cycle by over-expression of PC might be another promising strategy to increase the efficient usage of glucose by simultaneously decreasing the overflow metabolism to lactate. In addition, a knock-down of PDHK might increase the activity of PDH, thus reducing lactate production and eventually increasing the volumetric A1AT production as was shown by Zhou et al. [211] for an antibody producing CHO cell line. Furthermore, over-expression of the GLNase gene might increase the intracellular glutamate pool and thus increase glutamine utilization, potentially leading to the generation of more energy and precursors for biosynthesis [42]. Due to the rather high maximum enzyme activity of GS during the batch cultivations, it might also be worthwhile to explore the impact of a knock-down of the GS, because GLNase and GS are usually not expressed simultaneously in normal cells in the human body [192, 193]. Strategies focusing on the increase of the glutamine flux, would probably increase the amount of cell toxic ammonia concentration in the medium. Therefore, another promising strategy could be the adaptation of the cells to glutamine-free medium, after focusing on the increase of the intracellular glutamate pool, as it was found that the activity of GS was theoretically high enough in AGE1.HN.AAT cells to ensure the synthesis of glutamine from glutamate. An increase of the intracellular glutamate pool might be achieved either directly by

increasing the specific glutamate uptake or indirectly through the increased uptake of other amino acids.

Another promising strategy to improve the overall yield of A1AT might be the increase of the biomass yield on glucose. To achieve this, the specific glucose uptake rate should be controlled at a low value during fedbatch cultivations, eventually leading to a metabolic shift towards a highly efficient glucose metabolism, as was observed during the continuous cultivations. In addition, this might be especially promising after the above mentioned adaptation of the cells to glutamine-free medium, as a prolonged fedbatch cultivation time probably leads to higher and potentially cell toxic ammonia concentrations. Furthermore, for fedbatch cultivations, it might be beneficial to control the intracellular metabolite pools (e.g. of pyruvate) at a low level via the nutrient uptake rates, to maintain the glucose efficent metabolic state and to prevent a shift towards lactate production. This might be achieved for example by establishing non-invasive and non-destructive NIR or NMR measurements of *in vivo* intracellular metabolite pools [212]. After a subsequent correlation of the NIR/NMR signal with the non-lactate producing state, eventually the glucose efficient metabolic state might be tracked and controlled online during fedbatch cultivations.

5.3 Follow up experiments

Mass balance analysis showed that by sampling and quenching the cells to 0 °C in 10 s, most metabolite concentrations remained unchanged, with the exception of 3PG, FBP, PEP, F6P, G6P, 2-KG, ADP, GDP and UDP. Further optimization of this method should focus on shortening the time needed to separate the cells from the supernatant. For example, by carefully selecting suitable spin columns with integrated filter membranes, it might be possible to reduce the time needed for separation and washing of the cells, and the extraction of intracellular metabolites. Furthermore, and more important regarding metabolic flux analysis (MFA), a method should be established, which allows for the discrimination between intracellular metabolites from different cell compartments (e.g. cytosol and mitochondria). Moreover, also the influence of macromolecular crowding on biochemical reactions should be taken into account, when optimizing the method for the quantification of intracellular metabolites [213].

To study the influence of the energy status on the dynamics of intracellular metabolites and maximum enzyme activities, different perturbation experiments during continuous cultivations could be performed, e.g. with specific activators or inhibitors of GLUT, with artificial electron acceptors to generate oxidative stress (similar to Bonarius et al. [62]), and with specific inhibitors of the respiratory chain or the ATP/ADP transporter. This might further increase our understanding of the central metabolism and its regulation in mammalian cells. In addition, after establishing a method to determine the ratio of $NAD^+/NADH$ (e.g. by direct measurement or by calculation), it would be interesting to determine this ratio in combination with the concentrations of intracellular metabolites during above mentioned pertubation experiments and combine this with metabolic flux analysis to determine the intracellular fluxes. Finally, a scale up of the established continuous cultivations to a greater volume would enable the combination of intracellular metabolite measurements together with the determination of maximum enzyme activities and analysis of the proteome and transcriptome during steady state and during perturbation experiments.

Bibliography

[1] Florian M Wurm. Production of recombinant protein therapeutics in cultivated mammalian cells. Nature Biotechnology, 22(11):1393–1398, November 2004.

[2] Michael Butler. Animal cell cultures: recent achievements and perspectives in the production of biopharmaceuticals. Applied Microbiology and Biotechnology, 68(3): 283–291, August 2005.

[3] Gary Walsh. Biopharmaceutical benchmarks 2010. Nature Biotechnology, 28(9): 917–924, September 2010.

[4] Jianwei Zhu. Mammalian cell protein expression for biopharmaceutical production. Biotechnology Advances, 30(5):1158–1170, 2012.

[5] Gary Walsh. Biopharmaceutical benchmarks 2014. Nature Biotechnology, 32(10): 992–1000, October 2014.

[6] Yao-Ming Huang, WeiWei Hu, Eddie Rustandi, Kevin Chang, Helena Yusuf-Makagiansar, and Thomas Ryll. Maximizing productivity of CHO cell-based fed-batch culture using chemically defined media conditions and typical manufacturing equipment. Biotechnology Progress, 26(5):1400–1410, 2010.

[7] David L Hacker, Maria De Jesus, and Florian M Wurm. 25 years of recombinant proteins from reactor-grown cells - where do we go from here? Biotechnology Advances, May 2009.

[8] W. M. Miller, H. W. Blanch, and C. R. Wilke. A kinetic analysis of hybridoma growth and metabolism in batch and continuous suspension culture: effect of nutrient concentration, dilution rate, and ph (reprinted from biotechnology and bioengineering, vol. 32, pp 947-965 (1988)). Biotechnology and Bioengineering, 67(6):853–871, March 2000. Reprinted from Biotechnology and Bioengineering, Vol. 32, Pp 947-965 (1988).

[9] S. S. Ozturk and B. O. Palsson. Growth, metabolic, and antibody production kinetics of hybridoma cell culture: 1. analysis of data from controlled batch reactors. Biotechnology Progress, 7(6):471–480, 1991.

[10] R. Pörtner, A. Bohmann, I. Lüdemann, and H. Märkl. Estimation of specific glucose uptake rates in cultures of hybridoma cells. Journal of Biotechnology, 34(3):237–246, May 1994.

[11] L. Fitzpatrick, H. A. Jenkins, and M. Butler. Glucose and glutamine metabolism of a murine b-lymphocyte hybridoma grown in batch culture. Applied Biochemistry and Biotechnology, 43(2):93–116, November 1993.

[12] M. Linz, A. P. Zeng, R. Wagner, and W. D. Deckwer. Stoichiometry, kinetics, and regulation of glucose and amino acid metabolism of a recombinant bhk cell line in batch and continuous cultures. Biotechnology Progress, 13(4):453–463, 1997.

[13] H. J. Cruz, A. S. Ferreira, C. M. Freitas, J. L. Moreira, and M. J. Carrondo. Metabolic responses to different glucose and glutamine levels in baby hamster kidney cell culture. Applied Microbiology and Biotechnology, 51(5):579–585, May 1999.

[14] Michael W. Glacken. Catabolic control of mammalian cell culture. Bio/Technology, 6 (9):1041–1050, September 1988.

[15] S. S. Ozturk, M. R. Riley, and B. O. Palsson. Effects of ammonia and lactate on hybridoma growth, metabolism, and antibody production. Biotechnology and Bioengineering, 39(4):418–431, February 1992.

[16] Cruz, Freitas, Alves, Moreira, and Carrondo. Effects of ammonia and lactate on growth, metabolism, and productivity of bhk cells. Enzyme and Microbial Technology, 27(1-2):43–52, July 2000.

[17] Maria De Jesus and Florian M. Wurm. Manufacturing recombinant proteins in kg-ton quantities using animal cells in bioreactors. European Journal of Pharmaceutics and Biopharmaceutics, 78(2):184–188, June 2011.

[18] J. B. Griffiths. Animal cell culture processes–batch or continuous? Journal of Biotechnology, 22(1-2):21–30, January 1992.

[19] M. W. Glacken, R. J. Fleischaker, and A. J. Sinskey. Reduction of waste product excretion via nutrient control: Possible strategies for maximizing product and cell yields on serum in cultures of mammalian cells. Biotechnology and Bioengineering, 28(9):1376–1389, September 1986.

[20] J. Ljunggren and L. Häggström. Catabolic control of hybridoma cells by glucose and glutamine limited fed batch cultures. Biotechnology and Bioengineering, 44(7): 808–818, September 1994.

[21] A. Gambhir, A. F. Europa, and W. S. Hu. Alteration of cellular metabolism by consecutive fed-batch cultures of mammalian cells. Journal of Bioscience and Bioengineering, 87(6):805–810, 1999.

[22] Helder J. Cruz, Jose L. Moreira, and Manuel J.T. Carrondo. Metabolically optimised bhk cell fed-batch cultures. Journal of Biotechnology, 80:109–118, 2000.

[23] A. F. Europa, A. Gambhir, P. C. Fu, and W. S. Hu. Multiple steady states with distinct cellular metabolism in continuous culture of mammalian cells. Biotechnology and Bioengineering, 67(1):25–34, January 2000.

[24] N. Irani, M. Wirth, J. van Den Heuvel, and R. Wagner. Improvement of the primary metabolism of cell cultures by introducing a new cytoplasmic pyruvate carboxylase reaction. Biotechnology and Bioengineering, 66(4):238–246, 1999.

[25] S. L. Bell, C. Bebbington, M. F. Scott, J. N. Wardell, R. E. Spier, M. E. Bushell, and P. G. Sanders. Genetic engineering of hybridoma glutamine metabolism. Enzyme and Microbial Technology, 17(2):98–106, February 1995.

[26] K. Chen, Q. Liu, L. Xie, P. A. Sharp, and D. I. Wang. Engineering of a mammalian cell line for reduction of lactate formation and high monoclonal antibody production. Biotechnology and Bioengineering, 72(1):55–61, January 2001.

[27] M. Butler and A. Christie. Adaptation of mammalian cells to non-ammoniagenic media. Cytotechnology, 15(1-3):87–94, 1994.

[28] A. Christie and M. Butler. The adaptation of BHK cells to a non-ammoniagenic glutamate-based culture medium. Biotechnology and Bioengineering, 64(3):298–309, August 1999.

[29] C. Altamirano, C. Paredes, A. Illanes, J. J. Cairo, and F. Godia. Strategies for fed-batch cultivation of t-PA producing CHO cells: substitution of glucose and glutamine and rational design of culture medium. Journal of Biotechnology, 110(2):171–179, May 2004.

[30] Y. Genzel, J. B. Ritter, S. König, R. Alt, and U. Reichl. Substitution of glutamine by pyruvate to reduce ammonia formation and growth inhibition of mammalian cells. Biotechnology Progress, 21(1):58–69, 2005.

[31] C. Altamirano, A. Illanes, S. Becerra, J. J. Cairo, and F. Godia. Considerations on the lactate consumption by CHO cells in the presence of galactose. Journal of Biotechnology, 125(4):547–556, October 2006.

[32] Ewa Urbanczyk-Wochniak, Alexander Luedemann, Joachim Kopka, Joachim Selbig, Ute Roessner-Tunali, Lothar Willmitzer, and Alisdair R. Fernie. Parallel analysis of transcript and metabolic profiles: a new approach in systems biology. EMBO Reports, 4(10):989–993, October 2003.

[33] N. Saito, M. Robert, H. Kochi, G. Matsuo, Y. Kakazu, T. Soga, and M. Tomita. Metabolite profiling reveals yihu as a novel hydroxybutyrate dehydrogenase for alternative succinic semialdehyde metabolism in escherichia coli. Journal of Biological Chemistry, 284(24):16442–16451, June 2009. doi: 10.1074/jbc.M109.002089.

[34] R. Sulpice, S. Trenkamp, M. Steinfath, B. Usadel, Y. Gibon, H. Witucka-Wall, E.-T. Pyl, H. Tschoep, M. C. Steinhauser, M. Guenther, M. Hoehne, J. M. Rohwer, T. Altmann, A. R. Fernie, and M. Stitt. Network analysis of enzyme activities and metabolite levels and their relationship to biomass in a large panel of arabidopsis accessions. Plant Cell, 22(8):2872–2893, August 2010.

[35] S. Hori, S. Nishiumi, K. Kobayashi, M. Shinohara, Y. Hatakeyama, Y. Kotani, N. Hatano, Y. Maniwa, W. Nishio, T. Bamba, E. Fukusaki, T. Azuma, T. Takenawa, Y. Nishimura, and M. Yoshida. A metabolomic approach to lung cancer. Lung Cancer, 74(2):284–292, November 2011. doi: 10.1016/j.lungcan.2011.02.008.

[36] S. H. G. Khoo and M. Al-Rubeai. Metabolomics as a complementary tool in cell culture. Biotechnology and Applied Biochemistry, 47:71–84, June 2007.

[37] Panagiotis K Chrysanthopoulos, Chetan T Goudar, and Maria I Klapa. Metabolomics for high-resolution monitoring of the cellular physiological state in cell culture engineering. Metabolic Engineering, 12:212–222, November 2009. doi: 10.1016/j.ymben.2009.11.001.

150

[38] S. Dietmair, M. P. Hodson, L.-E. Quek, N. E. Timmins, P. Chrysanthopoulos, S. S. John, P. Gray, and L. K. Nielsen. Metabolite profiling of CHO cells with different growth characteristics. <u>Biotechnology and Bioengineering</u>, 109(6):1404–1414, March 2012.

[39] T. Ryll and R. Wagner. Intracellular ribonucleotide pools as a tool for monitoring the physiological state of in vitro cultivated mammalian cells during production processes. <u>Biotechnology and Bioengineering</u>, 40(8):934–946, October 1992.

[40] J. Neermann and R. Wagner. Comparative analysis of glucose and glutamine metabolism in transformed mammalian cell lines, insect and primary liver cells. <u>Journal of Cellular Physiology</u>, 166(1):152–169, January 1996.

[41] M. Doverskog, J. Ljunggren, L. Ohman, and L. Häggström. Physiology of cultured animal cells. <u>Journal of Biotechnology</u>, 59(1-2):103–115, December 1997.

[42] L. Häggström. Cell metabolism, animal. In Raymond E. Spier, editor, <u>Encyclopedia of cell technology</u>, volume 1 of <u>[A - Cu]</u>, pages 392–411. New York: Wiley, 2000.

[43] Véronique Blanchard, Xi Liu, Susann Eigel, Matthias Kaup, Silke Rieck, Sabina Janciauskiene, Volker Sandig, Uwe Marx, Peter Walden, Rudolf Tauber, and Markus Berger. N-glycosylation and biological activity of recombinant human alpha1-antitrypsin expressed in a novel human neuronal cell line. <u>Biotechnology and Bioengineering</u>, 108(9):2118–2128, September 2011. doi: 10.1002/bit.23158.

[44] Jens Niklas, Eva Schräder, Volker Sandig, Thomas Noll, and Elmar Heinzle. Quantitative characterization of metabolism and metabolic shifts during growth of the new human cell line AGE1.HN using time resolved metabolic flux analysis. <u>Bioprocess and Biosystems Engineering</u>, 34(5):533–545, June 2011.

[45] Jens Niklas, Volker Sandig, and Elmar Heinzle. Metabolite channeling and compartmentation in the human cell line AGE1.HN determined by 13C labeling experiments and 13C metabolic flux analysis. <u>Journal of Bioscience and Bioengineering</u>, 112(6): 616–623, December 2011.

[46] Jens Niklas, Christian Priesnitz, Thomas Rose, Volker Sandig, and Elmar Heinzle. Primary metabolism in the new human cell line AGE1.HN at various substrate levels: increased metabolic efficiency and alpha(1)-antitrypsin production at reduced pyruvate load. <u>Applied Microbiology and Biotechnology</u>, 93(4):1637–1650, August 2011.

[47] Christian Priesnitz, Jens Niklas, Thomas Rose, Volker Sandig, and Elmar Heinzle. Metabolic flux rearrangement in the amino acid metabolism reduces ammonia

stress in the alpha(1)-antitrypsin producing human AGE1.HN cell line. Metabolic Engineering, January 2012.

[48] Eva Schräder, Sebastian Scholz, Jens Niklas, Alexander Rath, Oscar Barradas, Uwe Jandt, Volker Sandig, Thomas Rose, Ralf Pörtner, Udo Reichl, and et al. Characterisation of cultivation of the human cell line AGE1.HN.AAT. BMC Proceedings, 5 (Suppl 8):P87, 2011. ISSN 1753-6561.

[49] Oscar Platas Barradas, Uwe Jandt, Linh Da Minh Phan, Mario E. Villanueva, Martin Schaletzky, Alexander Rath, Susann Freund, Udo Reichl, Eva Skerhutt, Sebastian Scholz, Thomas Noll, Volker Sandig, Ralf Pörtner, and An-Ping Zeng. Evaluation of criteria for bioreactor comparison and operation standardization for mammalian cell culture. Engineering in Life Sciences, 5:518–528, 2012.

[50] Susann Freund, Alexander Rath, Oscar Platas Barradas, Eva Skerhutt, Sebastian Scholz, Jens Niklas, Volker Sandig, Thomas Rose, Elmar Heinzle, Thomas Noll, et al. Batch-to-batch variability of two human designer cell lines AGE1. HN and AGE1. HN. AAT carried out by different laboratories under defined culture conditions using a mathematical model. Engineering in Life Sciences, 13(6):580–592, 2013.

[51] Sebastian Scholz, Miriam Luebbecke, Alexander Rath, Eva Schraeder, Thomas Rose, Heino Büntemeyer, Thomas Scheper, Udo Reichl, and Thomas Noll. Characterization of the human AGE1.HN cell line: a systems biology approach. BMC Proceedings, 5 (Suppl 8):P78, 2011. ISSN 1753-6561.

[52] Steffen Borchers, Susann Freund, Alexander Rath, Stefan Streif, Udo Reichl, and Rolf Findeisen. Identification of growth phases and influencing factors in cultivations with AGE1.HN cells using set-based methods. PLOS ONE, 8(8):e68124, 2013.

[53] Jens Niklas, Christian Priesnitz, Thomas Rose, Volker Sandig, and Elmar Heinzle. Metabolism and metabolic burden by α1-antitrypsin production in human AGE1.HN cells. Metabolic Engineering, 16:103–114, February 2013.

[54] Robert Janke. Investigation of mammalian cell metabolism by quantification of key metabolic enzyme activities. PhD thesis, Otto-von-Guericke University Magdeburg, December 2012.

[55] Joachim Ritter. Charakterisierung tierischer Zellkulturen anhand einer Quantifizierung intrazellulärer Metaboliten aus dem Zentralstoffwechsel. PhD thesis, Otto-von-Guericke University Magdeburg, 2009.

[56] P. M. Hayter, E. M. Curling, M. L. Gould, A. J. Baines, N. Jenkins, I. Salmon, P. G. Strange, and A. T. Bull. The effect of the dilution rate on cho cell physiology and recombinant interferon-gamma production in glucose-limited chemostat culture. Biotechnology and Bioengineering, 42(9):1077–1085, November 1993.

[57] J. L. Goergen, A. Marc, and J. M. Engasser. Comparison of specific rates of hybridoma growth and metabolism in batch and continuous cultures. Cytotechnology, 10(2): 147–155, 1992.

[58] M. S. Lao and D. Toth. Effects of ammonium and lactate on growth and metabolism of a recombinant chinese hamster ovary cell culture. Biotechnology Progress, 13(5): 688–691, 1997.

[59] M. Yang and M. Butler. Effects of ammonia on cho cell growth, erythropoietin production, and glycosylation. Biotechnology and Bioengineering, 68(4):370–380, May 2000.

[60] M. Al-Rubeai, A. N. Emery, and S. Chalder. The effect of pluronic f-68 on hybridoma cells in continuous culture. Applied Microbiology and Biotechnology, 37(1):44–45, April 1992.

[61] M. B. Gu, P. Todd, and D. S. Kompala. Analysis of foreign protein overproduction in recombinant cho cells. effect of growth kinetics and cell cycle traverse. Annals of The New York Academy Of Sciences, 721:194–207, May 1994.

[62] Hendrik P.J. Bonarius, José H.M. Houtman, Georg Schmid, Cornelis D. de Gooijer, and Johannes Tramper. Metabolic-flux analysis of hybridoma cells under oxidative and reductive stress using mass balances. Cytotechnology, 32:97–107, 2000.

[63] M. S. Lee and G. M. Lee. Effect of hypoosmotic pressure on cell growth and antibody production in recombinant chinese hamster ovary cell culture. Cytotechnology, 36 (1-3):61–69, July 2001.

[64] Sung Kwan Yoon, Sung Hyun Kim, and Gyun Min Lee. Effect of low culture temperature on specific productivity and transcription level of anti-4-1Bb antibody in recombinant chinese hamster ovary cells. Biotechnology Progress, 19(4):1383–1386, 2003.

[65] Stephen R Fox, Upasana A Patel, Miranda G S Yap, and Daniel I C Wang. Maximizing interferon-gamma production by chinese hamster ovary cells through temperature shift optimization: experimental and modeling. Biotechnology and Bioengineering, 85(2):177–184, January 2004.

[66] Chaya Mohan, Yeon-Gu Kim, Jane Koo, and Gyun Min Lee. Assessment of cell engineering strategies for improved therapeutic protein production in cho cells. Biotechnology Journal, 3(5):624–630, May 2008.

[67] Li Fan, Liang Zhao, Zhaoyang Ye, Yating Sun, Tianci Kou, Yan Zhou, and Wen-Song Tan. Effect of culture temperature on tnfr-fc productivity in recombinant glutamine synthetase-chinese hamster ovary cells. Biotechnology Letters, 32(9):1239–1244, September 2010.

[68] G. B. Nyberg, R. R. Balcarcel, B. D. Follstad, G. Stephanopoulos, and D. I. Wang. Metabolism of peptide amino acids by Chinese hamster ovary cells grown in a complex medium. Biotechnology and Bioengineering, 62(3):324–335, February 1999.

[69] Y. Genzel, I. Behrendt, S. König, H. Sann, and U. Reichl. Metabolism of MDCK cells during cell growth and influenza virus production in large-scale microcarrier culture. Vaccine, 22(17-18):2202–2208, June 2004.

[70] Fang Zhang, Xiangming Sun, Xiaoping Yi, and Yuanxing Zhang. Metabolic characteristics of recombinant chinese hamster ovary cells expressing glutamine synthetase in presence and absence of glutamine. Cytotechnology, 51(1):21–28, May 2006.

[71] J. B. Ritter, A. S. Wahl, S. Freund, Y. Genzel, and U. Reichl. Metabolic effects of influenza virus infection in cultured animal cells: intra- and extracellular metabolite profiling. BMC Systems Biology, 4(1):61, May 2010.

[72] Emma Petiot, Emmanuel Guedon, Fabrice Blanchard, Cécile Gény, Hervé Pinton, and Annie Marc. Kinetic characterization of vero cell metabolism in a serum-free batch culture process. Biotechnology and Bioengineering, 107(1):143–153, September 2010.

[73] Jun Luo, Natarajan Vijayasankaran, Jennifer Autsen, Rodell Santuray, Terry Hudson, Ashraf Amanullah, and Feng Li. Comparative metabolite analysis to understand lactate metabolism shift in chinese hamster ovary cell culture process. Biotechnology and Bioengineering, 109(1):146–156, January 2012.

[74] C. Altamirano, J. J. Cairo, and F. Godia. Decoupling cell growth and product formation in chinese hamster ovary cells through metabolic control. Biotechnology and Bioengineering, 76(4):351–360, December 2001.

[75] Suzanne D. Conzen. Cellular transformation, characteristics. In Raymond E. Spier, editor, Encyclopedia of cell technology, volume 1 of [A - Cu], pages 507–519. New York: Wiley, 2000.

154

[76] F. L. Graham and A. J. van der Eb. Transformation of rat cells by DNA of human adenovirus 5. Virology, 54(2):536–539, August 1973.

[77] V. Krougliak and F. L. Graham. Development of cell lines capable of complementing E1, E4, and protein IX defective adenovirus type 5 mutants. Human Gene Therapy, 6(12):1575–1586, December 1995.

[78] Kamilla Swiech, Virgínia Picanço-Castro, and Dimas Tadeu Covas. Human cells: new platform for recombinant therapeutic protein production. Protein Expression and Purification, 84(1):147–153, July 2012.

[79] Robin J Parks. Adenovirus protein IX: a new look at an old protein. Molecular Therapy, 11(1):19–25, January 2005.

[80] Emer Kelly, Catherine M. Greene, Tomas P. Carroll, Noel G. McElvaney, and Shane J. O'Neill. Alpha-1 antitrypsin deficiency. Respiratory Medicine, 104(6):763–772, June 2010.

[81] S. Gholami and T. Hamzehloei. Hereditary of alpha-1-antitrypsin deficiency. Shiraz E-Med J, 14(1):63–75, 2013. ISSN 1735-1391.

[82] L. Xie and D. I. Wang. Integrated approaches to the design of media and feeding strategies for fed-batch cultures of animal cells. Trends in Biotechnology, 15(3): 109–113, March 1997.

[83] W. Zhou, J. Rehm, and W. S. Hu. High viable cell concentration fed-batch cultures of hybridoma cells through on-line nutrient feeding. Biotechnology and Bioengineering, 46(6):579–587, June 1995.

[84] K. B. Konstantinov, Y. Tsai, D. Moles, and R. Matanguihan. Control of long-term perfusion chinese hamster ovary cell culture by glucose auxostat. Biotechnology Progress, 12(1):100–109, 1996.

[85] R. Heidemann, D. Lütkemeyer, H. Büntemeyer, and J. Lehmann. Effects of dissolved oxygen levels and the role of extra- and intracellular amino acid concentrations upon the metabolism of mammalian cell lines during batch and continuous cultures. Cytotechnology, 26(3):185–197, May 1998.

[86] Paul A Hoskisson and Glyn Hobbs. Continuous culture–making a comeback? Microbiology, 151(Pt 10):3153–3159, October 2005. doi: 10.1099/mic.0.27924-0.

[87] Chetan T. Goudar, Nigel Titchener-Hooker, and Konstantin Konstantinov. Integrated continuous biomanufacturing: A new paradigm for biopharmaceutical production. Journal of Biotechnology, 213:1–2, nov 2015.

[88] H. P. Bonarius, V. Hatzimanikatis, K. P. Meesters, C. D. de Gooijer, G. Schmid, and J. Tramper. Metabolic flux analysis of hybridoma cells in different culture media using mass balances. Biotechnology and Bioengineering, 50(3):299–318, May 1996.

[89] N. Vriezen, B. Romein, K. C. Luyben, and J. P. van Dijken. Effects of glutamine supply on growth and metabolism of mammalian cells in chemostat culture. Biotechnology and Bioengineering, 54(3):272–286, May 1997.

[90] Y. K. Lee, P. K. Yap, and A. P. Teoh. Correlation between steady-state cell concentration and cell death of hybridoma cultures in chemostat. Biotechnology and Bioengineering, 45(1):18–26, January 1995.

[91] C. Altamirano, A. Illanes, A. Casablancas, X. Gamez, J. J. Cairo, and C. Godia. Analysis of CHO cells metabolic redistribution in a glutamate-based defined medium in continuous culture. Biotechnology Progress, 17(6):1032–1041, 2001.

[92] Helene Faustrup Kildegaard, Deniz Baycin-Hizal, Nathan E. Lewis, and Michael J. Betenbaugh. The emerging cho systems biology era: harnessing the 'omics revolution for biotechnology. Current Opinion in Biotechnology, 24(6):1102–1107, December 2013.

[93] Peter M. O'Callaghan and David C. James. Systems biotechnology of mammalian cell factories. Briefings in Functional Genomics and Proteomics, 7(2):95–110, March 2008. doi: 10.1093/bfgp/eln012.

[94] Andrew R. Joyce and Bernhard Ø. Palsson. The model organism as a system: integrating 'omics' data sets. Nature Reviews. Molecular Cell Biology, 7(3):198–210, March 2006.

[95] J. B. Ritter, Y. Genzel, and U. Reichl. High-performance anion-exchange chromatography using on-line electrolytic eluent generation for the determination of more than 25 intermediates from energy metabolism of mammalian cells in culture. Journal of Chromatography, 843(2):216–226, November 2006.

[96] J. B. Ritter, Y. Genzel, and U. Reichl. Simultaneous extraction of several metabolites of energy metabolism and related substances in mammalian cells: Optimization using experimental design. Analytical Biochemistry, 373:349–369, November 2008.

[97] Silas G Villas-Bôas, Jesper Højer-Pedersen, Mats Akesson, Jørn Smedsgaard, and Jens Nielsen. Global metabolite analysis of yeast: evaluation of sample preparation methods. <u>Yeast</u>, 22(14):1155–1169, October 2005.

[98] C. L. Winder, W. B. Dunn, S. Schuler, D. Broadhurst, R. Jarvis, G. M. Stephens, and R. Goodacre. Global metabolic profiling of escherichia coli cultures: an evaluation of methods for quenching and extraction of intracellular metabolites. <u>Analytical Chemistry</u>, 80(8):2939–2948, April 2008.

[99] Quincy Teng, Wenlin Huang, Timothy W. Collette, Drew R. Ekman, and Chalet Tan. A direct cell quenching method for cell-culture based metabolomics. <u>Metabolomics</u>, 5:199–208, 2009.

[100] M. A. Lorenz, C. F. Burant, and R. T. Kennedy. Reducing time and increasing sensitivity in sample preparation for adherent mammalian cell metabolomics. <u>Analytical Chemistry</u>, 2011.

[101] S. Dietmair, N. E. Timmins, P. P. Gray, L. K. Nielsen, and J. O. Krömer. Towards quantitative metabolomics of mammalian cells - development of a metabolite extraction protocol. <u>Analytical Biochemistry</u>, April 2010.

[102] J. Kronthaler, G. Gstraunthaler, and C. Heel. Optimizing high-throughput metabolomic biomarker screening: a study of quenching solutions to freeze intracellular metabolism in CHO cells. <u>Omics</u>, 16(3):90–97, March 2012.

[103] C. A. Sellick, R. Hansen, A. R. Maqsood, W. B. Dunn, G. M. Stephens, R. Goodacre, and A. J. Dickson. Effective quenching processes for physiologically valid metabolite profiling of suspension cultured mammalian cells. <u>Analytical Chemistry</u>, 81:174–183, December 2009.

[104] C. Wiendahl, J. J. Brandner, C. Kueppers, B. Luo, U. Schygulla, T. Noll, and M. Oldiges. A microstructure heat exchanger for quenching the metabolism of mammalian cells. <u>Chemical Engineering & Technology</u>, 30(3):322–328, March 2007. ISSN 0930-7516.

[105] M. Volmer, S. Northoff, S. Scholz, T. Thüte, H. Büntemeyer, and T. Noll. Fast filtration for metabolome sampling of suspended animal cells. <u>Biotechnology Letters</u>, 33(3): 495–502, March 2011.

[106] R. V. Kapoore, R. Coyle, C. A. Staton, N. J. Brown, and S. Vaidyanathan. Cell line dependence of metabolite leakage in metabolome analyses of adherent normal and cancer cell lines. <u>Metabolomics</u>, 11(6):1743–1755, jul 2015.

[107] Paulo Canas Rodrigues. Principal component analysis of dependent data. In 15th European Young Statisticians Meeting, page 5, 2007.

[108] Jerome Friedman Trevor Hastie, Robert Tibshirani. The Elements of Statistical Learning. Springer New York, 2009.

[109] Waltraud Kessler. Multivariate Datenanalyse für die Pharma-, Bio- und Prozessanalytik. WILEY-VCH Verlag GmbH & Co KGaA, Weinheim, 2007.

[110] Steven Holland. Principal components analysis (PCA). Department of Geology, University of Georgia, May 2008. Lecture notes.

[111] H. Wold. Path Models with latent variables: The NIPALS approach. Acad. Press, 1975.

[112] Hervé Abdi and Lynne J. Williams. Principal component analysis. WIREs Computational Statistics, 2(4):433–459, June 2010.

[113] Jens Niklas, Yannic Nonnenmacher, Thomas Rose, Volker Sandig, and Elmar Heinzle. Quercetin treatment changes fluxes in the primary metabolism and increases culture longevity and recombinant α_1-antitrypsin production in human AGE1.HN cells. Applied Microbiology and Biotechnology, 94(1):57–67, April 2012.

[114] Klaas Van't Riet and Johannes Tramper. Basic Bioreactor Design (Electrical Engineering & Electronics). CRC Press, 1991. ISBN 0824784464.

[115] P. Bonvillani, M.P. Ferrari, E.M. Ducrós, and J.A. Orejas. Theoretical and experimental study of the effects of scale-up on mixing time for a stirred-tank bioreactor. Brazilian Journal of Chemical Engineering, 23(1):1–7, 2006. cited By (since 1996) 2.

[116] Felix Garcia-Ochoa and Emilio Gomez. Bioreactor scale-up and oxygen transfer rate in microbial processes: an overview. Biotechnology advances, 27(2):153–176, 2009.

[117] Klaas Van't Riet. Review of measuring methods and results in nonviscous gas-liquid mass transfer in stirred vessels. Industrial & Engineering Chemistry Process Design and Development, 18(3):357–364, 1979.

[118] Andreas Bock. Untersuchung einer sterilen und totvolumenfreien Probeentnahme für die Zellkultur Methodenvalidierung am Beispiel des Enzymsensors YSI 2700. PhD thesis, Otto von Guericke Universität Magdeburg, Oktober 2002.

[119] Wolfgang Gottwald. Statistik für Anwender. Wiley-Vch Weinheim, 2000.

[120] Norman R Draper and Harry Smith. Applied regression analysis (wiley series in probability and statistics). Wiley-Interscience, 1998.

[121] Yvonne Genzel, Susanne König, and Udo Reichl. Amino acid analysis in mammalian cell culture media containing serum and high glucose concentrations by anion exchange chromatography and integrated pulsed amperometric detection. Analytical Biochemistry, 335(1):119–125, December 2004a.

[122] Heino Büntemeyer. Entwicklung eines Perfusionssystems zur kontinuierlichen Kultivierung tierischer Zellen in Suspension. PhD thesis, Universität Hannover, 1988.

[123] Ralf Steuer, Katja Morgenthal, Wolfram Weckwerth, and Joachim Selbig. A gentle guide to the analysis of metabolomic data. Methods in Molecular Biology, 358:105–126, 2007.

[124] M. Tremblay, M. Perrier, C. Chavarie, and J. Archambault. Optimization of fed-batch culture of hybridoma cells using dynamic programming: single and multi feed cases. Bioprocess Engineering, 7(5):229–234, January 1992.

[125] S. S. Ozturk and B. O. Palsson. Chemical decomposition of glutamine in cell culture media: effect of media type, ph, and serum concentration. Biotechnology Progress, 6(2):121–128, 1990.

[126] H. Schmidt and M. Jirstrand. Systems biology toolbox for MATLAB: a computational platform for research in systems biology. Bioinformatics, 22(4):514–515, nov 2005.

[127] H.M Princen, J.Th.G Overbeek, and S.G Mason. The permeability of soap films to gases. Journal of Colloid and Interface Science, 24(1):125–130, May 1967.

[128] D.W. Murhammer and E.C. Pfalzgraf. Effects of pluronic f-68 on oxygen transport in an agitated, sparged bioreactor. Biotechnology Techniques, 6(3):199–202, 1992. ISSN 0951-208X.

[129] John D. Sheppard and David G. Cooper. The effects of a biosurfactant on oxygen transfer in a cyclone column reactor. Journal of Chemical Technology & Biotechnology, 48(3):325–336, April 1990.

[130] S. Zhang, A. Handa-Corrigan, and R. E. Spier. Oxygen transfer properties of bubbles in animal cell culture media. Biotechnology and Bioengineering, 40(2):252–259, June 1992.

[131] Robert W Potter and David Leslie Brown. <u>The volumetric properties of aqueous</u> <u>sodium chloride solutions from 0degC to 500degC at pressures up to 2000 bars based</u> <u>on a regression of available data in the literature</u>. US Government Printing Office, 1977.

[132] Joseph Kestin, H Ezzat Khalifa, and Robert J Correia. <u>Tables of the dynamic and</u> <u>kinematic viscosity of aqueous NaCl solutions in the temperature range 20-150 C</u> <u>and the pressure range 0.1-35 MPa</u>. American Chemical Society and the American Institute of Physics for the National Bureau of Standards, 1981.

[133] H. Eagle, V. I. Oyama, M. Levy, C. L. Horton, and R. Fleischman. The growth response of mammalian cells in tissue culture to l-glutamine and l-glutamic acid. <u>Journal of</u> <u>Biological Chemistry</u>, 218(2):607–616, Feb 1956.

[134] J. B. Griffiths. The effects of adapting human diploid cells to grow in glutamic acid media on cell morphology, growth and metabolism. <u>Journal of Cell Science</u>, 12(2): 617–629, Mar 1973.

[135] V. Lohr, O. Haedicke, Y. Genzel, I. Jordan, H. Buentemeyer, S. Klamt, and U. Reichl. The avian cell line AGE1.CR.pIX characterized by metabolic flux analysis. <u>BMC</u> <u>Biotechnology</u>, 14:72, 2014.

[136] M.G. Pau, C. Ophorst, M.H. Koldijk, G. Schouten, M. Mehtali, and F. Uytdehaag. The human cell line PER.C6 provides a new manufacturing system for the production of influenza vaccines. <u>Vaccine</u>, 19:2716–2721, 2001.

[137] Liangzhi Xie, Warren Pilbrough, Christian Metallo, Tanya Zhong, Lana Pikus, John Leung, John G. Aunins, and Weichang Zhou. Serum-free suspension cultivation of PER.C6 cells and recombinant adenovirus production under different pH conditions. <u>Biotechnology and Bioengineering</u>, 80(5):569–579, 2002.

[138] Liangzhi Xie, Christian Metallo, James Warren, Warren Pilbrough, Joseph Peltier, Tanya Zhong, Lana Pikus, Amanda Yancy, John Leung, John G. Aunins, and Weichang Zhou. Large-scale propagation of a replication-defective adenovirus vector in stirred-tank bioreactor per.c6 Cell culture under sparging conditions. <u>Biotechnology</u> <u>and Bioengineering</u>, 83(1):45–52, 2003.

[139] David Jones, Nathalie Kroos, Regina Anema, Bart van Montfort, Andre Vooys, Sven van der Kraats, Esmeralda van der Helm, Shirley Smits, Jan Schouten, Kirsten Brouwer, Fija Lagerwerf, Patrick van Berkel, Dirk-Jan Opstelten, Ton Logtenberg, and Abraham Bout. High-level expression of recombinant igg in the human cell line per.c6. <u>Biotechnology Progress</u>, 19(1):163–168, 2003.

[140] M.J.E Havenga, L. Holterman, I. Melis, S. Smits, J. Kaspers, E. Heemskerk, R. van der Vlugt, M. Koldijk, G.J. Schouten, G. Hateboer, K. Brouwer, R. Vogels, and J. Goudsmit. Serum-free transient protein production system based on adenoviral vector and PER.C6 technology: High yield and preserved bioactivity. Biotechnology and Bioengineering, November 2007.

[141] J. Capiaumont, C. Legrand, D. Carbonell, B. Dousset, F. Belleville, and P. Nabet. Methods for reducing the ammonia in hybridoma cell cultures. Journal of Biotechnology, 39(1):49–58, Feb 1995.

[142] R. H. McDermott and M. Butler. Uptake of glutamate, not glutamine synthetase, regulates adaptation of mammalian cells to glutamine-free medium. Journal of Cell Science, 104 (Pt 1):51–58, Jan 1993.

[143] J. Paul and Pf Fottrell. Mechanism of D-glutamyltransferase repression in mammalian cells. Biochimica et Biophysica Acta, 67:334–336, Feb 1963.

[144] A. Sanfeliu and G. Stephanopoulos. Effect of glutamine limitation on the death of attached chinese hamster ovary cells. Biotechnology and Bioengineering, 64(1):46–53, July 1999.

[145] R. Janke, Y. Genzel, N. Händel, A. Wahl, and U. Reichl. Metabolic adaptation of mdck cells to different growth conditions: effects on catalytic activities of central metabolic enzymes. Biotechnology and Bioengineering, 108(11):2691–2704, November 2011.

[146] Thomas M. Annesley. Ion suppression in mass spectrometry. Clinical Chemistry, 49 (7):1041–1044, July 2003.

[147] Dajana Vuckovic. Current trends and challenges in sample preparation for global metabolomics using liquid chromatography-mass spectrometry. Analytical and Bioanalytical Chemistry, 403(6):1523–1548, June 2012.

[148] WJ Ball, Jr and D. E. Atkinson. Adenylate energy charge in saccharomyces cerevisiae during starvation. Journal of Bacteriology, 121(3):975–982, March 1975.

[149] Andre B. Canelas, Cor Ras, Angela ten Pierick, Jan C. van Dam, Joseph J. Heijnen, and Walter M. van Gulik. Leakage-free rapid quenching technique for yeast metabolomics. Metabolomics, 4:226–239, February 2008.

[150] Alexander G. Rath, Markus Rehberg, Robert Janke, Yvonne Genzel, Sebastian Scholz, Thomas Noll, Thomas Rose, Volker Sandig, and Udo Reichl. The influence

of cell growth and enzyme activity changes on intracellular metabolite dynamics in AGE1.HN.AAT cells. Journal of Biotechnology, March 2014. ISSN 0168-1656.

[151] M. Al-Rubeai, R. P. Singh, M. H. Goldman, and A. N. Emery. Death mechanisms of animal cells in conditions of intensive agitation. Biotechnology and Bioengineering, 45(6):463–472, March 1995. doi: 10.1002/bit.260450602.

[152] Yusuf Chisti. Hydrodynamic damage to animal cells. Critical reviews in biotechnology, 21(2):67–110, 2001. doi: 10.1080/20013891081692.

[153] Lorea Legazpi, Adriana Laca, and Mario Díaz. Kinetic analysis of hybridoma cells viability under mechanical shear stress with and without serum protection. Bioprocess and Biosystems Engineering, 32(6):717–722, October 2009. doi: 10. 1007/s00449-008-0295-4.

[154] Mike Mollet, Ruben Godoy-Silva, Claudia Berdugo, and Jeffrey J Chalmers. Acute hydrodynamic forces and apoptosis: a complex question. Biotechnology and Bioengineering, 98(4):772–788, November 2007. doi: 10.1002/bit.21476.

[155] Ibrahim Abu-Reesh and F. Kargi. Biological responses of hybridoma cells to defined hydrodynamic shear stress. Journal of Biotechnology, 9(3):167–178, feb 1989.

[156] S.K.W. Oh, A.W. Nienow, M. Al-Rubeai, and A.N. Emery. The effects of agitation intensity with and without continuous sparging on the growth and antibody production of hybridoma cells. Journal of Biotechnology, 12(1):45–61, oct 1989.

[157] Julian T. Keane, David Ryan, and Peter P. Gray. Effect of shear stress on expression of a recombinant protein by chinese hamster ovary cells. Biotechnol. Bioeng., 81(2): 211–220, nov 2002.

[158] Stéphanie Tissot, Agata Oberbek, Martino Reclari, Matthieu Dreyer, David L Hacker, Lucia Baldi, Mohamed Farhat, and Florian M Wurm. Efficient and reproducible mammalian cell bioprocesses without probes and controllers? N Biotechnol, February 2011.

[159] L. K. Nielsen, S. Reid, and P. F. Greenfield. Cell cycle model to describe animal cell size variation and lag between cell number and biomass dynamics. Biotechnology and Bioengineering, 56(4):372–379, November 1997.

[160] J. Ljunggren and L. Häggström. Specific growth rate as a parameter for tracing growth-limiting substances in animal cell cultures. Journal of Biotechnology, 42(2): 163–175, September 1995.

[161] M Dalili, G D Sayles, and D F Ollis. Glutamine-limited batch hybridoma growth and antibody production: experiment and model. Biotechnology and bioengineering, 36: 74–82, Jun 1990. ISSN 0006-3592.

[162] Chetan T Goudar, Klaus Joeris, Konstantin B Konstantinov, and James M Piret. Logistic equations effectively model mammalian cell batch and fed-batch kinetics by logically constraining the fit. Biotechnology Progress, 21(4):1109–1118, 2005.

[163] M. Rehberg, J. B. Ritter, Y. Genzel, D. Flockerzi, and U. Reichl. The relation between growth phases, cell volume changes and metabolism of adherent cells during cultivation. Journal of Biotechnology, February 2013.

[164] W. Zhou and W. S. Hu. On-line characterization of a hybridoma cell culture process. Biotechnology and Bioengineering, 44(2):170–177, June 1994. doi: 10.1002/bit.260440205.

[165] M. A. Bree, P. Dhurjati, RF Geoghegan, Jr, and B. Robnett. Kinetic modelling of hybridoma cell growth and immunoglobulin production in a large-scale suspension culture. Biotechnology and Bioengineering, 32(8):1067–1072, October 1988. doi: 10.1002/bit.260320814.

[166] Lars Möhler, Andreas Bock, and Udo Reichl. Segregated mathematical model for growth of anchorage-dependent mdck cells in microcarrier culture. Biotechnology Progress, 24(1):110–119, 2008. doi: 10.1021/bp0701923.

[167] M. W. Glacken, E. Adema, and A. J. Sinskey. Mathematical descriptions of hybridoma culture kinetics: I. initial metabolic rates. Biotechnol. Bioeng., 32(4):491–506, aug 1988.

[168] Rafael Moreno-Sanchez, Sara Rodriguez-Enriquez, Alvaro Marin-Hernandez, and Emma Saavedra. Energy metabolism in tumor cells. FEBS Journal, pages 1393–1418, 2007.

[169] Sybille Mazurek. Pyruvate kinase type m2: a key regulator of the metabolic budget system in tumor cells. International Journal of Biochemistry and Cell Biology, 43(7): 969–980, July 2011.

[170] Matthew G. Vander Heiden, Jason W. Locasale, Kenneth D. Swanson, Hadar Sharfi, Greg J. Heffron, Daniel Amador-Noguez, Heather R. Christofk, Gerhard Wagner, Joshua D. Rabinowitz, John M. Asara, and Lewis C. Cantley. Evidence for an alternative glycolytic pathway in rapidly proliferating cells. Science, 329(5998):1492–1499, September 2010.

[171] J. E. Pessin and G. I. Bell. Mammalian facilitative glucose transporter family: structure and molecular regulation. Annual Review of Physiology, 54:911–930, 1992.

[172] M. Hatanaka. Saturable and nonsaturable process of sugar uptake: effect of oncogenic transformation in transport and uptake of nutrients. Journal of Cellular Physiology, 89(4):745–749, December 1976.

[173] S. Decker and F. Lipmann. Transport of d-glucose by membrane vesicles from normal and avian sarcoma virus-transformed chicken embryo fibroblasts. Proceedings of the National Academy of Sciences of the United States of America, 78(9):5358–5361, September 1981.

[174] Otto Warburg, Franz Wind, and Erwin Negelein. The metabolism of tumors in the body. The Journal of General Physiology, pages 519–530, 1927.

[175] Matthew G. Vander Heiden, Lewis C. Cantley, and Craig B. Thompson. Understanding the warburg effect: the metabolic requirements of cell proliferation. Science, 324(5930):1029–1033, May 2009.

[176] D. Rivenzon-Segal, E. Rushkin, S. Polak-Charcon, and H. Degani. Glucose transporters and transport kinetics in retinoic acid-differentiated t47d human breast cancer cells. Am J Physiol Endocrinol Metab, 279(3):E508–E519, September 2000.

[177] S. Rodríguez-Enríquez, A. Marín-Hernández, J. C. Gallardo-Pérez, and R. Moreno-Sánchez. Kinetics of transport and phosphorylation of glucose in cancer cells. Journal of Cellular Physiology, 221(3):552–559, December 2009.

[178] Christian D Young, Andrew S Lewis, Michael C Rudolph, Marisa D Ruehle, Matthew R Jackman, Ui J Yun, Olesya Ilkun, Renata Pereira, E. Dale Abel, and Steven M Anderson. Modulation of glucose transporter 1 (glut1) expression levels alters mouse mammary tumor cell growth in vitro and in vivo. PLOS ONE, 6(8): e23205, 2011.

[179] M. Rehberg, A. Rath, J. B. Ritter, Y. Genzel, and U. Reichl. Changes in intracellular metabolite pools during growth of adherent mdck cells in two different media. Applied Microbiology and Biotechnology, 98(1):385–397, January 2013.

[180] G. Schmid and T. Keller. Monitoring hybridoma metabolism in continuous suspension culture at the intracellular level. i. steady-state responses to different glutamine feed concentrations. Cytotechnology, 9(1-3):217–229, 1992.

[181] G. A. Dunaway. A review of animal phosphofructokinase isozymes with an emphasis on their physiological role. Molecular and Cellular Biochemistry, 52(1):75–91, 1983.

[182] E Eigenbrodt. Glycolysis - one of the keys to cancer? Trends in Pharmacological Sciences, 1(2):240–245, 1980.

[183] S. Mazurek, W. Zwerschke, P. Jansen-Dürr, and E. Eigenbrodt. Effects of the human papilloma virus hpv-16 e7 oncoprotein on glycolysis and glutaminolysis: role of pyruvate kinase type m2 and the glycolytic-enzyme complex. Biochemical Journal, 356 (Pt 1):247–256, May 2001.

[184] K. Ashizawa, M. C. Willingham, C. M. Liang, and S. Y. Cheng. In vivo regulation of monomer-tetramer conversion of pyruvate kinase subtype m2 by glucose is mediated via fructose 1,6-bisphosphate. Journal of Biological Chemistry, 266(25):16842–16846, September 1991.

[185] L. G. Baggetto. Deviant energetic metabolism of glycolytic cancer cells. Biochimie, 74(11):959–974, November 1992.

[186] L. J. Reitzer, B. M. Wice, and D. Kennell. Evidence that glutamine, not sugar, is the major energy source for cultured hela cells. Journal of Biological Chemistry, 254(8): 2669–2676, April 1979.

[187] H. R. Zielke, C. L. Zielke, and P. T. Ozand. Glutamine: a major energy source for cultured mammalian cells. Federation Proceedings, 43(1):121–125, January 1984.

[188] P. Newsholme, M M R. Lima, J. Procopio, T. C. Pithon-Curi, S. Q. Doi, R. B. Bazotte, and R. Curi. Glutamine and glutamate as vital metabolites. Brazilian Journal of Medical and Biological Research, 36(2):153–163, February 2003.

[189] Aljoscha Wahl, Yury Sidorenko, Michael Dauner, Yvonne Genzel, and Udo Reichl. Metabolic flux model for an anchorage-dependent MDCK cell line: characteristic growth phases and minimum substrate consumption flux distribution. Biotechnology and Bioengineering, 101(1):135–152, September 2008.

[190] T. J. Piva and E. McEvoy-Bowe. Oxidation of glutamine in hela cells: role and control of truncated tca cycles in tumour mitochondria. Journal of Cellular Biochemistry, 68 (2):213–225, February 1998.

[191] C. Lobo, M. A. Ruiz-Bellido, J. C. Aledo, J. Márquez, I. Núñez De Castro, and F. J. Alonso. Inhibition of glutaminase expression by antisense mrna decreases growth and tumourigenicity of tumour cells. Biochemical Journal, 348 Pt 2:257–261, June 2000.

[192] R. Gebhardt and D. Mecke. Heterogeneous distribution of glutamine synthetase among rat liver parenchymal cells in situ and in primary culture. <u>EMBO Journal</u>, 2 (4):567–570, 1983.

[193] John D. McGivan and Claire I. Bungard. The transport of glutamine into mammalian cells. <u>Frontiers In Bioscience</u>, 12:874–882, JAN 1 2007. ISSN 1093-9946.

[194] Subiao Lu, Xiangming Sun, and Yuanxing Zhang. Insight into metabolism of cho cells at low glucose concentration on the basis of the determination of intracellular metabolites. <u>Process Biochemistry</u>, 40(5):1917–1921, 2005. ISSN 1359-5113.

[195] S. T. Sharfstein, S. N. Tucker, A. Mancuso, H. W. Blanch, and D. S. Clark. Quantitative in vivo nuclear magnetic resonance studies of hybridoma metabolism. <u>Biotechnology and Bioengineering</u>, 43(11):1059–1074, May 1994.

[196] Rashmi Korke, Marcela de Leon Gatti, Ally Lei Yin Lau, Justin Wee Eng Lim, Teck Keong Seow, Maxey Ching Ming Chung, and Wei-Shou Hu. Large scale gene expression profiling of metabolic shift of mammalian cells in culture. <u>Journal of Biotechnology</u>, 107(1):1–17, January 2004.

[197] Huong Le, Santosh Kabbur, Luciano Pollastrini, Ziran Sun, Keri Mills, Kevin Johnson, George Karypis, and Wei-Shou Hu. Multivariate analysis of cell culture bioprocess data–lactate consumption as process indicator. <u>Journal of Biotechnology</u>, 162(2-3): 210–223, December 2012.

[198] B. D. Follstad, R. R. Balcarcel, G. Stephanopoulos, and D. I. Wang. Metabolic flux analysis of hybridoma continuous culture steady state multiplicity. <u>Biotechnology and Bioengineering</u>, 63(6):675–683, June 1999.

[199] Aljoscha S Wahl. <u>Entwicklung von biologisch motivierten Methoden zur Vereinfachung kinetischer Modelle Dissertation</u>. PhD thesis, Universität Siegen, 2007.

[200] Theodor I. Linardos, Nicolas Kalogerakis, Leo A. Behie, and Louis R. Lamontagne. The effect of specific growth rate and death rate on monoclonal antibody production in hybridoma chemostat cultures. <u>The Canadian Journal of Chemical Engineering</u>, 69(2):429–438, 1991.

[201] Florian Lang. Effect of cell hydration on metabolism. <u>Nestle Nutr Inst Workshop Ser</u>, 69:115–26; discussion126–30, 2011.

[202] F. Lang, G. L. Busch, M. Ritter, H. Völkl, S. Waldegger, E. Gulbins, and D. Häussinger. Functional significance of cell volume regulatory mechanisms. Physiological Reviews, 78(1):247–306, January 1998.

[203] Anshu Gambhir, Rashmi Korke, Jongchan Lee, Peng-Cheng Fu, Anna Europa, and Wei-Shou Hu. Analysis of cellular metabolism of hybridoma cells at distinct physiological states. Journal of Bioscience and Bioengineering, 95(4):317–327, 2003.

[204] Vicente Bernal, Francisca Monteiro, Nuno Carinhas, Raquel Ambrósio, and Paula M Alves. An integrated analysis of enzyme activities, cofactor pools and metabolic fluxes in baculovirus-infected spodoptera frugiperda sf9 cells. Journal of Biotechnology, 150(3):332–342, November 2010.

[205] H. J. Cruz, J. L. Moreira, and M. J. Carrondo. Metabolic shifts by nutrient manipulation in continuous cultures of bhk cells. Biotechnology and Bioengineering, 66(2): 104–113, 1999.

[206] Ralph J. DeBerardinis, Nabil Sayed, Dara Ditsworth, and Craig B. Thompson. Brick by brick: metabolism and tumor cell growth. Current Opinion in Genetics and Development, 18(1):54–61, February 2008.

[207] Xuemei Tong, Fangping Zhao, and Craig B. Thompson. The molecular determinants of de novo nucleotide biosynthesis in cancer cells. Current Opinion in Genetics and Development, 19(1):32–37, February 2009.

[208] Paolo Dell' Antone. Energy metabolism in cancer cells: how to explain the warburg and crabtree effects? Medical Hypotheses, 79(3):388–392, September 2012.

[209] William Pooi Kat Chong, Shu Hui Thng, Ai Ping Hui, Dong-Yup Lee, Eric Chun Yong Chan, and Ying Swan Ho. Lc-ms-based metabolic characterization of high monoclonal antibody-producing chinese hamster ovary cells. Biotechnology and Bioengineering, June 2012.

[210] C. Kent and G. M. Carman. Interactions among pathways for phosphatidylcholine metabolism, CTp synthesis and secretion through the golgi apparatus. Trends in Biochemical Sciences, 24(4):146–150, April 1999.

[211] Meixia Zhou, Yongping Crawford, Domingos Ng, Jack Tung, Abigail F J. Pynn, Angela Meier, Inn H. Yuk, Natarajan Vijayasankaran, Kimberly Leach, John Joly, Bradley Snedecor, and Amy Shen. Decreasing lactate level and increasing antibody production in chinese hamster ovary cells (cho) by reducing the expression of lactate

dehydrogenase and pyruvate dehydrogenase kinases. Journal of Biotechnology, 153 (1-2):27–34, April 2011. doi: 10.1016/j.jbiotec.2011.03.003.

[212] Miroslava Cuperlović-Culf, David A Barnett, Adrian S Culf, and Ian Chute. Cell culture metabolomics: applications and future directions. Drug Discov Today, 15(15-16):610–621, August 2010. doi: 10.1016/j.drudis.2010.06.012.

[213] A. P. Minton. The influence of macromolecular crowding and macromolecular confinement on biochemical reactions in physiological media. Journal of Biological Chemistry, 276(14):10577–10580, April 2001.

List of publications

Journal publications

- Cammann, C.; Rath, A.; Reichl, U.; Lingel, H.; Brunner-Weinzierl, M.; Simeoni, L.; Schraven, B.; Lindquist, J. A (2016), "Early changes in the metabolic profile of activated CD8+ T cells", BMC Cell Biology, Springer Nature, 17, https://doi.org/10.1186%2Fs12860-016-0104-x.
  A. Rath performed HPLC measurements of intracellular metabolites and data evaluation.

- Rath, A.; Rehberg, M.; Scholz, S.; Noll, T.; Janke, R.; Genzel, Y.; Rose, T.; Sandig, V.; Reichl, U (2014), "The influence of cell growth and enzyme activity changes on intracellular metabolite dynamics in AGE1.HN.AAT cells", Journal of Biotechnology, http://dx.doi.org/10.1016/j.jbiotec.2014.03.012.
  A. Rath performed sampling, extraction and measurement of intracellular metabolites for all batch cultivations, sampling for analysis of maximum enzyme activities, determined cell and extracellular metabolite concentrations for the 2.5 L and 0.5 L bioreactor cultivations, performed modelling of cell growth and substrate consumption for all batch cultivations, analysed the data and wrote the publication.

- Rehberg, M.; Rath, A.; Ritter, J. B.; Genzel, Y.; Reichl, U. (2013), "Changes in intracellular metabolite pools during growth of adherent MDCK cells in two different media.", Applied Microbiology and Biotechnology, 98, 385–397, http://dx.doi.org/10.1007/s00253-013-5329-4.
  A. Rath assisted in interpreting and analysing the data and reviewed the publication.

- Freund, S.; Rath, A.; Platas Baradas, O.; Schräder, E.; Scholz, S.; Niklas, J.; Sandig, V.; Rose, T.; Heinzle, E.; Noll, T.; Pörtner, R.; Zeng, A.P.; Reichl, U. (2013), "Batch-to-batch variability of two human designer cell lines AGE1.HN and AGE1.HN.AAT carried out by different laboratories under defined culture conditions using a mathematical model", Engineering in Life Sciences, 13, 580–592, http://dx.doi.org/10.1002/elsc.201200111.
  A. Rath performed shaker flask and bioreactor cultivations with both cell lines, measured cell and extracellular metabolite concentrations and performed data analysis.

- Borchers, S.; Freund, S.; Rath, A.; Streif, S.; Reichl, U.; Findeisen, R. (2013), "Identification of growth phases and influencing factors in cultivations with AGE1.HN cells using set-based methods", PLOS ONE, 8, e68124, http://dx.doi.org/10.1371/journal.pone.0068124.
  A. Rath performed the shaker flask and the bioreactor cultivation, measured cell and extracellular metabolite concentrations and performed data analysis.

- Platas Barradas, O.; Jandt, U.; Da Minh Phan, L.; Villanueva, M. E.; Schaletzky, M.; Rath, A.; Freund, S.; Reichl, U.; Skerhutt, E.; Scholz, S.; Noll, T.; Sandig, V.; Pörtner, R. & Zeng, A. (2012), "Evaluation of criteria for bioreactor comparison and operation standardization for mammalian cell culture", Engineering in Life Sciences 5, 518–528, http://dx.doi.org/10.1002/elsc.201100163.
  A. Rath performed the 0.5 L bioreactor cultivations with the DasGip System, measured and analysed cell and extracellular metabolite concentrations and reviewed the publication.

- Lohr*, V.; Rath*, A.; Genzel, Y.; Jordan, I.; Sandig, V. & Reichl, U. (2009), "New avian suspension cell lines provide production of influenza virus and MVA in serum-free media: studies on growth, metabolism and virus propagation", Vaccine 27, 4875–5026, http://dx.doi.org/10.1016/j.vaccine.2009.05.083 *Authors contributed equally.
  A. Rath performed and analysed all experiments with the influenza virus and reviewed the publication.

Proceedings

- Platas Barradas, O.; Jandt, U.; Da Minh Phan, L.; Villanueva, M.; Rath, A.; Reichl, U.; Schräder, E.; Scholz, S.; Noll, T.; Sandig, V.; Pörtner, R. & Zeng, A. (2011), "Criteria for bioreactor comparison and operation standardisation during process development for mammalian cell culture.", BMC Proceeding 5 Suppl 8, P47.
  A. Rath performed the 0.5 L bioreactor cultivations with the DasGip System and measured and analysed cell and extracellular metabolite concentrations.

- Scholz, S.; Luebbecke, M.; Rath, A.; Schraeder, E.; Rose, T.; Büntemeyer, H.; Scheper, T.; Reichl, U. & Noll, T. (2011), "Characterization of the human AGE1.HN cell line: a systems biology approach.", BMC Proceeding 5 Suppl 8, P78.
  A. Rath performed sampling, extraction and analysis of intracellular metabolite concentrations.

- Schräder, E.; Scholz, S.; Niklas, J.; Rath, A.; Barradas, O. P.; Jandt, U.; Sandig, V.; Rose, T.; Pörtner, R.; Reichl, U.; Zeng, A.; Heinzle, E. & Noll, T. (2011), "Characterisation of cultivation of the human cell line AGE1.HN.AAT.", BMC Proceeding 5 Suppl 8, P87.
  A. Rath performed shaker flask and bioreactor cultivations and measured and analysed cell and extracellular metabolite concentrations.

- Lohr, V.; Rath, A.; Jordan, I.; Sandig, V.; Genzel, Y. & Reichl, U. (2009), "Avian Designer Cells AGE1.CR as Candidates for MVA and Influenza Vaccine Production", in 'Proceedings from the 21tst Annual Meeting of the European Society for Animal Cell Technology (ESACT)', 615-631.
  A. Rath performed and analysed all experiments with the influenza virus.

Talks at conferences

- Rath, A.; Scholz, S.; Noll, T.; Janke, R.; Genzel, Y.; Rose, T.; Sandig, V. & Reichl, U. (2012), "Insights into mammalian energy metabolism: connecting intracellular metabolites and maximum enzyme activities", Talk at the GVC/DECHEMA Vortrags- und Diskussionstagung - Biopharmazeutische Produktion in Freiburg, Germany.
  A. Rath performed and analysed the experiments and gave the talk.

- Rath, A.; Lohr, V.; Genzel, Y.; Schwarzer, J.; Rapp, E.; Sandig, V.; Jordan, I. & Reichl, U.(2008), "Influenza and modified vaccinia Ankara (MVA) production in avian designer cells", Talk at the Bioperspectives in Hannover, Germany.
  A. Rath performed and analysed all experiments with the influenza virus and gave the talk.

Poster presentations

- Rath, A.; Prehm, C.; Janke, R.; Genzel, Y.; Sandig, V.; Rose, T. & Reichl, U. (2011), "Intracellular metabolite pools and enzyme activities of AGE1.HN.AAT cells during continuous cultivations", 22nd ESACT Meeting in Vienna, Austria.
  A. Rath designed and analysed the experiments and presented the poster.

- Rath, A.; Gern, T.; Genzel, Y.; Sandig, V.; Rose, T. & Reichl, U. (2010), "Continuous cultivation of human AGE1.HN.AAT cells: Cell physiology under glucose limitation", 8th European Symposium on Biochemical Engineering Science (ESBES) in Bologna, Italy.
  A. Rath designed and analysed the experiments and presented the poster.

- Rath, A.; Genzel, Y.; Sandig, V.; Rose, T. & Reichl, U. (2009), "Cell Growth and Metabolism of a Novel Human Designer Cell Line", 21st ESACT Meeting in Dublin, Ireland.
  A. Rath designed, performed and analysed the experiments and presented the poster.

List of supervised bachelor theses

- Thomas Gern (2010), „Einfluss der Wachstumsrate auf Metabolismus, Wachstum und Produktivität der humanen Designerzelllinie AGE1.HN.AAT", Bachelor Thesis, Fakultät Angewandte Naturwissenschaften - Hochschule Esslingen, 106 pages.

- Florian Fleischhacker (2010), „Untersuchungen zur Zelllyse verschiedener Suspensionszelllinien", Bachelor Thesis, Abteilung Naturwissenschaftliche Technik - Fachhochschule Emden/Leer, 70 pages.

- Christina Prehm (2011), „Charakterisierung des Wachstums, des Metabolismus und der Produktbildung der humanen Suspensionszelllinie AGE1.HN.AAT in Batch- und Chemostatkultivierungen", Bachelor Thesis, Fakultät für Elektrotechnik und Informationstechnik - Otto von Guericke Universität Magdeburg, 58 pages.

- Vivien Fischer (2011), „Physikalische Charakterisierung orbital geschüttelter Systeme mit anschließender Kultivierung", Bachelor Thesis, Fakultät für Elektrotechnik und Informationstechnik - Otto von Guericke Universität Magdeburg, 68 pages.

List of figures

List of tables

Appendix

A.1 Supplementary data

A.1.1 Table: List of chemicals

Table A.1: List of chemicals used in this thesis.

Name	Supplier	Order No.
3-(N-morpholino)-propansulfonsäure	Sigma	M1254
5,5-dithiobis (2-nitrobenzoic acid) 99 % Ellman´s reagent	Sigma	D218200
6-phosphogluconate	Fluka	79455
α-ketoglutaric acid disodium salt dihydrate	Sigma	75892
α-ketoglutaric acid sodium salt (2-oxoglutarate)	Sigma	K1875
acetyl-CoA	Roche	10101893001
adenosine-5-diphosphat disodium salt	Fluka	01897
adenosine-5-monophosphate disodium salt	Fluka	01930
adenosine-5-triphosphate disodium salt	Sigma	A2383
alcohol dehydrogenase	Roche	10127558001
aldolase	Sigma	A8811
ammoniumacetate	Sigma	A7330
anti-human alpha1-Antitrypsin (rabbit, polyclonal)	DiaSorin	80252
anti-human alpha1-Antitrypsin (rabbit, polyclonal)	Acris	AP01066PU-N
anti-human alpha1-Antitrypsin-Perox. (polyclonal)	The Binding Side	PP034
aspartate transaminase	Sigma	G2751
benzamidine	Fluka	12072
calcium chloride	Merck	1.02381.1000
citrate	Sigma	C1909
citrate synthase	Sigma	C3260
coenzyme A trilithium salt, from yeast	Sigma	C3019

creatine kinase	Roche	10127566001
D-fructose 6-phosphate dipotassium salt	Sigma	F1502
diaphorase from Clostridium kluyveri	Sigma	D5540
dihydroxyacetone phosphate	Sigma	D7137
dipotassium phosphate	Merck	1.05099.1000
disodium phosphate	Merck	1.06585.5000
dithiothreitol	Fluka	43819
DL-glyceraldehyde 3-phosphate diethyl acetyl barium salt	Sigma	G5376
e-aminocaproic acid	Sigma	A7824
EDTA	Sigma	ED2SS
EGTA	Roth	3054
erythrose 4-phosphate	Sigma	E0377
ethanol	Roth	9065.3
fructose 1,6-bisphosphate	Sigma	47810
fumarate	Sigma	F1506
gelatine	Roche	1112589
glucose	Sigma	G8270
glucose	Roth	X997.3
glucose 6-phosphate	Sigma	G7879
glucose-6-phosphate dehydrogenase (G6PDH), grade I	Roche	10127655001
glucose-6-phosphate dehydrogenase, grade II	Roche	10127671001
glutamate dehydrogenase	Sigma	G2626
glycerokinase	Sigma	G6278
glycerol	Sigma	G7757
glycerol 3-phosphate oxidase	Sigma	G4388
glycerol-3-phosphate dehydrogenase	Roche	10127752001
guanosine 5'-diphosphate	Sigma	G7127
Hepes	Roth	9105
human alpha1-Antitrypsin	Calbiochem	178251
hydrochloric acid, 37 hydroxylamine-HCl	Fluka	55460
imidazole, puriss. p.a. >99,5 %	Fluka	56750
iodine	Roth	7935
iron(III) chloride hexahydrate	Sigma	31232
isocitrate	Sigma	I1252
lactate dehydrogenase	Roche	10127876001
L-alanine	Sigma	A7627
L-aspartic acid	Sigma	A9256
L-aspartic acid sodium salt monohydrate	Fluka	A6683
L-carnitine	Sigma	C0283
leupeptin hemisulfat	Roth	CN33
L-glutamic acid monosodium salt	Sigma	G2834
L-glutamine	Sigma	G3126
magnesium chloride hexahydrate	Roth	2189
magnesium sulfate heptahydrate	Roth	P027
malate	Sigma	M1125
malate dehydrogenase	Roche	10127256001
malonyl coenzyme A lithium salt	Sigma	M4263
monopotassium phosphate	Merck	1.04873.1000

NADH, disodium salt, grade II, approx. 98 %	Roche	10128023001
NADP, disodium salt approx. 98 %	Roche	10128040001
NADPH, tetrasodium salt, approx. 98 %	Roche	10107824001
oxaloacetate	Sigma	O4126
oxamic acid sodium salt	Fluka	75791
oxamic acid sodium salt	Sigma	O2751
phenazine ethosulfate	Sigma	P4544
phenylmethylsulfonylfluorid	Roth	6367
phophoglycerate kinase	Sigma	P7634
phospho creatine di (tris) salt), Enzymatic	Sigma	P1937
phosphoenolpyruvate	Sigma	860077
potassium bicarbonate	Fluka	60339
potassium chloride	Merck	1.04935.5000
potassium iodide	Merck	105043
seramun blau slow	Seramun	S-004-2-TMB
sodium carbonat	Sigma	S2127
sodium chloride	Roth	P029.3
sodium hydrogen carbonat	Sigma	S6014
sodium hydroxide 99 % p.a.,	Roth	6771.1
sodium pyruvate	Sigma	P8574
sodium thiosulfate	Roth	HN25
starch from potatoes	Roth	9441.1
sulfuric acid	Merck	100731
thiamine pyrophosphate	Sigma	C8754
thiazolyl blue (MTT)	Roth	4022.2
trichloroacetic acid	Sigma	T4885
tricine	Roth	6977
triose-phosphate isomerase	Sigma	T2391
triton X-100	Sigma	X100
Tween20	Roth	9127
uridine 5-triphosphate tris salt, type VI	Sigma	U6875
uridine 5-triphosphate trisodium salt hydrate	Sigma	U6625
uridine 5-diphosphoglucose disodium salt	Sigma	94335
xylulose 5-phosphate	Sigma	X0754

A.1.2 Stock solution for quantification of intracellular metabolites

Table A.2: List of chemicals and their concentration in the standard stock solution for quantification of intracellular metabolites.

Substance	Concentration (µM)	Supplier	Order number
2-phospho-D-glyceric acid	25	Sigma	P-0257
3-phosphoglyceric acid	25	Sigma	P-8877
Acetat	100	Sigma	71185
ADP	200	Sigma	A-2754
AMP	100	Merck	A-1752
ATP	400	Sigma	A-2383
CDP	25	Sigma	C-9755
sodium chloride	100	Roth	3957.1
cis-aconitate	25	Sigma	A-3412
citrate	385	Sigma	C-1909
CMP	25	Sigma	C-1006
CTP	40	Sigma	C-1506
formiat	100	Sigma	1.06443
fructose 1,6-bisphosphate	228	Sigma	F6803
fructose 1-phosphate	35	Sigma	F-0877
fructose 6-phosphate	35	Sigma	F-3627
fumarate	50	Sigma	F-2752
GDP	40	Sigma	G-7127
glucose 1-phosphate	35	Sigma	G-7000
glucose 6-phosphate	35	Sigma	G-7772
GMP	25	Sigma	G-8377
GTP	79.2	Sigma	G-8877
isocitrate	25	Sigma	I-1252
2-ketoglutarate	100	Sigma	K-1750
lactate	160	Sigma	L-7022
malate	200	Sigma	M-0875
sodium nitrate	100	Merck	1.05537
phosphoenolpyruvate	25	Sigma	P-0564
pyruvate	200	Sigma	P-8574
ribose 5-phosphate	25	Sigma	R-7750
succinate	200	Sigma	S-0141
sodium sulfate	800	Merck	1.06637
UDP	25	Sigma	U-4125
UDP-GalNAc	60	Sigma	U-5252
UDP-GlcNAc	200	Sigma	U-4375
UDP-glucose	69.8	Sigma	U-4625
UMP	25	Sigma	U-6375
UTP	200	Sigma	U-6625

A.1.3 Standard operating procedures

Table A.3: Overview of the in this work applied standard operating procedures.

SOP Title	Author	Version/date
Production of PBS solution	A. Neumann	10.12.2008
Kurzanleitung Zellzählgerät ViCell XR	J. Schulze-Horsel	08.08.2008
Alpha1-Antitrypsin Sandwich-ELISA	A. Rath	06.06.2013
Metabolitbestimmung aus Zellkultur	V. Lohr	07.04.2010

A.1.4 Table: Bioreactor, stirrer and baffle dimensions

Table A.4: Determined dimensions and characteristic numbers of the DasGip bioreactors for the physical characterization of the bioreactor systems.

Dimension	Unit	BS0500TPSS (wv=0.5 L)	DR03C (wv=2.5 L)
H_B	m	0.165	0.254
H	m	0.065	0.202
D	m	0.100	0.128
Bottom shape	-	flat	torispherical
Type of aeration	-	dip tube	dip tube
h_{sp}	m	0.005	0.010
di_{tube}	mm	2.0	2.0
Stirrer type	-	pitched impeller	pitched impeller
d	m	0.054	0.048
d_w	m	0.016	0.008
h_B	m	0.056	0.050
α	°	35	35
number of stirrers, z	-	1	2
number of blades, i	-	3 segments	3 segments
h1	m	0.015	0.025
h2	m	-	0.083
h3	m	-	-
Direction of flow	-	axial	axial
V_{total}	liter	1.30	3.20
V_{cult}	liter	0.50	2.50
V_{min}	liter	0.35	0.70
V_{max}	liter	0.60	2.70
min. aeration rate	$^{NL}/_{min}$	0.008	0.008
max. aeration rate	$^{NL}/_{min}$	0.833	0.833
Min drive	$^{1}/_{min}$	2	30
Max drive	$^{1}/_{min}$	180	500
Torque	mNm	-	35-40
Motor output	W	1-10	1-10
H/D	-	0.65	1.58
d/D	-	0.54	0.38
h2/d	-	-	1.73

A.1.5 Matlab-scripts

Cell growth model 2 - glucose and glutamine limitation

```
function dydt = growthmodelARv21(t,y,mumax,Kgln,Kglc,Yglc,Ygln,Ypyr,mglc,mgln,
mpyr,Kd,Sglc,Sgln,Spyr)
% Definition der Differentialgleichungen
% dy/dt = f(y)
CVv=y(1);
Glc=y(2);
Gln=y(3);
Pyr=y(4);

%% MODEL VARIABLES
mu   = mumax * Glc/(Glc+Kglc) * Gln/(Gln+Kgln);
kdeg = 0.0015; % 1/h bestimmt im DasGip Bioreaktor
RGlc = (mglc * Glc/(Glc+Sglc) + mu/Yglc);
RGln = (mgln * Gln/(Gln+Sgln) + mu/Ygln);
RPyr = (mpyr * Pyr/(Pyr+Spyr) + mu/Ypyr);

%% MODEL STATES
dydt=ones(4,1);
dydt(1) =  mu*CVv - Kd*CVv;
dydt(2) = -RGlc*CVv;
dydt(3) = -(RGln*CVv+kdeg*Gln);
dydt(4) = -RPyr*CVv;
```

Script for simulation of batch cultivations with cell growth model 2

```
%% Simulation Ergebnisse BHB6 mit einfachen Wachstumsmodell
% A. Rath 2013
% Modell Publikation Zentralexperimente
clc
clear all
%%
csvData = importdata( 'Datensatz.csv' );
%(von:bis,von:bis)=(Zeile:Zeile,Spalte:Spalte)
t_m   = csvData.data( 1:end, 1 );          % time-vector [h]
CVv_m = csvData.data( 1:end, 4 );
CVd_m = csvData.data( 1:end, 6 );
```

```matlab
Glc_m = csvData.data( 1:end, 2 );
Gln_m = csvData.data( 1:end, 3 );
Pyr_m = csvData.data( 1:end, 5 );
l_S = csvData.textdata( 3:end );
c_M_all = csvData.data( 1:end, 3:end );

%% Definition der Modellparameter (=optimierte Parameter für Model 2)
mumax = 0.0242867       % 1/h
Kgln = 0.01013          % mmol/L
Kglc = 0.000306619      % mmol/L
Yglc = 79072.8          % uL/umol
Ygln = 3.82575e+007     % uL/umol
Ypyr = 2.39094e+007     % uL/umol
mglc = 0.0464925        % umol/(uL*h)
mgln = 0.00976736       % umol/(uL*h)
mpyr = 0.0212928        % umol/(uL*h)
Kd = 0.00864526         % 1/h
Sglc = 0.88833          % mmol/L
Sgln = 0.393399         % mmol/L
Spyr = 1.47591          % mmol/L

%tsim = t_m;
tsim = [0:1:165]; %Simulationszeitraum
options = odeset('RelTol',1e-20); %Definition der Toleranz

%% Setzen der Anfangsbedingungen (Vektor y0)
CVv0=1.58559 % (Experiment 1)
Glc0=29.9683 % (Experiment 1)
Gln0=3.45293 % (Experiment 1)
Pyr0=2.47696 % (Experiment 1)
y0(1) = CVv0;
y0(2) = Glc0;
y0(3) = Gln0;
y0(4) = Pyr0;

%% Aufruf der Simulation (Zustandsvektor y)
[t,y] = ode23tb(@growthmodelARv21,tsim,y0,options,mumax,Kgln,Kglc,Yglc,
Ygln,Ypyr,mglc,mgln,mpyr,Kd,Sglc,Sgln,Spyr);
```

```
% Ergebnisse werden von y in andere Variablen kopiert
CVv=y(:,1);
Glc=y(:,2);
Gln=y(:,3);
Pyr=y(:,4);

%% Berechnung der Raten:
mu = mumax .* Gln./(Gln+Kgln).* Glc./(Glc+Kglc);
RGlc = (1/Yglc.*mu + mglc .* Glc./(Glc+Sglc)).*1000 ; % [nmol/(uL*h)]
RGln = (1/Ygln.*mu + mgln .* Gln./(Gln+Sgln)).*1000 ; % [nmol/(uL*h)]
RPyr = (1/Ypyr.*mu + mpyr .* Pyr./(Pyr+Spyr)).*1000 ; % [nmol/(uL*h)]

%% Model Events
mu(mu<0)=0;
Glc(Glc<0)=0;
Gln(Gln<0)=0;
Pyr(Pyr<0)=0;

%% Diagramme
figure(6);
subplot(2,2,1);plot(t,CVv,'--k',t_m,CVv_m,'squarer','linewidth',2);
hold on
hold off
title('CVv')
xlabel('Zeit [h]');
ylabel('Volumen');
hold on
subplot(2,2,2);plot(t,Glc,'--k',t_m,Glc_m,'squareg','linewidth',2);
title('Glc')
xlabel('Zeit [h]');
ylabel('Konzentration [mM]');
hold on
subplot(2,2,3);plot(t,Gln,'--k',t_m,Gln_m,'squarem','linewidth',2);
title('Gln')
xlabel('Zeit [h]');
ylabel('Konzentration [mM]');
hold on
```

```
subplot(2,2,4);plot(t,Pyr,'--k',t_m,Pyr_m,'squarec','linewidth',2);
title('Pyr')
xlabel('Zeit [h]');
ylabel('Konzentration [mM]');
hold on
```

A.1.6 DasGip scripts

Volume controlled feed

```
'Volume Controlled feed
'Version 1.0, 2010/11/24, (c) DASGIP AG
'Profile Script
'Select V.PV as Profile Source
'x = V.PV


'Script parameters:
Dim LevelVolumn as double = 500 '[ml]
Dim maxFlow as double = 7.5 ' [ml/h]Flow at LevelVolumn
Dim Con as double = maxFlow/LevelVolumn ' --> calculation of the dilution rate
Dim dV as double 'delta Volumn --> sampling volume
if P isNot Nothing Then
  with P
    .SampleTime = 10 '[s]

    'Init Storege
    if s is Nothing then
      dim a(3) as double
      'a(1) = t(n-1)
      'a(2) = Volumn(n-1)
      'a(3) = real Volumn
      a(1) = .Runtime_H
      a(2) = .VPV
      a(3) = .VPV
      if a(3) > LevelVolumn then
        a(3) = LevelVolumn
      end if
      s = a
    else
```

```
    dV = x - s(2)
    s(2) = x
    s(3) = s(3) + dV
    if s(3) > LevelVolumn then
      s(3) = LevelVolumn
    end if
    if dV < 0 then
      .logMessage ( "Calculated Volumn after Probe VCalc = " & s(3))
    end if
  end if
  dbg.writeln("calcV = " & s(3))

  'new Flow
  y = con * s(3)
  end with
end if
```

Dilution rate calculation

```
'Mass flow
'Version 1.2, 2011/07/06, (c) DASGIP AG

'Reactor Script

Dim Mr as double = 500   'Masse Reaktor (g)
dim interval_H as double = 15/60 'Interval (h)
Dim maxDeltaM as double = 1 'max delta Masse between samples (g)
Dim Fm as double          'Massenstrom (g/h)
Dim D as double           'Verdünnungsrate (1/h)
dim MPV as double         'Masse (g)
dim MPVn_1 as double      'Masse (n-1) (g)
dim dMPV as double        'delta Masse (g)
dim calM as double        'berechnete Masse
dim m1 as double          'Masse begin Interval
dim m2 as double          'Masse ende Interval
dim dt as double          'delta time


if P isNot Nothing Then
```

```
  with P

    MPV = .MAPV

    'Init Storege
    if s is Nothing then
      dim a(3) as double
      a(1) = -1 'MPVn_1
      a(2) = 0  'calM
      a(3) = 0  'Masse begin Interval
      .phase = 1
      s = a
    end if

    'read storage
    MPVn_1 = s(1)
    calM = s(2)

    if MPVn_1 <> -1 then
      dMPV = math.abs(MPVn_1 - MPV)
      if dMPV >= maxDeltaM then
        .logwarning("delta MPV high= " & Format(dMPV, "#0.00") & " > "
& Format(maxDeltaM,"#0.00"))
      else
        calM = calM + dMPV
      end if
    end if

    select case .phase
      case 1 ' init Interval
        s(3) = calM ' m1
        .phase = .phase + 1
      case 2 'end Interval calculate and log new values
        dt = (.Runtime_h - .PhaseStart_H)
        if dt > Interval_H then
          m1 = s(3)
          m2 = calM
          Fm = (m2 - m1)/(dt)
```

```
        D = Fm / Mr
        'Log to Interval Values
        .logMessage("New Values M.PV=" & Format(calM, "#0.00")
& " Fm=" & Format(Fm, "#0.00") & " D=" & Format(D, "#0.00"))
        .IntA = Fm
        .IntB = D
        .phase = .phase - 1
      end if
   end select

   'write storge
   s(1) = MPV
   s(2) = calM

  end with
end if
```
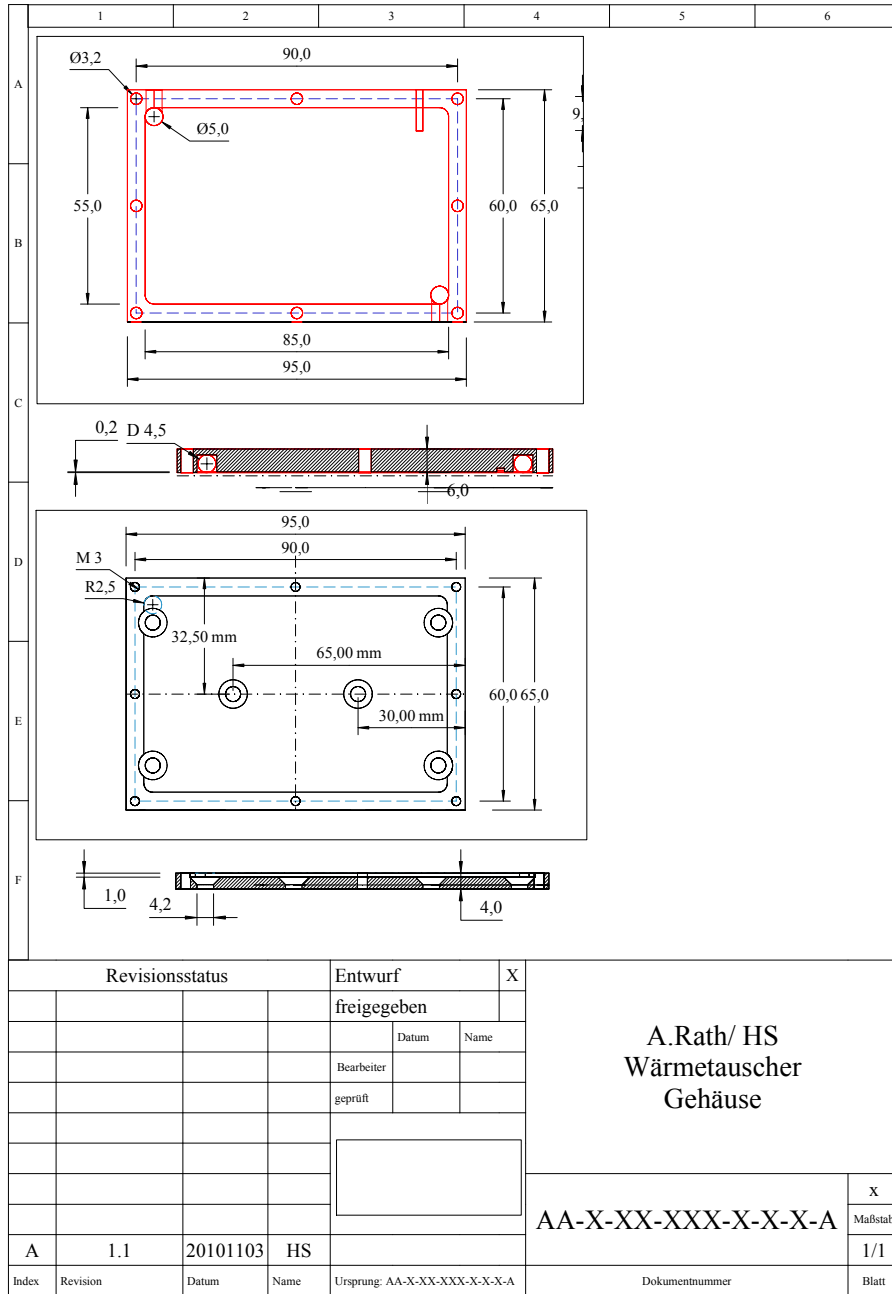
A.1.7 Mechanical drawings of the heat exchanger
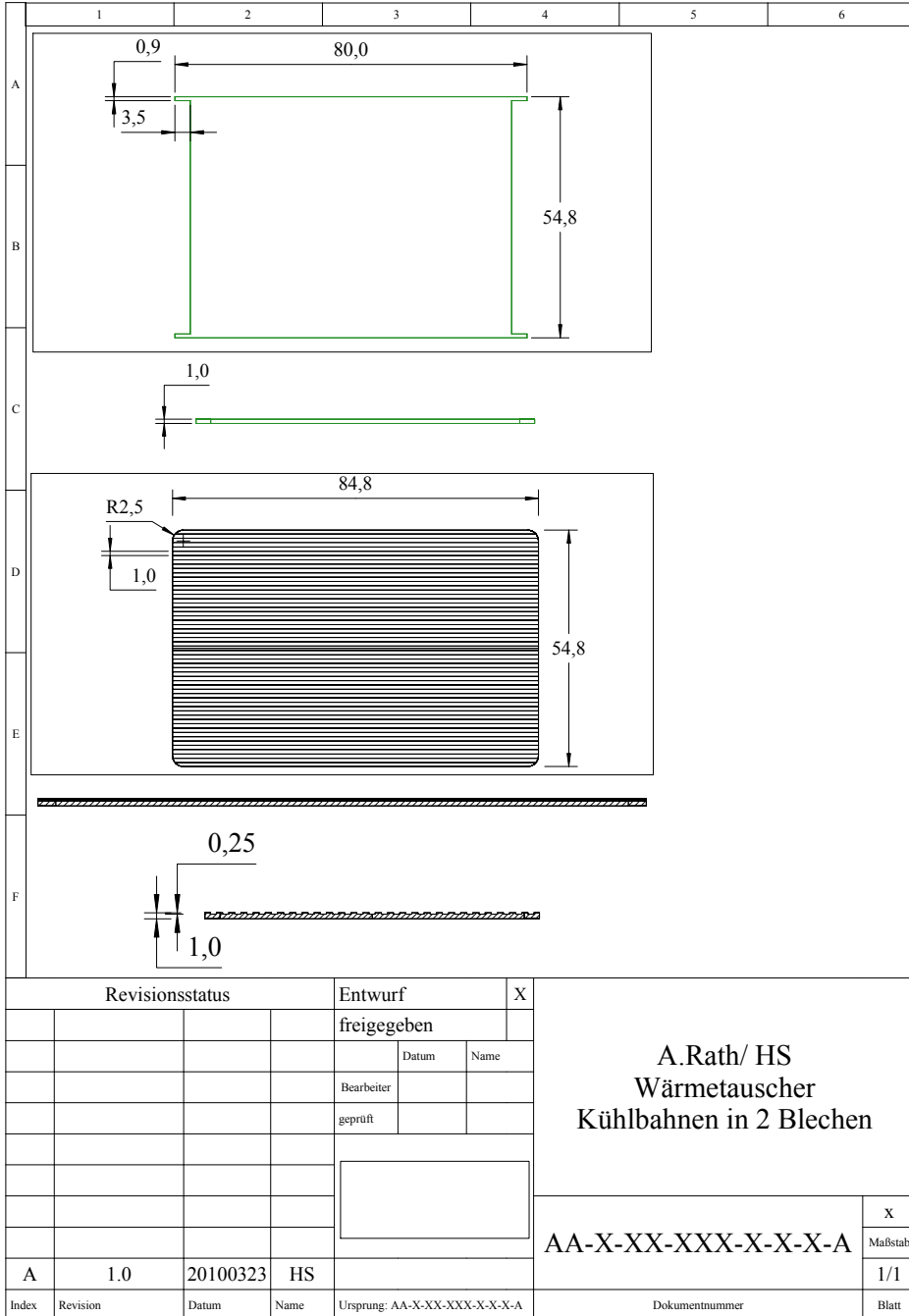

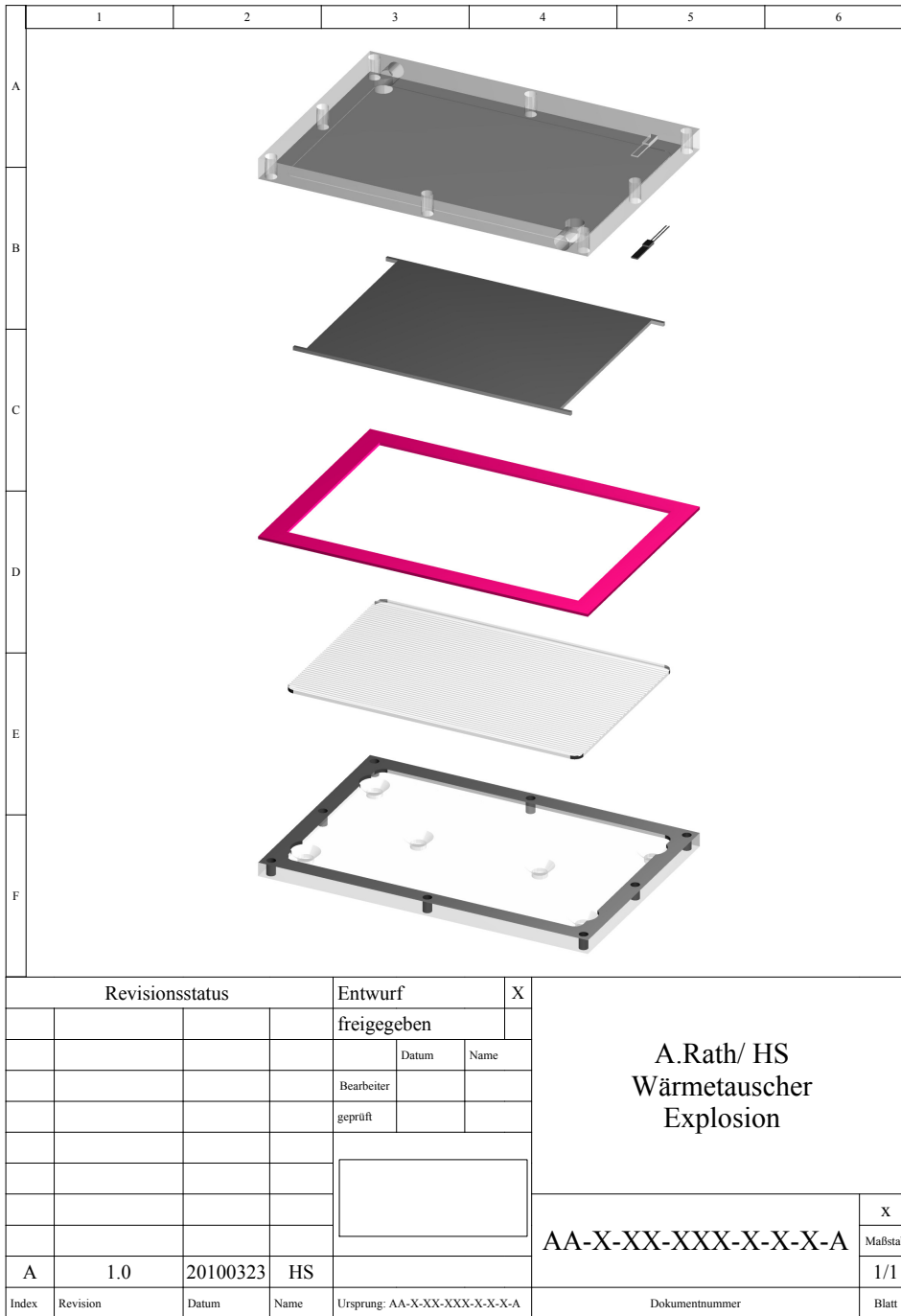**Figure A.1:** Mechanical drawing heat exchanger 1

Figure A.2: Mechanical drawing heat exchanger 2

Figure A.3: Mechanical drawing heat exchanger 3

Curriculum vitae

Personal Details

Name	Alexander Rath
Adress	Zum Lindenweiler 104, 39110 Magdeburg
E-mail	Alexander-Rath@gmx.de
Date of Birth	13. September 1978
Place of Birth	Penang, Malaysia
Nationality	German

Work experience

10/2016 – present	**Research and Development Engineer, Amino GmbH, Frellstedt, Germany:** responsible for product and process development for amino acid production.
04/2015 – 09/2016	**Division manager, Oncotec Pharma Produktion GmbH, Dessau-Rosslau, Germany:** responsible for aseptic production of cytostatic drugs.
10/2013 – 02/2015	**Prozess manager, Sandoz, Kundl, Austria:** responsible for upstream production (fermentation) of antibiotics.
12/2006 – 08/2007	**Design Draftsman, Ritterwand Metall Systembau, Nufringen, Germany:** part-time work as design draftsman.
03/2005 – 12/2005	**Industrial mechanic, Robert Bosch GmbH, Stuttgart-Feuerbach, Germany:** part-time work as mechanic.
09/2001 – 08/2002	**Civilian service, German Red Cross, Stuttgart-Bad Cannstadt, Germany:** driving and caring of elderly and disabled persons.
02/1999 – 08/2000	**Industrial mechanic, Robert Bosch GmbH, Waiblingen, Germany:** work as mechanic in the special purpose machinery manufacture department.

Education

06/2008 – 08/2013	Doctor of Engineering (Biotechnology), Dissertation, Max-Planck-Institute for Dynamics of Complex Technical Systems, Magdeburg, Germany
10/2003 – 04/2008	Diploma in Biotechnology Engineering, University of Applied Sciences, Esslingen, Germany
10/2002 – 07/2003	Two semesters Supply and Environment Engineering, University of Applied Sciences, Esslingen, Germany
09/2000 – 07/2001	Technical High School, Stuttgart, Germany
09/1995 – 02/1999	Apprenticeship as industrial mechanic, Robert Bosch GmbH, Waiblingen, Germany
09/1989 – 06/1995	Hermann Hesse Middle School, Fellbach-Schmiden, Germany.
09/1985 – 07/1989	Primary School, Fellbach-Oeffingen, Germany.

Internships

02/2006 – 09/2006	**Bioprocessing Technology Institute, Singapore:** Semester internship in the Stem Cell Research Group of Dr. Steve Oh.
09/2004 – 02/2005	**Analytical Institute Bostel, Stuttgart, Germany:** Chemical and microbiological analysis of edibles and pharmaceuticals.
02/2003 – 03/2003	**Robert Bosch GmbH, Stuttgart-Feuerbach, Germany:** Internship in the department plant maintenance and basic supply at the Robert Bosch GmbH.

(Date, Signature)